Polymers functionalized with chromophores for applications in photovoltaics, photonics and medicine

Aurel Diacon

2011
N° d'ordre : **1190**

Polymers functionalized with chromophores for applications in photovoltaics, photonics and medicine

Thèse de doctorat en cotutelle

University Politehnica of Bucharest – Roumanie
Spécialité : Ingénierie chimique

Université d'Angers - France
Spécialité : Chimie Organique
École doctorale 3MPL

Présentée et soutenue publiquement
Le 30 septembre 2011 à Bucarest

Par Aurel DIACON

Devant le jury ci-dessous :

M. Horia IOVU, *Professeur*, University Politehnica of Bucharest	*Président*
M. Roger C. HIORNS, *Chargé de Recherches,* Université de Pau et des Pays de l'Adour	*Rapporteur*
M. Andrei SARBU, *Directeur de Recherches,* ICECHIM Bucharest	*Rapporteur*
M. Marc SALLE, *Professeur,* Universite d'Angers	*Examinateur*
M. Stefan TOMAS, *Maître de Conférences,* University Politehnica of Bucharest	*Examinateur*
M. Piétrick HUDHOMME, *Professeur,* Université d'Angers	*Directeur de Thèse*
M. Corneliu CINCU, *Professeur,* University Politehnica of Bucharest	*Directeur de Thèse*

Laboratory Moltech Anjou
UMR CNRS 6200
Université d'Angers
UFR Sciences-2, Bd Lavoisier
49045 ANGERS CEDEX 01

Laboratory of Macromolecular Chemistry
University Politehnica of Bucharest
Calea Victoriei n° 149
BUCHAREST

ED n°500-3MPL

UNIVERSITY POLITEHNICA OF BUCHAREST
UNIVERSITY OF ANGERS

Year ***2011***
No. **1190**

Polymers functionalized with chromophores for applications photovoltaics, photonics and medicine

Ph.D. THESIS

in: Chemical Engineering
Organic Chemistry

Doctoral school of Faculty of Applied Chemistry and Materials Science, Bucharest
Doctoral school "Matière, Molécules, Matériaux en Pays de la Loire"

Presented and publicly sustained at
30th September 2011 at University POLITEHNICA of Bucharest

by **Aurel DIACON**

Jury:

President:	**H. Iovu**, *Professor*, University Politehnica of Bucharest
Reviewers:	**R. C. Hiorns**, *Chargé de Recherche, Université de Pau et des Pays de l'Adour*
	A. Sârbu, *Researcher grad I, ICECHIM Bucharest*
Examinateurs :	**M. Sallé**, *Professor*, Université d'Angers
	S. Tomas, *Lecturer*, University Politehnica of Bucharest
Scientific advisors:	**C. Cincu**, *Professor*, University Politehnica of Bucharest
	P. Hudhomme, *Professor*, Université d'Angers

Laboratory of Macromolecular Chemistry, Calea Victoriei No. 149, Bucharest, Romania
Laboratory Moltech Anjou– University of Angers, boulevard Lavoisier, Angers, France

Contents

Acknowledgements

I would like to offer special thanks to the members of the jury for accepting to participate at the thesis defence and for the patience to read it.

This co-joint thesis was made between the University Politehnica of Bucharest, Faculty of Applied Chemistry and Materials Science and University of Angers, Faculty of Science, Moltech Anjou Laboratory.

I would like to thank dr. eng. Corneliu Cincu, professor at University Politehnica of Bucharest for the accepting to be my scientific advisor, giving me the opportunity to develop this research work, for guidance, support and encouragement during my formation.

I am most grateful to dr. Piétrick Hudhomme, professor at University of Angers for receiving me in his laboratory in this co-joint thesis. I would like to thank him for making possible for me to work during two stages in Angers, and for all his support, attention and advices.

I would like to express a special thanks to dr. Edina Rusen, lecturer at University Politehnica of Bucharest, who offered her guidance and support in much of my work during the thesis and allowed me to work in her lab. I'm grateful also to dr. Bogdan Mărculescu for many interesting talks and ideas. I need to say that it was a pleasure to work in their lab along side with a great colleague, Alexandra Mocanu.

Important thanks go to dr. Cristian Boscornea, lecturer at University Politehnica of Bucharest for providing an insight into light-material interaction and many interesting talks. Also, to dr. Stefan Tomas and Cristina Pop I would like to thank for allowing me to work in their lab and suggesting me to start this thesis. For the many funny moments spent together I would like to thank to Raul-Augustin Mitran.

I would like to thank the wonderful people at Moltech Anjou, especially to my lab partner Marie Hardouin-Lerouge; Luc Sero, Lionel Sanguinet and Ghislain Tsague-Kenfack also a big thanks for providing each Friday with moral nourishment.

The "Romanian group" at Moltech Anjou provided me with much needed support in accommodating during my stages in Angers. My warm-hearted thanks go to Paul Ionut Dron- for his many advices and beer time, Flavia Piron - for her opinions on synthesis and purification and great walks, also, to Diana Branzea, Ion Danila and Dora Demeter for a great company.

I want to thank my PhD colleagues Cristinel Degeratu and Ramona Tudora for their team spirit and support.

An important person in my academic life, to whom I need to thank for guiding my first steps into the chemistry world, for showing me her passion for it and for having confidence in my abilities is Diana Antonia Petcu, my high school chemistry teacher: a big “Mulțumesc”.

Last but not least, I wish to thank my family and Ramona for their support and for their outstanding patience with me during these years.

The present thesis has been supported by the Sectoral Operational Programme Human Resources Development 2007-2013 of the Romanian Ministry of Labour, Family and Social Protection through the Financial Agreement POSDRU/6/1.5/S/16

ABBREVIATIONS

DSSC(s)	Dye sensitized solar cell(s)
TCO/ITO	Transparent conductive oxide/Indium tin oxide-tin-doped indium oxide
HOMO	Highest occupied molecular orbital
LUMO	Lowest unoccupied molecular orbital
V_{oc}	Open circuit voltage
I_{sc}	Short circuit intensity
FF	Fill factor
ICPE	Incident photon-to-current efficiency
AM 1.5	Air Mass 1.5
LHE	Light-harvesting efficiency
CIE	Charge injection efficiency
CCE	Charge collection efficiency
ZnPc	Zinc phthalocyanine
QD	Quantum dot
DMSO	Dimethyl sulfoxide
DMF	Dimethylformamide
NMP	N-methyl pyrrolidone
PANI	Polyaniline
PT	Polythiophene
SEM	Scanning electron microscopy
AFM	Atomic force microscopy
XRD	X-ray diffraction
IR	Infrared
DBU	1,8-diazabicyclo[5.4.0]undecene-7
EDAX	Energy-dispersive X-ray spectroscopy
AMPSA	2-acrylamido 2-methylpropane sulfonic acid
PAMPSA	Poly (2-acrylamido 2-methylpropane sulfonic acid)
CNT	Carbon nanotube
ATP	Adenosine triphosphate
OPV	Oligophenylenevinylene
EDC	N-(3-dimethylaminopropyl) N'-carbodiimide
HOBt	Hydroxybenzotriazole
DSC	Differential scanning calorimetry
TGA	Thermogravimetric analysis
COSY	Correlation SpectroscopY
HMBC	Heteronuclear Multiple Bond Correlation
HMQC	Heteronuclear Multiple Quantum Coherence
DEPT	Distortionless Enhancement by Polarization Transfer
FFT	Fast Fourier Transform filtering
PCBM	[6,6]-Phenyl C61 butyric acid methyl ester
SAM	Self-assembled monolayer
PDT	Photodynamic therapy
TETA	Triethylentetramine (*N*,*N*′-bis (2-aminoethyl) ethane -1,2-diamine)
PANI/ES/EB	Polyaniline/Emeraldine salt/Emeraldine Base
Rh	Rhodamine B

Introduction

The key characteristics in current scientific research are the interconnectivity and pluridisciplinarity. Thus, the present thesis follows the modern trend by putting into contact materials science, polymer chemistry, organic chemistry and physics.

As the title suggests, the thesis purpose has been to study the interaction and utilization of polymers and dyes for possible practical applications. One of the two components studied being a dye, it was only logical to consider light as common element. Thus, all the applications and interaction studied are based on the response of the materials to light sources.

The envisaged applications and the function we gave to each component are presented in Figure 0-1.

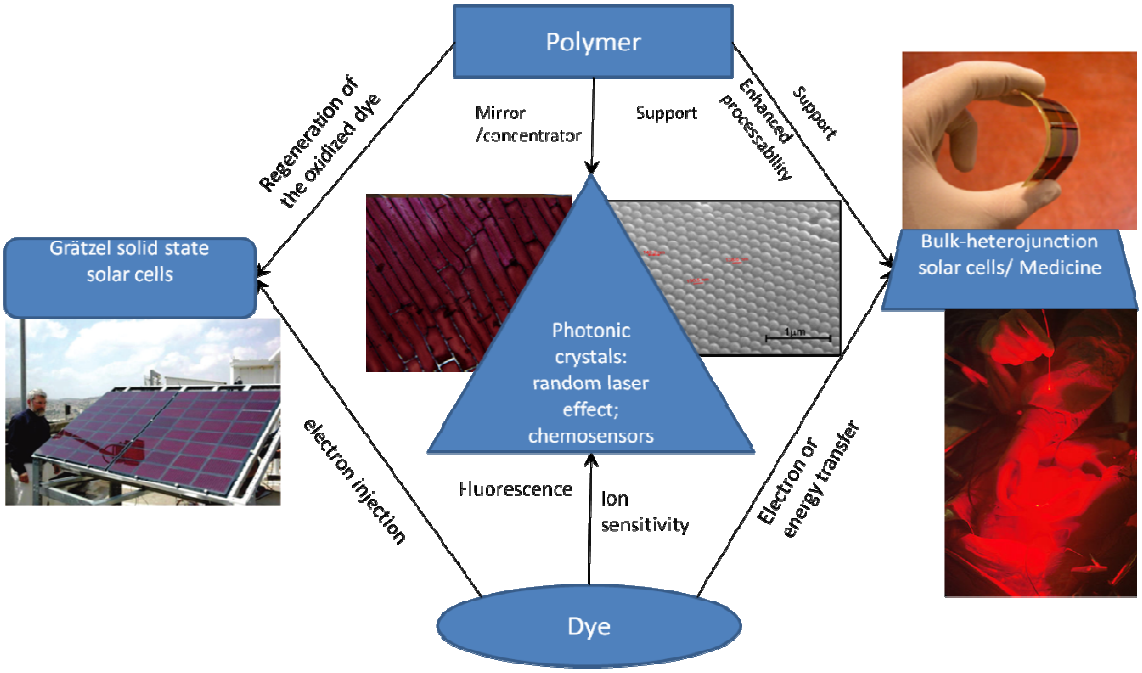

Figure 0-1 Interactions followed during the thesis

An important part of the research work of this thesis was dedicated to applications in photovoltaics. The first direction of the research consisted in the obtaining of new materials in order to obtain solid-state Grätzel solar cells. Thus, the role of the dye is to act as the sensitizer, injecting an electron upon excitation into the conduction band of the semiconductor layer. The role of the polymer utilized in this application is to regenerate the oxidized dye. Different approaches have been studied in order to improve the efficiency of the obtained solar cells (see Chapter I).

The second direction with applications in photovoltaics is represented by the molecular design of PDI-C_{60} dyads that can allow further developments. Previous results

obtained by the group of P. Hudhomme indicated the possibility to use PDI-C_{60} light-harvesting dyads in bulk-heterojunction solar cells by replacing the PCBM. In this case the dyad has been grafted onto a polymeric chain with the intent to enhance the processability of the dyad. Energy transfer has been observed through fluorescence spectroscopy and cyclic voltammetry has been performed in order to characterize the dyad. Additional possibility of use in medicine (PDT - photodynamic therapy-cancer treatment) can be envisaged for the dyad due to the dye characteristics which is able to reach triplet state capable to generate single oxygen species.

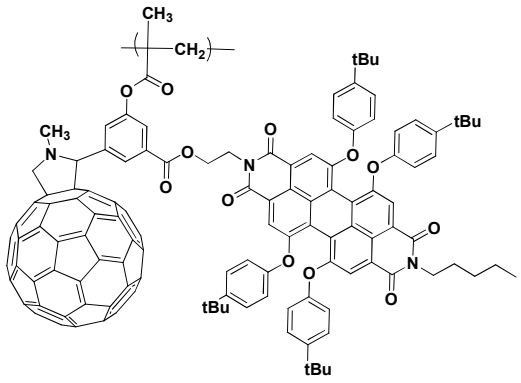

Pol 3

The third direction has been the developing of photonic crystals systems. Thus, the polymer particles through their size and arrangement also interact with the light (the stop-band). The first objective has been to study the effect of photonic crystals on the emission properties of fluorescent dyes. The dye was also placed inside the polymer particles comprising the photonic crystals, thus obtaining different emission characteristics. The photonic crystals doped with dye in this manner may be suitable for applications for the obtaining of random laser effect.

The second approach regarding photonic crystals involved the obtaining photonic crystal heterostructures using monodisperse polymer particles dispersion and a colloidal gold solution. The obtained structures served as platform for the self-assembly of aliphatic chains containing hydroxy-thiol groups (HO-R-SH). Rhodamine B was attached to the SAM. The fluorescence properties of the obtained structure have been compared to a Rhodamine B film deposited on a simple glass surface. Also, by modifying Rhodamine B with TETA (triethylentetraamine) the chemosensor properties of the obtained materials have been investigated.

CHAPTER I: Dye sensitized solar cells

I. Dye sensitized solar cells presentation

1. History

Humanity's demand for energy is constantly increasing. Faced with this impending colossal demand, many researchers are pointing to the sun as a necessary source of energy. The challenge remains how to harness that energy in a cost-effective, environmentally friendly way.

Until recently, commercially available solar cells were based on inorganic materials, which require high costs and highly energy consuming preparation methods. Also, several materials, such as CdTe are toxic and have low natural abundance. The organic-based solar cells, however, for the moment, are still a long way behind those obtained with purely inorganic photovoltaic systems.

Scientists have shown a lot of interest to the photoelectric interactions starting with the discovery of photography more than 100 years ago. The first panchromatic film, able to remit image in black and white, followed the work of the german chemist Herman W. Vogel. His accidental discovery in 1873, when he found that a plate treated with the coralline to reduce light scatter of halation also had increased the emulsion's sensitivity to yellow-green light[1]. In is only in the 1960s that a clear correlation between photographic and photoelectrode sensitization is made[2,3]. Improvement of concept came in the next years by using chemisorption in order to attach the dye to the semiconductor surface[4]. Another important improvement was to use dispersed particles to provide a sufficient interface and then to use photoelectrodes[5]. In 1991[6], the first dye-sensitized nanocrystalline solar cell with a conversion yield of 7.1 % was announced. The use of a mesoporous semiconductor electrode with a high internal surface area was one of the key improvements brought by Grätzel, this, coupled with the dye used as the photosensitizer marked an exponential increase given to research in this field. Until, this moment, the basic problem was the belief that only smooth conductor surface could be used which limited the amount of absorption that could be reached even with dyes that have high extinction coefficients. At present, in the official table of world record efficiencies for solar cells, the record is held by the Sharp company in Japan at $10.3 \pm 0.3\%$.[6]

[1] M. R. Peres, *Focal encyclopedia of photography: digital imaging, theory and applications, history, and science*. Elsevier/Focal Press: 20071.
[2] S. Namba and Y. Hishiki, *The Journal of Physical Chemistry,* **1965,** *69*, 774-779.
[3] H. Tributsch and H. Gerischer, *Berichte der Bunsengesellschaft für physikalische Chemie,* **1969,** *73*, 251-260.
[4] H. Tsubomura, M. Matsumura, Y. Nomura and T. Amamiya, *Nature,* **1976,** *261*, 402-403.
[5] J. Desilvestro, M. Graetzel, L. Kavan, J. Moser and J. Augustynski, *Journal of the American Chemical Society,* **1985,** *107*, 2988-2990.
[6] M. A. Green, K. Emery, Y. Hishikawa and W. Warta, *Progress in Photovoltaics: Research and Applications,* **2011,** *19*, 84-92.

2. Principle

The dye sensitized solar cell (DSSC), also called Grätzel[7] cell, is a photoelectrochemical device that combines light-absorbing dye molecules with semiconductor nanoparticles and a redox electrolyte in order to generate electricity using sunlight.

A typical DSSC is composed of:

1) a nanoporous metal oxide (TiO_2, NiO, ZnO) infiltrated with sensitizer dye molecules (Ru complexes or other organic dyes) and deposited on a transparent conductive oxide (TCO) electrode

2) electrolyte containing I^-/I_3^- redox system filling the pores of the metal oxide

3) a platinum counter electrode[8]; figure I.-1

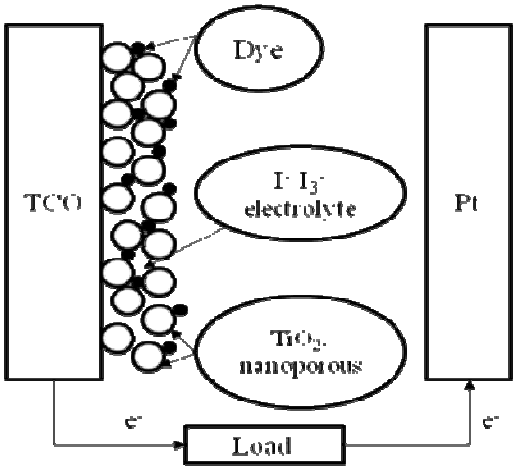

Figure I-1 Structure of DSSC

After light absorption, an electron is excited from a low-energy level (highest occupied molecular orbital, HOMO) to a high-energy state (lowest unoccupied molecular orbital, LUMO) of the dye. The excited state of the dye is relaxed by electron injection to the semiconductor layer (TiO_2, ZnO etc) conduction band and the oxidized dye is regenerated by electron capture from the redox electrolyte. The electron moves by diffusion in the TiO_2 layer until it is collected at the TCO contact of the photoelectrode and it is returned to the redox electrolyte in an electrochemical reaction at the counter electrode. The electrical circuit is closed by ionic transport between the photoelectrode and counter electrode[9,10,11]. (Figure I-2)

[7] B. O'Regan and M. Gratzel, *Nature,* **1991,** *353*, 737-740.
[8] M. Grätzel, *Inorganic Chemistry,* **2005,** *44*, 6841-6851.
[9] M. Grätzel, *Journal of Photochemistry and Photobiology C: Photochemistry Reviews,* **2003,** *4*, 145-153.
[10] A. Hagfeldt and M. Graetzel, *Chemical Reviews,* **1995,** *95*, 49-68.
[11] A. Hagfeldt, G. Boschloo, L. Sun, L. Kloo and H. Pettersson, ibid. **2010,** *110*, 6595-6663.

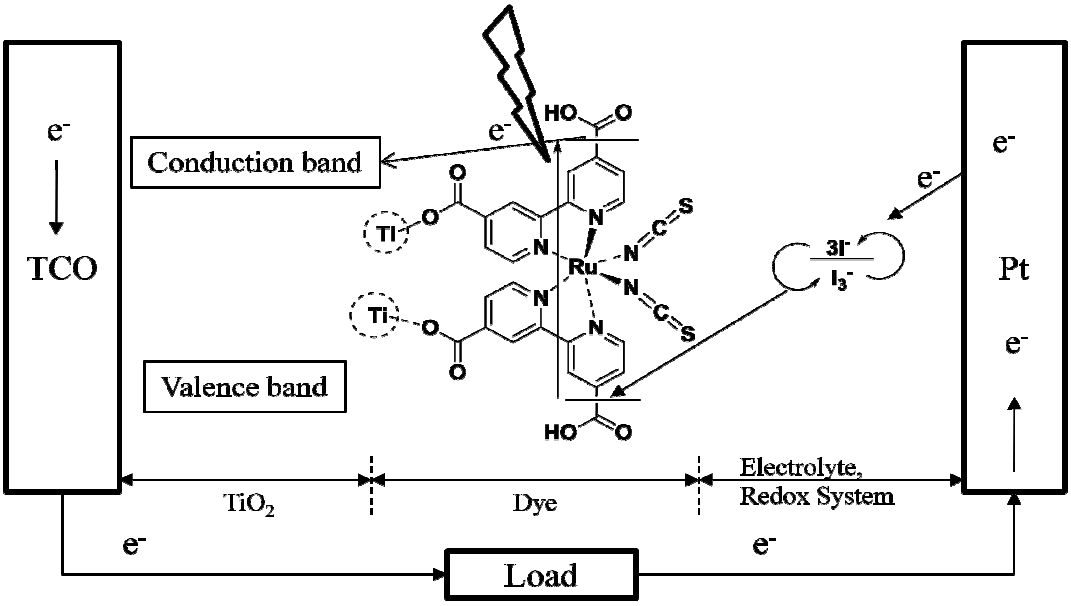

Figure I-2 Scheme of working principle of DSSC

The operating cycle of the cell can be summarized this way:

$S + h\nu \rightarrow S^*$ light absorption by the sensitizer (1)

$S^* \rightarrow S^+ + e^-_{injected}$ electron injection in the semiconductor layer (2)

$I_3^- + 2e^-_{(cathode)} \rightarrow 3I^-_{(cathode)}$ electrolyte reduction on the cathode (3)

$S^+ + \frac{3}{2} I^- \rightarrow S + \frac{1}{2} I_3^-$ dye regeneration (4)

Also, some undesirable reactions, resulting in a decrease of cell efficiency occur. They are the recombination of the injected electrons either with the oxidized sensitizer or with the oxidized redox couple at the TiO_2 surface.

$S^+ + e^-_{(TiO_2)} \rightarrow S$ (5)

$I_3^- + 2\, e^-_{(TiO_2)} \rightarrow 3I^-_{(anode)}$

A solid-state version of the cell is the sensitized heterojunction. The electrolyte is replaced by a wide bang gap inorganic semiconductor of p-type such as CuI[12] or CuSCN[13] or a hole-transmitting solid.

[12] K. Tennakone and et al., *Semiconductor Science and Technology,* **1995,** *10*, 1689.
[13] B. O'Regan and D. T. Schwartz, *Journal of Applied Physics,* **1996,** *80*, 4749-4754.

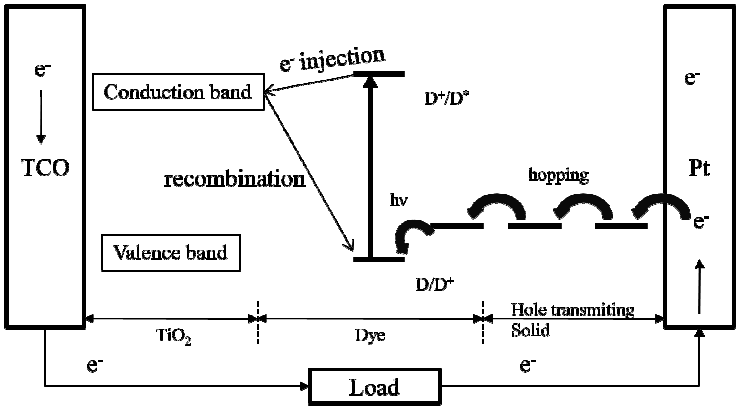

Figure I-3 Dye-sensitized heterojunction solar cell, the electrolyte is replaced by an organic hole conductor

The total efficiency of the DSSC depends on the optimization and compatibility of each of its constituents.

Performance characterization

The photovoltaic performance of a solar cell can be establish using the current-voltage (I=f(V)) curve. The utilization of the curve allows the determination of the parameters:

- V_{oc} (V), the open circuit voltage, is the potential between the two electrodes when the external load is very large (for I=0);
- I_{sc} ($A \cdot cm^{-2}$), is the maximum current delivered by the solar cell at any illumination level, it corresponds to a zero external resistance (V=0);
- the maximum power point (MPP), it allows the determination of the P_{max} ($W \cdot cm^{-2}$):

$$P_{max} = V_{max} \cdot I_{max}$$

- the filling factor (FF) is defined as:

$$FF = \frac{I_{max} \cdot V_{max}}{V_{oc} \cdot I_{sc}} = \frac{P_{max}}{V_{oc} \cdot I_{sc}}$$

- the photon-to-current conversion efficiency (ICPE), sometimes referred to as external quantum efficiency (EQE), is defined as the number of electrons generated by light in the external circuit divided by the number of incident photons and represents the ratio between the maximum power produced by the cell ($W \cdot m^{-2}$) and the incident light intensity P_{in} ($W \cdot m^{-2}$)

$$\eta = \frac{P_{max}}{P_{in}}$$

The standard conditions relevant for terrestrial applications are: light intensity 1000 $W \cdot m^2$, spectral distribution according to AM 1.5 global standard solar spectrum, and cell temperature 25°C. The power output of the solar cell in these conditions is called nominal power of the cell and it is indicated by reporting the date in units of W_p, called peak watt.

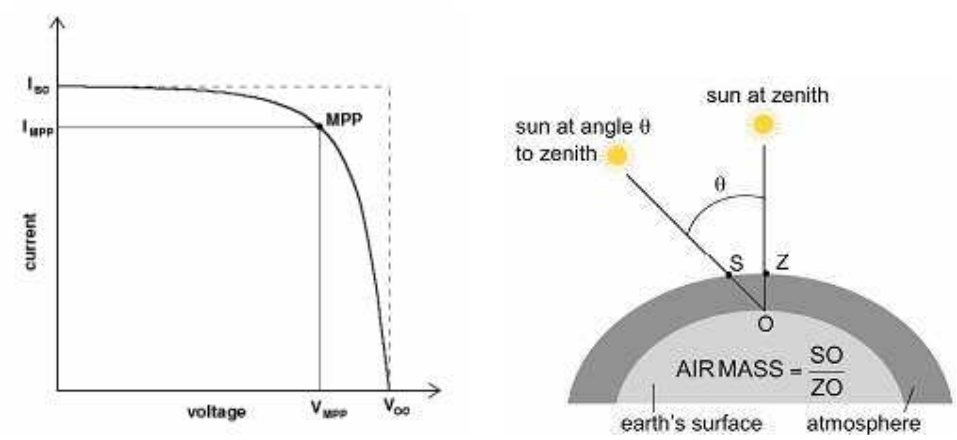

Figure I-4 curve and conditions for cell illumination for testing

The incident photon-to-current conversion efficiency (IPCE) is determined by light-harvesting efficiency (LHE), charge injection efficiency (CIE) and charge collection efficiency (CCE). LHE is the ratio between the absorbed photons and the total incoming photons and depends on the absorption coefficient of dye and the density or the thickness of absorbed dye on the nanoporous electrode.

CIE is determined by the potential difference between the conduction band edge of TiO_2 and LUMO of the dye, acceptor density in TiO_2 and spatial distance between the surfaces of TiO_2 and the dye.

The diffusion length of electrons in TiO_2 (L) influences CCE and the thickness of the TiO_2 electrode must be less than L. The length L is defined as: $L = (D\tau)^{1/2}$ where D is the electron diffusion coefficient and τ is electron lifetime in nanoporous TiO_2.

For a Grätzel type cell with nanoporous TiO_2 electrode and Ru complex dyes, 10-30 μm thickness (L) is required to achieve high LHE values.[14]

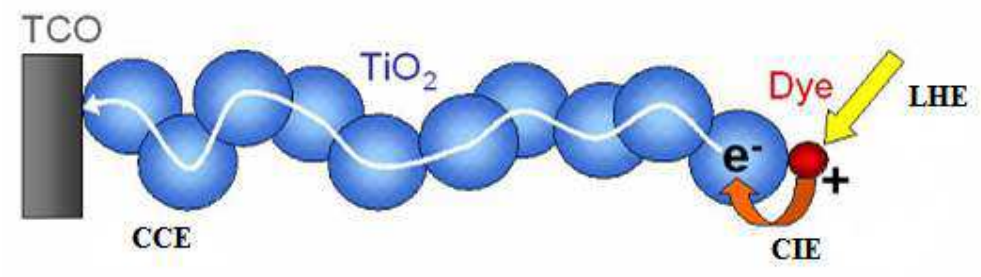

Figure I-5 The output of the DSSC depends on the LHE, CIE and CCE[15]

[14] M. Grätzel, *Journal of Photochemistry and Photobiology A: Chemistry,* **2004,** *164*, 3-14.
[15] J. Halme, P. Vahermaa, K. Miettunen and P. Lund, *Advanced Materials,* **2010,** *22*, E210-E234.

3. Sensitizers

The ideal sensitizer for a DSSC should absorb all light below 920 nm, it should also present functional groups that allow attachment on the semiconductor layer such as carboxy or phosphate. The process of absorption must be followed by electron injection into the conduction band of the solid with a CIE of 1. The energy level of the HOMO of the sensitizer should be in accordance with the energy level of the conduction band of the oxide in order to obtain a good working tension and to minimize the energy loses during the electron transfer. For the regeneration step, its redox potential should be sufficiently positive to allow regeneration by a redox electrolyte or a hole conductor. Finally, the stability should sustain about 10^8 turnover cycles corresponding to about 20 years of exposure to natural light.

Intense research in dye chemistry has been devoted to the identification, synthesis of dyes that satisfy these demands, while retaining sufficient photostability. Functional groups allow the attachment of the dye through spontaneous assembly of molecules on the semiconductors surface immersed in a dye solution. This molecular dispersion permits a high probability that, after a photon is absorbed, the relaxation of the excited state of the dye will take place by electron injection in the semiconductor conduction band.

Discovered in 1993[16] the photovoltaic performance of N_3, was not surpassed for 8 years by hundreds of other synthesized and compounds. However, in 2001, a new record was achieved by the "black dye" tri(cyanato)-2.2'2''-terpyridyl-4,4',4''-tricarboxylate)Ru(II) at 10.4%.

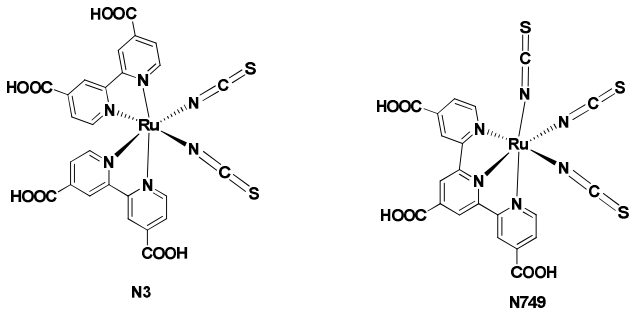

Scheme I-1 Structures of N3 and N749 "black dye"

In the search for a better sensitizer many different types of dyes have been tested: porphyrins[17], phthalocyanines[18], coumarins[19], transition metal complexes[20], perylene[21], cyanines and azulene[22].

[16] M. K. Nazeeruddin, A. Kay, I. Rodicio, R. Humphry-Baker, E. Mueller, P. Liska, N. Vlachopoulos and M. Graetzel, *Journal of the American Chemical Society,* **1993,** *115*, 6382-6390.
[17] H. Mao, H. Deng, H. Li, Y. Shen, Z. Lu and H. Xu, *Journal of Photochemistry and Photobiology A: Chemistry,* **1998,** *114*, 209-212.

One of the drawbacks of ruthenium complexes is the limited absorption in the near-infrared region of the solar spectrum. Porphyrin and phthalocyanine systems exhibit intense spectral response bands in the near-IR region and possess good chemical, photo-, and thermal stability, providing good potential candidates for photovoltaic applications.

Due to their role in photosynthesis, porphyrins and chlorophylls have been tested as photosensitizers in DSSCs. The appropriate LUMO and HOMO energy levels and the strong absorption of Soret band in the 400-450 nm, as well as Q-band 500-700 nm,[23] make the porphyrins suitable as panchromatic sensitizers for DSSCs. The effect of different anchoring groups and substitution positions on a series free porphyrins base on DSSC has been studied by Bignozzi and co-workers.[24] They found that only when anchoring group is changed there is no real modification in efficiency. However, the position of the anchoring group is important; this could be due to differences in orientation and distance between the chromophores and the TiO_2 layer. Nazeeruddin and co-workers developed a family of porphyrin dyes with different central metal ions (Cu(II) or Zn(II)) and different anchoring groups (COOH or PO_3H_2).[25] They concluded that for porphyrins with carboxylic binding groups, the diamagnetic metalloporphyrins containing Zn showed very high IPCE values in comparison to that of the paramagnetic metalloporphyrins containing Cu. Moreover, porphyrins with a phosphonate anchoring group showed lower efficiencies than those with a carboxylate anchoring group. A method of employing porphyrins is to construct $D-\pi-A$ structures. Tan and co-workers reported several new porphyrin dyes with a $D-\pi-A$ structure: the porphyrin acted as a donor and cyanoacrylic acid acted as an acceptor/anchoring group; different thiophene derivatives acted as a π bridge to broaden the absorption of the dyes.[26] They found that the thiophene π-conjugation unit can extend the spectral response region of porphyrin dyes, and the alkyl chain on this unit can improve the photovoltaic performance of DSCs.

---

[18] M. K. Nazeeruddin, R. Humphry-Baker, M. Gratzel and B. A. Murrer, *Chemical Communications,* **1998**, 719-720.
[19] J. M. Rehm, G. L. McLendon, Y. Nagasawa, K. Yoshihara, J. Moser and M. Gratzel, *The Journal of Physical Chemistry,* **1996,** *100*, 9577-9578.
[20] A. S. Polo, M. K. Itokazu and N. Y. Murakami Iha, *Coordination Chemistry Reviews,* **2004,** *248*, 1343-1361.
[21] S. Ferrere, A. Zaban and B. A. Gregg, *The Journal of Physical Chemistry B,* **1997,** *101*, 4490-4493.
[22] B. C. O'Regan, I. López-Duarte, M. V. Martínez-Díaz, A. Forneli, J. Albero, A. Morandeira, E. Palomares, T. Torres and J. R. Durrant, *Journal of the American Chemical Society,* **2008,** *130*, 2906-2907.
[23] R. K. Lammi, R. W. Wagner, A. Ambroise, J. R. Diers, D. F. Bocian, D. Holten and J. S. Lindsey, *The Journal of Physical Chemistry B,* **2001,** *105*, 5341-5352.
[24] F. Odobel, E. Blart, M. Lagree, M. Villieras, H. Boujtita, N. El Murr, S. Caramori and C. Alberto Bignozzi, *Journal of Materials Chemistry,* **2003,** *13*, 502-510.
[25] M. K. Nazeeruddin, R. Humphry-Baker, D. L. Officer, W. M. Campbell, A. K. Burrell and M. Grätzel, *Langmuir,* **2004,** *20*, 6514-6517.
[26] Y. Liu, N. Xiang, X. Feng, P. Shen, W. Zhou, C. Weng, B. Zhao and S. Tan, *Chemical Communications,* **2009**, 2499-2501.

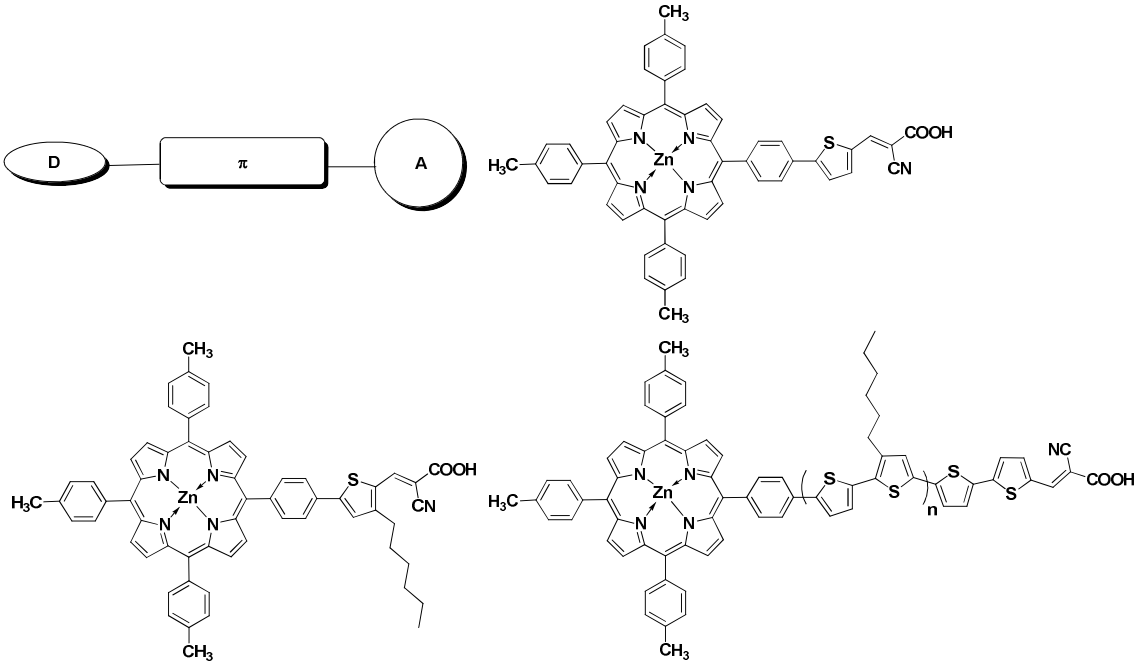

Scheme I-2 Porphyrin containing donor-π-acceptor system used in DSSC

Phthalocyanines present the advantage of having high molecular coefficients and absorption in this area, but come with problems like aggregation and low solubility. They are of interest to use as near IR photosensitizers for DSSCs. A large number of phthalocyanine dyes have been synthesized for applications in DSSC.

An important work on phthalocyanines has been realized by Nazeerudin and co-workers[27]. They synthesized a series of Zn and Al phthalocyanines with COOH or SO_3H as anchoring group. They found that there is no real difference between the two groups regarding the cell efficiency. Also, they concluded that the introduction of –O- or $–CH_2$- between the macrocycle and the anchoring groups, the IPCE drops to one-half of the value observed for phthalocyanine derivatives with no spacer. They obtained a cell efficiency of 1% for the tetracarboxy derivative (scheme I-3).

The solubility restrictions of the phthalocyanines can be surpassed by proper choice of substituents on the macrocycle periphery. An interesting approach that involved the developing of new methods of anchoring the dye was employed by He et al.[28]. They employed a butyl ester of tetracarboxyphthalocyanine, and the TiO_2 layer was pretreated with $(CH_3)_3COLi$ to change the surface hydroxyl groups into deprotonated oxygen anions, thus

[27] M. K. Nazeeruddin, R. Humphry-Baker, M. Gratzel, D. Wohrle, G. Schnurpfeil, G. Schneider, A. Hirth and N. Trombach, *J. Porphyrins Phthalocyanines,* **1999,** *3*, 230-237.
[28] J. He, A. Hagfeldt, S.-E. Lindquist, H. Grennberg, F. Korodi, L. Sun and B. Åkermark, *Langmuir,* **2001,** *17*, 2743-2747.

making the surface more reactive toward the ester-functionalized phthalocyanines. According to this method, the dye used (scheme I-3) gave a 4.3% IPCE value at 690 nm. A phthalocyanine dye with tyrosine groups was synthesized.[29] The tyrosine group plays an important role in the photosynthetic oxygen-evolving photosystem II (PSII) reaction center, because it can donate an electron to the oxidized chlorophylls. The introduction of tyrosine units into phthalocyanine should result in an electron-transfer process from tyrosine to the oxidized ZnPc, thereby suppressing the back-electron transfer. Also the bigger substituting tyrosine groups can reduce the dye aggregation on the semiconductor surface. With this dye they obtained DSSCs, an IPCE value of ~24% at 690 nm and an overall conversion efficiency of 0.54%. The tyrosine substituted phthalocyanine was investigated by femtosecond spectroscopy which revealed that the electron injection from the excited state of the dye to the conduction band of the TiO_2 is very fast. But, the charge recombination is also fast. This can explain the low efficiency of DSSC based on this type of dye.

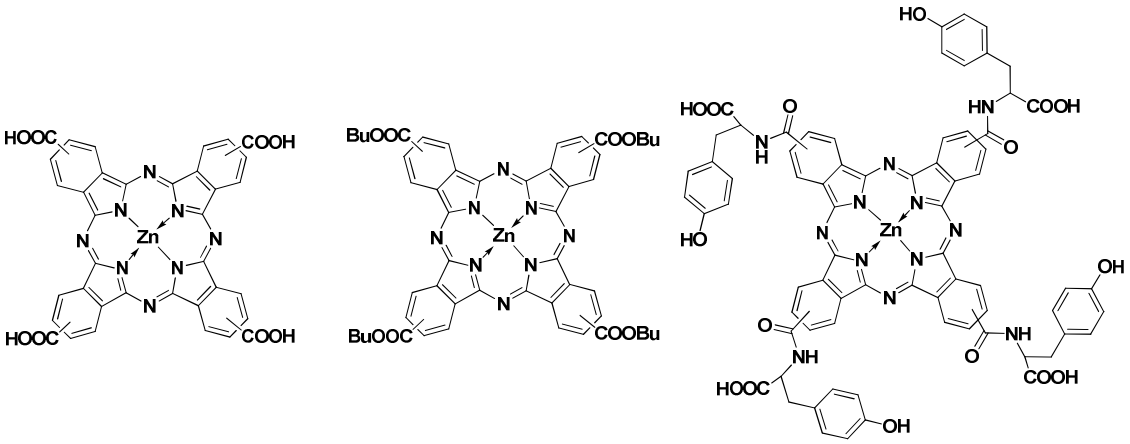

Scheme I-3 Examples of phthalocyanines tested in DSSC

There are several ways in which molecular adsorption can take place on host surfaces[30]:

a) covalent attachment brought about by directly linking groups of interest or via linking agents;
b) electrostatic interactions, brought about via ion exchange, ion-pairing or donor-acceptor interactions;
c) hydrogen bonding;
d) hydrophobic interactions leading to self-assembly of long-chain fatty acid derivatives;

[29] J. He, G. Benkö, F. Korodi, T. Polívka, R. Lomoth, B. Åkermark, L. Sun, A. Hagfeldt and V. Sundström, *Journal of the American Chemical Society,* **2002,** *124*, 4922-4932.
[30] K. Kalyanasundaram and M. Grätzel, *Coordination Chemistry Reviews,* **1998,** *177*, 347-414.

e) van der Waals forces involved in physisorption of molecules on solid surfaces;

f) physical entrapment inside the pores of cavities of host such as cyclodextrins, micelles.

To construct a functional and efficient DSSC, the dye must be adsorbed intimately on the semiconductor surface. The first type of adsorption, is the best suited for this type of interaction. For this take place, the dye must poses an anchoring group which can react with the semiconductor surface. The most common anchoring group for sensitizers is carboxylic (-COOH).

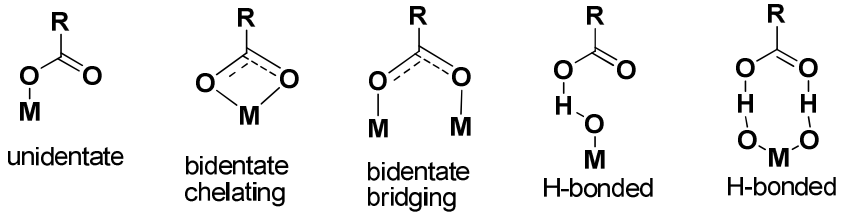

$$-Ti\text{-}OH + (CH_3)_3COLi \longrightarrow -Ti\text{-}O^{-}\,Li^{+} + (CH_3)_3COH$$

$$-Ti\text{-}O^{-}\,Li^{+} + ZnPc\text{-}COOBu \longrightarrow -Ti\text{-}OOC\text{-}ZnPc + BuOLi$$

Scheme I-4 Different biding modes between the semiconductor (oxide) layer and the carboxylic anchoring group

Other anchoring groups tested include sulfonate ($-SO_3^-$), silane (SiX_3 or $Si(OX)_3$) and also phosphonic acid ($-H_2PO_3$) which did not present desorption in the presence of water compared to carboxyl[31].

4. Combination of dyes

A strategy used in order to increase the spectral response of the DSSC is the use of a combination of dyes. A good example for this is the work of Spitler[32] that combined cyanine dyes absorbing in the red, yellow and blue regions which resulted in photocurrents increased compared to the single dyes. Also, a method for dye absorption in a double layer has been developed. It employs an ultrathin film of aluminum oxide deposited over the first dye. The adsorption of the second is done on top of this film. Using this method, Choi et al. obtained 8.7% efficiency by combining two organic dyes.[33]

[31] P. Pechy, F. P. Rotzinger, M. K. Nazeeruddin, O. Kohle, S. M. Zakeeruddin, R. Humphry-Baker and M. Gratzel, *J. Chem. Soc., Chem. Commun.,* **1995**, 65-66.
[32] A. Ehret, L. Stuhl and M. T. Spitler, *The Journal of Physical Chemistry B,* **2001,** *105*, 9960-9965.
[33] H. Choi, S. Kim, S. O. Kang, J. Ko, M.-S. Kang, J. N. Clifford, A. Forneli, E. Palomares, M. K. Nazeeruddin and M. Grätzel, *Angewandte Chemie International Edition,* **2008,** *47*, 8259-8263.

Another approach of using a combination of dyes is the use of energy relay dyes: the introduction of highly fluorescent dyes either in the liquid electrolyte[34] or in the solid hole conductor[35]. The energy relay dye participates to the generation of photocurrent by Förster resonant energy transfer to the sensitizing dye adsorbed on the TiO_2 layer. This method allows a broader spectral absorption, while reducing the design requirements for the sensitizing dye.

5. Quantum Dots

When considering the designing of DSSC with panchromatic sensitizers, an alternative are semiconductor quantum dots. These are II-VI and III-V type semiconductors particles whose size (less than about 25 nm to 10 nm depending upon effective mass) allows them to produce quantum confinement effects. When charge carriers are confined by potential barriers in three spatial dimensions, this regime is termed a quantum dot (QD). The absorption spectrum of such quantum dots can be adjusted by controlling the particle size. Quantum dots (QDs) can be formed either by epitaxial growth from the vapor phase (molecular beam epitaxy or metallo-organic chemical vapor deposition process) or via chemical synthesis (colloidal chemistry or electrochemistry).

6. Electrolytes

The record cell fabricated by Grätzel and O'Regan in 1991, used an electrolyte that was based on mixture 80:20 (v) of ethylene carbonate and acetonitrile. The redox components were added as 0.5 M tetrapropylammonium iodide and 0.04 M iodine, and no extra additives were used. The composition of the electrolyte was adjusted using lower concentrations of lithium or potassium iodide, however not producing higher conversion than the simplest composition.

The imposed requirements for the liquid redox electrolyte are:

- it should be chemically stable
- to have low viscosity in order to minimize transport problems
- it has to be a good solvent for the redox components and various additives but at the same time not cause significant dissolution of adsorbed dye or even the semiconducting

[34] B. E. Hardin, E. T. Hoke, P. B. Armstrong, J.-H. Yum, P. Comte, T. Torres, J. M. J. Frechet, M. K. Nazeeruddin, M. Gratzel and M. D. McGehee, *Nat Photon,* **2009,** *3*, 406-411.
[35] J.-H. Yum, B. E. Hardin, S.-J. Moon, E. Baranoff, F. Nüesch, M. D. McGehee, M. Grätzel and M. K. Nazeeruddin, *Angewandte Chemie International Edition,* **2009,** *48*, 9277-9280.

material of the electrodes. Water and reactive protic solvents are normally not good choices, due the fact that many organometallic sensitizing dyes are sensitive to hydrolysis

- it should be compatible with a suitable sealing material to avoid losses by evaporation or leakage

The initial solvent choice for liquid electrolyte consisted in organic carbonates, or a mixture with organic solvent. Another use of this solution is in lithium batteries, also due to their high permittivity. When a considering the use of an organic solvent an important factor to take into consideration is the sealing of the cell which might be sensitive to it.

The influence of a large number of common organic solvents, including DMF, DMSO with LiI/I_2 has been studied by Hara et al.[36]. Another, interesting study is the one did by Wu et al.[37], they studied pure and mixed electrolytes based on propylene carbonate, γ-butyrolactone, N-methylpyrrolidone, and pyridine. They obtained similar results as Hara et al. concluding that stronger donating solvents enhance the photovoltage, but decrease the photocurrent. For DSSC using organic dyes, the use of a protic solvent is possible, O'Regan and Schwartz[38] using ethanol in combination with cyanine dyes.

7. Ionic liquids

In order to gain long-term stability, by obtaining non volatile electrolyte solvents, ionic liquids were tested. The first ionic liquids have been tested by Grätzel et al.[39], and were imidazolium derivatives, molten at room temperature. The DSSC obtained presented good photoelectrochemical performance and stability. The mechanism in which this ionic liquids present high conductivity was verified to be Grotthus[40] - type electron exchange (at higher iodine concentrations used to compensate for mass transport limitations due to the viscous nature of the environment). (see Figure I-6) The ionic properties depend both on the organic cations and anions.

$$I_3^- + I^- \rightarrow I^- – I_2 \cdots I^- \rightarrow I^- \cdots I_2 – I^- \rightarrow I^- + I_3^-$$

Figure I-6 Representation of Grotthus-type carrier mechanism for I_2

[36] K. Hara, T. Horiguchi, T. Kinoshita, K. Sayama and H. Arakawa, *Solar Energy Materials and Solar Cells,* **2001,** *70*, 151-161.
[37] J. Wu, Z. Lan, J. Lin, M. Huang and P. Li, *J. Power Sources,* **2007,** *173*, 585-591.
[38] B. O'Regan and D. T. Schwartz, *Chemistry of Materials,* **1995,** *7*, 1349-1354.
[39] N. Papageorgiou, Y. Athanassov, M. Armand, P. Bonhote, H. Pettersson, A. Azam and M. Gratzel, *J. Electrochem. Soc.,* **1996,** *143*, 3099-3108.
[40] S. Cukierman, *Biochimica et Biophysica Acta (BBA) - Bioenergetics,* **2006,** *1757*, 876-885.

A recent review by Gorlov and Kloo [41] divided the liquid electrolytes into two sections, pure ionic liquids and quasi-solid electrolytes based on ionic liquids. Imidazolium-based electrolytes dominate the area. In conclusion, they stated, that photochemical stability and low viscosity-and thus ion mobility remains a challenge. Another conclusion is that the different components in the DSSC need to be specifically adapted to new electrolyte classes, and new sensitizing dyes need to be designed. In this direction, Grätzel et al. obtained an efficiency of 7.2% for an indoline dye and an ionic liquid based electrolyte[42]. An important development towards optimizing the use of ionic liquids was the use of eutectic mixtures in order to reduce melting points and in this way to reduce mass transport limitations. This approach was highly successful resulting in cells with performances over 8%.[43] In introduction of nanotubes of titania has been investigated in order to increase charge transport. In conclusion, the current two strategies to overcome the mass transport problems in ionic liquid electrolytes are: to use eutectic multicomponent melts in order to lower melting points and minimize internal melt structures affecting viscosity and ion mobility or to include solid components to enhance the conductivity.

8. Gel and polymer electrolytes

Another approach to increase the long term stability of the solar cells is to use gels, polymers or dispersion of polymeric materials obtained using electrolytes base on organic solvents and ionic liquids. The inclusion of gelating or polymeric materials results in the obtaining of quasi-solid electrolytes. [44] This approach is different from the hole conductors through the fact that the redox mediator is included and that the charge transport occurs generally by diffusion of molecules instead of hoping of charge. When a large concentration of iodine is added, a Grotthus mechanism of charge conduction can occur in gelated media, as suggested by the data presented by Kubo et al. [45], supporting the formation of polyiodides. However, a recent study, suggests that the Grotthus mechanism may be overestimated by neglecting the possible impact of ion association. [46]

[41] M. Gorlov and L. Kloo, *Dalton Transactions,* **2008**, 2655-2666.
[42] D. Kuang, S. Uchida, R. Humphry-Baker, S. M. Zakeeruddin and M. Grätzel, *Angew. Chem.,* **2008,** *120*, 1949-1953.
[43] Y. Bai, Y. Cao, J. Zhang, M. Wang, R. Li, P. Wang, S. M. Zakeeruddin and M. Gratzel, *Nat Mater,* **2008,** *7*, 626-630.
[44] W. Kubo, K. Murakoshi, T. Kitamura, Y. Wada, K. Hanabusa, H. Shirai and S. Yanagida, *Chem. Lett.,* **1998,** *27*, 1241-1242.
[45] W. Kubo, K. Murakoshi, T. Kitamura, S. Yoshida, M. Haruki, K. Hanabusa, H. Shirai, Y. Wada and S. Yanagida, *The Journal of Physical Chemistry B,* **2001,** *105*, 12809-12815.
[46] F. Call and N. A. Stolwijk, *The Journal of Physical Chemistry Letters,* **2010,** *1*, 2088-2093.

Typically, these quasi-solid electrolytes show conversion efficiencies that are slightly lower than that of the host liquid redox electrolyte. This effect may be attributed to limitations in the mobility of the redox couple components within the quasi-solid electrolyte.

A large portion of the gelated electrolytes is made up of more or less complex composites: various pure (of different molecular weight), mixed, and composite electrolytes involving nanocomposites with silica, titania, and many other inorganic additives. The molecular weight was proven to influence conductivity and photochemical properties and suggest the existence of an optimal chain length.[47] Recent developments include complex and multicomponent systems such as quasi-solid systems composed of polymer, oligomers and nonofiller resulting in a boost of efficiency (≈7.2%)[48].

Nogoeira et al[49] reported the use of a solid polymer, poly(epichlorohydrin-co-ethylene oxide) (Epichloromer), containing NaI and I_2 and traces of solvent to obtain solar efficiency of 2.6%, due to the reduced crystallinity of the polymer chains. Better results for solvent-free polymers were obtained using polymer electrolytes comprised of poly(vinyl pyridine) iodides, efficiencies reaching up to 5.6%.[50]

Plastic molecular crystals have been utilized as electrolytes in battery and fuel cell and have also been successfully in DSSC. They are compounds in which the molecules or ions exhibit rotational disorder, while their centers of mass occupy ordered sites in the crystalline lattice structure. An electrolyte based on succinonitrile doped with N-methyl-N-butylpyrrolidinium iodide and iodine, gave good results in DSSC, resulting in efficiencies of 5%.[51]

The work on gel electrolytes with uses in DSSC could not benefit of the extensive for done on the subject with uses in lithium ion batteries. The addition of acrylic monomers (gelators) and radical initiators in liquid electrolytes followed by cross-linking is the most convenient method to obtain gel electrolyte. This method could not be applied in DSSC because the iodine inhibited the cross-linking reactions. The following conditions are imposed in order to obtain gels for use in DSSCs[52]:

- polymerization must occur in the presence of iodine
- polymerization must occur at a temperature below which the dye would not decompose

[47] Z. Lan, J. Wu, J. Lin, M. Huang, S. Yin and T. Sato, *Electrochim. Acta,* **2007,** *52*, 6673-6678.
[48] M.-S. Kang, K.-S. Ahn and J.-W. Lee, *J. Power Sources,* **2008,** *180*, 896-901.
[49] A. F. Nogueira, J. R. Durrant and M. A. De Paoli, *Advanced Materials,* **2001,** *13*, 826-830.
[50] J. Wu, S. Hao, Z. Lan, J. Lin, M. Huang, Y. Huang, P. Li, S. Yin and T. Sato, *Journal of the American Chemical Society,* **2008,** *130*, 11568-11569.
[51] P. Wang, Q. Dai, S. M. Zakeeruddin, M. Forsyth, D. R. MacFarlane and M. Grätzel, ibid. **2004,** *126*, 13590-13591.
[52] S. Murai, S. Mikoshiba, H. Sumino and S. Hayase, *Journal of Photochemistry and Photobiology A: Chemistry,* **2002,** *148*, 33-39.

- polymerization should initiate and complete even under some impurities such as oxygen, water, ions and others
- polymerization has to be completed without generating byproducts that could decrease the photovoltaic performance
- polymerization must proceed without an initiator because the resultant decomposition products of the initiator may decrease the photovoltaic performance

In the past years, many gel polymer systems have been employed. Some examples are: amino acid derivatives with phenyl or alkyl groups, poly(ethylene oxide) modified with cross-linkable groups (Figure I-7 Structures of some gel polymer precursors).[53] An interesting alternative is to use polysaccharides as electrolyte solidifiers.[54]

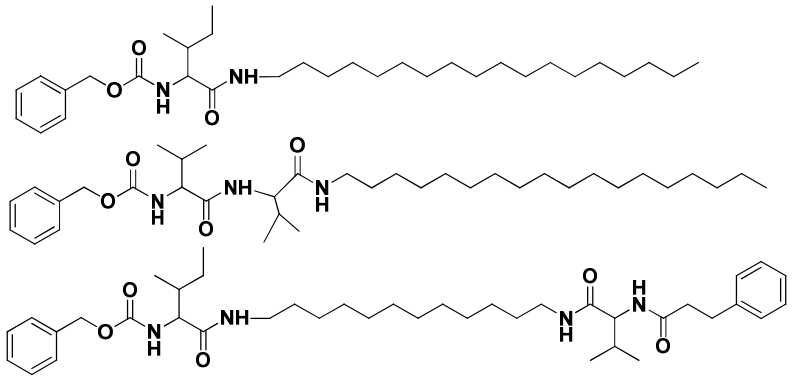

Amino acid gelators

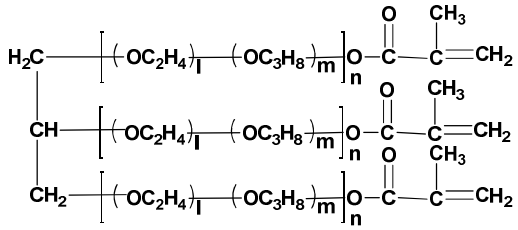

Poly(ethylene oxide-co-propylene oxide) trimethacrylate oligomer

Figure I-7 Structures of some gel polymer precursors

Complex systems of quaternary ammonium functionalized polymers involving poly(ethylene oxide) and other functional groups have been employed as conducting electrolytes.[55,56]

[53] B. Li, L. Wang, B. Kang, P. Wang and Y. Qiu, *Solar Energy Materials and Solar Cells,* **2006,** *90*, 549-573.
[54] J. Nemoto, M. Sakata, T. Hoshi, H. Ueno and M. Kaneko, *J. Electroanal. Chem.,* **2007,** *599*, 23-30.
[55] J. Kang, W. Li, X. Wang, Y. Lin, X. Xiao and S. Fang, *Electrochim. Acta,* **2003,** *48*, 2487-2491.
[56] J. Kang, W. Li, X. Wang, Y. Lin, X. Li, X. Xiao and S. Fang, *J. Appl. Electrochem.,* **2004,** *34*, 301-304.

9. Redox couples

Although I^-/I_3^- has been demonstrated as the most efficient redox couple for regeneration the oxidized dye, its severe corrosion for many sealing materials, especially metals[57], causes a difficult assembling and sealing for large scale DSSCs and poor long-term stability. Therefore, other redox couples such as Br^-/Br_2 [58], $SCN^-/(SCN)_2$, $SeCN^-/(SeCN)_2$ were investigated. But, due to their energy unmatchable with the sensitizer or their intrinsic low diffusion coefficients in electrolyte, the utilization of these redox couples resulted in DSSCs with lower efficiency than with I^-/I_3^-. Another direction was to use transition metal based systems, like bypiridine cobalt (III/II) complexes[59].

In a recent paper, Rowley et al.[60], discuss the redox chemistry, and photochemistry of iodine and its implication in DSSC. They focus on the making and breaking of I-I bonds and the importance in obtaining high-efficiency solar cells, an important role in the success of this redox couple being its photochemistry.

Many iodide salts have been tested in liquid electrolyte DSSCs. In aprotic solvents, the position of the TiO_2 conduction band edge depends on the type and the concentration of cations in the electrolyte. It was found that Li^+ and Mg^{2+} bind specifically onto the mesoporous TiO_2 electrode and in this way modifying the conduction band position. [61] Liu et al. found that V_{oc} of DSSC increases as function of cation in the order: $Li^+ < Na^+ < K^+ < Rb^+ < Cs^+$. [62] In a study of the effects of monovalent to trivalent maingroup iodides on solar cell performance, it was found that the higher the cation charge density, the larger effects on photoelectrochemical properties were observed caused by the expected band shifts and recombination losses.[63] Beside the modification of the conduction band edge, adsorption of cations onto the TiO_2 surface affects the local iodide concentration, as was demonstrated by Pelet et al. [64] The higher the effective charge of the cation, the stronger the positive effects for dye regeneration. The concentration of lithium cations in the electrolyte was shown to significantly affect the electron transport in the titania film, suggesting ambipolar diffusion.[65]

[57] M. Toivola, F. Ahlskog and P. Lund, *Solar Energy Materials and Solar Cells,* **2006,** *90*, 2881-2893.
[58] Z.-S. Wang, K. Sayama and H. Sugihara, *The Journal of Physical Chemistry B,* **2005,** *109*, 22449-22455.
[59] H. Nusbaumer, J.-E. Moser, S. M. Zakeeruddin, M. K. Nazeeruddin and M. Grätzel, ibid. **2001,** *105*, 10461-10464.
[60] J. G. Rowley, B. H. Farnum, S. Ardo and G. J. Meyer, *The Journal of Physical Chemistry Letters,* **2010,** *1*, 3132-3140.
[61] G. Redmond and D. Fitzmaurice, *The Journal of Physical Chemistry,* **1993,** *97*, 1426-1430.
[62] Y. Liu, A. Hagfeldt, X.-R. Xiao and S.-E. Lindquist, *Solar Energy Materials and Solar Cells,* **1998,** *55*, 267-281.
[63] H. Wang, J. Bell, J. Desilvestro, M. Bertoz and G. Evans, *The Journal of Physical Chemistry C,* **2007,** *111*, 15125-15131.
[64] S. Pelet, J.-E. Moser and M. Grätzel, *The Journal of Physical Chemistry B,* **2000,** *104*, 1791-1795.
[65] S. Nakade, S. Kambe, T. Kitamura, Y. Wada and S. Yanagida, ibid. **2001,** *105*, 9150-9152.

10. Hole conductors

An alternative to liquid electrolyte, in order to obtain long-term stability, is represented by solid state hole conductors. Several aspects are essential for any p-type semiconductor in a DSSC[66]:

- it must be able to transfer holes from the sensitizing dye after the dye has injected electrons into the TiO_2 conduction band; this means the upper edge of the valence band of p-type semiconductors must be located above the ground state of the dye;
- it must be able to be deposited within the porous nanocrystalline layer;
- the deposition of the p-type semiconductors must be done without dissolving or degrading the monolayer of dye on TiO_2 layer;
- it must be transparent in the visible spectrum, of, if it absorbs light, it must be as efficient in electron injection as the dye.

Many inorganic p-type semiconductors satisfy several of the above demands, however, the well known, large-gap p-semiconductors such as SiC and GaN, due to the high-temperature deposition, are not suited for application in DSSC. The solutions found after extensive testing were copper based p-semiconductors, like CuI, CuBr or CuSCN, which satisfy all the requirements. These materials can be casted from solution of vacuum deposited to form the hole-conductive layer, CuI and CuSCN presenting good conductivity in excess of 10^{-2} $S \cdot cm^{-1}$, which assists their hole conductive properties.

The first solid-state DSSC using CuI was obtained by Tennakone et al. in 1995[12]. The short-circuit was about 1.5-2.0 mA cm^{-2} in sunlight (about 800 W m^{-2}), a record for solid-state DSSC at that time. The solar cell has been improved by replacing the sensitizer with a Ru-bipyridyl complex and using as n-type semiconductor a film comprised of zinc and tin(IV) oxide, resulting in an efficiency of 2.4%.[67] However, the photodegradation appears to be a larger problem than it is in liquid cells. One of the reasons responsible for the degradation is that CuI tends to be oxidized under continuous illumination.[68]

One alternative to using CuI is employing CuSCN, which does not decompose to SCN^- an there is no indication that stoichiometrically excessive SCN^- creates surface traps in CuSCN. This is consistent with the observation that solid-state DSSC based on CuSCN have more stable performance.[69] Despite the extensive testing, the performance of cells using

[66] G. P. Smestad, S. Spiekermann, J. Kowalik, C. D. Grant, A. M. Schwartzberg, J. Zhang, L. M. Tolbert and E. Moons, *Solar Energy Materials and Solar Cells,* **2003,** *76*, 85-105.
[67] K. Tennakone and et al., *Journal of Physics D: Applied Physics,* **1999,** *32*, 374.
[68] G. R. A. Kumara, S. Kaneko, M. Okuya and K. Tennakone, *Langmuir,* **2002,** *18*, 10493-10495.
[69] V. P. S. Perera and K. Tennakone, *Solar Energy Materials and Solar Cells,* **2003,** *79*, 249-255.

CuSCN is still lower than of cells with CuI, probably due to the relatively lower hole conductance.

Inorganic semiconductors other than Cu complexes include NiO. This was first used in DSSC, in 2005, by Barbara et al.[70] NiO was prepared by dipping TiO_2 electrodes in $NiSO_4$ solution for 3 h, and then sintered at 400°C for 30 min. In this type of solid-state DSSC, dye was adsorbed on the surface of the NiO-coated TiO_2 film and charge carriers were transported to different layers by tunneling. The current of this kind of DSSC was 0.15 mA and voltage 480 mV, not as high as DSSC utilizing Cu complexes. However, the described method allows the fabrication of a very stable DSSC.

11. Organic hole conductors

Organic p-type semiconductors present the advantages of having great diversity, easy film formation and low cost. This type of materials has been widely used in organic solar cells, organic thin film transistors and organic light-emitting diodes.

In organic hole conductors, positive charge moves by a hoping mechanism between neighboring molecules, as opposed to redox electrolytes where charge transport is due to movement of redox molecules. The hole conductors usually contain additives, salts, allowing some ionic conductivity. Organic hole conductors used in DSSC can be divided in two classes, conducting polymes and molecular hole conductors.

12. Polymers as semiconductors

The conducting polymers and the ability to dope these polymers over the full range from insulator to metal, has been discovered in 1976 by Nobel laureates Alan MacDiarmid, Hideki Shirakawa and Alan J. Heejer.[71,72] Their discovery was at the boundary between chemistry and condensed-matter physics, and led to a great number of possibilities.

[70] J. Bandara and H. Weerasinghe, ibid. **2005,** *85*, 385-390.
[71] C. K. Chiang, C. R. Fincher, Y. W. Park, A. J. Heeger, H. Shirakawa, E. J. Louis, S. C. Gau and A. G. MacDiarmid, *Physical Review Letters,* **1977,** *39*, 1098.
[72] H. Shirakawa, E. J. Louis, A. G. MacDiarmid, C. K. Chiang and A. J. Heeger, *J. Chem. Soc., Chem. Commun.,* **1977**, 578-580.

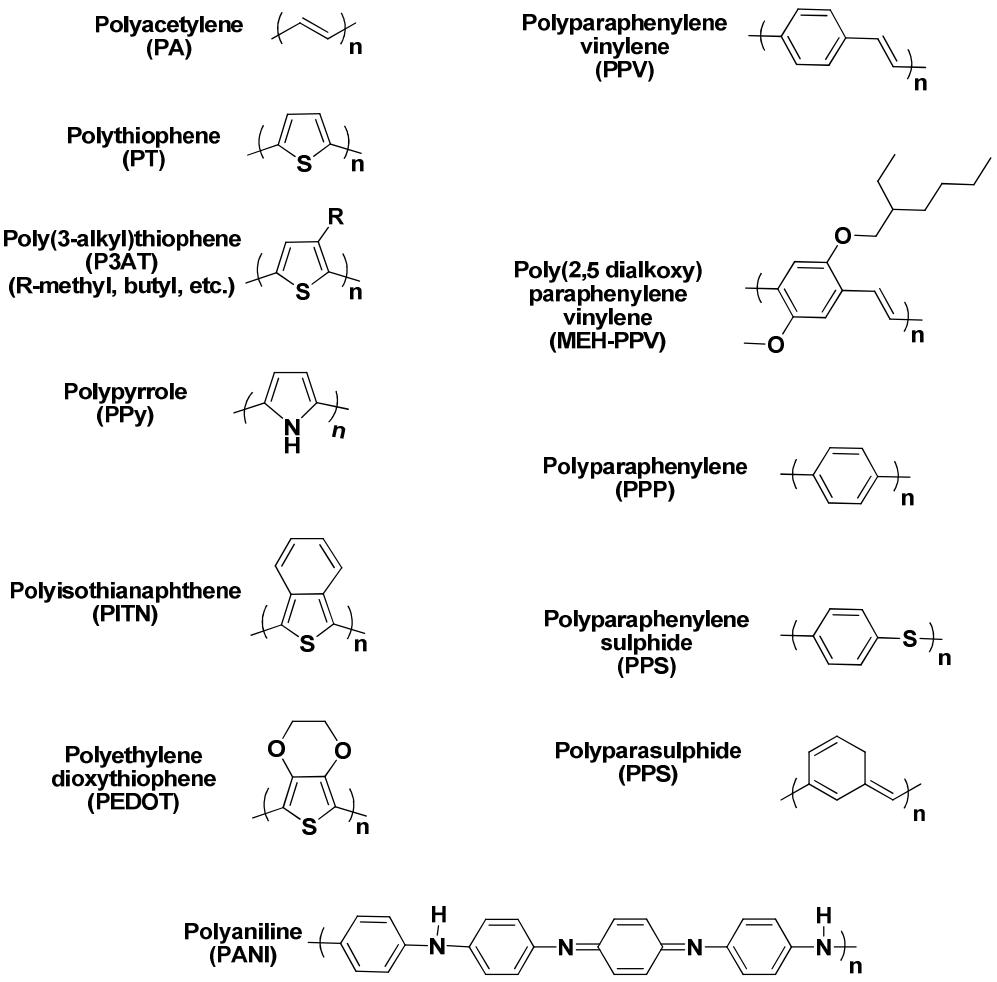

Figure I-8 Molecular structures of examples of conjugated polymers

Reversible "doping" of conducting polymers, with associated control of the dielectrical conductivity over the full range from insulator to metal, can be accomplished either by chemical doping or electrochemical doping. Concurrent with the doping, the electrochemical potential (Fermi level) is moved either by redox reaction or an acid-base reaction into a region of energy where there is a high density of electronic states. The charge neutrality is maintained by introduction of counterions. Metallic polymers are, therefore, salts. The electrical conductivity results from the existence of charge carriers (through doping) and from the ability of those carriers to move along the π-bonded "highway". Consequently, doped conjugated polymers are good conductors for two reasons:

- doping introduces carriers into the electronic structure. Since every repeat unit is a potential redox site, conjugated polymers can be doped n type (reduced) or p type (oxidized) to a relatively high density of charge carriers.

- the attraction of an electron is one repeat unit to the nuclei in the neighboring units leads to carrier delocalization along the polymer chain and to charge-carrier mobility, which is extended into three dimensions through interchain electron transfer.

Examples of **chemical doping** by charge transfer:

-p type:

$$(\pi - polymer)_n + \frac{3}{2}ny(I_2) \rightarrow (((\pi - polymer)^{+y}(I_3^-)_y)_n$$

-n type

$$(\pi - polymer)_n + (Na^+(C_{10}H_8)^*)_y \rightarrow ((Na^+)_y(\pi - polymer)^{-y})_n + (C_{10}H_8)^0$$

In **electrochemical doping**, the electrode supplies the redox charge to the conducting polymer, while ions diffuse into (or out of) the polymers structure from the nearby electrolyte to compensate the electronic charge. The doping level is determined by the voltage between the conducting polymer and the counterelectrode. At equilibrium, the doping level is perfectly controlled by the voltage. This permits any level of doping to be achieved by controlling the setting of the electrochemical cell.

-p type:

$$(\pi - polymer)_n + (Li^+(BF_4^-))_{solution} \rightarrow ((\pi - polymer)^{+y}(BF_4^-)_y)_n + Li_{electrode}$$

-n type

$$(\pi - polymer)_n + Li_{electrode} \rightarrow (Li^+(\pi - polymer)^{-y})_n + (Li^+(BF_4^-))_{solution}$$

Polyaniline provides the protypical example of a chemically distinct doping mechanism, **doping by acid-base chemistry**[73]. This leads to an internal redox reaction and conversion from semiconductor (the emeraldine base) to metal (the emeraldine salt) (see Figure I-9). The chemical structure of semiconducting emeraldine base (EB) is of an alternative copolymer. Upon protonation of the emeraldine base to the emeraldine salt, the proton induced spin unpairing mechanism leads to a structural change with one unpaired spin per repeating unit, but with no change in the number of electrons. The result is half filled band and, potentially, a metallic state in which there is a positive charge in each repeating unit and an associated counterion (Cl^-, HSO_4^- etc.).

[73] S. Stafström, J. L. Brédas, A. J. Epstein, H. S. Woo, D. B. Tanner, W. S. Huang and A. G. MacDiarmid, *Physical Review Letters,* **1987,** *59*, 1464.

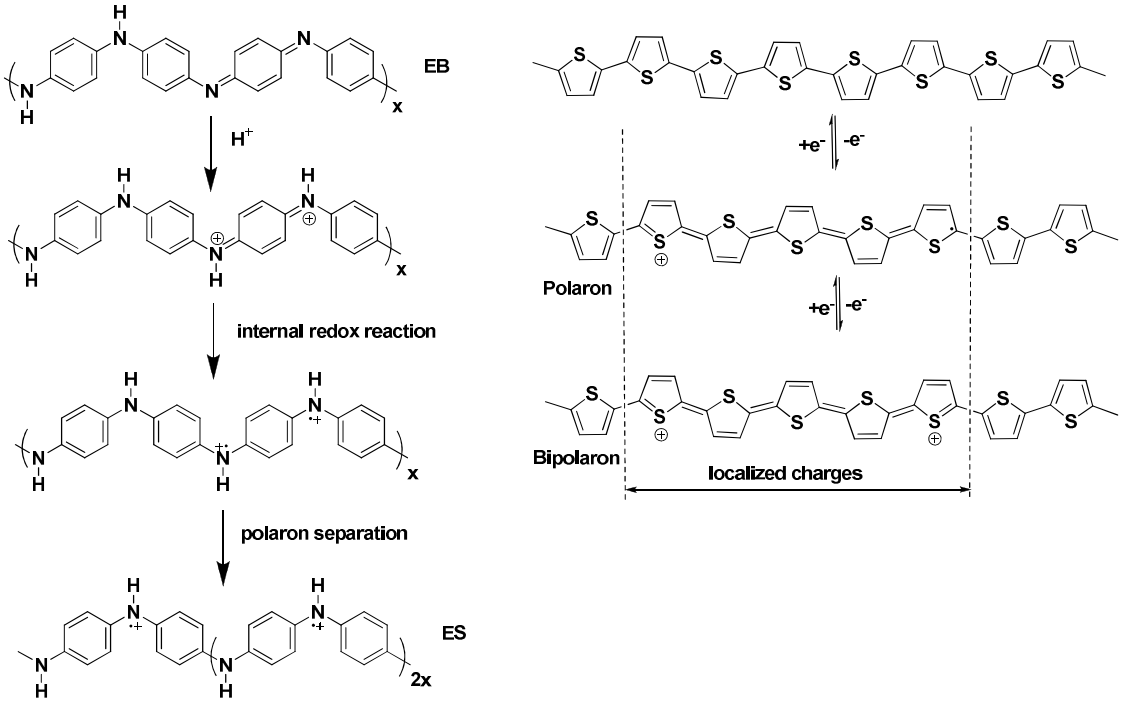

Figure I-9 Proton induced doping in polyaniline; formation of bipolarons and polarons (the counterion is not presented) and thiophene doping and polaron state.

The polarons and bipolarons are positive or negative charges associated with local deformation of a polymer chain that is changing from the aromatic form to a quinoid form. Polarons are delocalized over a few units and exibit spin-charge relations that differ from those of solitons, as they are simultaneously charge ($q=\pm e$) and spin carriers ($S=^1/_2$). The displacement (coherent or by hopping) of polarons along or between macromolecules contributes to the bulk electronic transport of the material. By removing (or adding) another electron to the existing polaron, a new species, a bipolaron is created. In bipolarons, the two charges are adapted in the same local deformation of the chain. A bipolaron is in effect a dication that has zero spin. (Figure I-9).

Although, well known, the processing advantages of polymers, in the case of conducting polymers of this nature, proved very difficult to be obtained. So, even in 1990, there were no known examples of stable metallic polymers which could be processed in their metallic form. This major problem was first solved with polyaniline, PANI. By using functionalized protonic acids to convert the polymer to the metallic form, simultaneously, the resulting PANI complex was rendered soluble in common organic solvents.[74] The functionalized counterion acts like a "surfactant" in that the charged head is ionically bound to the oppositely charged protonated PANI chain, and the "tail" is chosen to be compatible

[74] Y. Cao, P. Smith and A. J. Heeger, *Synthetic Metals,* **1992,** *48*, 91-97.

with nonpolar or weakly polar organic liquids (in the case of solutions) or host polymer (in the case of blends) with a variety of host polymers. This enhanced processibility induced by the counterion has made possible the fabrication of various materials with conducting properties.

The first report of conducting polymers used in DSSC was in 1997, by Murakoshi et al., who utilized polypyrrole doped with $LiClO_4$ in order to obtain an efficiency of 0.1%[75]. They fabricated the polymer film by electropolymerization in situ in the pores of the TiO_2 layer.

The most important requirement for a conducting polymer, to be used in DSSC as a hole transporting materials, is represented by its wetability, the ability of the polymer solution to infiltrate in the pores of the dye covered TiO_2 layer. This ability must allow a good contact with the absorbed dye.

Pioneering work on the use of conducting polymers as hole transporting materials in DSSC has been realized by Gebeyehu et al., using poly(3-octylthiophene) or a thiophene-isothianaphthelene-based copolymer, obtaining an efficiency of 0.16%.[76] The possibility to use poly(3-undecyl-2,2'-bithiophene) as a sensitizer has been studied by Grant et al.[77], concluding that the relative size of the sensitizer molecule and the pores of nanocrystalline films may be a critical factor to consider in designing photovoltaic devices such as solar cells based on nanoporous materials.

An interesting approach in the use of conducting polymers as hole transporting materials, is to obtain a multicomponent film, using a dual-function supramolecular conductor to allow molecular level control of the local chemical composition at the nanostructured inorganic/organic semiconductor heterojunction. For this approach Haque et al. developed lithium doped dual-functional hole transporting material. Their approach allows the tailoring of properties at the interface region.[78] The importance of the interface between the conducting polymer and the sensitizer has been studied by Zhu et al., demonstrating that by modifying the interface higher efficiencies can be obtained.[79]

One of the most intense studied hole conducting polymers is poly(3,4-ethylenedioxythiophene) (PEDOT). Important work involving this polymer has been realized

[75] K. Murakoshi, R. Kogure, Y. Wada and S. Yanagida, *Chem. Lett.,* **1997,** *26*, 471-472.
[76] D. Gebeyehu, C. J. Brabec, N. S. Sariciftci, D. Vangeneugden, R. Kiebooms, D. Vanderzande, F. Kienberger and H. Schindler, *Synthetic Metals,* **2001,** *125*, 279-287.
[77] C. D. Grant, A. M. Schwartzberg, G. P. Smestad, J. Kowalik, L. M. Tolbert and J. Z. Zhang, *J. Electroanal. Chem.,* **2002,** *522*, 40-48.
[78] S. A. Haque, T. Park, C. Xu, S. Koops, N. Schulte, R. J. Potter, A. B. Holmes and J. R. Durrant, *Advanced Functional Materials,* **2004,** *14*, 435-440.
[79] R. Zhu, C.-Y. Jiang, B. Liu and S. Ramakrishna, *Advanced Materials,* **2009,** *21*, 994-1000.

by Yanagida et al. [80]. The influence of the doping anions on cell efficiency was also studied.[81] An alternative to solution processing and film formation is to obtain the polymer by polymerization in situ. In a recent article, Liu et al. used in situ polymerization of bis-EDOT and D149 dye sensitized to obtain a DSSC with an average efficiency of 6.1%.[82] The authors underline the importance in having a good polymer penetration in the TiO_2/sensitizer layer, and also importance of choosing the dye in relation with the polymer used.

Another, very recent, article used solid state polymerization of dibromo 3,4-ethylenedioxythiophene (DBEDOT) by heating at mild temperature[83]. The advance of this method is that the monomer is small enough to penetrate into the nanopores of the TiO_2 layer, improving the interface contact. They obtained a solid state DSSC with 5.4% efficiency, using N719 sensitizer.

Improvement of the interface between conducting polymer and the TiO_2/layer has been obtained, also, by modification of the polymeric chain with carboxy groups. Using this approach, Lee et al.[84] synthesized a copolymer poly(3-hexylthiophene)-co-(3-thiopheneacetic acid). They compared the obtained efficiencies with the use of poly(3-hexylthiophene), concluding that the improved efficiency is due to the better adsorption on TiO_2 layer.

Conducting polymers have also been used in more complex systems like composites. One of such examples is what Ikeda et al.[85] and Lee et al.[86] report. They obtain solid state DSSC using a PANI/carbon black/ionic liquid composite. The, I^-/I_3^-, redox system is generated using the ionic liquid iodide derivative without addition of I_2. The advantage of such systems is high stability and good reported efficiencies of 3-4%.

13. Molecular hole conductors

Triarylamine-based compounds, such as 2,2',7,7'-tetrakis (N,N-di-p-metoxy phenylamine)-9,9'-spirobifluorene (spiroMeOTAD), are the most popular molecular hole conductors in solid state DSSC. (see Figure I-10). Since the first report on this system in

[80] R. Senadeera, N. Fukuri, Y. Saito, T. Kitamura, Y. Wada and S. Yanagida, *Chemical Communications,* **2005**, 2259-2261.
[81] J. Xia, N. Masaki, M. Lira-Cantu, Y. Kim, K. Jiang and S. Yanagida, *Journal of the American Chemical Society,* **2008,** *130*, 1258-1263.
[82] X. Liu, W. Zhang, S. Uchida, L. Cai, B. Liu and S. Ramakrishna, *Advanced Materials,* **2010,** *22*, E150-E155.
[83] J. K. Koh, J. Kim, B. Kim, J. H. Kim and E. Kim, ibid. **2011,** *23*, 1641-1646.
[84] J.-K. Lee, W.-S. Kim, H.-J. Lee, W. S. Shin, S.-H. Jin, W.-K. Lee and M.-R. Kim, *Polym. Adv. Technol.,* **2006,** *17*, 709-714.
[85] N. Ikeda, K. Teshima and T. Miyasaka, *Chemical Communications,* **2006**, 1733-1735.
[86] C.-P. Lee, P.-Y. Chen, R. Vittal and K.-C. Ho, *Journal of Materials Chemistry,* **2010,** *20*, 2356-2361.

1998[87], the efficiencies obtained have been constantly increasing, the highest reported conversion being of 5%[88].

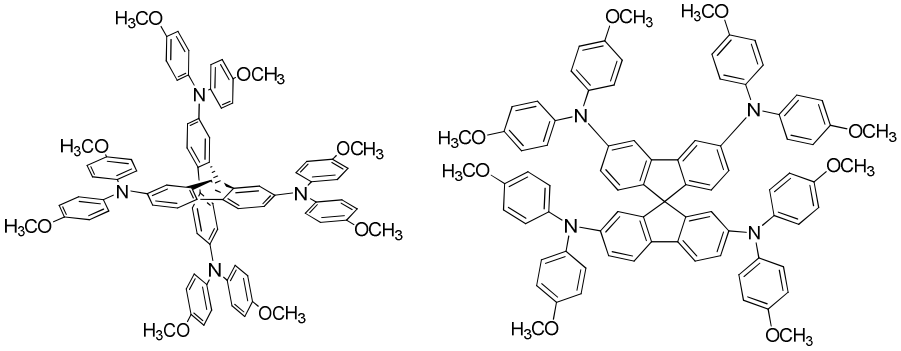

Figure I-10 Structure of spiro-bisfluorene triarylamine type hole conductor

The main advantage of this material is its high glass transition temperature of ca. 120°C. It forms amorphous layers, which are useful in complete pore filling.

14. Additives

Additives play an important role in the enhancement of photoelectrochemical performance of DSSC. Most additives are understood at a fairly phenomenological level, and their effects are often attributed to modification of redox couple potential, band shifts of the semiconducting material, effects of surface blocking, or surface dye organization. A first example of the use of additives is the introduction of 4-tert-butylpyridine, which resulted in a remarkable increase of V_{oc}, of the cells in combination with LiI-based electrolyte. The effect consists in the shifting of the TiO_2 band edge toward higher energy levels.[89] Thus upon adsorption on the TiO_2 surface the pyridine ring induces electron density into the TiO_2 creating a surface dipole. The band edge shifting reduces the driving force for electron injection and thus the I_{sc} is a bit lower than in untreated cells.

Another approach in decreasing the recombination rate in DSSC is the use of coadsorbers. They are added to the dye bath upon dye adsorption. Coadsorbers can occupy spaces between dye molecules and can help to avoid aggregation, which is a problem for many organic dyes. Usually they are added in a large concentration and bind weakly to the TiO_2 layer being replaced by the dye upon adsorption. Examples of this type of additives are the cholic acid derivatives.

[87] U. Bach, D. Lupo, P. Comte, J. E. Moser, F. Weissortel, J. Salbeck, H. Spreitzer and M. Gratzel, *Nature,* **1998,** *395*, 583-585.
[88] H. J. Snaith, A. J. Moule, C. Klein, K. Meerholz, R. H. Friend and M. Grätzel, *Nano Letters,* **2007,** *7*, 3372-3376.
[89] G. Schlichthörl, S. Y. Huang, J. Sprague and A. J. Frank, *The Journal of Physical Chemistry B,* **1997,** *101*, 8141-8155.

II. Hybrid dye sensitized solar cells (Original contribution)

This part of the chapter will present the objectives and results of the work on the DSSC subject. As it was presented in the first part of the chapter, polymers can be used in DSSC in order to replace the liquid electrolyte. Our main objective was to obtain solid state solar cells using polymers to replace the liquid electrolyte. Furthermore, strategies for improving the cell efficiency by using a dye with better anchoring capacity on the TiO_2 layer, and the use of quantum-dots particles for the increasing of the electron injection rate have been tested. The set up of the cell is presented in Figure I-11.

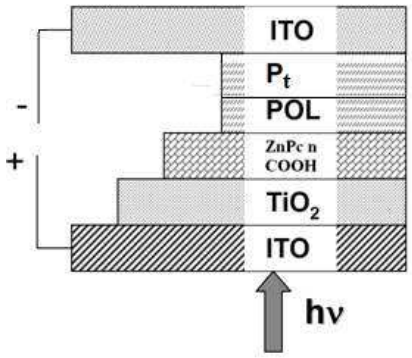

Figure I-11 Set up of the solar cell

In order to satisfy the main objective, it was necessary to obtain a working solar cell with a good reproducibility. The sensitizers chosen were based on carboxyphthalocyanines.

1. The nanoporous TiO_2 layer

Analyses were performed in order to determine the obtained TiO_2 layer characteristics. This include: crystallization (if the anatase form is kept during the sinterization), the thickness of the layer and its rugosity.

The XRD analysis of TiO_2 layer deposited on conductive glass (Figure I-12) confirms the crystallization form of anatase for TiO_2.

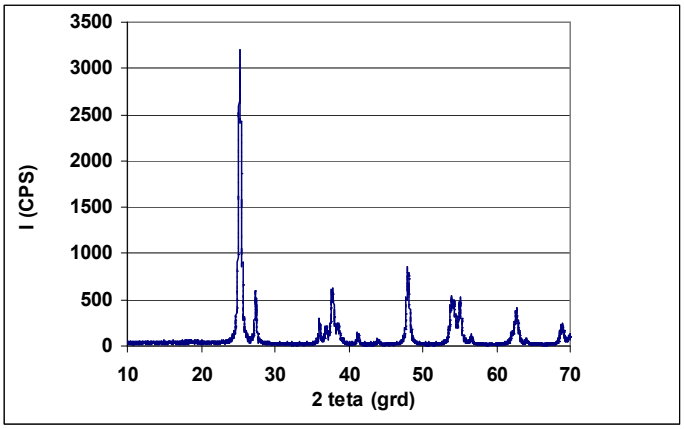

Figure I-12 XRD diagram for TiO_2-anatase

The SEM analysis of the TiO_2 layer (Figure I-13) deposited on the conductive glass shows the presence of nanoparticles with a size of 25 nm and the existence of agglomerates.

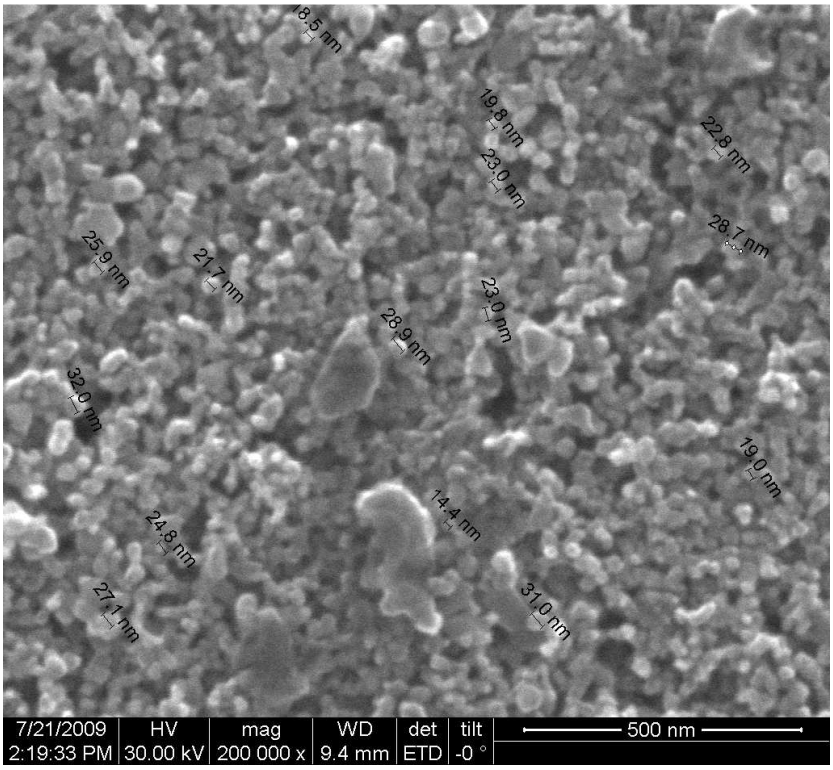

Figure I-13 SEM analysis of the TiO_2 layer, particle dimensions of 25 nm

AFM analysis allowed the observation of this agglomerates and also to the surface characteristics. The rugosity of the film is important as it influences the concentration of the adsorbed dye onto the semiconducting layer. (Figure I-14)

According to the literature[90], the thickness of the TiO_2 layer has a strong influence on the cell efficiency. SEM analysis of the transversal section allowed the evaluation of the layer thickness, the value being approximately 2.3µm (Figure I-15).

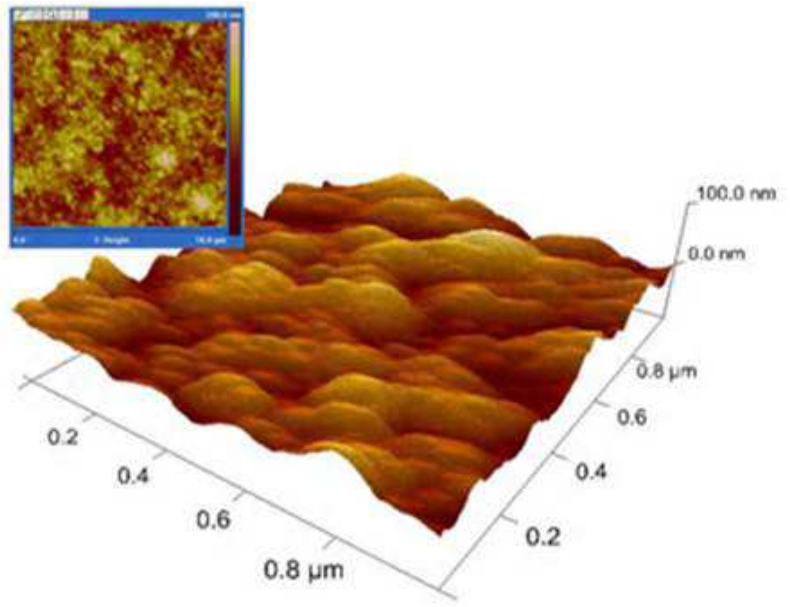

Figure I-14 AFM analysis of the TiO_2 layer showing the rugosity of the film

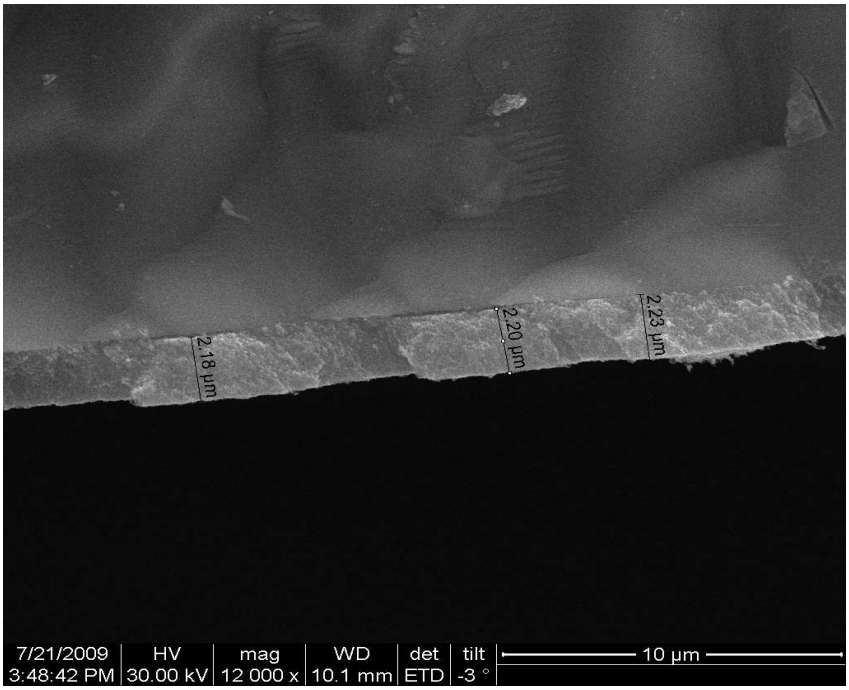

Figure I-15 SEM analysis of the transversal section for TiO2 layer

[90] C. J. Barbé, F. Arendse, P. Comte, M. Jirousek, F. Lenzmann, V. Shklover and M. Grätzel, *Journal of the American Ceramic Society,* **1997,** *80*, 3157-3171.

The method used for the obtaining of the 2.3μm thick TiO_2 layer proved to be facile reproducible. However, the thickness obtained is lower than the standard 10 μm utilized in general in DSSC. Thus, the quantity of adsorbed sensitizer is lower. The experiments for increasing this thickness proved to have, for the moment, lower reproducibility.

2. Dye synthesis and adsorption

The sensitizers chosen were based on carboxyphthalocyanine derivatives. Phthalocyanines possess intense absorption bands in the IR region and are known for their excellent stability. Depending on the substituents phthalocyanines present p- or n-semiconducting properties.[91] Zinc (II) phthalocyanines are used as photosensitizer in photo-oxidation[92] and in photodynamic therapy due to their capability to generate oxygen singlet species from their triplet energy state by energy transfer. Their semiconducting properties allowed the use of phthalocyanine derivatives in sensors.[93]

Due to the necessity of having anchoring groups, the phthalocyanines derivatives used possess carboxy groups. In order to see if an increased number of groups is beneficial for the attachment of the dye, octa and tetracarboxy substituted phthalocyanines were used.

The synthesis of the two chromophores is presented in Scheme I-5 and Scheme I-6. As catalyst $Mo_7(NH_4)_6O_{24}$ and DBU (1,8-diazabicyclo(5.4.0)undecene-7) were used. The starting materials were the trimellitic and the perimellitic anhydrides, which make the procedure cheaper than using the corresponding nitriles.

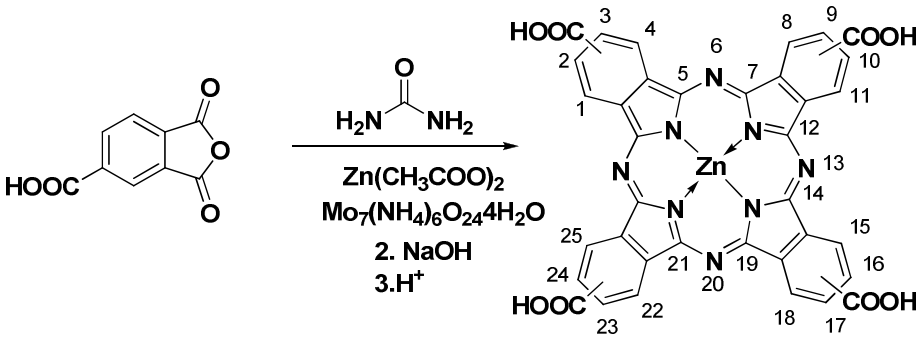

Scheme I-5 Reaction scheme for the synthesis of the 2,9,16,23-tetracarboxyphthalocyanine zinc (II)

[91] C. C. Leznoff; A. B. P. Lever, *Phthalocyanines: properties and applications*. VCH: 1996.
[92] G. Schneider, D. Wohrle, W. Spiller, J. Stark and G. Schulz-Ekloff, *Photochemistry and Photobiology,* **1994,** *60*, 333-342.
[93] C. Boscornea, L. Hinescu, C. Moldovan, S. Tomas and A. Diacon, *Proceedings of the 16th Romanian International Conference on Chemistry and Chemical Engineering RICCCE XVI 9-12 September 2009,* **2009**, S. VI.2-S.VI.11.

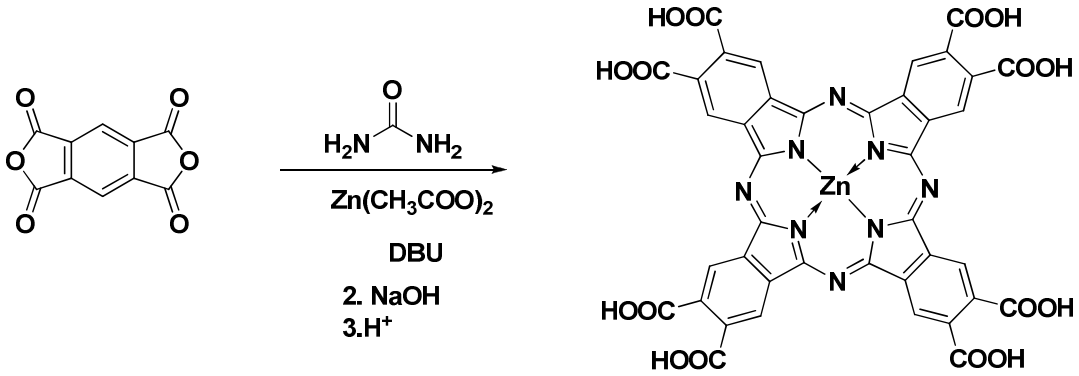

Scheme I-6 Synthesis scheme of 2,3,9,10,16,17,23,24-octacarboxyphthalocyanine zinc(II)

Firstly, the synthesized dyes have been characterized by FT-IR and UV-VIS spectroscopy. The following characteristic peaks (cm^{-1}) could be observed in FT-IR spectra: 3300 cm^{-1}(ν_{O-H}), 3103 cm^{-1}, 3078 cm^{-1}, 3042 cm^{-1} (ν_{C-H}), 1710 cm^{-1} ($\nu_{C=O}$), 1654 cm^{-1}, 1590 cm^{-1} (ν_{C-C}), 1484 cm^{-1}, 1446 cm^{-1}, 1284 cm^{-1}, 1173 cm^{-1} (δ_{C-O}), 1228 cm^{-1}, 1088 cm^{-1} (δ_{C-H}), 1004 cm^{-1}, 880 cm^{-1}, 770 cm^{-1}, 705 cm^{-1}, 570 cm^{-1}, 499 cm^{-1}, 435 cm^{-1}. The peaks observed are in according with the literature confirming the structures of the carboxylic derivatives of zinc phthalocyanine.

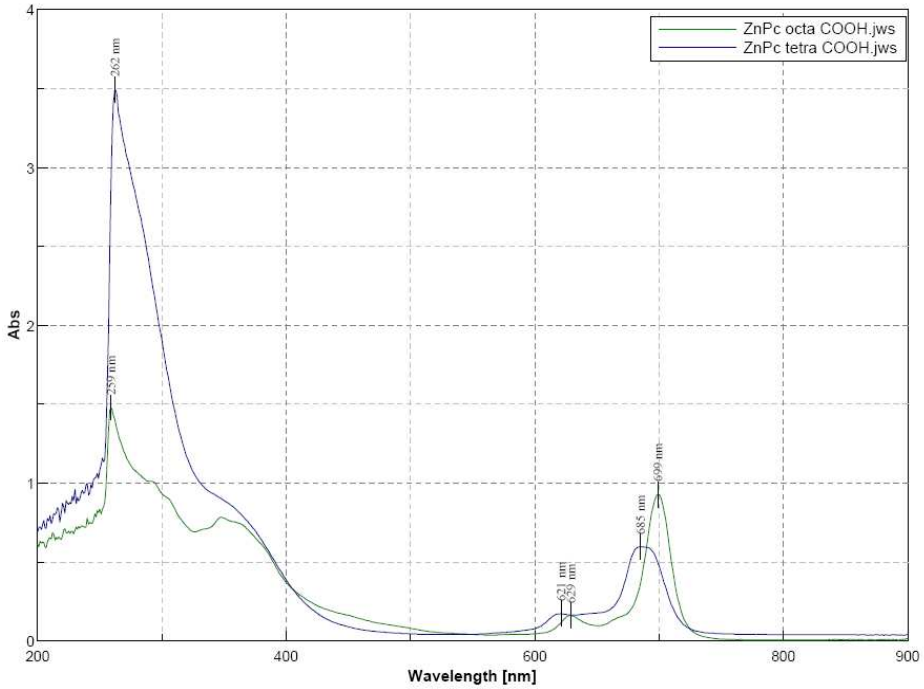

Figure I-16 UV-Vis spectra for the synthesized carboxyphthalocyanine derivatives in DMF

For further confirmation the UV-Vis spectra were also recorded (Figure I-16). A strong absorption in the UV region, the Soret band, is noticed for both phthalocyanines. The characteristic peaks of the phthalocyanines are 621 and 685 nm for

tetracarboxyphthalocyanine zinc (II), whereas 629 and 699 nm for octacarboxyphthalocyanine zinc (II). They represent the Q band, which is attributed to the allowed π-π* transition.

The reflectance of the films was measured and then it was converted into absorption to compare it with the spectra of the dyes in solution. UV-VIS spectra (Figure I-17) of the TiO_2 films with different dyes reveal a stronger absorption in the case of octacarboxy phthalocyanine due to its higher concentration on the TiO_2 layer. This behavior could be explained by the enhanced ability of this dye to anchor onto the TiO_2 layer with the carboxyl groups. Also, the absorption signal may be due to the presence of dye aggregates.

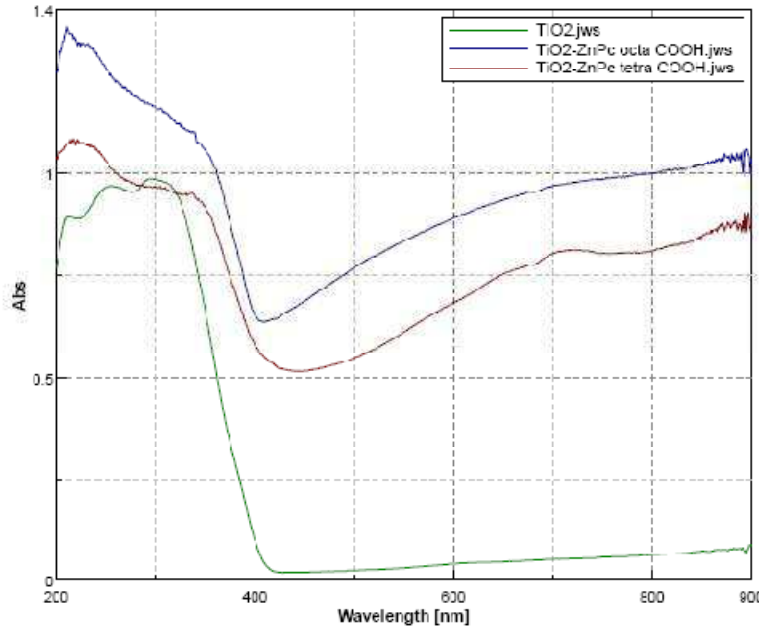

Figure I-17 UV-Vis spectra of dye adsorbed on TiO_2 film

The fluorescence of dyes activates the TiO_2 surface and enhances the electrons injection from the dye to the electrode.

The 3D fluorescence spectra for tetracarboxy phthalaocyanine zinc(II) (A) and octacarboxy phthalocyanine zinc(II) (B) (Figure I-18) presents the fluorescence emission intensity depending on the excitation wavelength. It can be concluded that the dyes have a high emission response for excitation wavelength over 650 nm. This characteristic allows the formation of excited state singlet that can transfer an electron in the conduction band of the TiO_2.

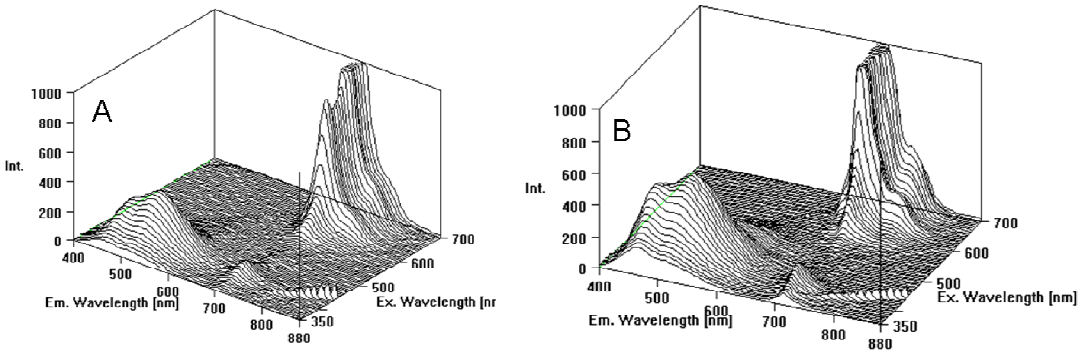

Figure I-18 3D Fluorescence spectra for: (A) tetracarboxy phthalaocyanine zinc(II) and (B) octacarboxy phthalocyanine zinc(II)

The adsorption of the dye onto the surface of the TiO_2 was also evaluated by SEM. It is well-known that the mode in which the dye is bound is crucial for obtaining good solar cell efficiency. Figure I-19 shows the selective adsorption of the dye on the conductive layer, the dark areas were found to present higher concentration of dye. This has been determined by measuring the nitrogen procentage using the EDAX probe. An explanation of this higher concentration is the existence of zones characterized by higher specific surfaces along TiO_2 layer (light and dark zones).

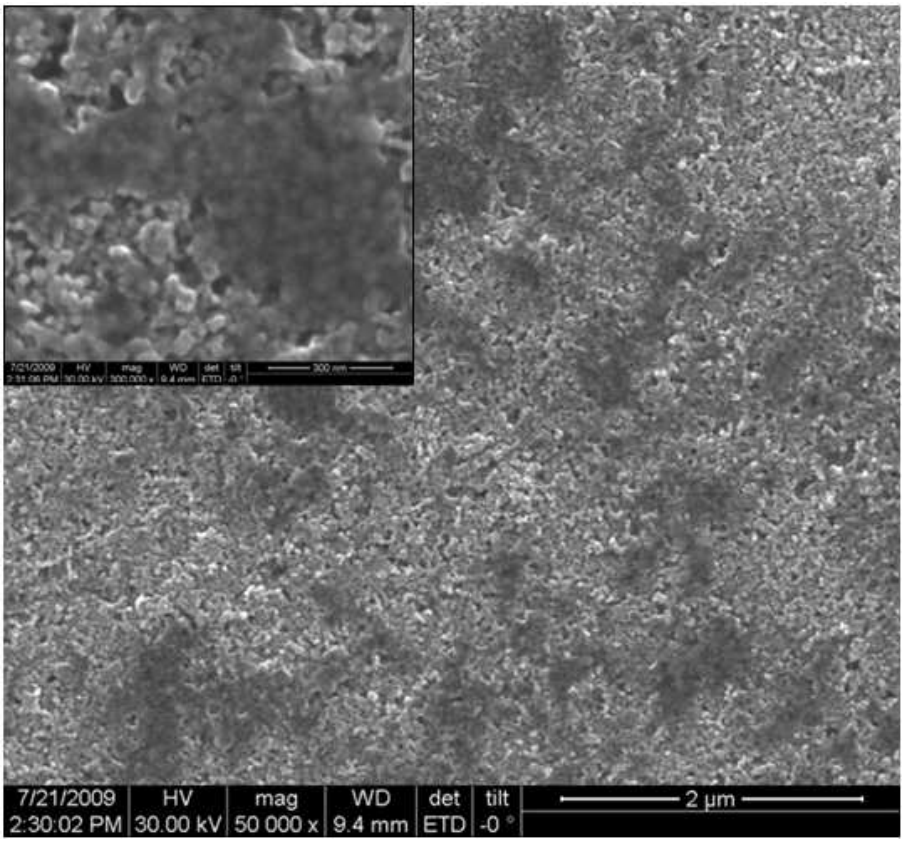

Figure I-19 SEM images of TiO_2 covered with dye

3. Polymer layer

The liquid electrolyte in DSSC represents a major drawback due to their volatility, sealing related problems and overall lifetime stability. As presented in the first part of the chapter there are different ways to address this problem such as the use of: ionic liquids, gel and polymers and hole conductive materials.

Thus, polymers were used to replace the liquid electrolyte. Two strategies were utilized in order to obtain solid-state DSSC. One is based on the use of hole conducting polymers obtained by chemical means and the other is the use of a high mobility polymer (a low Tg of the polymer) containing quaternary ammonium salts in the pending chain and iodine dispersed in the polymer matrix.

In parallel for both solutions the utilization of quantum dots as a co-sensitizer has been explored in order to increase the electron injection reactions.

A. Hole conducting polymers[94]

The conducting polymers chosen were polythiophene (PT) and polyaniline (PANI). Both polymers have been obtained by chemical methods. To enhance their conductivity several doping methods have been tested.

Polythiophene has been obtained by the well known method of chemical oxidation using $FeCl_3$ (Sugimoto and Yoshino) method. The method was proposed by Sugimoto and Yoshino in 1986.[95] They proposed oxidation of thiophene and 3-alkyl derivatives with transition metal salts. The most used is $FeCl_3$, but also can be used $MoCl_5$ or $RuCl_3$. The catalyst also serves as the doping agent in this synthesis.

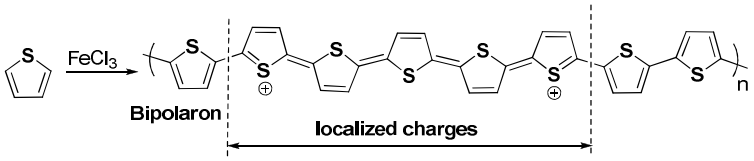

Scheme I-7 Polythiophene synthesis

The first mechanism was proposed by Niemi et. al[96], it was the radical type presented in Scheme I-8. They based their mechanism on the two suppositions:

[94] A. Diacon, E. Rusen, C. Boscornea, C. Zaharia and C. Cincu, *Journal of Optoelectronics and Advanced Materials,* **2010,** *12*, 199-204.
[95] R. D. McCullough, *Advanced Materials,* **1998,** *10*, 93-116.
[96] V. M. Niemi, P. Knuuttila, J. E. Österholm and J. Korvola, *Polymer,* **1992,** *33*, 1559-1562.

- the active sites of the polymerization are at the surface of the solid $FeCl_3$, this is based on the fact that the reaction takes place in solvents in which $FeCl_3$ is either partially or completely insoluble (like chloroform, toluene, carbon tetrachloride, pentane).
- they determined by quantum chemical calculation that the most negative carbon from 3-methylthiophene is carbon 2 and the carbon with the highest odd electron population is also carbon 2. By calculation the total energy of the species with radicals at the 2 or 5 carbons, determined that the second is more stable. Thus, the more stable radical could react with the neutral species resulting in head-to-tail bond formation.

The carbocation mechanism was proposed by Anderson et. al[97], who tried to explain the regioselectivity observed for the polymerization of 3-(4-octylpheyl)thiophene upon slow addition of $FeCl_3$. They concluded that due to the selectivity of couplings and the strong oxidizing conditions, the reaction could proceed by a carboncation mechanism.

The radical mechanism was questioned by the findings of Olinga and François[98] who presented the polymerization of thiophene in acetonitrile, a solvent in which $FeCl_3$ is soluble, contradicting the predictions of the radical polymerization mechanism.

The radical cation mechanism was proposed by Barbarella et al. [99]. They studied the regioselective oligomerization of 3-(alkylsulfanyl)thiophenes with $FeCl_3$. Using quantum mechanical calculations and consideration regarding enhanced stability of the radical cation when delocalized over planar conjugated oligomers they concluded that a radical cation mechanism was more likely to be responsible for the regioselectivity.

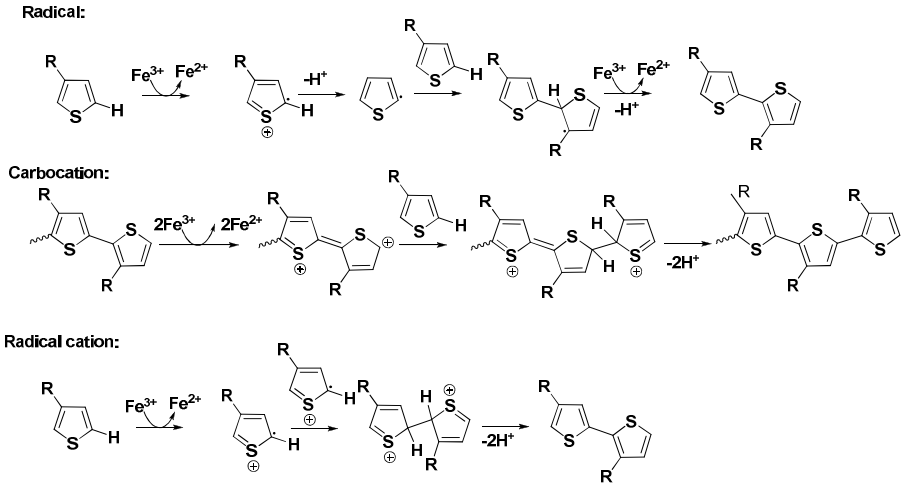

Scheme I-8 Proposed mechanism for the oxidative polymerization of thiophene with $FeCl_3$

[97] M. R. Andersson, D. Selse, M. Berggren, H. Jaervinen, T. Hjertberg, O. Inganaes, O. Wennerstroem and J. E. Oesterholm, *Macromolecules,* **1994,** *27*, 6503-6506.
[98] T. Olinga and B. François, *Synthetic Metals,* **1995,** *69*, 297-298.
[99] G. Barbarella, M. Zambianchi, R. Di Toro, M. Colonna, D. Iarossi, F. Goldoni and A. Bongini, *The Journal of Organic Chemistry,* **1996,** *61*, 8285-8292.

FT-IR spectrum of PT shows the signals at 3100 cm^{-1} characteristic to ν_{CH}, 1500 cm^{-1} specific to $\nu_{C=C}$ and 700 cm^{-1} specific to γ_{CH}. UV-Vis spectrum (Figure I-20) reveals peaks at 271 nm ($\pi \rightarrow \pi^*$ transition of the cyclopentadiene ring) and 297 nm ($n \rightarrow \pi^*$ transition of the un-paired electrons of the S atom).

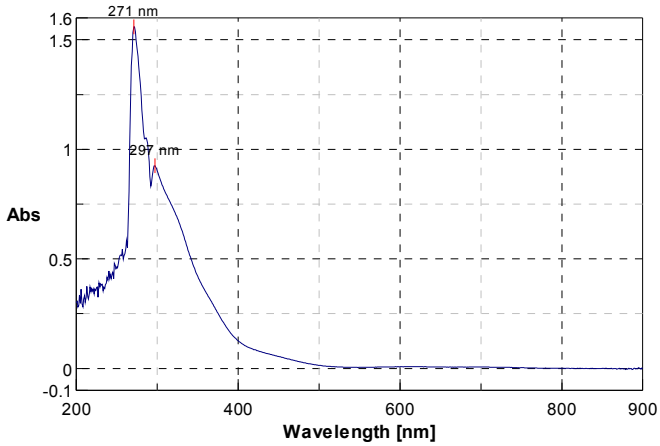

Figure I-20 UV-Vis spectrum of PT

PANI-ES was prepared by chemical oxidation of aniline with potassium persulfate in acid medium. (Scheme I-9).

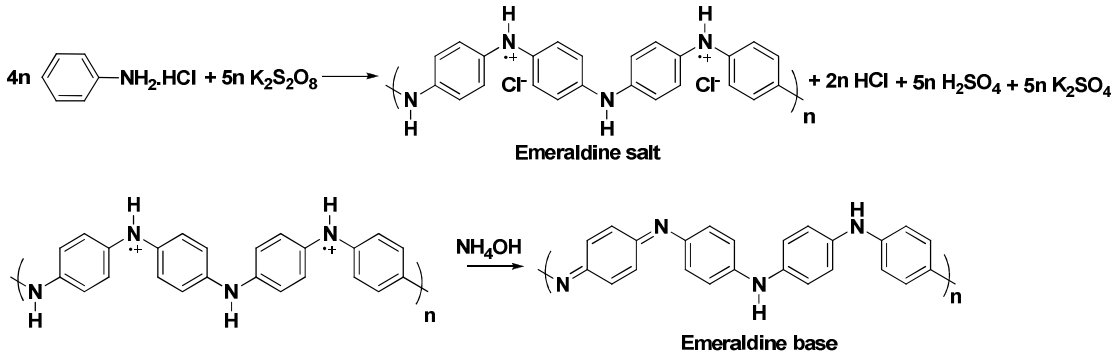

Scheme I-9 PANI synthesis

Polyaniline (PANI) exists in a variety of forms that differ in chemical and physical properties. The most common green protonated emeraldine has a conductivity on a semiconductor scale 10 $S \cdot cm^{-1}$, many orders of magnitude higher than of common polymers ($<10^{-9}$ $S \cdot cm^{-1}$) but lower that of typical metals ($>10^{4}$ $S \cdot cm^{-1}$).

As alternatives for doping agents the alternatives chosen consist in:

- Utilizing Poly (2-acrylamido 2-methylpropane sulfonic acid) - PAMPSA
- Self doping by using sulfonic acid groups on the polyaniline backbone

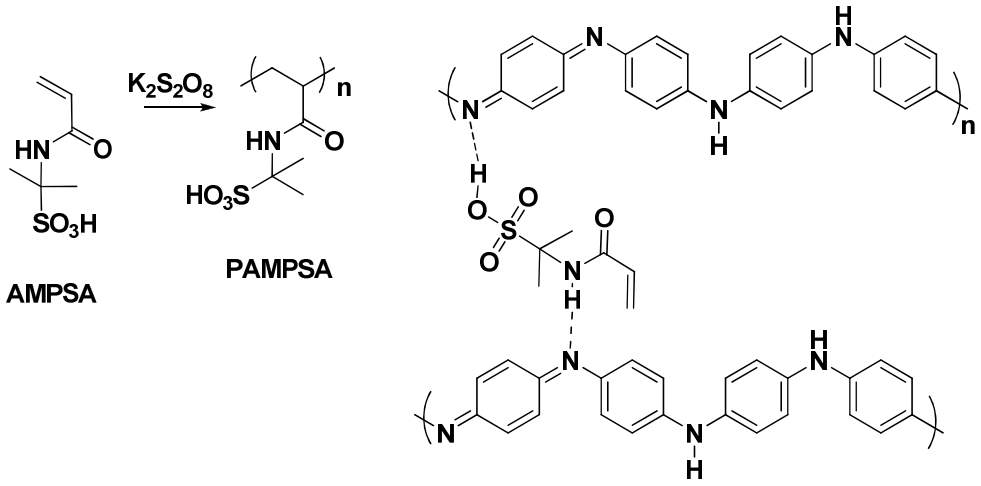

Scheme I-10 Synthesis of PAMPSA, interaction with PANI-EB

The synthesis of PAMPSA is presented in Scheme I-10. Yang et. al[100] studied a competing reaction with the protonation of PANI-EB in the case of the monomer, and studied the obtaining of gels. By using the polymer and performing the oxidation polymerization of aniline in the polymer solution, weak gelation has been observed.

The second type of doping has been obtained by adding sulfonation of PANI-EB.

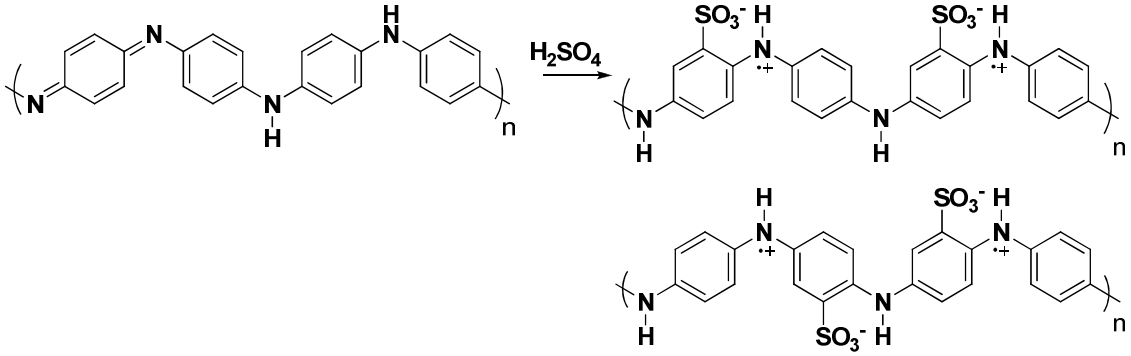

Scheme I-11 Self doping aniline (sulfonated polyaniline) PANI-SO_3H

For the characterization of the PANI polymers FT-IR technique has been used. The following characteristic peaks (cm^{-1}) could be assigned in the case of PANI: 3500 ν_{NH2} as vibration, 3400 ν_{NH2} sim, 788 γ_{NH2}, 3005 ν_{CH}, 1500 $\nu_{C=C}$, 863 γ_{CH}. In the case of PANI doped with HCl the characteristic peak is 540 cm^{-1}, as compared to PANI doped with PAMPSA where the characteristic peak is 1735 cm^{-1} specific for $\nu_{C=O}$ (ester group).

UV spectrum for PANI-EB (Figure I-21) shows two absorption bands: 634 nm (shifting of the electron from the benzene structure to quinone structure) and 303 nm ($\pi \rightarrow \pi^*$ transition of the benzene ring). In the case of PANI-ES we noticed 3 signals: 790 nm (shifting

[100] D. Yang, P. N. Adams, L. Brown and B. R. Mattes, *Synthetic Metals,* **2006,** *156*, 1225-1235.

of the electron from the benzene structure to quinone structure), 393 nm ($\pi \rightarrow \pi^*$ transition of the benzene ring) and 260 nm ($\pi \rightarrow \pi^*$ electron jump of C=N) which is in accordance with the literature.[101,102]

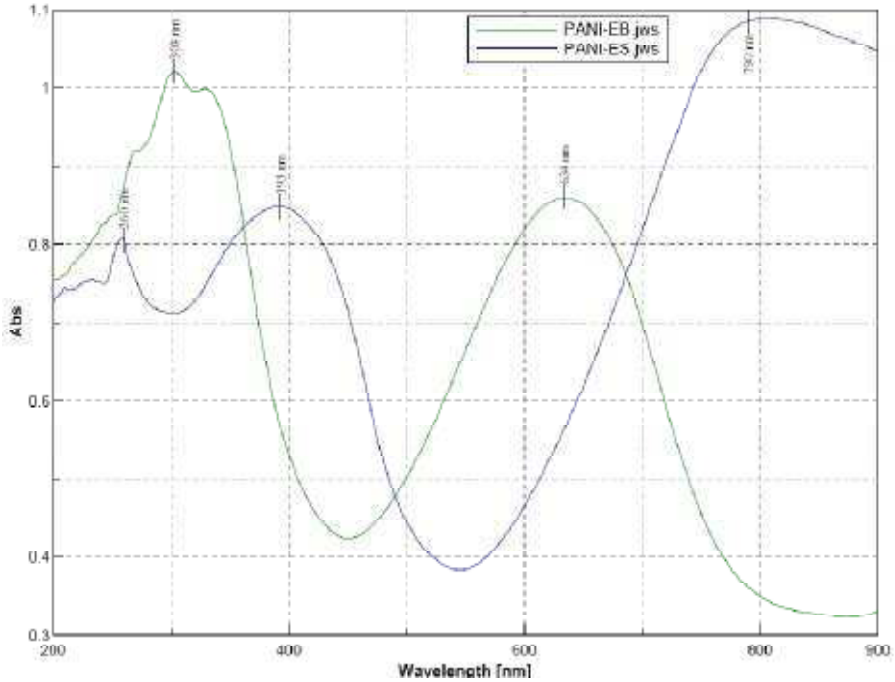

Figure I-21 UV-VIS spectra for PANI-EB and PANI-ES

For the characterization of PT doped with PbS there were recorded various X-ray diffraction spectra shown in Figure I-22. The peaks with 2θ values of 26.0, 30.1, 43.1, 51.0, 53.5, 62.6, 68.9, 70.9 and 79.0 correspond to the crystal planes (111), (200), (220), (311), (222), (400), (331), (420) and (422), which may be indexed to the pure cubic phase for PbS (JCPDF card no. 5-0592). The strong and sharp diffraction peaks suggest that the PbS is well crystallized.

[101] S. W. Ng, K. G. Neoh, J. T. Sampanthar, E. T. Kang and K. L. Tan, *The Journal of Physical Chemistry B,* **2001,** *105*, 5618-5625.
[102] V. P. Parkhutik and E. Matveeva, ibid. **1998,** *102*, 1549-1555.

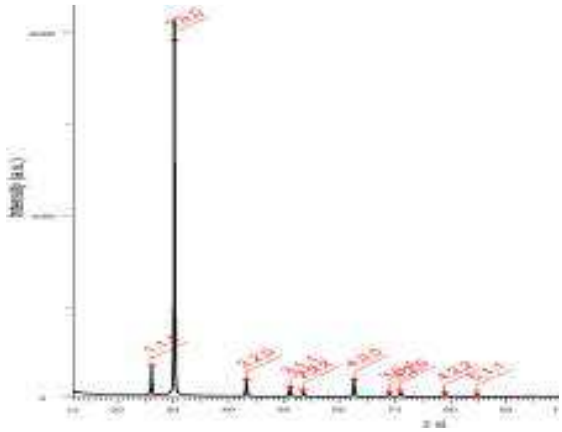

Figure I-22 X-ray diffraction spectrum of PbS generated in the presence of PT

The synthesis of PbS in the presence of PT followed the increase of quantum efficiency of the cell, knowing that PbS has excellent semiconductor properties at nanometric level. Additionally, it has advantageous properties like solar spectrum matching, multiple electron hole generation ability and tailor made which make them suitable candidate as a sensitizer/co-sensitizer in solar cells.[103] A quantum dot is a granule of a semiconductor material whose size is on the nanometer scale. These nanocrystallites behave essentially as a 3-dimensional potential well for electrons (i.e., the quantum mechanical "particle in a box").[104]

The influence of the polymer film on the absorption was evaluated by UV-VIS spectra of the films TiO_2/dye/polymer (Figure I-23). The minimum influence of the polymer upon the dye absorption in the visible spectrum is observed.

[103] R. J. Ellingson, M. C. Beard, J. C. Johnson, P. Yu, O. I. Micic, A. J. Nozik, A. Shabaev and A. L. Efros, *Nano Letters,* **2005,** *5*, 865-871.
[104] R. P. Raffaelle, S. L. Castro, A. F. Hepp and S. G. Bailey, *Progress in Photovoltaics: Research and Applications,* **2002,** *10*, 433-439.

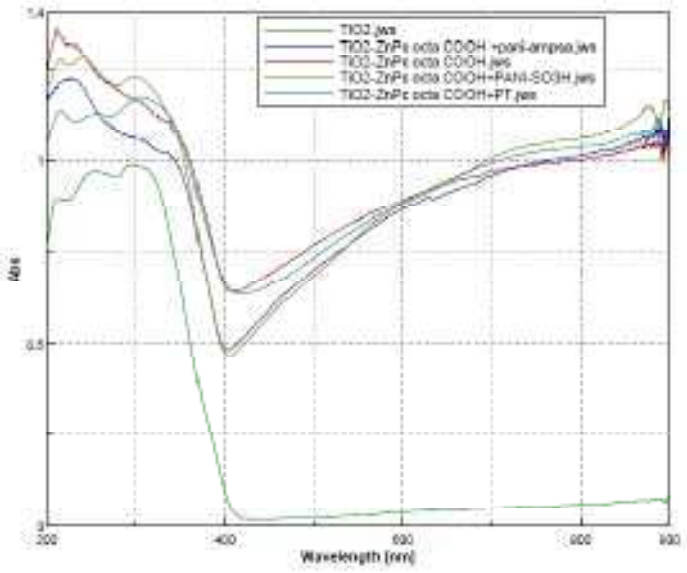

Figure I-23 UV-VIS absorption spectrum of films TiO2/dye/polymer

Next step, after the characterization of the compounds for the solar cell, consisted in the manufacture of the solar cells and the measuring their properties. The set up scheme is shown in Figure I-11.

The cell parameters for the obtained cells are presented in table 1.

Table I-1 Voltage and intensity of the solar cells measuread at light intensity of 100 mW/cm^2

Symbol	Cell	Voltage (mV)	Intensity (µA)
C1	ITO+TiO_2 + 4 COOH ZnPc+ electrolyte of I_2/KI + Graphite	178	3.6
C2	ITO+TiO_2 + 8COOH ZnPc+ electrolyte of I_2/KI + Graphite	256	5.1
C3	ITO+TiO_2 + 8COOH + PT + ITO	0.2	0.01
C4	ITO+TiO_2 + 8COOH + PT + electrolyte of I_2/KI+ ITO	4.2	1.2
C5	ITO+TiO_2 + 8COOH + PT/PbS+ ITO	35	0.3
C6	ITO+TiO_2 + 8COOH + PANI/PAMPSA+ ITO	38	0.01
C7	ITO+TiO_2 + 8COOH + PANI-SO3H+ ITO	20	0.01

The data from this table could be analyzed in a comparative manner and they show an increase both of the intensity and voltage in the case of octacarboxyphthalocyanine Zn (II). This could be explained, on one hand, by the high concentration of the sensitizer due to a good anchorage on the TiO_2 layer (high intensity) and on the other hand by a difference between the energy level of the excited state and the conduction band of TiO_2 (high voltage). This fact led to the use of this dye to manufacture the new hybrid cells. Comparing the values for C3 and C4 we may notice the increase of the efficiency when using the classic electrolyte. This is explained by the improvement of the regeneration ability of the polymer through charge carriers with high mobility. In the case of quantum dots (C5) we may notice the increase of the efficiency when using PbS nanoparticles. In the case of C6 and C7 the voltage is increased by using PANI-PAMPSA.

B. Polymer electrolyte[105]

Polymers containing quaternary ammonium iodine salts represent another polymer-involving alternative to the use of liquid electrolytes in DSSC that was tested. For this a suitable polymer had to be chosen. The conditions imposed for the polymer are: the possibility of obtaining quaternary ammonium salts and high mobility of the ions in the polymer matrix.

A literature search revealed the previous use of: poly(N-alkyl-4-vinyl-pyridine iodide)[50], polysiloxane with quaternary ammonium side groups[56], polysiloxane with oligo(oxyethylene) side chains and quaternary ammonium groups[55]. The structures are presented in Figure I-24:

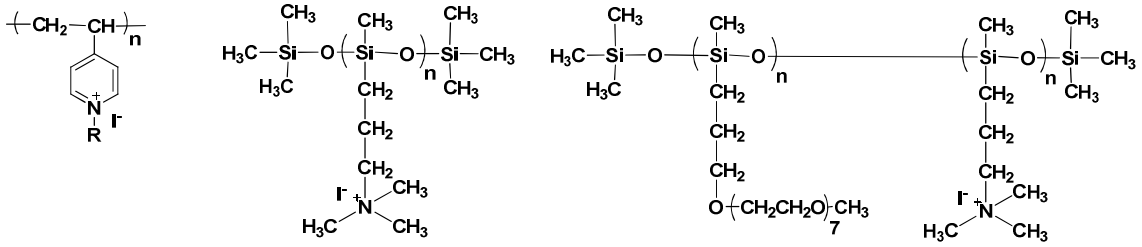

Figure I-24 Examples of previous used polymers containing quaternary ammonium slats

However, there is no mention for the use of poly-2-(diethylamino)ethyl methacrylate (PDEAEMA). The synthesis of the used polymer is presented in scheme Scheme I-12. The quaternary salts (PDEAEMA-q) are the result of a polymer analogous reaction using CH_3I.

[105] A. Diacon, L. Fara, C. Cincu, M. R. Mitroi, C. Zaharia, E. Rusen, C. Boscornea, C. Rosu and D. Comaneci, *Optical Materials,* **2010,** *32*, 1583-1586.

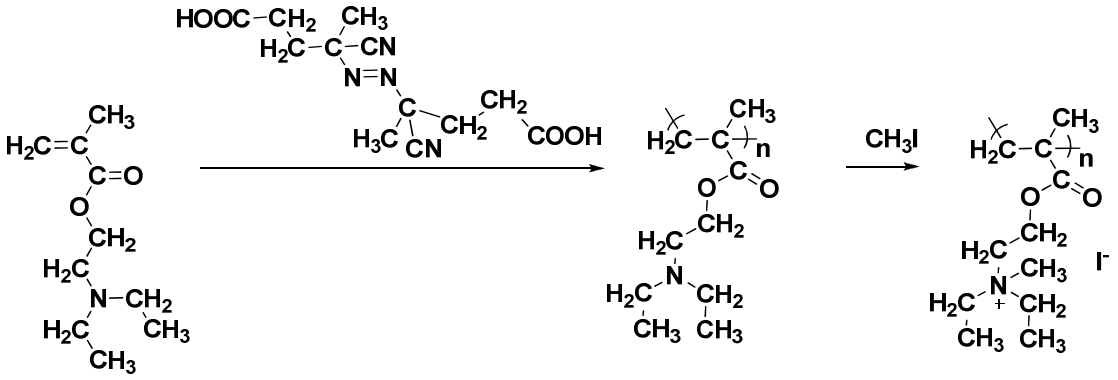

Scheme I-12 Synthesis PDEAEMA and PDEAEMA-q

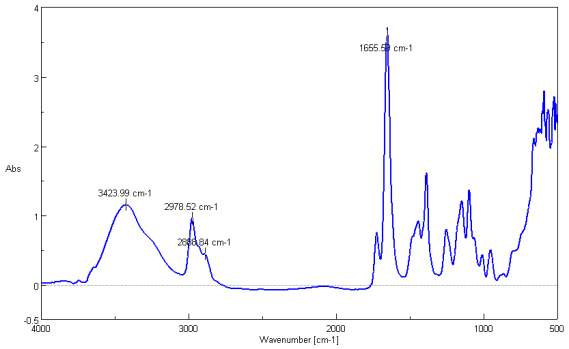

Figure I-25 spectrum of the analogous polymer derivative PDEAEMA-q

FT-IR spectrum confirms the polymer structure by the existence of the characteristic peaks: 1655 cm^{-1} corresponding to $\nu_{C=O}$, from the ester group, 2978-2888 cm^{-1} ν_{CH3} aliphatic, a low intensity of the signal for ν_{N-C} vibration from the tertiary amine. This fact supports the idea of a polymer analogous reaction.

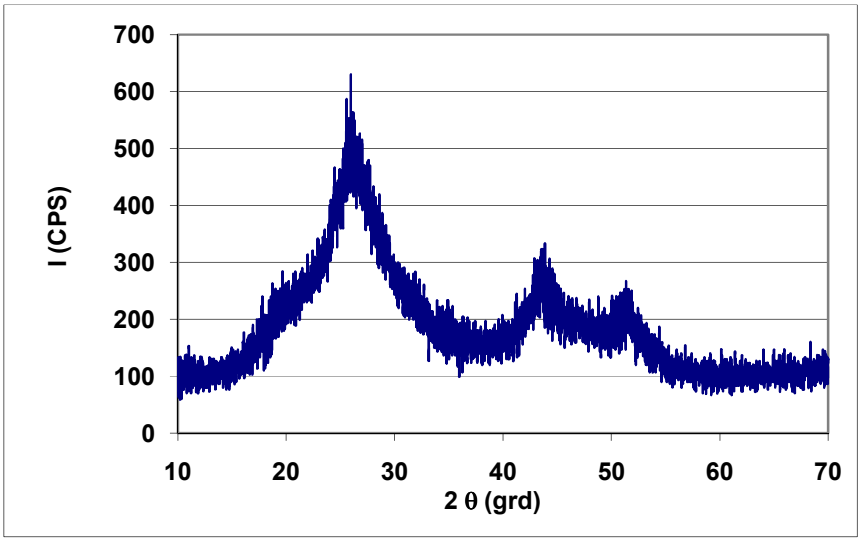

Figure I-26 XRD analysis for CdS

In the case of CdS quantum-dots generated in the presence of PDEAEMA, the XRD pattern exhibits the prominent broad peaks at 2θ values of 26.778, 43.928 and 51.678º. The three broadened peaks match the peaks assignable to (111), (220) and (311) lattice planes of cubic crystalline CdS. By using the Scherrer equation the size of the nanoparticles can be estimated.[106]

$$B(2\theta) = \frac{K\lambda}{L\cos\theta}, \text{ where}$$

K - is the Scherrer constant depending on the crystallite shape (0.89)

λ - X-ray wavelength

B-FWHM (full width at half max) or integral breadth

L-crystallite size

θ – Bragg angle.

Using this equation an estimated size of 10 nm was determined for the CdS nanoparticles.

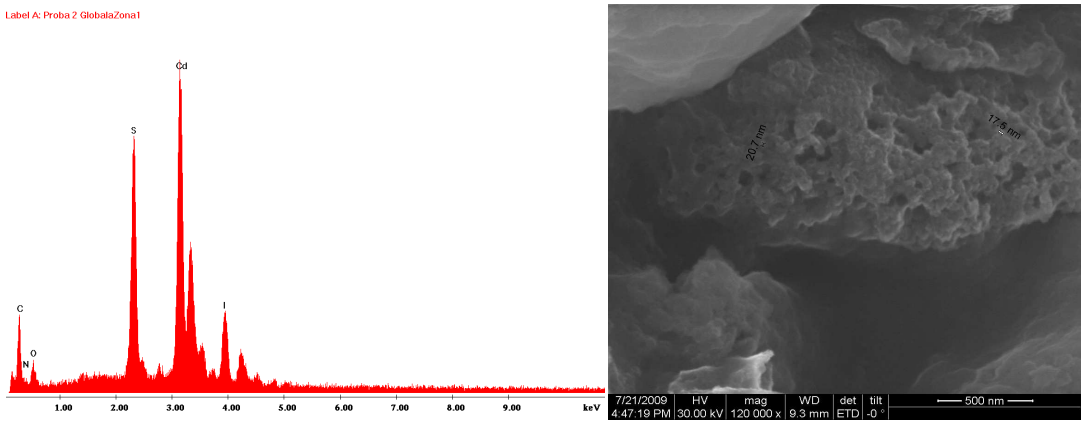

Figure I-27 EDAX and SEM for the CdS nanoparticles inside PDEAEMA-q polymer

In order to confirm the value of the nanoparticles given by the XRD and to examine the polymer-quantum dot morphology, we have studied using SEM coupled with an EDAX probe a film obtained by deposition of the quantum dots suspension in a polymer solution. The analysis confirmed the elemental composition of the two components and allowed the observation of nanoparticles imbedded in the polymer matrix.

The initial values for the short-circuit I_{sc} and open circuit voltage V_{oc} are presented in Table I-2 . Values are not stable in time, after o certain time the cells behave as photo-resistors.

[106] J. I. Langford and A. J. C. Wilson, *J. Appl. Crystallogr.,* **1978,** *11*, 102-113.

Table I-2 The values for: open circuit voltage and short-circuit intensity using PDEAEMA-q polymer electrolyte

Sensitizer	V_{oc} (V·cm^{-2})	I_{sc} (μA·cm^{-2})
Tetracarboxyphthalocyanine Zn(II)	0.021	0.3
Octacarboxyphthalocyanine Zn(II)	0.130	3.3
Octacarboxyphthalocyanine Zn(II) with PbS quantum dots	0.134	4.3
Octacarboxyphthalocyanine Zn(II) with CdS quantum dots	0.140	5.8

Conclusions

Porous nanostructurated films of TiO_2 have obtained and characterized by SEM and XRD analysis. These films were used for the depositions by self assembly on their surface of photochemical resistant dyes who serves as sensitizer for DSSC. The fluorescence characteristics of the dyes were investigated.

The influence of the functional groups upon the anchorage of the dye on the TiO_2 layer was established. A study concerning the manufacture of hybrid dye sensitized solar cells using polythiophene and polyaniline with different doping agents was realized. The performance of the hybrid cells utilizing hole conducting polymers and quantum dots as co-sensitizers is promising.

In order to obtain a new design for a hybrid dye sensitized solar cell a polymer with enhanced mobility based on quaternary salts was synthesized and used to replace the classic electrolyte system, this kind of polymer has not been mentioned in the literature so far for the obtaining of DSSC.

Considering the solar cell as a diode it is known that the series resistance of the diode junction depends on the technological process. This fact is very important during simulated solar irradiation when the photo current of the solar cell is high. Its change leads to the variation of the cell parameters V_{oc} and J_{sc}. This aspect explains the time degradation of the solar cells. Though values for V_{oc} and J_{sc} are stable over time, they show the possibility of using these materials for the manufacturing of hybrid solar cells. The differences between the obtained results are due to the influence of the increased values for V_{oc} and J_{sc}, in the case of quantum dot solar cells.

PbS and CdS nanoparticles were chemically generated in the presence of the polymer electrolyte solution. The best results were obtained in the case of CdS where the dimension of the generated nanoparticle was 10 nm. The performance of quantum dots based photovoltaics is dramatically influenced by dimension, respectively dispersion of these nanoparticles.

III. *Outlook*

The use of carbon nanotubes (CNTs) in solar cells attracted a lot of attention recently. One future strategy could be the utilization of CNTs in the polymer electrolyte. What would be interesting to study is the interaction with the dye and the overall conductivity and charge mobility in a polymer electrolyte comprised of CNTs having grafted on their surface the polymer electrolyte, the influence of the CNTs on the I_2 contained in the electrolyte and the effect on the Grotthus mechanism.

Initial research has been made in the attempt to explore the possibility of modifying carbon nanotubes with the polymer electrolyte. A new method that allows the superficial grafting of polymers from the carbon nanotubes has been explored by using for the moment water soluble polymers such as polyacrylamide and poly(2-hydroxyethylacrylate) (PHEA).[107]

The modification of the CNTs with water soluble polymers (PHEA) allowed them to form stable dispersions in water. The use of the DEAEMA monomer for the moment proved to be more difficult to control using our method.

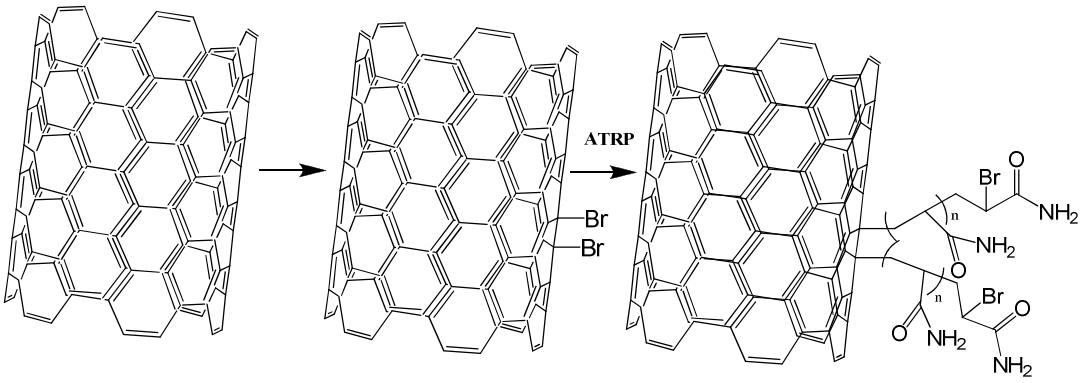

[107] A. Diacon, E. Rusen, B. Mărculescu, C. Andronescu, C. Cotruţ, C. Zaharia, A. Mocanu and C. Cincu, *International Journal of Polymer Analysis and Characterization,* **2011,** *16*, 1 - 8.

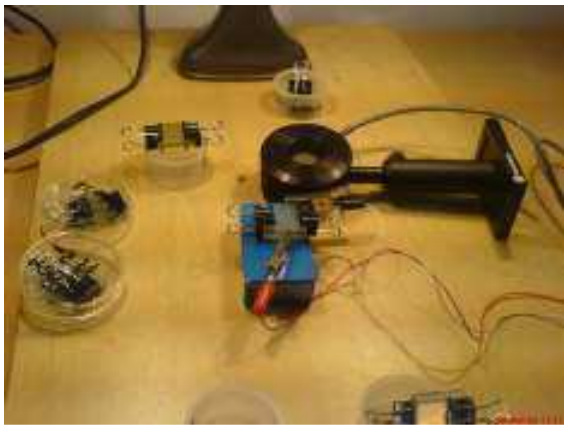


1. Experimental

Cell set-up

1. Obtaining of TiO_2 paste

2 g of TiO_2 were mixed with 1 mL of acetic acid solution (pH=3-4) in three portions and the mixture was grinded to obtain a homogeneous paste. Finally Triton X 100 was added as a surfactant.

2. Deposition of TiO_2 layer and sinterization stage

The surface of the conductive glass was covered with TiO_2, the excess being removed by spin-coating technique.

The conductive plate with TiO_2 layer was placed in the oven at 450°C for 30 minutes.

3. Deposition of the dye

The conductive glass with TiO_2 layer was introduced after sinterization in a dye DMF solution ($c=3x10^{-4}$ M). After 24h immersion, the solvent was removed by vacuum evaporation at 80°C.

4. Deposition of polymer film

The polymer film was obtained by solution spin coating. The solvent layer was removed by vacuum evaporation of the plates at 80°C.

5. Closing the cell circuit

For closing the circuit, we may use as counter-electrode the conductive glass (ITO) and to improve the interaction with the electrolyte we use a thin layer of graphite. We have used as electrolyte a solution of KI (0.5 M) and I_2 (0.05 M) in ethyleneglycol.

Synthesis of the 2,9,16,23-tetracarboxyphthalocyanine zinc(II) (Scheme I-5)

In a three-neck flask equipped with stirrer and thermometer trimellitic anhydride (15 g, 0.078 moles), urea (44 g, 0.73 moles), ammonium molibdate (0.4 g), zinc acetate (3.6 g, 0.0195 moles) and 100 ml of nitrobenzene were added. The mixture was heated at 185°C for 4h. After cooling, 100 ml of water were added and the mixture was stirred at reflux and then filtrated. It was washed with methanol to remove the nitrobenzene traces. The precipitate was added to 250 ml, 10% NaOH solution and it was hydrolyzed for 12h at reflux. It was filtrated hot and the filtrate was acidified with HCl up to positive reaction with Congo red. The precipitate was filtrated and washed with water. For a supplementary purification, the dried product was dissolved in concentrated H_2SO_4 and then it was poured over water. Yield 30%.

Synthesis of zinc octacarboxy phthalocyanine (Scheme I-6)

In a flask equipped with stirring and condenser pyromellitic anhydride (7.5 g, 0.035 moles), urea (39 g, 0.66 moles), 1,8-diazabicyclo(5.4.0) undec-7-ene (0.2-0.4 ml) and zinc acetate (8.6 g) were added. The reaction mixture was heated at 250°C for 3h. The reaction product was washed with water, HCl solution (15 ml in 50 ml of H_2O) and was hydrolyzed in basic medium with 10% NaOH solution. Then it was introduced in a flask equipped with stirrer and condenser together with 100 ml of 10% NaOH solution and refluxed for 18h, after which it was filtrated. The filtrate was acidified with HCl up to positive reaction with Congo red paper, filtrated and washed with water. For a supplementary purification, the dried product was dissolved in concentrated H_2SO_4 and poured over water. Yield 40%.

Synthesis of PT (Scheme I-7**)**

60 ml of chloroform were added to 3 ml of thiophene and then 10 g of ferric chloride were added to the solution. The mixture was kept under stirring over night. After which it was precipitated in methanol and dried under vacuum to constant mass.

Synthesis of PbS in the presence of PT

A mixture of 30 ml of toluene, 10 ml of dimethylsulfoxide, 5 µl of dodecyl mercaptane, 0.1 g of lead acetate and 0.3 g of PT was stirred and heated at 100°C for 20 minutes. 0.1 g sulfur was dissolved in 10 ml of toluene and injected in the first solution. The reaction mixture was kept at the same temperature for 10 minutes, and then it was precipitated in ethanol, filtrated and dried under vacuum to constant mass.

Synthesis of PANI (PANI-ES) (Scheme I-9**)**

In a 500 ml reactor equipped with stirrer, pouring funnel and thermometer, 0.1 moles of fresh distilled aniline were added. The temperature was kept at 0°C. Then 0.1 moles of 35% HCl were added to obtain the aniline clorhydrate. This product is quickly formed as a white-yellow precipitate accompanied by a high volume of HCl vapours. After 45 minutes, 0.1 moles of potassium persulfate in 75 ml of demineralised water were drop added for 60 minutes. A blue precipitate was formed and the reaction mass was kept overnight at 0°C. The obtained precipitate was washed with distilled water on the filter paper and dried in vacuum to constant mass. The yield was 94%.

Synthesis of poly 2-acrylamido 2-methylpropane sulfonic acid (PAMPSA)

2-acrylamido 2-methylpropane sulfonic acid (AMPSA) (7 g, 0.033 moles) was dissolved in 50 ml of distilled water and potassium persulfate (0.1 g) was added. Nitrogen was bubbled for 10 minutes within the reaction mixture. The mixture was then placed in a thermostatic bath at 80°C for 5 hours. The polymer was precipitated in acetone, filtrated and dried in vacuum to constant mass.

Synthesis of PANI doped with PAMPSA

PAMPSA (5.8 g) was dissolved in 375 ml of distilled water and then aniline (3 ml) was added and stirred for 1 h at room temperature. Separately a solution of potassium persulfate (7.3 g) in 20 ml of distilled water was prepared, and then was added to the initial solution at 0°C. The reaction was kept at this temperature for 6 h, after which the mixture was precipitated in acetone, it was filtrated and the precipitate was dried in vacuum to constant mass.

Synthesis PANI - emeraldine base (PANI-EB)

PANI (0.5 g) was added to 100 ml solution of 0.1 M ammonia. The reaction was kept under stirring for 24 h at room temperature. The reaction product was filtrated and dried under vacuum.

Synthesis of sulfonated PANI (PANI-SO_3H) (Scheme I-11**)**

PANI-EB (0.5 g) was added to 40 ml of H_2SO_4. The mixture was stirred for 2 hours at room temperature. Then 200 ml of methanol were drop-added for 20 minutes on an ice bath

and finally 100 ml of acetone were added. The precipitate was filtrated and washed with methanol up to pH=7. Finally the product was dried under vacuum to constant mass.

Synthesis of poly(2-(diethylamino)ethyl methacrylate) (PDEAEMA)

In a 50 ml round bottom flask 10 ml of 2-(diethylamino)ethyl methacrylate are introduced and 0.014 g of 4,4'-Azobis (4-cyanovaleric acid) are added, the mixture is heated to 60°C and stirred for 6 h. The resulting polymer (poly 2-(diethylamino)ethyl methacrylate - PDEAEMA) is then precipitated in diethyl ether, filtered, dried and kept in a dessicator.

Quaternization of poly 2-(diethylamino)ethyl methacrylate (PDEAEMA-q)

In a 25 ml round bottom flask 2 g of poly 2-(diethylamino)ethyl methacrylate are dissolved in DMF and 2 ml of methyl iodide are added. The reaction mixture is kept to 15°C for 24 h. The final polymer (PDEAEMA-q) is precipitated in petroleum ether and then filtered, dried and kept in a dessicator.

The generation of PbS in the presence of PDEAEMA-q

In a reactor 1 g of PDEAEMA-q is dissolved in 10 ml of water, to this solution 0.05 g of $Pb(CH_3COO)_2$ and 0.06 g of thioacetamide are added. The mixture is then heated at 80°C and stirred for 24 h. The polymer containing PbS is then precipitated in methanol, filtered, dried and kept in an dessicator.

The generation of CdS in the presence of PDEAEMA-q

In a reactor 1 g of PDEAEMA-q is dissolved in 10 ml of water, to this solution 0,08 g of $Cd(CH_3COO)_2$ and 0,075 g $Na_2S{\cdot}9H_2O$ are added. The mixture is stirred at room temperature for 24 h. The polymer containing CdS is then precipitated in methanol, filtered, dried and kept in a dessicator.

CHAPTER II: Light-harvesting systems involving C_{60}

I. *Introduction - light harvesting antennas in nature (Photosynthesis)*

Nature's most sophisticated and important solar energy harvesting and storage system is found in photosynthetic organisms, like, plants, algae and a variety of types of bacteria. Sunlight is absorbed and converted to electrochemical potential energy (used for the formation of ATP) by photoinduced electron transfer in the reaction center.

In normal condition, one chlorophyll molecule acting as antenna would capture a photon once every few seconds, the charge separation in photochemical reactions has half-times in this range, so photosynthesis with an antenna of this magnitude would be inefficient. In order to attain an efficient use of solar energy, the photosynthetic organisms have developed during evolution light harvesting antennas, which allow the cooperation of pigments in the collection of light for a single reaction center. The size of the antenna is adjusted to suit the intensity of the available light in many photosynthetic systems. The antenna is the key for growth at low light intensity.

The light-harvesting antennas (LH2) are usually located at the interior of the photosynthetic membrane, near the reaction center, that is also surrounded by a complex representing the interior antenna (LH1).

The first determination of the structure of LH2 has been made by McDermott et al. in 1995.[108] It represents a light-harvesting antenna consisting in two concentric cylinders of helical protein subunits which enclose the pigment molecules. These pigments, which can be carotenoids or chlorophylls[109], are close and orientated parallel to each other. The absorption of the LH2 complexes covers a high part of the spectrum, in the UV region (carotenoids) and up to 1000 nm (bacteriochlorophylls- 870 and 890 nm (Bchla) or at 1020 nm (Bchlb)). The high efficiency of the antenna is due to the specific structure of the proteins involved which need to bind the pigments in order to maximize absorption. Also, the optimal orientation, configuration and excited state energy levels of the pigments must be ensured in order to allow efficient energy transfer.[110] Interaction between complexes is important, this protein-protein interaction allowing the energy transfer between complexes. One of the most important factors to take into account is that chlorophyll must be arranged in order to suppress the tendency for excited state to dissipate by non-radiate process. The concentration of chlorophyll in LH2 is 0.6 M. If chlorophyll would be dissolved in an organic solvent, or in solid polymer matrix like PMMA at this concentration all absorbed energy would be

[108] G. McDermott, S. M. Prince, A. A. Freer, A. M. Hawthornthwaite-Lawless, M. Z. Papiz, R. J. Cogdell and N. W. Isaacs, *Nature,* **1995,** *374*, 517-521.
[109] H. Zuber, *Trends Biochem. Sci,* **1986,** *11*, 414-419.
[110] H. van Amerongen and R. van Grondelle, *The Journal of Physical Chemistry B,* **2000,** *105*, 604-617.

dissipated via close interactions, dimers or excimers, process that take place at quenching concentration.[111] These characteristics suggest that the protein acts as a special "solvent", an environment that allows a high chlorophyll concentration without the quenching from due to associations. The environment is due to the formation of hydrophobic binding pockets, liganding of chlorophyll Mg atoms by amino acid residues of the alpha helices and hydrogen bonding to the porphyrins ring.[112]

The structure of the interior LH1 was established by X-ray diffraction by Karrasch et al.in 1995, showing the same molecular components as LH2. However, LH1 is larger than the LH2 in order to be able to accommodate the reaction center at the interior (Figure II-1)

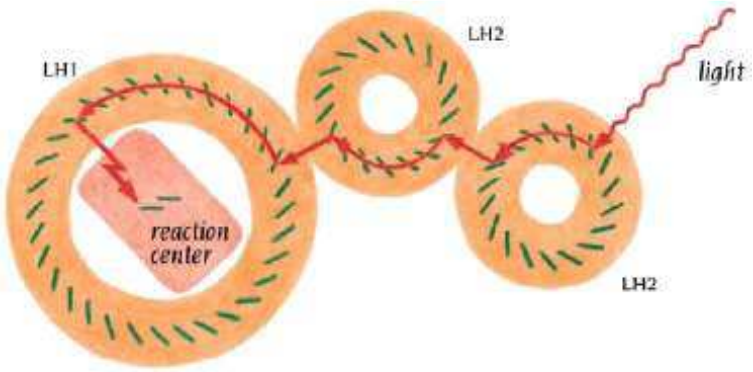

Figure II-1 Light harvesting complex and light capturing pathway from LH2 to reaction center[113]

The photon absorption by the pigments contained in the LH2 results in the generation of an exited state. This is rapidly propagated from one pigment to another inside the complex LH2 due to the arrangement of the molecules and their susceptibility to undergo this type of processes. The energy can be further transferred from one pigment to another at the interior of complex LH1. Thus, the energy provided by the absorption of one photon is transported very rapidly (less than 1 picosecond) and with a minimum loss of energy from the collection area to the reaction center. Inside the reaction center is where the transformation of the supplied energy is transformed into chemical energy used by the living cells in order to undergo the necessary transformation for obtaining the necessary nutrients. (Figure II-2)

[111] G. S. Beddard and G. Porter, *Nature,* **1976,** *260*, 366-367.
[112] Z. Liu, H. Yan, K. Wang, T. Kuang, J. Zhang, L. Gui, X. An and W. Chang, ibid. **2004,** *428*, 287-292.
[113] Brändén, C. I.; Tooze, J., *Introduction to protein structure*. Garland Pub.: 1999;

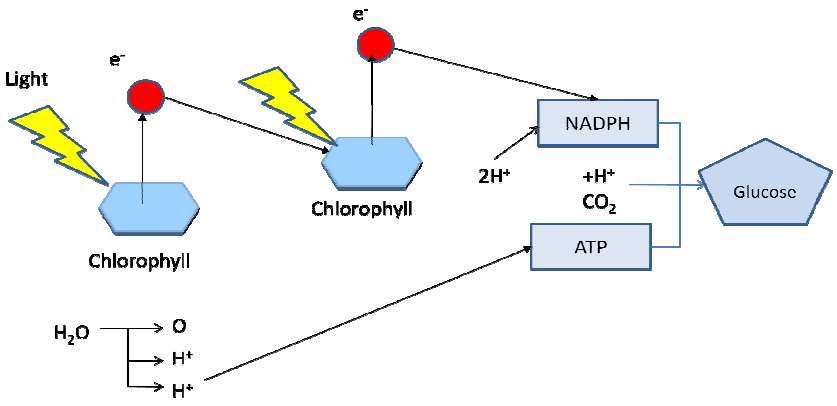

Figure II-2 Transformation of sunlight energy (NADPH-nicotinamide adenine dinucleotide phosphate; ATP-Adenosine-5'-triphosphate)

Having in mind this kind of interactions, the goal of many chemists is to obtain artificial systems, less complicated, that would present the antenna and the energy transfer properties of natural systems.

II. *Energy and electron transfer*

Photoinduced energy and electron transfer are the governing processes in photosynthesis, photo-imaging, photoinduced chemical reactions and optoelectronic devices. The study of these processes in artificial systems may lead to a better understanding of the first events in biological processes and to the development of new devices.

Following the absorption of a photon the molecule passes from the ground state S_0 to an excited state S_1. The excess energy due to light absorption can be dissipated through unimolecular processes either as radiation (emission) or by radiationless transitions. Also, the transfer can be to other molecules through bimolecular processes.

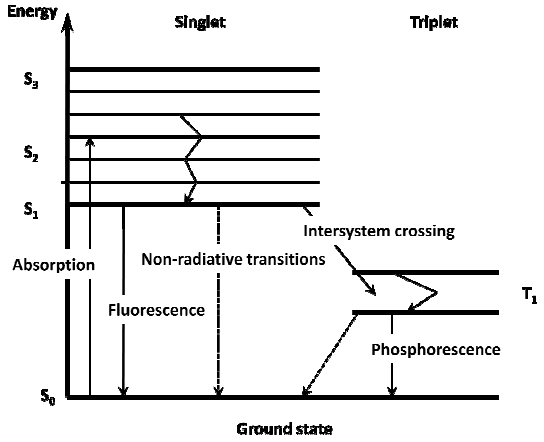

Figure II-3 Jablonski diagram: photoinduced processes

1. Light induced electron transfer

The light induced electron transfer is often the cause for fluorescence quenching. It is a process involved in many chemical reactions and in many essential biological processes. It represents a process in which an electron is transferred from an electron donating species (D) to an electron accepting species (A). The process is described in Figure II-4. The result of the light induced electron transfer is the formation of the charge-separated state. This can be reached by two paths depending on which of the components forms the excited state:

a. If the photon is absorbed by the donor, an electron from its HOMO orbital is transferred to its LUMO orbital from where is transferred to the LUMO orbital of the acceptor; resulting in the formation of charge-separated state

b. The acceptor can also absorb a photon and have an electron from its HOMO orbital transferred to its LUMO orbital, this is followed by the transfer of an electron from the HOMO orbital level of the donor to the HOMO orbital of the acceptor resulting in the obtaining of the charge-separated state.

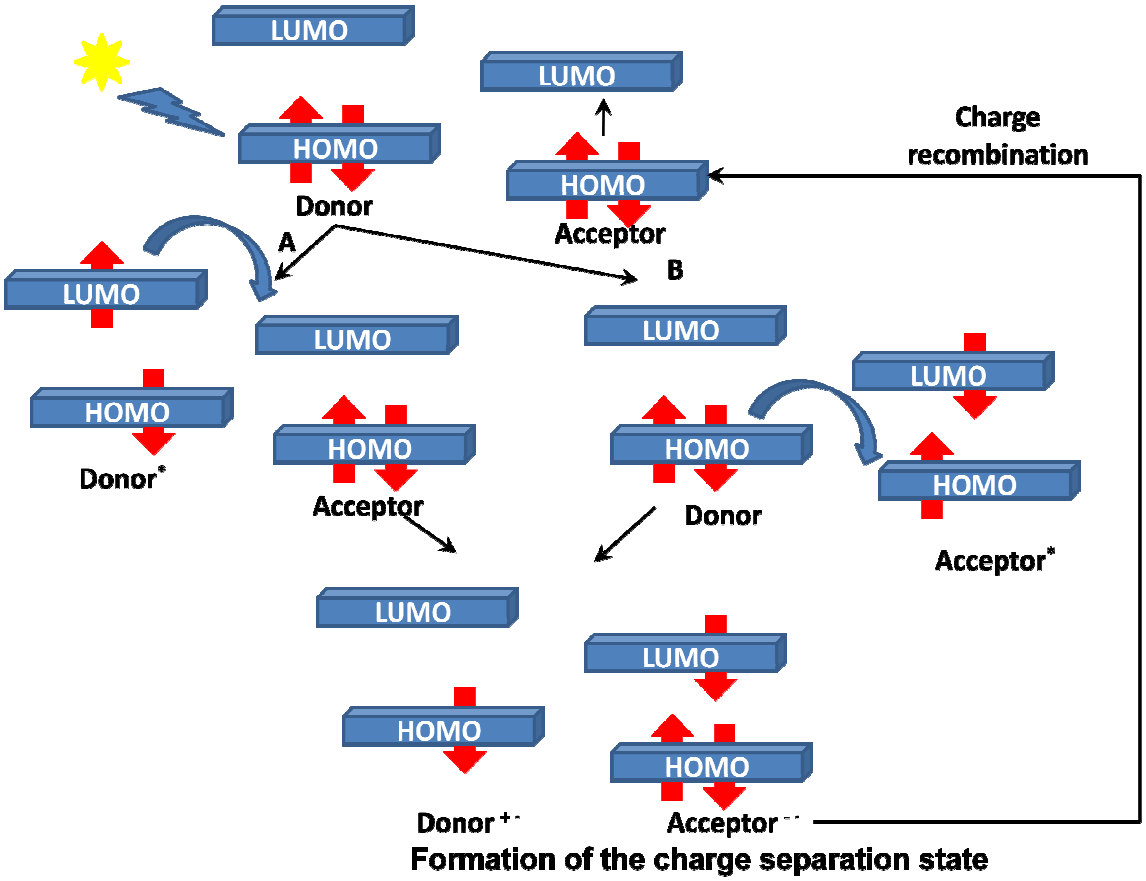

Figure II-4 Electron transfer, formation of charge-separated state

Electron transfer is in correlation with the redox properties of the donor-acceptor couple and with the excitation energy.

2. Energy transfer

In an energy transfer process, the excitation of the donor is transferred to the acceptor, which has an energy lower excited state. Thus, the donor returns to the ground state while the acceptor reaches its excited state. The donor molecules typically emit at shorter wavelengths which overlap with the absorption spectrum of the acceptor. There are two basic Förster and Dexter mechanisms for energy transfer (Figure II-5).[114]

Förster energy transfer[115] – also called "coulombic", "dipole-dipole" or "resonance" energy transfer – takes places through the interaction of the oscillating dipole of the excited donor with that of the acceptor. The critical condition for energy to be transferred by this mechanism, besides thermodynamics, is a good overlap between the emission spectrum of the donor and the absorption spectrum of the acceptor. Due to the fact that the electrons involved in the energy transfer process are not exchanged between the two chromophores, there is no dependence of the donor-acceptor orbital overlap on the dynamics. The dipole-dipole interaction is long-range (~100 Å) and the rate of the energy transfer by Förster mechanism decay inversely with the sixth power of the interchromophore separation.

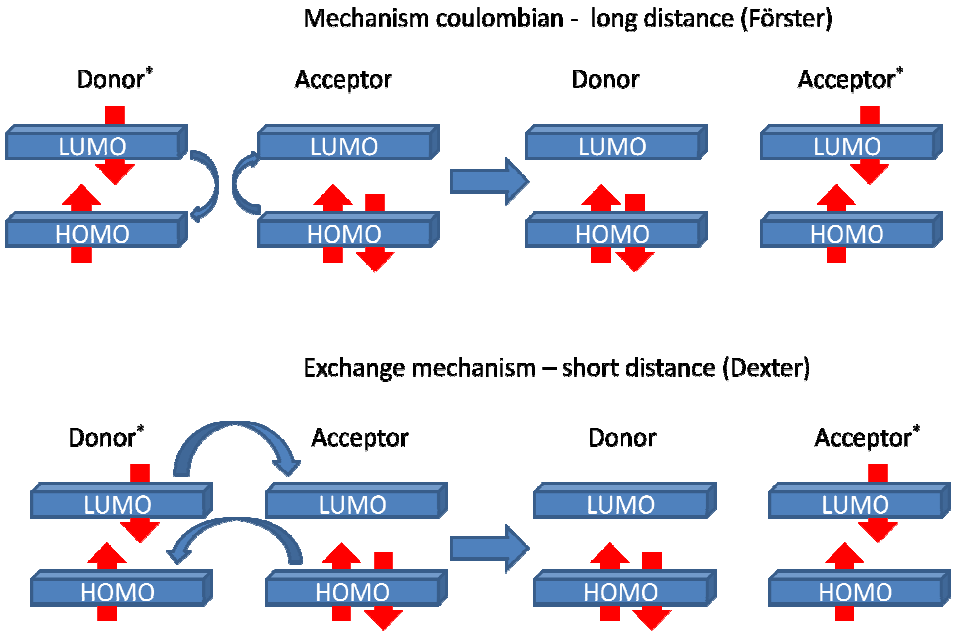

Figure II-5 Mechanisms for energy transfer

[114] Paddon-Row, M. N., *Electron and Energy Transfer*. Wiley-VCH Verlag GmbH & Co. KGaA: 2005; p 267-291.
[115] T. Forster, *Discussions of the Faraday Society,* **1959,** *27*, 7-17.

The Dexter mechanism[116] – also called "exchange" mechanism – can be regarded as a double electron transfer, one electron moving from the LUMO of the donor to the acceptor LUMO and the other from the acceptor HOMO to the donor LUMO. This electron exchange requires strong D-A orbital overlap and is therefore a short-range (<10 Å) interaction that decreases exponentially with distance.

Singlet-singlet energy transfer is "spin-allowed" for both the Förster and the Dexter mechanism. Triplet-triplet energy transfer is not allowed by a coulombic mechanism (Förster) due the low extinction of the acceptor, but can take place by the exchange (Dexter). In the Dexter mechanism, the bridging ligand, its electronic nature, geometry and rigidity are the most important factors that determine the electronic coupling between the donor and acceptor moieties and in this way the energy transfer rate. The properties of the chromophores, the transition dipole moment and spectral overlap of donor emission and acceptor absorption as well as the distance between the chromophores play the most important role in the Förster mechanism.

III. *Photoinduced electron/energy transfer in fullerene containing assemblies*

Covalently linked donor-acceptor systems involving fullerene-C_{60} have received a lot of interest due to fact that they can exhibit characteristic electronic and excited state properties. These kind of molecular assemblies are of particular interest, representing attracting candidates for the investigation of photoinduced electron transfer processes and long-lived charge-separated state $D^{+\bullet}$-$A^{-\bullet}$. The formation of the excited state is followed by a series of changes in the electronic and geometrical structure and simultaneously induces changes in the interaction with the environment. In excited states molecules undergo also inter- or intramolecular dynamic processes and reactions, out of which the photoinduced electron transfer is the most important from the fundamental point of view.

During the last decades, an increasing number linked donor-acceptor (D-A) systems with fullerene-C_{60} as acceptor have been obtained with a certain degree of control over the distance and arrangement between the donor and acceptor pairs, fused or covalently bounded by a single or a rigid bridge.

Photoinduced electron transfer has been studied between donor and fullerene because C_{60} can give rise in electron transfer processes to a rapid photoinduced charge separation and slow charge recombination. This interesting ability of fullerenes in electron transfer has been

[116] D. L. Dexter, *The Journal of Chemical Physics,* **1953,** *21*, 836-850.

correlated with their small reorganization energy.[117] Thus, the acceleration effect of photoinduced charge separation as well as charge shift and the deceleration effect on charge recombination in donor-linked fullerenes can be explained.

These outstanding properties made organo-fullerenes containing electro-donor species a much studied topic and target for synthesis. The design of the molecules aims the obtaining of arrays that exhibit optimized electron transfer capabilities and minimize loss of the excited-state energy of back-electron transfer. The initial steps in artificial photosynthesis process are collection of light energy and energy transfer to the photosynthetic reaction center[118] [119]. Fullerene can bring much improvement to both of these steps.

1. General presentation of fullerene-C_{60}

The "superaromaticity" of fullerene-C_{60} has been predicted for the first time by Osawa in 1970[120, 121]. However, the actual existence of C_{60} was proven by H.W. Kroto, R.F. Curl and R.E. Smalley, who discovered a remarkably stable cluster of 60 C atoms vaporizing graphite by laser irradiation in their quest for the structure of carbon in space. Fullerenes represent after graphite and diamond the third allotropic form of carbon.

The first method for the production of macroscopic quantities of fullerene has been established by Krätschmer and Hufman in 1990.[122] Thus, a new chapter in organic chemistry had the possibility to be developed. The interest in fullerenes was also increased by the discovery made by Iijima et al.[123] of another allotropic form of carbon, the carbon nanotubes.

The name "fullerene" was given to these structures as a tribute to architect and inventor Richard Buckminster Fuller, the creator of geodesic dome concept.

Fullerene-C_{60}, is made up of 12 pentagons and 20 hexagons arranged in spherical shape, football-like. Only two types of bond are present: the 5:6 bonds (also called simple bonds) which constitute the pentagons with bond length of 1.45 Å and the 6:6 bonds (also called double bonds) that are present in the hexagons with a bond length of 1.38 Å (Figure II-6). Thus, all the carbon atoms are equivalents (intermediary hybridization sp^2-sp^3), which is confirmed by the ^{13}C NMR spectra that shows a single peak at 143 ppm. (Figure II-7)

---

[117] H. Imahori, K. Hagiwara, T. Akiyama, M. Aoki, S. Taniguchi, T. Okada, M. Shirakawa and Y. Sakata, *Chemical Physics Letters,* **1996,** *263*, 545-550.
[118] M. R. Wasielewski, *Chemical Reviews,* **1992,** *92*, 435-461.
[119] D. M. Guldi, *Chemical Society Reviews,* **2002,** *31*, 22-36.
[120] E. Osawa, *Kagaku,* **1970,** *25*, 854-863.
[121] Z. Yoshida and E. Osawa, *Hokozokusei (Aromaticity),* **1971**, 174.
[122] W. Kratschmer, L. D. Lamb, K. Fostiropoulos and D. R. Huffman, *Nature,* **1990,** *347*, 354-358.
[123] S. Iijima, ibid. **1991,** *354*, 56-58.

Figure II-6 Fullerene-C_{60} front view and the Schlegel diagram

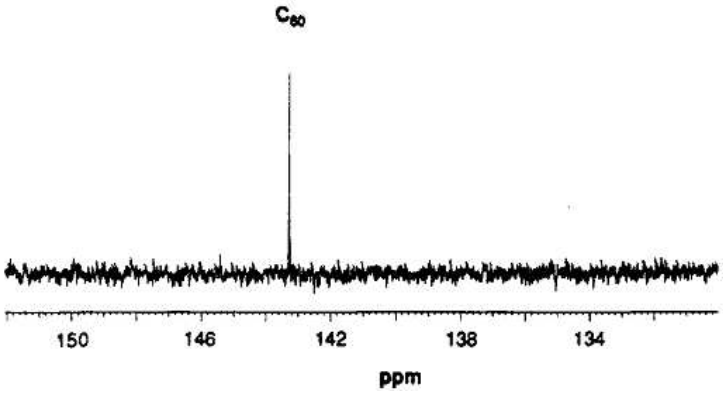

Figure II-7 ^{13}C NMR spectrum of fullerene-C_{60} in benzene-d_6[124]

As mentioned above one of the most important properties of fullerene are the electrochemical properties due to its particular structure. In fact C_{60} has the capacity to reversibly accept up to 6 successive electrons through electrochemical reduction, as proven by Xie et al.[125]. This property is due to its triple-degenerate low-lying LUMOs (1.5-2.0 eV above the HOMO). [126](Figure II-8)

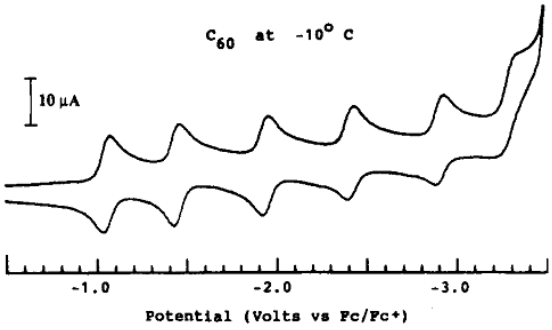

Figure II-8 Cyclic voltammetry of C_{60} in CH_3CN/toluene at -10°C[127]

Besides the acceptor capabilities that are presented in the cyclic voltammetry, it is important to note that the first reduction potential is at a relative low value (~1 V). This has been shown to vary depending on the solvent. These two findings allow the fullerene-C_{60} to play an important role in donor-acceptor systems.

[124] H. Ajie, M. M. Alvarez, S. J. Anz, R. D. Beck, F. Diederich, K. Fostiropoulos, D. R. Huffman, W. Kraetschmer, Y. Rubin and et al., *The Journal of Physical Chemistry,* **1990,** *94*, 8630-8633.
[125] Q. Xie, E. Perez-Cordero and L. Echegoyen, *Journal of the American Chemical Society,* **1992,** *114*, 3978-3980.
[126] Kadish, K. M.; Ruoff, R. S., *Fullerenes: chemistry, physics, and technology*. Wiley-Interscience: 2000.124.
[127] Q. Xie, F. Arias and L. Echegoyen, *Journal of the American Chemical Society,* **1993,** *115*, 9818-9819.

Fullerene-C_{60} has a low absorption in the visible domain ($\varepsilon_{520}^{toluene} = 826\ Lmol^{-1}$) [128]. The absorption spectrum of C_{60} in hexane presents large characteristic absorption bands at 211, 256 and 328 nm (the extinction depends on the used solvent)[129], a weak absorption at 405 nm and a very weak absorption characteristic from 430 to 650 nm. (Figure II-9)

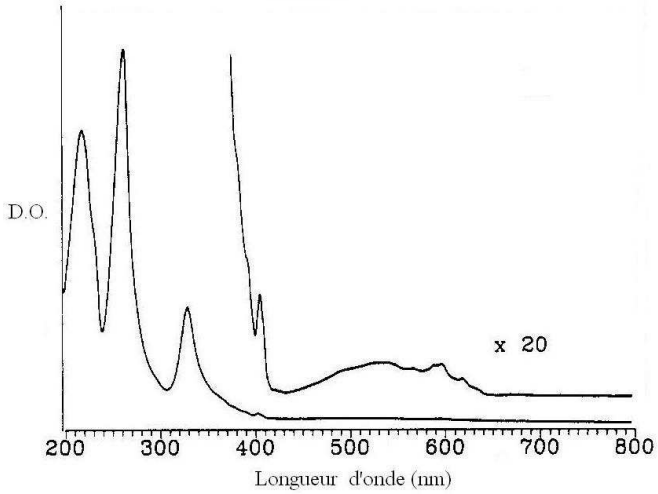

Figure II-9 Absorption spectrum of fullerene-C_{60} in hexane[124]

2. Functionalization of fullerene-C_{60}

Although, initially were thought to be unreactive, aromatic-like molecule, the fullerenes take part in wide variety of reactions characteristic of alkenes. This is due to the particular delocalization of the π electrons. A large number of cycloaddition products are demonstration of this characteristic. Fullerenes exhibit also electron deficient alkyne characteristics reacting with electron rich species. The majority of reactions take place at a 6:6 bond due to the presence of a higher electron density.

As presented in Scheme II-1 there is available a large variety of functionalization methods for fullerenes.[130]

[128] J. Catalán, J. L. Saiz, J. L. Laynez, N. Jagerovic and J. Elguero, *Angewandte Chemie International Edition in English,* **1995,** *34*, 105-107.
[129] S. Leach, M. Vervloet, A. Desprès, E. Bréheret, J. P. Hare, T. John Dennis, H. W. Kroto, R. Taylor and D. R. M. Walton, *Chem. Phys.,* **1992,** *160*, 451-466.
[130] R. Taylor and D. R. M. Walton, *Nature,* **1993,** *363*, 685-693.

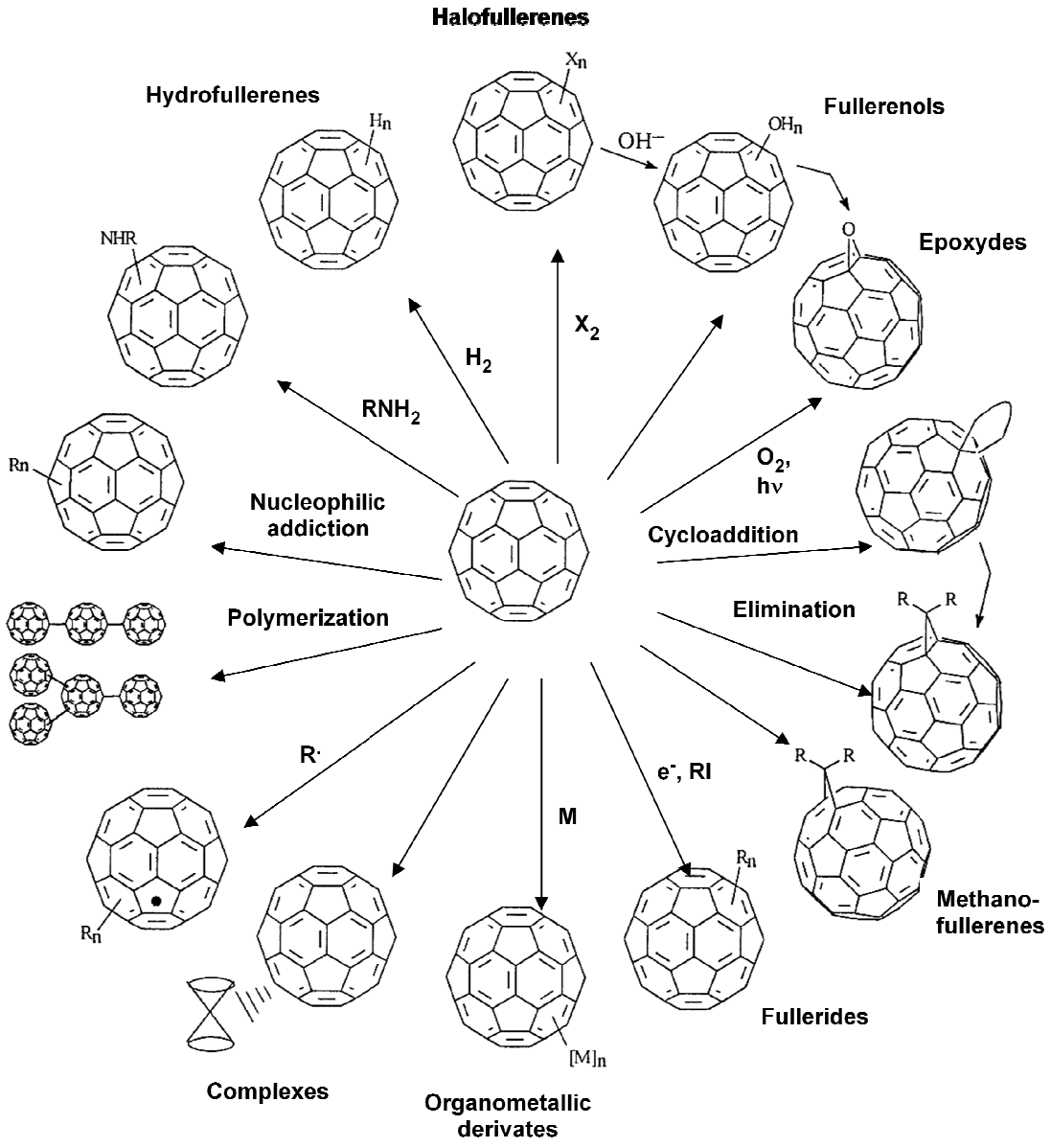

Scheme II-1 Functionalization methods for fullerenes [131]

Reaction with amines

Different aliphatic amines react with fullerene. The obtained derivative is usually the result of a nucleophilic addition and the mechanism consists in a first step of single-electron transfer from the amine to C_{60} resulting in the formation of an radical anion. The formation of the anion can be followed by ESR spectroscopy[132]. The next step is a charge recombination between the radical cation of the amine and the radical anion present on the fullerene resulting

[131] Hirsch, A., *The chemistry of the fullerenes*. G. Thieme Verlag: 1994.
[132] A. Skiebe, A. Hirsch, H. Klos and B. Gotschy, *Chemical Physics Letters,* **1994,** *220*, 138-140.

in zwitterions intermediates of green color. The transfer of the proton from the nitrogen to the C_{60} permits the obtaining of the final product. (Figure II-10)

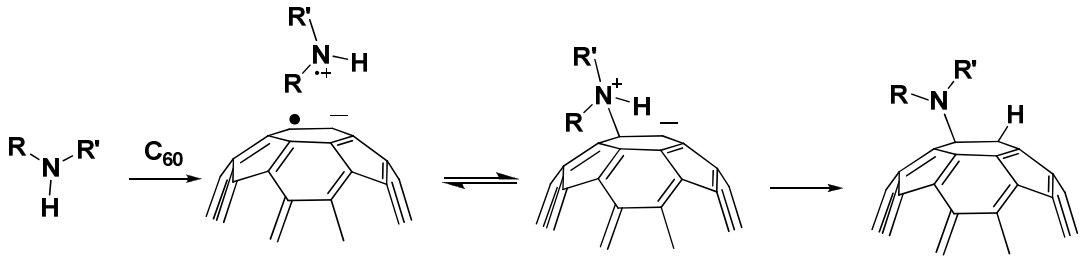

Figure II-10 Mechanism for nucleophilic addition of amines to C_{60}

Although reactions of fullerene-C_{60} with amines, either in solution or with the pure amine, proceed very easily, only a few cases of the isolation of defined aminofullerenes have been reported because complex mixtures of aminoadducts are very often obtained.[133]

Cycloadditions

A highly utilized reactions set for fullerene is represented by cycloadditions[134]. Due to its electron deficiency, C_{60} can play the role of a dienophile or 1,3-dipolarophile. Thus, all types of cycloaddition are available involving the 6:6 bonds. Examples of possible types of reactions include: [2+1][135] cycloadditions corresponding to carbene insertion, [4+2][136] cycloadditions corresponding to Diels-Alder reactions, [2+2][137] cycloadditions or 1,3 dipolar [3+2][138] cycloadditions (Figure II-11).

[133] A. Hirsch, *J. Phys. Chem. Solids,* **1997,** *58*, 1729-1740.
[134] M. A. Yurovskaya and I. V. Trushkov, *Russ. Chem. Bull.,* **2002,** *51*, 367-443.
[135] A. Vasella, P. Uhlmann, C. A. A. Waldraff, F. Diederich and C. Thilgen, *Angewandte Chemie International Edition in English,* **1992,** *31*, 1388-1390.
[136] M. Prato, T. Suzuki, H. Foroudian, Q. Li, K. Khemani, F. Wudl, J. Leonetti, R. D. Little and T. White, *Journal of the American Chemical Society,* **1993,** *115*, 1594-1595.
[137] M. Prato, M. Maggini, G. Scorrano and V. Lucchini, *The Journal of Organic Chemistry,* **1993,** *58*, 3613-3615.
[138] M. Maggini, G. Scorrano and M. Prato, *Journal of the American Chemical Society,* **1993,** *115*, 9798-9799.

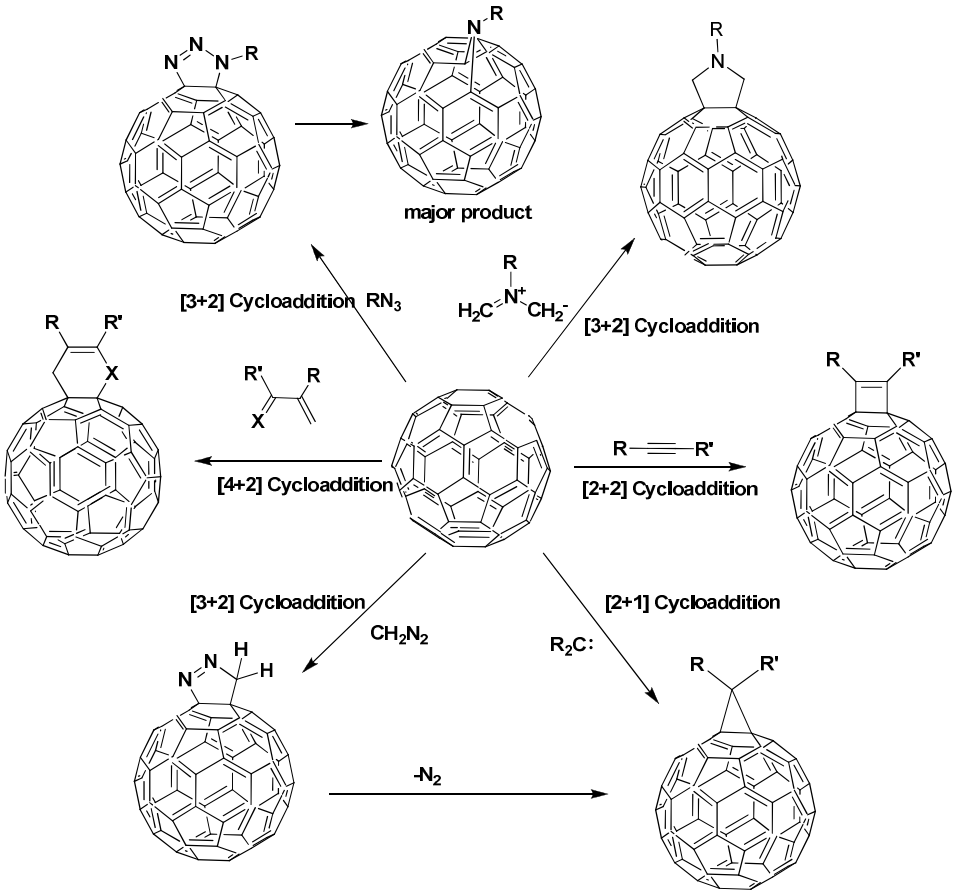

Figure II-11 Different cycloaddition possibilities

Addition of azides

Organic azides can act as 1,3-dipoles and react with a fullerene in a [3+2] cycloaddition to the 6:6 double bonds resulting in a triazole intermediate, which after thermal nitrogen elimination allows the formation of aza-bridge fullerenes. Cases et al.[139] using theoretical calculation suggested a stepwise mechanism in which the N-N bond is cleaved before C-N. During the loss of N_2, the steric effects of the living molecule prevent the addition of the nitrene substituent to the 6:6 bond initially attacked and conduct the addition to a neighboring 5:6 bond. (Figure II-10)

[139] M. Cases, M. Duran, J. Mestres, N. Martín and M. Solà, *The Journal of Organic Chemistry,* **2000,** *66*, 433-442.

Cyclopropanation: Bingel reaction

The cyclopropanation reaction of C_{60} was discovered by C. Bingel[140] in 1993 (Figure II-12) and it involves an addition elimination mechanism involving α-halocarbanion stabilized by the C_{60}.

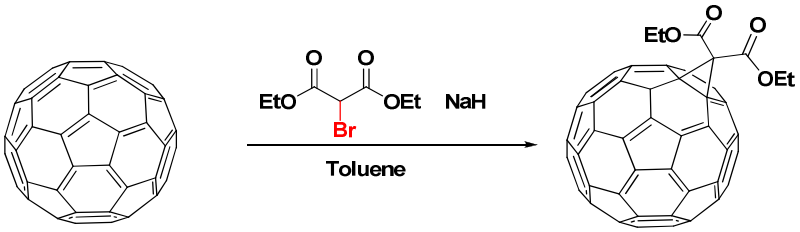

Figure II-12 Bingel reaction: C_{60} cyclopropanation

The mechanism can be divided into two stages: in the first in situ generation of the stabilized α-halocarbanion using as base NaH which allows the nucleophilic attack on C_{60}. The second stage consists of an intramolecular nucleophilic substitution allowing the formation of the cyclopropanation product. (Figure II-13)

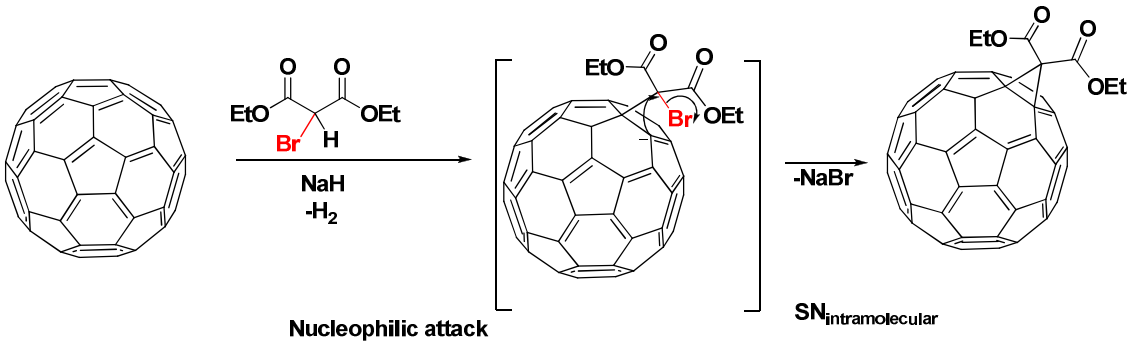

Figure II-13 Bingel reaction mechanism

Alternatives of Bingel's cyclopropanation have been developed by F. Diederich[141] and A. Hirsch[142]. (Figure II-14) These methods involve in situ the generation of iodomalonate or bromomalonate utilizing iodide or CBr_4.

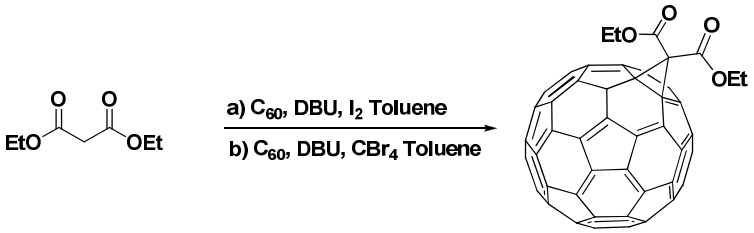

Figure II-14 Alternatives for Bingel's cyclopropanation reaction

[140] C. Bingel, *Chemische Berichte,* **1993,** *126*, 1957-1959.
[141] J.-F. Nierengarten, V. Gramlich, F. Cardullo and F. Diederich, *Angewandte Chemie International Edition in English,* **1996,** *35*, 2101-2103.
[142] X. Camps and A. Hirsch, *J. Chem. Soc., Perkin Trans. 1,* **1997**, 1595-1596.

Prato reaction: Addition of azomethine ylides

This reaction was developed by Prato and Maggini[138] and evolved into one of the most utilized methods for fullerene functionalization. One reason for its intense use is the high selectivity presented; only the 6:6 bond is attacked and a wide range of functional groups are tolerated. The nitrogen atom in the obtained fulleropyrrolidines is about six orders of magnitude less basic and three orders of magnitude less reactive than in the corresponding pyrrolidines without C_{60}[143]. The azomethine ylide can be generated in situ from various materials, one of the easiest approaches to produce them involves the decarboxylation of immonium salts resulted from the condensation of α-amino acids with aldehydes and ketones.

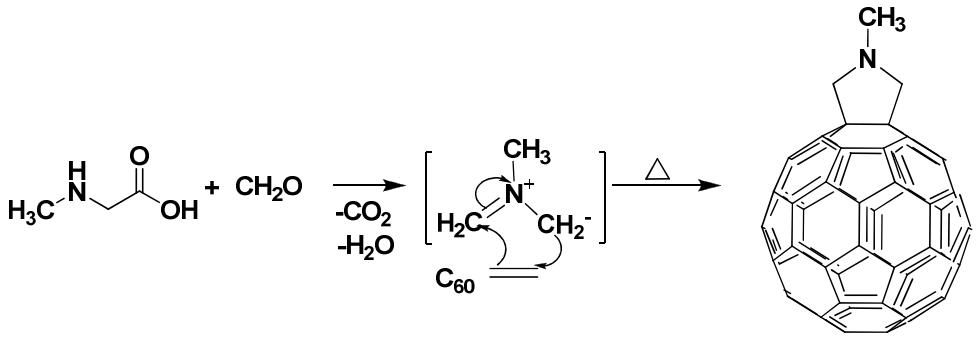

Figure II-15 Example of Prato reaction using paraformaldehyde and sarcosine (N-methylglycine)

IV. *Electroactive systems involving fullerene-C_{60}*

In 1992 Sariciftci et al.[144] proved the existence of a photoinduced intermolecular electron transfer between a conducting polymer and fullerene-C_{60}. This discovery was followed by the developing of many donor-acceptor systems containing C_{60} susceptible of generating electron or energy transfer.

An important step was the synthesis of electroactive dyads involving fullerene-C_{60} displaying an intramolecular electron transfer. The first active fullerene dyad was obtained by Liddell et al.[145] consisting in a porphyrins-C_{60} derivative in which the two components are linked by a bicyclic bridge obtained by Diels-Alder reaction (Figure II-16).). The fluorescence measurements revealed quenching of the porphyrins singlet lifetimes (≤17 ps in toluene) due to single-singlet energy transfer from ^{1}ZnP* (2.1 eV) and $^1H_2P^*$ (1.9 eV) to C_{60}. The lifetime of ZnP-$^1C_{60}^*$ is ~5 ps in toluene, while the singlet lifetime of an appropriate C_{60}

[143] A. Bagno, S. Claeson, M. Maggini, M. L. Martini, M. Prato and G. Scorrano, *Chemistry – A European Journal,* **2002,** *8*, 1015-1023.
[144] C. G. Claessens, U. Hahn and T. Torres, *The Chemical Record,* **2008,** *8*, 75-97.
[145] P. A. Liddell, J. P. Sumida, A. N. Macpherson, L. Noss, G. R. Seely, K. N. Clark, A. L. Moore, T. A. Moore and D. Gust, *Photochemistry and Photobiology,* **1994,** *60*, 537-541.

model compound is 1.2 ns. This quenching is due to electron transfer to yield ZnP^{+}-C_{60}^{-}. In toluene, H_2P-$^1C_{60}^{*}$ is not quenched because the non-polar solvent pushes up the level of the charge separated state. In this solvent, an oxygen-sensitive transient species, assigned to $^3C_{60}^{*}$, with an absorption maximum at 700 nm and lifetime of ~10 μs, was detected using transient absorption spectroscopy. In the more polar benzonitrile, H_2P-$^1C_{60}^{*}$ and ZnP-$^1C_{60}^{*}$ undergo photoinduced electron transfer to give H_2P^{+}-C_{60}^{-} and ZnP^{+}-C_{60}^{-}. These intramolecular photochemical processes can be interpreted as direct through space interaction of the π electron systems, rather than through bond interaction.[146]

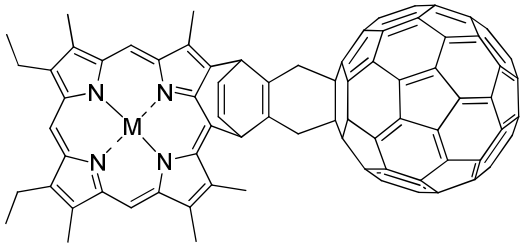

Figure II-16 Dyad C60-porphyrine

Soon after Liddell's dyad, Williams et al. reported the photophysical properties of a dyad system involving aniline derivative and C_{60} (Figure II-17). The photophysical of properties of C_{60}[3]DMA[147] are very solvent dependent presenting fluorescent and phosphorescent properties in methylcyclohexane, but complete emission and triplet quenching in benzonitrile. In solvents of medium polarity, charge recombination to a local C_{60} triplet-state was evidenced.

In the case of C_{60}[3]TMPD[148] a very efficient electron transfer (~95%) was observed in non-polar solvents and there is only a minor solvent dependece. The compound was synthesized using a two phase water/toluene reaction system.

The C_{60}[11]DMA was synthesized by Lawson et al.[149] using a Diels-Alder reaction of fullerene with 1,3-diene presenting the rigid, hybrid saturated polynorbarnane-byciclo[2.2.0] hexane ("norbornylogous") hydrocarbon bridge.

[146] H. Imahori and Y. Sakata, *Advanced Materials,* **1997,** *9*, 537-546.
[147] R. M. Williams, J. M. Zwier and J. W. Verhoeven, *Journal of the American Chemical Society,* **1995,** *117*, 4093-4099.
[148] R. M. Williams, M. Koeberg, J. M. Lawson, Y.-Z. An, Y. Rubin, M. N. Paddon-Row and J. W. Verhoeven, *The Journal of Organic Chemistry,* **1996,** *61*, 5055-5062.
[149] J. M. Lawson, A. M. Oliver, D. F. Rothenfluh, Y.-Z. An, G. A. Ellis, M. G. Ranasinghe, S. I. Khan, A. G. Franz, P. S. Ganapathi, M. J. Shephard, M. N. Paddon-Row and Y. Rubin, ibid., 5032-5054.

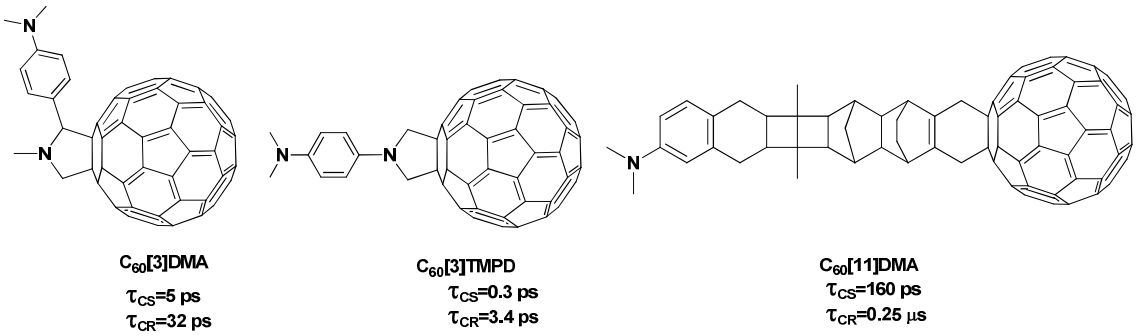

Figure II-17 Aniline and fullerene C_{60} derivatives: C_{60}[3]DMA (DMA-dimethylaniline), C_{60}[3]TMPD (TMPD-N,N,N',N'-tetramethyl-p-phenylene diamine). The characteristic times of charge separation (τ_{CS}) and of charge recombination (τ_{CR}) in benzonitrile and toluene (for C_{60}[3]DMA)are presented.

Other aniline-C_{60} derivatives were obtained and characterized by Thomas et al.[150] (Figure II-18). They studied the effect of orientation on photoinduced electron transfer. In the case of ortho substituted dyads evidence of folding of the aniline group is provided by the ^{1}H NMR studies. Through-space charge transfer processes in these dyads were investigated using steady state fluorescence spectroscopy. The decrease in special distance is reflected in a more efficient electron transfer. The marked increase in the singlet excited state deactivation rate constants and quantum yields of charge separation observed in the case of the ortho-substituted dyads, in benzonitrile, further support a topographically controlled electron transfer process.

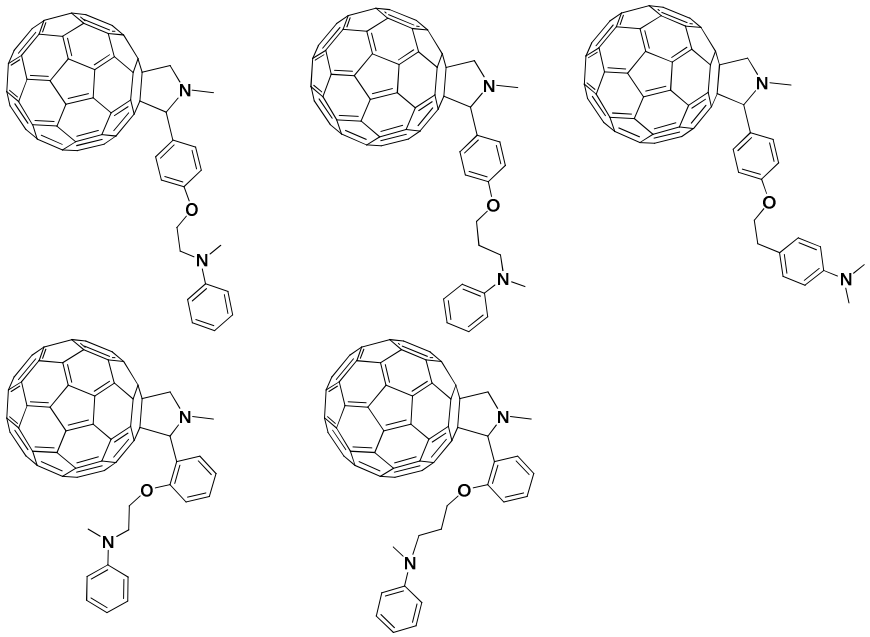

Figure II-18 other aniline-C_{60} derivatives

[150] K. G. Thomas, V. Biju, D. M. Guldi, P. V. Kamat and M. V. George, *The Journal of Physical Chemistry A,* **1999,** *103*, 10755-10763.

Kamat et al.[151] were able to study photoinduced charge separation and stabilization in a fullerene cluster using compound **1** in Figure II-18. Fullerene-aniline dyad, as well as the model fulleropyrolidine form transparent microscopic clusters in mixture (3:1) of acetonitrile and toluene at room temperature. The clusters present a high increase of the extinction coefficients in the visible range. Using steady-state and time-resolved fluorescence studies they concluded that the charge stabilization processes are highly efficient in the clusters of the dyads compared to homogenous medium. The remarkable stability of the charge separated intermediates in the clustered dyad is attributed to electron hopping between the fullerene molecules. The results of the photophysical studies in the clusters illustrate a model for circumventing the back-electron transfer processes in the donor-bridge-acceptor systems.

Another important electron donor that has been covalently bonded to fullerene-C_{60} is ferrocene. In Figure II-19 are presented dyads involving fullerene and ferrocene obtained by Prato reaction[152] and Bingel reaction[153]. Photophysical characterization in toluene of the first set of dyads revealed the formation of the singlet state that undergoes rapid intramolecular quenching caused by an intramolecular electron transfer Fc→C_{60} resulting in the formation of a charge separated state $Fc^{+\cdot}$-$C_{60}^{-\cdot}$. The nature of the spacer between C_{60} and ferrocene was found to determine the quenching mechanism. A through-bond electron transfer characterizes the first two presented examples and a transient intramolecular exciplex for the third system. The last dyad example in Figure II-19 presents liquid-crystal properties. Cholesterol is used as liquid-crystalline promoter. It was found that in such a smectic phase, C_{60} imposes the arrangement of other molecular moieties. Photophysical studies revealed also electron transfer occurs from the donor ferrocene to the accepting fullerene.

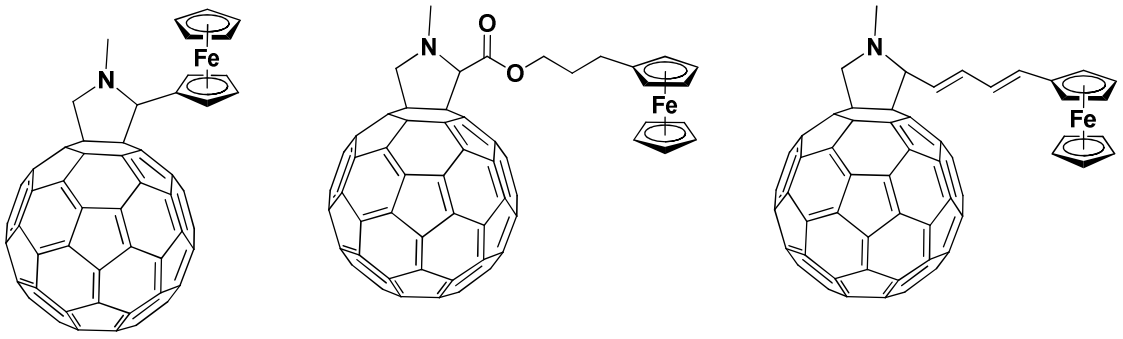

[151] K. G. Thomas, V. Biju, D. M. Guldi, P. V. Kamat and M. V. George, *The Journal of Physical Chemistry B,* **1999,** *103*, 8864-8869.
[152] D. M. Guldi, M. Maggini, G. Scorrano and M. Prato, *Journal of the American Chemical Society,* **1997,** *119*, 974-980.
[153] M. Even, B. Heinrich, D. Guillon, D. M. Guldi, M. Prato and R. Deschenaux, *Chemistry – A European Journal,* **2001,** *7*, 2595-2604.

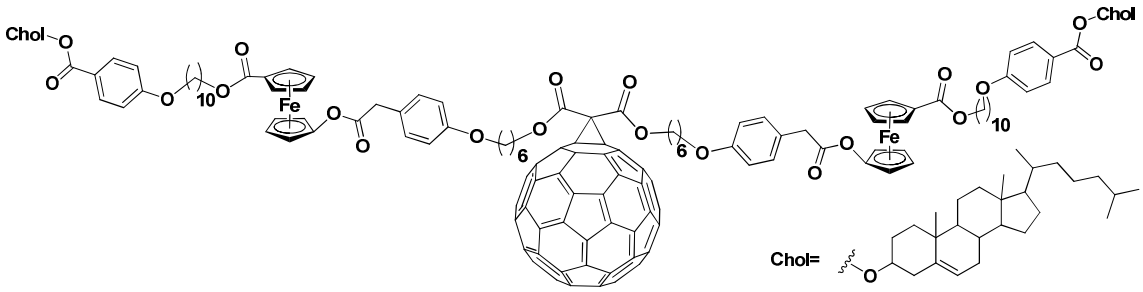

Figure II-19 examples of ferrocene-fullerene dyads

The ferrocene was also attached to fullerene using as a spacer a conducting polymer like polythiophene (Figure II-20)[154]. For the triad Fc-tm-nT-C_{60} two consecutive intramolecular electron transfers take place, in polar solvents, resulting in the formation of a first charge-separated state Fc-tm-nT$^{+\cdot}$- $C_{60}^{-\cdot}$ followed by the second Fc$^{+\cdot}$-tm-nT- $C_{60}^{-\cdot}$. The lifetime of the state depends on the length of the oligothiophene chain ranging from 22 to 330 ns. The triad Fc-nT-C_{60} allows the formation of the species (Fc-nT)$^{+\cdot}$-$C_{60}^{-\cdot}$ in which the positive charge is delocalized on the ferrocene and the oligothiophene and having a lifetime between 0.1 to 50 ns. These results present the importance of the distance in stabilizing the charge-separated state and reducing the charge recombination rate. Another important finding is that the prevention of π-conjugation between the ferrocene and thiophene moieties is more effective for maintaining the lifetime of the charge-separated state than the positive-charge delocalization between the Fc and nT moieties by extending π-conjugation.

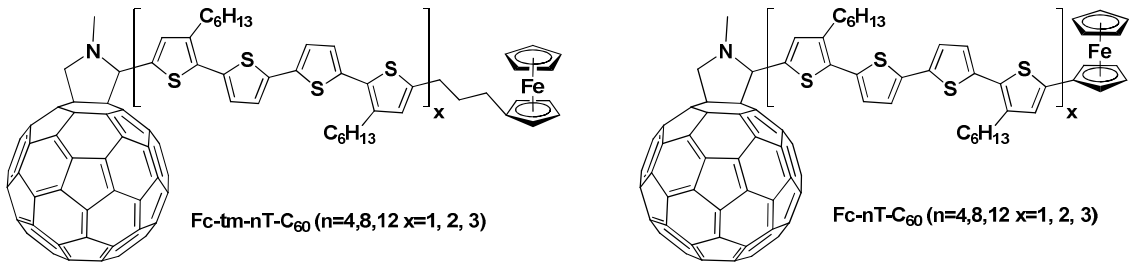

Figure II-20 Triades ferrocene-oligothiophene-C_{60}

Other examples of donors that have been covalently linked to C_{60} include: transition metal complexes[155], oligoacenes[156], carotenoids[157], oligothiophenes[158, 159], oligoacetylenes[160].

[154] T. Nakamura, H. Kanato, Y. Araki, O. Ito, K. Takimiya, T. Otsubo and Y. Aso, *The Journal of Physical Chemistry A,* **2006,** *110*, 3471-3479.
[155] M. Maggini, A. Dono, G. Scorrano and M. Prato, *J. Chem. Soc., Chem. Commun.,* **1995**, 845-846.
[156] J. A. Schlueter, J. M. Seaman, S. Taha, H. Cohen, K. R. Lykke, H. H. Wang and J. M. Williams, ibid. **1993**, 972-974.
[157] H. Imahori, S. Cardoso, D. Tatman, S. Lin, L. Noss, G. R. Seely, L. Sereno, J. C. d. Silber, T. A. Moore, A. L. Moore and D. Gust, *Photochemistry and Photobiology,* **1995,** *62*, 1009-1014.
[158] T. Otsubo, Y. Aso and K. Takimiya, *Journal of Materials Chemistry,* **2002,** *12*, 2565-2575.
[159] B. Jousselme, P. Blanchard, E. Levillain, R. de Bettignies and J. Roncali, *Macromolecules,* **2003,** *36*, 3020-3025.

(Figure II-21 presented in this order) An interesting approach is the obtaining of films by electropolymerization of thiophene derivatives resulting in a conducting polymer with fullerene pending groups.

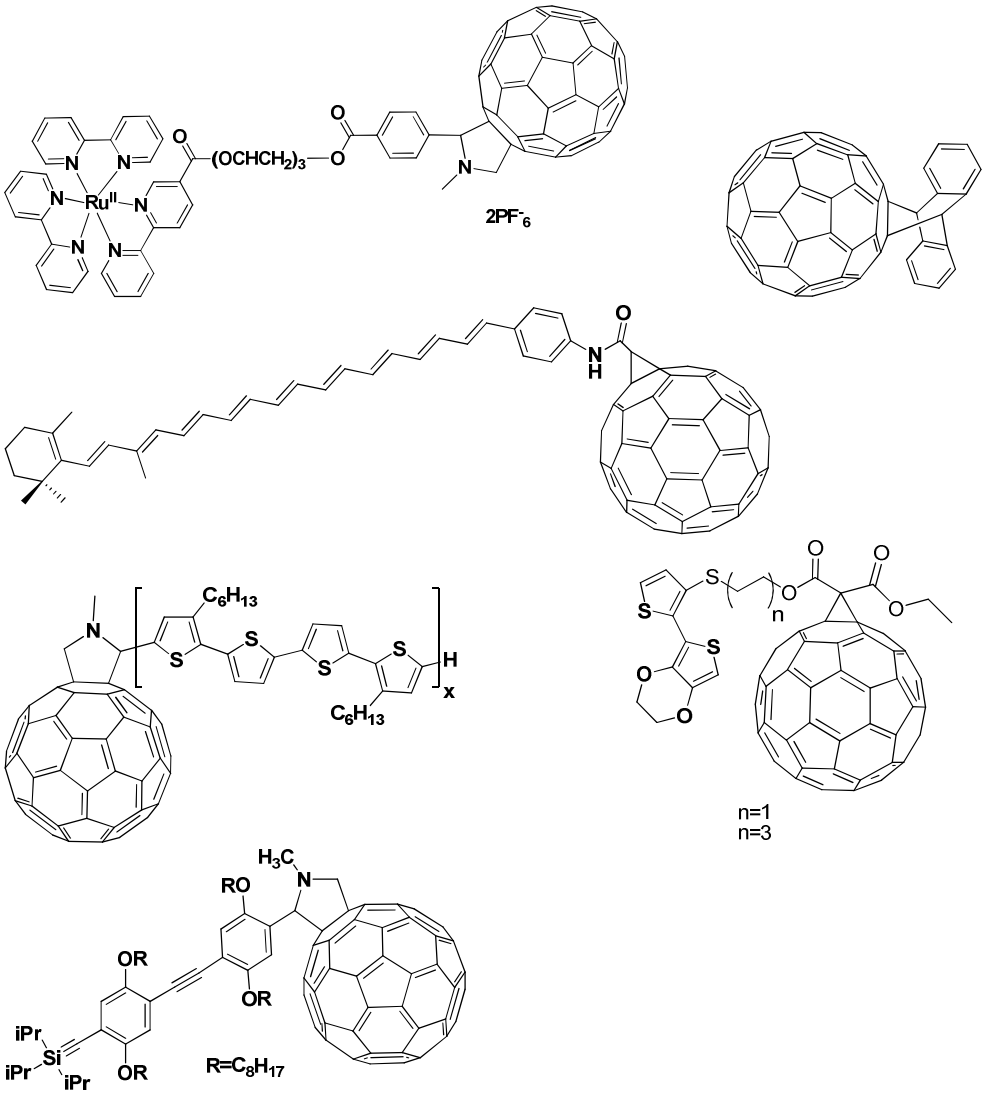

Figure II-21Examples of donors-C60 dyads

In most of the cases presented so far, the donor presents an aromatic character in its ground state that is usually replaced by π-radical cation species upon the transfer to fullerene. Having these transformations in mind, the strong donor tetrathiafulvalene (TTF) proves to be an interesting class of compounds. Thus, the gain of aromaticity associated with the oxidation TTF, to 1,3-dithiolium cations, is an interesting alternative for obtaining photoinduced stabilized charge separated state.[161] Using this approach, many sophisticated TTF-C_{60} dyads, TTF-C_{60}-TTF or C_{60}-TTF-C_{60} triads were synthesized through a flexible space with the aim of

[160] T. Gu and J.-F. Nierengarten, *Tetrahedron Letters,* **2001,** *42*, 3175-3178.
[161] N. Martín, L. Sánchez, B. Illescas, S. González, M. Angeles Herranz and D. M. Guldi, *Carbon,* **2000,** *38*, 1577-1585.

increasing interactions between the chromophores in the ground state and reaching long-lived charge separated radical pair.[162] (Figure II-22)

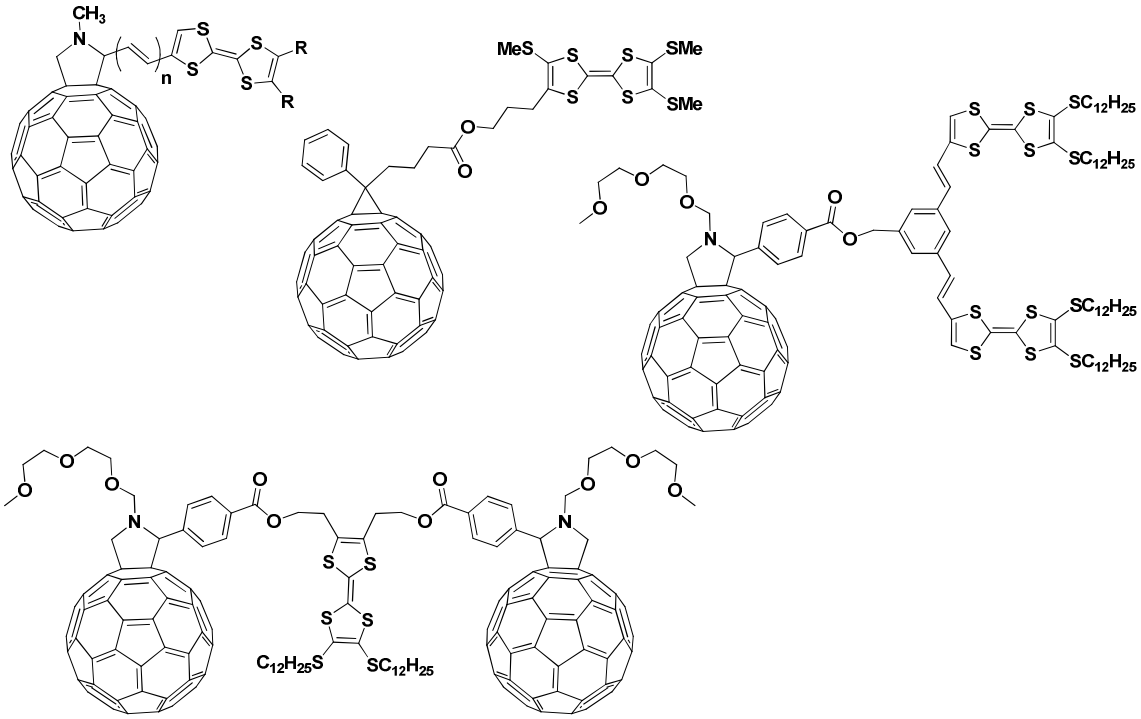

Figure II-22 Examples of TTF-C_{60} dyads, TTF-C_{60}-TTF or C_{60}-TTF-C_{60} triads Experimental

The intramolecular electronic interactions can be either through space or through bond. Thus, following another strategy that consists in controlling the relative orientation and distance between the partners, rigidified TTF-C_{60} dyads, $(TTF)_n$-C_{60}[163] and C_{60}-TTF-C_{60} dumbbell[164] triads were synthesized by [4+2] Diels-Alder cycloaddition. (Figure II-23) Thus, through-space interactions are expected to dominate because of special topology of the compounds with the close proximity and optimal orbital orientation between both units.

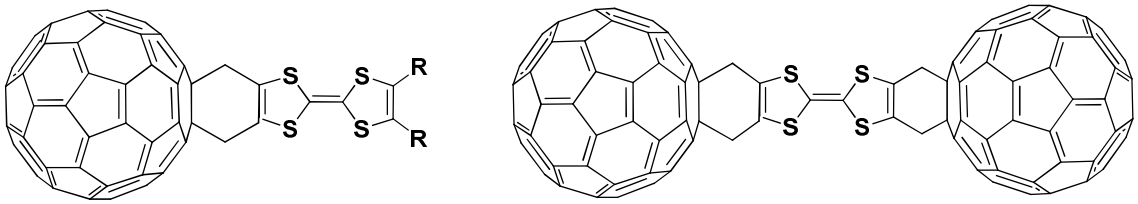

Figure II-23 TTF-C60 dyads and C_{60}-TTF-C_{60} dumbbell

[162] M. Bendikov, F. Wudl and D. F. Perepichka, *Chemical Reviews,* **2004,** *104*, 4891-4946.
[163] D. Kreher, S.-G. Liu, M. Cariou, P. Hudhomme, A. Gorgues, M. Mas, J. Veciana and C. Rovira, *Tetrahedron Letters,* **2001,** *42*, 3447-3450.
[164] S.-G. Liu, D. Kreher, P. Hudhomme, E. Levillain, M. Cariou, J. Delaunay, A. Gorgues, J. Vidal-Gancedo, J. Veciana and C. Rovira, ibid., 3717-3720.

Besides the gain of aromaticity, which leads to a stabilized charge separated state in the case of π-extended TTF derivatives (ex-TTF) Martin et al.[165] introduced the concept of the gain of planarity that also plays an important part. Indeed, the aromatization induced by the oxidation in π-extended TTF with p-quinonoid structures has a strong impact on the stabilization of the charge separated state. In effect, the lifetimes of the charge-separated states in C_{60}-π-extended TTF dyads are increased due to higher stability of the $C_{60}^{-\cdot}$ π-extended-$TTF^{+\cdot}$ pair. A clear example of this effect is present in the case of the triad C_{60}-$exTTF_1$-$exTTF_2$ in which sequential electron transfer by means of adjacent radical pair formation $C_{60}^{-\cdot}$- $exTTF_1^{+\cdot}$- $exTTF_2$ allows ultimately the transformation of the distant radical pair $C_{60}^{-\cdot}$-$exTTF_1$- $exTTF_2^{+\cdot}$ (Figure II-24). The lifetime for the distant radical pair charge separated state was determined to be of 111 μs, which is one of the highest values obtained for electroactive fullerene triads.[166]

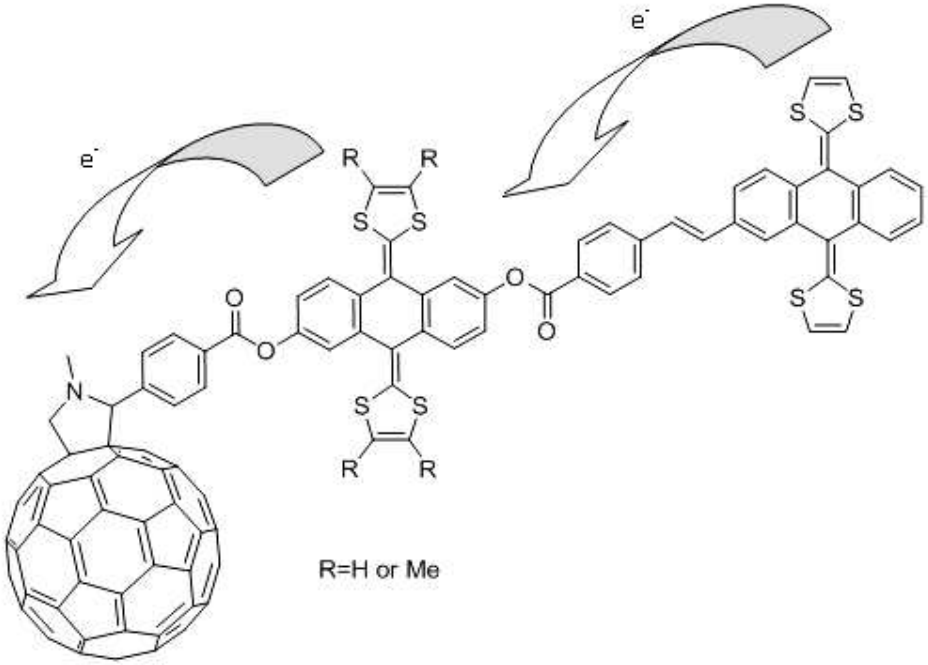

Figure II-24 C_{60} π-extended TTF triad (C_{60}-$exTTF_1$-$exTTF_2$) and cascade electron transfer process

These long-lived radical pairs species are susceptible to play an important role in future applications, mainly in organic solar cells.[167] Using covalent donor-C_{60} systems in solar cells, problems like phase segregation and clustering phenomena of fullerenes in bulk-

[165] N. Martin, L. Sanchez and D. M. Guldi, *Chemical Communications,* **2000**, 113-114.
[166] L. Sánchez, I. Pérez, N. Martín and D. M. Guldi, *Chemistry – A European Journal,* **2003,** *9*, 2457-2468.
[167] N. Martín, L. Sánchez, M. a. Á. Herranz, B. Illescas and D. M. Guldi, *Accounts of Chemical Research,* **2007,** *40*, 1015-1024.

heterojunction can be solved. This molecular approach also makes possible the correlation between structure and property in series of conjugated structures, thus allowing the fine tuning of important parameters such as the ratio, the distance, the relative orientation and the attachment mode the donor and acceptor moieties. A first example of using this approach is the utilization of oligophenylenevinylene (OPV) moiety covalently linked to C_{60}, specifically designed for use in photovoltaic conversion as molecular heterojunction, developed by Nierengarten et al.[168]

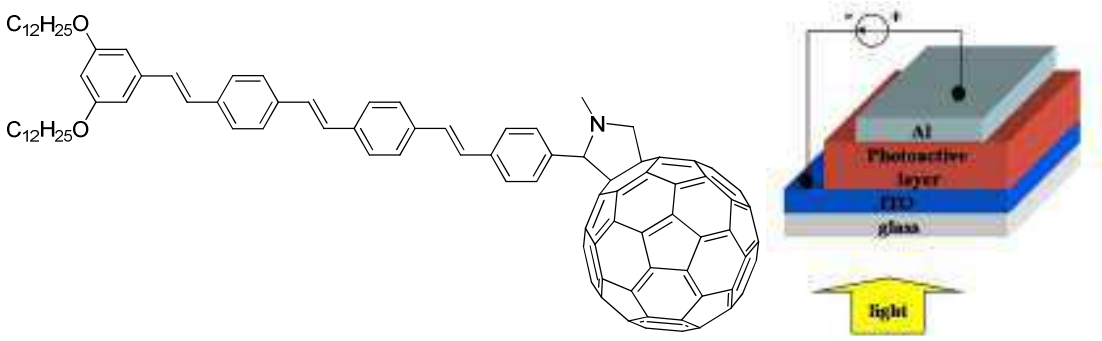

Figure II-25 OPV-C60 dyad and its use in organic solar cells

The device ITO/OPV-C_{60}/Al presented low power conversion efficiency (ICPE) of 0.01% under monochromatic irradiation (400 nm, 12 mW cm^{-2}). By increasing the length of the OPV chain from three to four units resulted in an increase of the efficiency up to 0.03%. The low overall efficiency of these devices was assigned to the competition between energy and electron transfer.[169]

The importance of the absorption parameter was proved by using an azothiophene-fullerene dyad that displays a wide absorption spectrum in the visible range at about 570 nm. The obtained device had an efficiency of 0.37% under white light-irradiation with an intensity of 80 mW cm^{-2}.[170] (Figure II-26) Although the good results, this approach is limited by the energy transfer that replaces the electron transfer in this type light-harvesting donor-C_{60} dyads. A solution for compensating this effect is combination with a donor polymer like poly 3-hexylthiophene (P3HT).[171]

[168] J.-F. Nierengarten, J.-F. Eckert, J.-F. Nicoud, L. Ouali, V. Krasnikov and G. Hadziioannou, *Chemical Communications,* **1999**, 617-618.
[169] J.-F. Eckert, J.-F. Nicoud, J.-F. Nierengarten, S.-G. Liu, L. Echegoyen, F. Barigelletti, N. Armaroli, L. Ouali, V. Krasnikov and G. Hadziioannou, *Journal of the American Chemical Society,* **2000,** *122*, 7467-7479.
[170] M. Maggini, G. Possamai, E. Menna, G. Scorrano, N. Camaioni, G. Ridolfi, G. Casalbore-Miceli, L. Franco, M. Ruzzi and C. Corvaja, *Chemical Communications,* **2002**, 2028-2029.
[171] C. M. Atienza, G. Fernandez, L. Sanchez, N. Martin, I. S. Dantas, M. M. Wienk, R. A. J. Janssen, G. M. A. Rahman and D. M. Guldi, ibid. **2006**, 514-516.

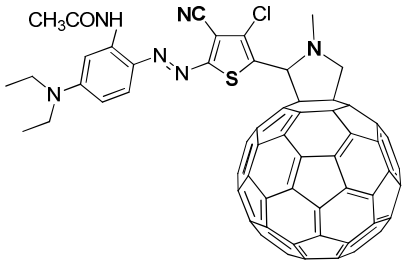

Figure II-26 Light-harvesting donor-C_{60} dyad

V. *Light-harvesting C_{60} –based dyads*

Photosynthesis is one of the most important natural processes, representing one of Nature's solutions to the need of energy in organisms' development and evolution. Thus, the understanding and mimicry of photosynthesis represents an important goal for scientists. They designed artificial light-harvesting antenna searching to achieve energy transfer over a long distance to a defined point. The uses of these antennas are not limited to understanding the photosynthesis process but can also find applications in photovoltaics, field-effect transistors and light-emitting devices. Due to the poor absorption of fullerenes in the visible region, the development of C_{60}-based dyads where the chromophoric units act as an electron donor was the focus of many researches.

1. Phthalocyanine-fullerene C_{60} light-harvesting dyads state of the art

As presented before porphyrins have been a logical choice in the attempt to create photoactive dyads with the intent to mimic nature. A similar choice is represented by the phthalocyanine chromophores which have the advantage of higher stability and increased absorption characteristic in the visible region due to their Q-bands. Another advantage of these types of systems is the minimal structure changes that follow electron injection. In order to minimize the morphological problems of the bulk-heterojunctions, such photoactive dyad has been incorporated into photovoltaic blends, but efficiencies are still very low.[172]

The first reported compound **A** was constructed by Hirsch et al in 1997 by using covalently linked phthalocyanine (Pc) and fullerene **(**Figure II-27)[173]. In phthalocyanine - fullerene dyads such as **B**[174] (Figure II-27), the role of the phthalocyanine is dual: first if

[172] P. Vivo, M. Ojala, V. Chukharev, A. Efimov and H. Lemmetyinen, *Journal of Photochemistry and Photobiology A: Chemistry,* **2009,** *203*, 125-130.
[173] T. G. Linssen, K. Durr, M. Hanack and A. Hirsch, *J. Chem. Soc., Chem. Commun.,* **1995**, 103-104.
[174] D. M. Guldi, A. Gouloumis, P. Vazquez and T. Torres, *Chemical Communications,* **2002**, 2056-2057.

functions as an antenna and then upon photoexcitation it acts as an electron donor to the fullerene. The initial photoexcitation is succeeded by an ultrafast electron transfer largely due to the strong electronic coupling between electron donor (Pc) and electron acceptor C_{60} generating radical ion pairs $Pc^{+\bullet}$-$C_{60}^{-\bullet}$ with lifetimes of several nanoseconds depending on the central metal atom and the solvent in which the measurements are conducted.[175] In the case of triad **C,** due the presence of an supplementary accepting fullerene unit, longer lifetime for the charge separated state were obtained, reaching up to 21 ns (in toluene).[176]

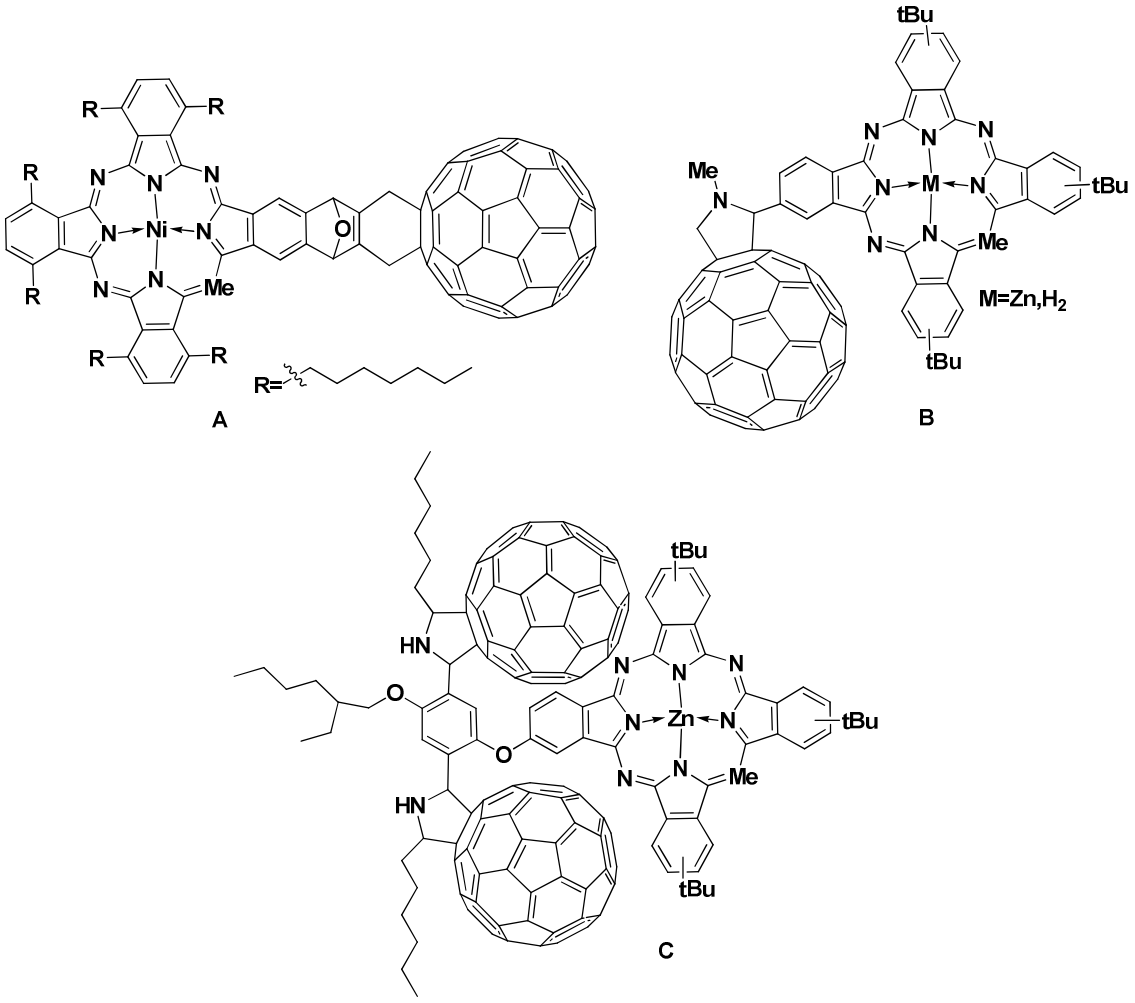

Figure II-27 Systems involving C_{60} and phthalocyanines

An interesting approach was to study the series presented in Figure II-28, in order to determine the influence of the spacer on the photoinduced electron transfer properties. The

[175] D. M. Guldi, I. Zilbermann, A. Gouloumis, P. Vázquez and T. Torres, *The Journal of Physical Chemistry B,* **2004,** *108*, 18485-18494.
[176] A. Gouloumis, A. de la Escosura, P. Vázquez, T. Torres, A. Kahnt, D. M. Guldi, H. Neugebauer, C. Winder, M. Drees and N. S. Sariciftci, *Organic Letters,* **2006,** *8*, 5187-5190.

dyads in Figure II-28 have been obtained by Quintiliani et al.[177] by using a synthesis strategy involving palladium-catalyzed cross-coupling reactions using monoiodo phthalocyanine to introduce the corresponding spacer, and subsequent Prato cycloaddition. The photophysical investigations proved the intramolecular electron transfer that takes place between the photoexcited ZnPc and C_{60}. The lifetimes of the corresponding formed radical ion pairs state depend on the solvent polarity: they increase as polarity decreases. Although the impact of the spacer (single, double or triple bound) on the charge-separated lifetimes is rather low, the triple bond system shows the highest lifetime.

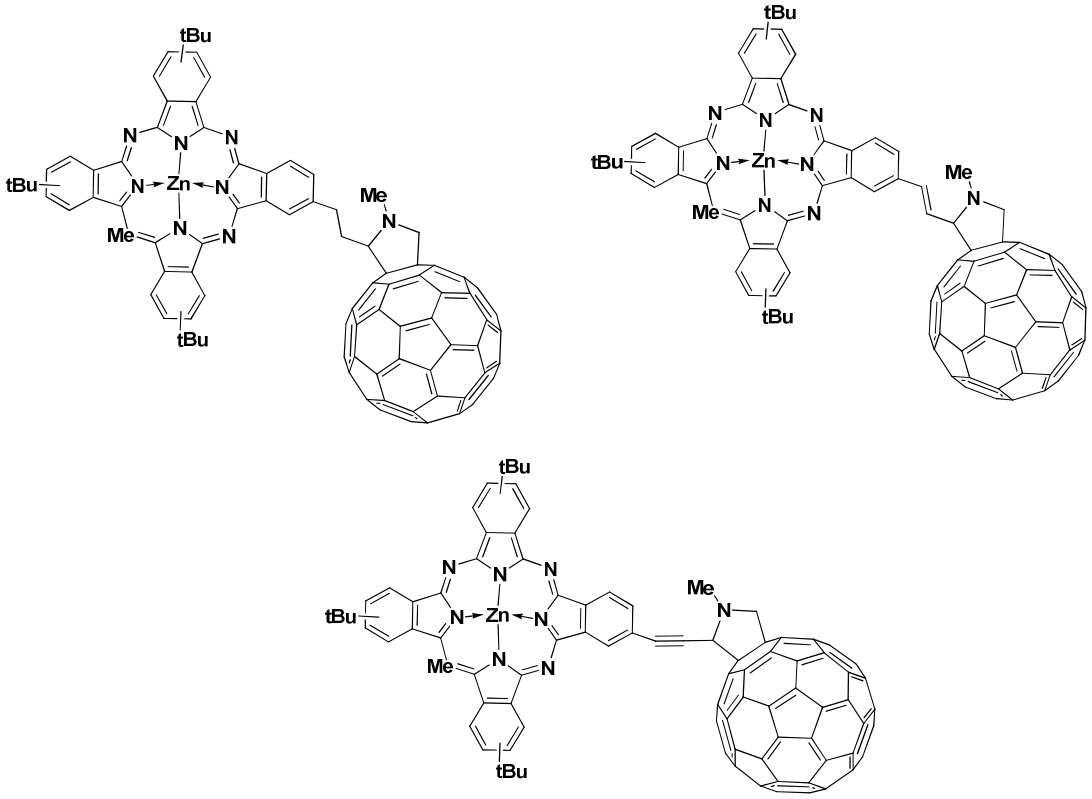

Figure II-28 ZnPc-C60 dyads with different spacers

An important characteristic of phthalocyanines is that in general the phthalocyanine macrocycle has a tendency to organize itself forming stacks in which there is an interaction between the large π-systems of adjacent rings, π-stacking. This characteristic leads to the obtaining of materials with metal-like properties behaving as one-dimensional semiconductors.[178]

The formation of long-range ordered assembly using the donor-acceptor system involving phthalocyanine-fullerene has also been investigated. One example of

[177] M. Quintiliani, A. Kahnt, T. Wölfle, W. Hieringer, P. Vázquez, A. Görling, D. M. Guldi and T. Torres, *Chemistry – A European Journal,* **2008,** *14*, 3765-3775.
[178] T. J. Marks, *Angewandte Chemie International Edition in English,* **1990,** *29*, 857-879.

supramolecular structure obtained from the assembly of the dyad is the 1D highly oriented nanotubules obtained by Guldi et al.[179] (Figure II-29). The self-assembling of the dyad may be due to the hydrophobic/hydrophilic nature of the components and also to possible π-π stacking interaction. The photoreactivity in terms of ultrafast charge separation and ultraslow charge recombination is remarkable. The charge separated lifetime is around 1.4 ms, compared to that of the monomeric ZnPc-C_{60} of about 3 ns, an impressive stabilization 6 order of magnitude.

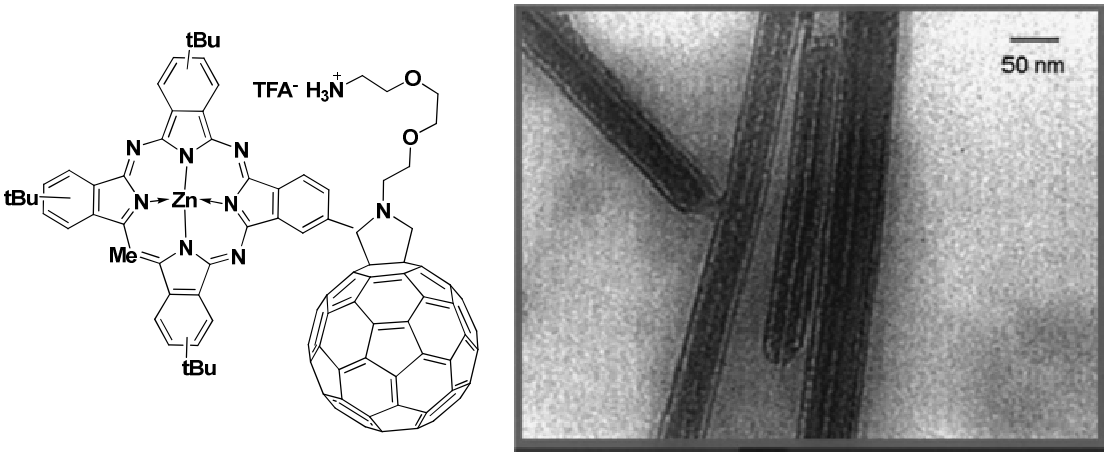

Figure II-29 Dyad structure and nanotubes formed in water and deposited on a TEM grid

The organization properties of the dyads have been also investigated on the surface of solids, one such example is presented in Figure II-30. The organization property of the donor-acceptor Pc-C_{60} dyad on highly oriented pyrolitic graphite was investigated by atomic force microscopy[180]. These studies revealed the formation of layers and micrometer-long fibers the hight and density of the latter being strongly dependent on the concentration of the drop-cast solution. The electrical properties of these supramolecularly assembled nanostructured architectures were also probed, obtaining outstanding electrical conductivity values, which were found to be related to the extremely high degree of molecular order of the Pc C60 conjugates within the nanostructures.

[179] D. M. Guldi, A. Gouloumis, P. Vázquez, T. Torres, V. Georgakilas and M. Prato, *Journal of the American Chemical Society,* **2005,** *127*, 5811-5813.
[180] G. Bottari, D. Olea, C. Gómez-Navarro, F. Zamora, J. Gómez-Herrero and T. Torres, *Angewandte Chemie International Edition,* **2008,** *47*, 2026-2031.

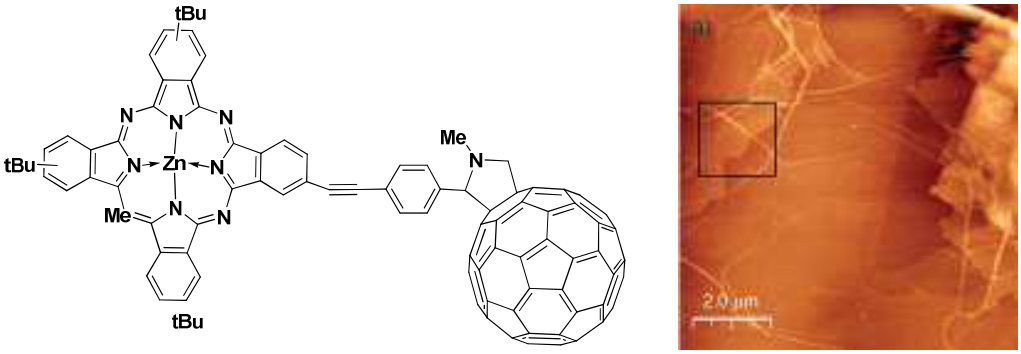

Figure II-30 Dyad structure and AFM topographic images of dyad drop-casted on highly oriented pyrolytic graphite

Phthalocyanine-fullenere dyads have been also prepared by utilizing the metal center of the phthalocyanine. Examples are presented in Figure II-31. In the first example a catechol derivative is used to axial coordinate the titanium metal center. This has been obtained independently by two groups Torres[181] et al and Ito et al.[182]. The charge separated lifetime was measured at ~2 µs. The presence of Ru as the metal center in the phthalocyanine allows one or two ligands to be attached in the axial positions; an example of an obtained triad utilizing pyridine[183] for coordination is presented in Figure II-31. The triad has shown an excellent redox behavior.

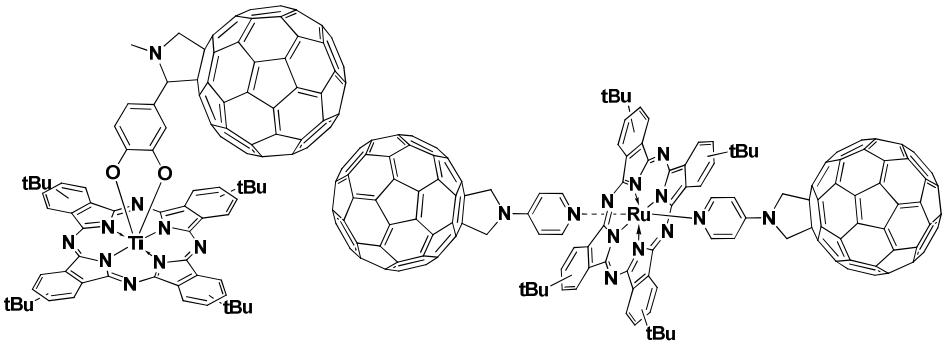

Figure II-31 Pc-C_{60} dyads utilizing the metal center

Recently, Bottari et al.[180] published a review article presenting the different synthetic strategies that have been pursued so far in the preparation of D-A phthalocyanine, subphthalocyanine and carbon nanostructures systems.

[181] B. Ballesteros, G. de la Torre, T. Torres, G. L. Hug, G. M. A. Rahman and D. M. Guldi, *Tetrahedron,* **2006,** *62*, 2097-2101.
[182] Y. Chen, M. E. Ei-Khouly, M. Sasaki, Y. Araki and O. Ito, *Organic Letters,* **2005,** *7*, 1613-1616.
[183] M. S. Rodríguez-Morgade, M. E. Plonska-Brzezinska, A. J. Athans, E. Carbonell, G. de Miguel, D. M. Guldi, L. Echegoyen and T. s. Torres, *Journal of the American Chemical Society,* **2009,** *131*, 10484-10496.

2. New phthalocyanine-fullerene derivatives (Original Contribution)

This part of the chapter will present the synthesis and characterization of some new phthalocyanine-fullerene derivatives. The attachment of the phthalocyanine derivatives on the fullerene has been realized using nucleophilic addition of amine phthalocyanine moieties or using azide groups cycloaddition reactions to fullerene.

The nucleophilic addition of amines to fullerene, as mentioned before (Reaction with amines), usually results in complex mixtures of aminoadducts. Thus, we opted to use tetraamino or tetraazide derivatives in combination with fullerene in order to obtain polymer-like structures involving the two components. (Figure II-32)

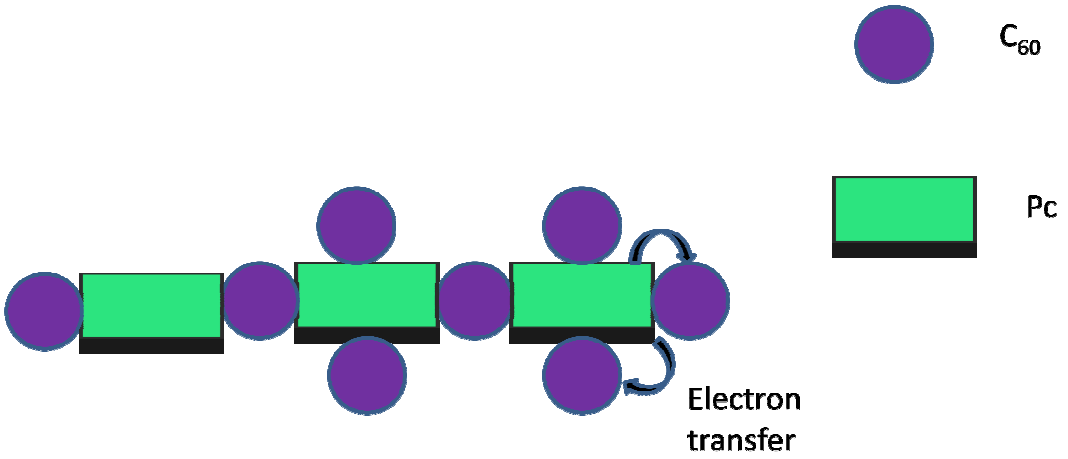

Figure II-32 Pc-C_{60} polymer-like structure

The first objective was to obtain the tetraaminophthalocyanine zinc (II) (**F0**), which was then reacted with fullerene (**F1**). The synthesis of **F0** was realized in two steps using 4-nitrophtalonitrile to obtain the tetranitrophthalocyanine zinc (II) which was then reduced using Na_2S (Figure II-33).

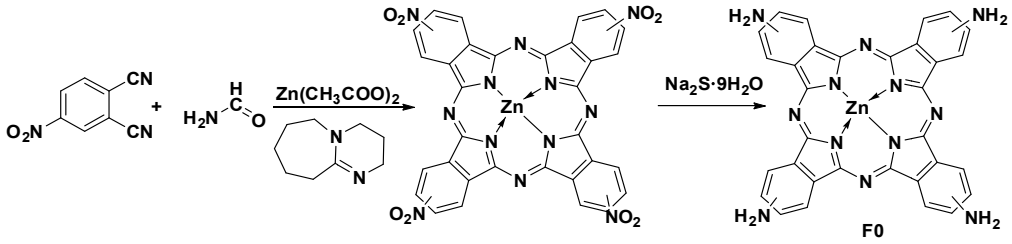

Figure II-33: Tetraamino phthalocyanine zinc (II) synthesis (isomers mixture)

The derivative **F2** resulted from the reaction between the tetraaminophthalocyanine zinc (II) (**F0**) and fullerene-C_{60} (**F1**). The synthesis and a possible structure are presented in

Figure II-34. The structure of **F2** allows subsequent attachment of phthalocyanine derivatives to the fullerene pending groups allowing the formation of a polymer-like structure. In parallel, the reaction was performed using a monoaminophthalocyanine zinc (II) affording compound **F4**.

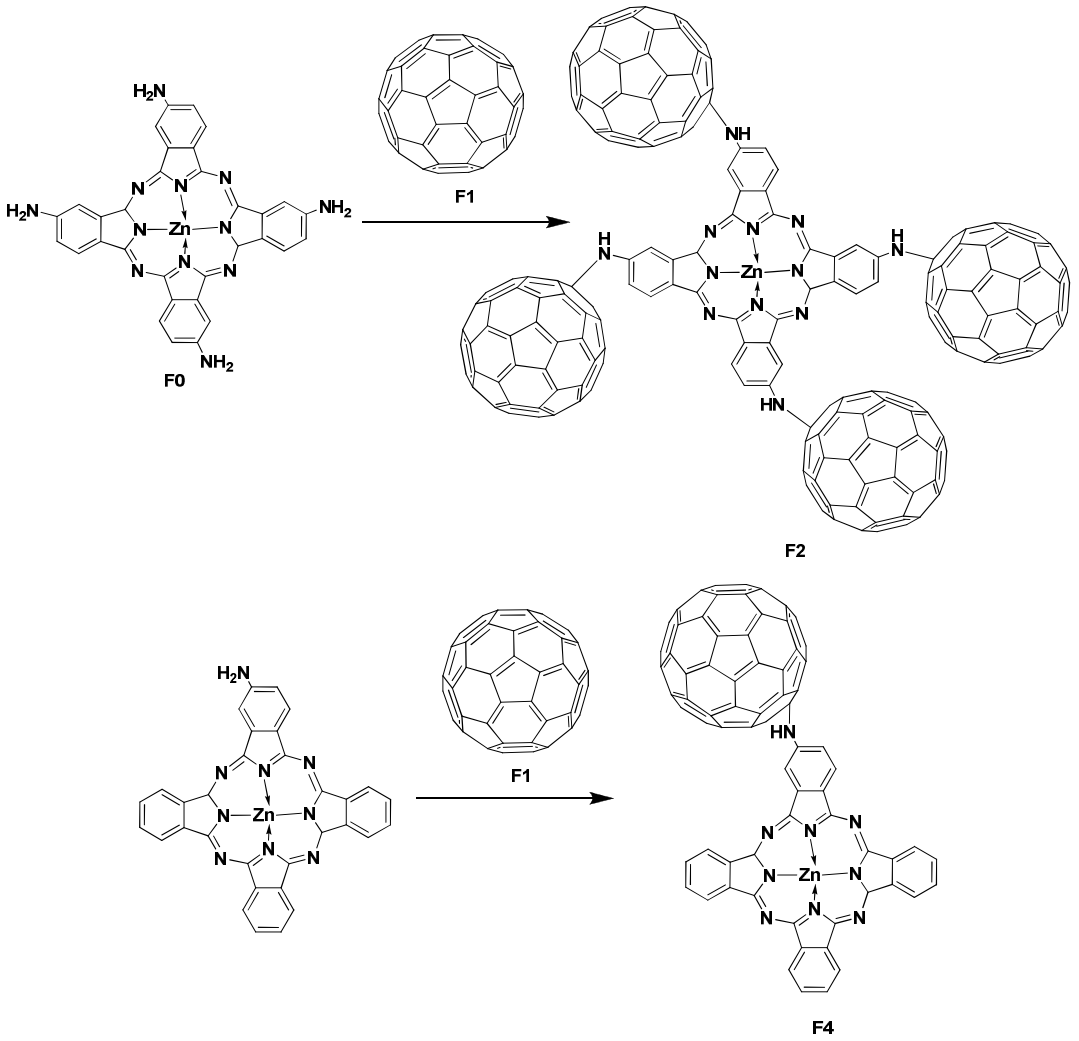

Figure II-34: Synthesis of F2, F4 fused adducts (possible structures)

The second alternative for covalently linking the phthalocyanine to the fullerene moiety has been through the use of a short spacer. This spacer has been obtained by reacting **F0** with epichlorohydrin and then the chlorine atom has substituted by an azide group which can easily react with fullerene. The azide high reactivity with fullerene allows also the obtaining of the envisaged polymer-like adducts. The spacer was introduced in order to study its effects on properties of the materials and also because the cycloaddition reaction of the azide to the fullerene is an efficient reaction.

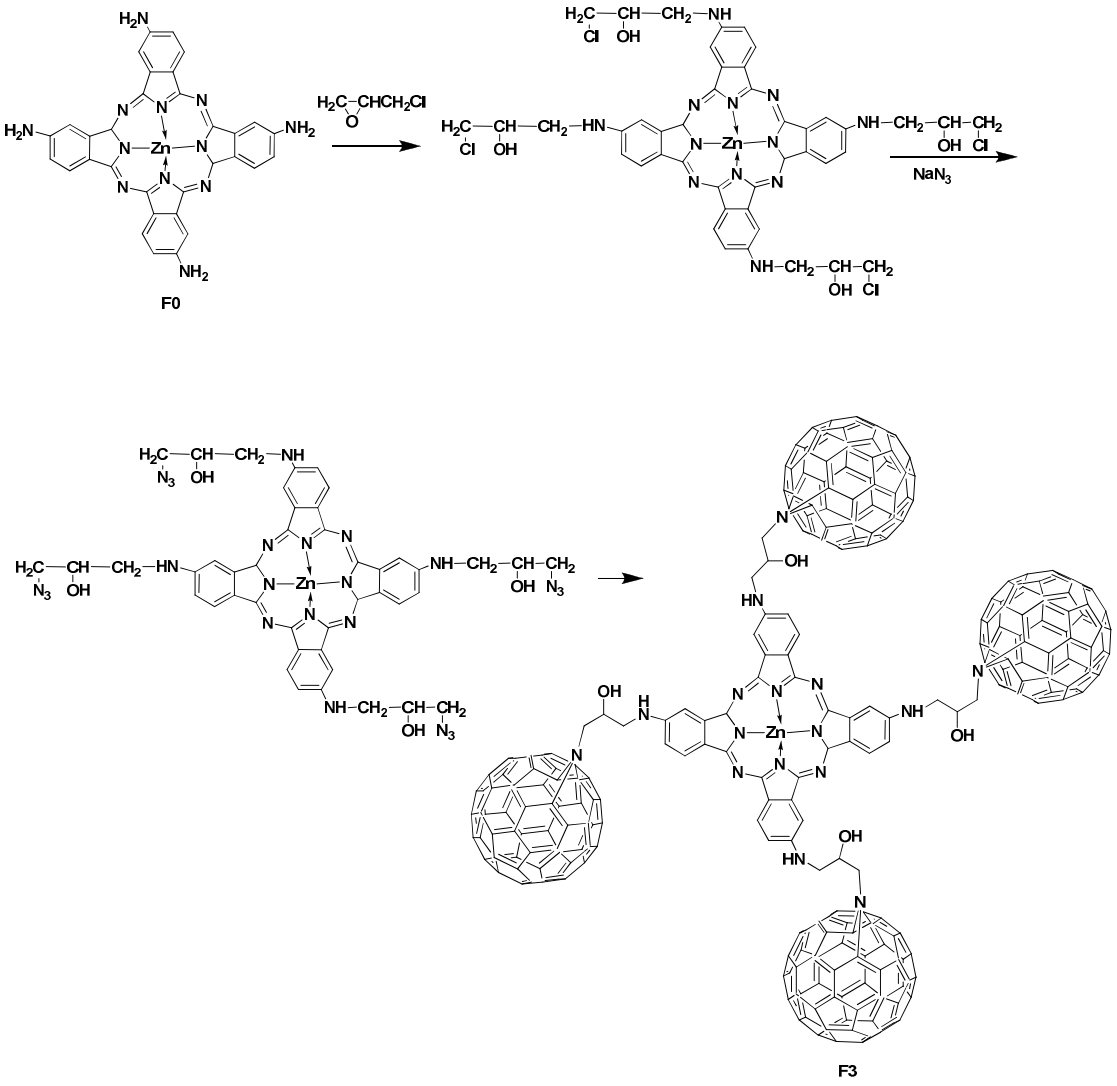

Figure II-35: Short spacer fullerene/phthalocyanine adducts (possible structures)

The first step in the study of the obtained compounds was the characterization of **F0** by IR and RAMAN spectroscopy, since synthesis method used is original. The IR spectra have shown signals at: 3326 cm^{-1} (NH_2), 3209 cm^{-1} (NH_2), 1604 cm^{-1} (C-N), 1487-1400 cm^{-1} (C-C aromatic), 1300-1400 cm^{-1} (C-H) which correspond to literature data[184].

[184] F.-D. Cong, B. Ning, X.-G. Du, C.-Y. Ma, H.-F. Yu and B. Chen, *Dyes and Pigments,* **2005,** *66*, 149-154.

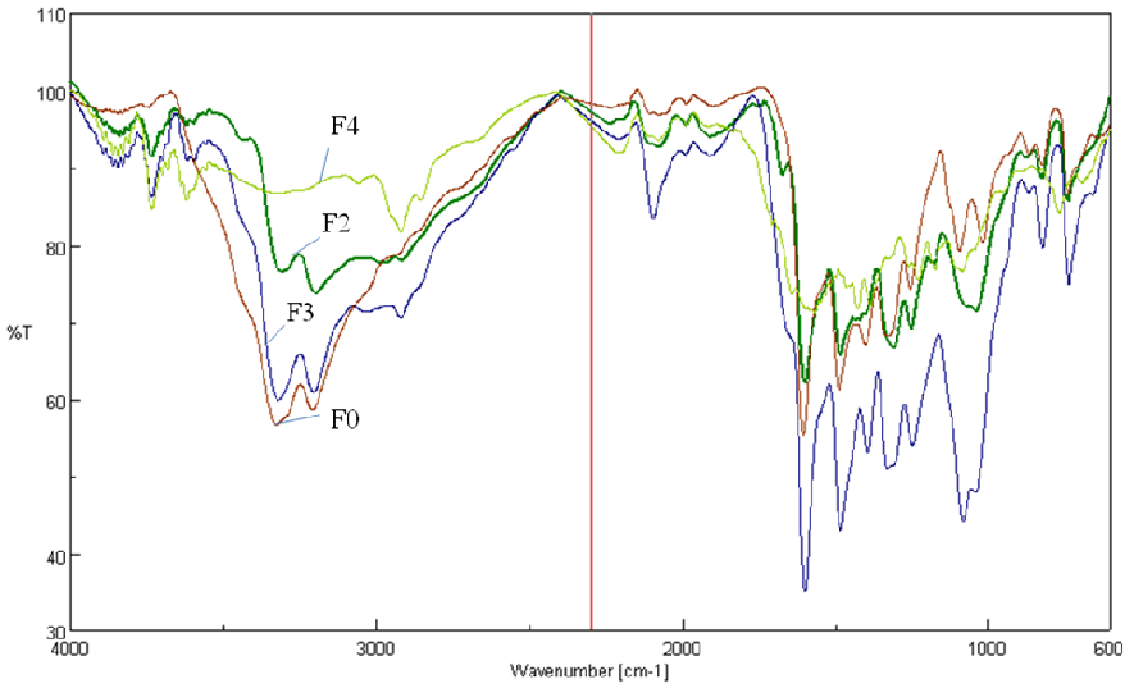

Figure II-36: IR spectra for F0, F2, F3 and F4

For the compound **F3**, the intermediates were characterized using IR spectroscopy. For the epichlorohydrin derivative signals at 3326 cm^{-1} (NH_2), 3209 cm^{-1} (NH_2), 1604 cm^{-1} (C-N), 1487-1400 cm^{-1} (C-C aromatic), 1300-1400 cm^{-1} (C-H), 650 cm^{-1} (C-Cl) have been registered. For the azide derivative the signal characteristic for the N≡N vibration at 2200 cm^{-1} was shown in the IR spectra.

To study the chemical linking of **F0** to the C_{60} in the case of all the dyads IR spectroscopy has been used as first investigation technique (Figure II-36). The characteristic signals for the amino group and the phthalocyanine were present in the spectra.

Another investigation technique used to characterize the adducts has been the RAMAN spectroscopy. The characteristic peaks for **F0** in RAMAN spectroscopy are: 700-900 cm^{-1} macrocycle ring stretching vibration[185], bending vibrations of the C-H groups 1000 to 1300 cm^{-1} and 1500 cm^{-1} for the symmetric NH_2 deformations[186]. For all adducts a change has been noticed in the interval 600-800 cm^{-1}, compared to the phthalocyanine spectrum. The change consists in an increase of the intensity at ≈ 750 cm^{-1}. This could be explained by the increase of the C-C bonds number; this corresponds to one of the characteristic signals of the fullerene (772 cm^{-1}). The other characteristic peaks are similar to those for the **F0** compound,

[185] R. Aroca, C. Jennings, G. J. Kovac, R. O. Loutfy and P. S. Vincett, *The Journal of Physical Chemistry,* **1985,** *89*, 4051-4054.
[186] M. Diem, P. L. Polavarapu, M. Oboodi and L. A. Nafie, *Journal of the American Chemical Society,* **1982,** *104*, 3329-3336.

with small shifts in the response. The RAMAN signals corresponding to the fullerene-C_{60} are at 275 cm^{-1}, 496 cm^{-1}, 772 cm^{-1} and 1467 cm^{-1}. (Figure II-37).

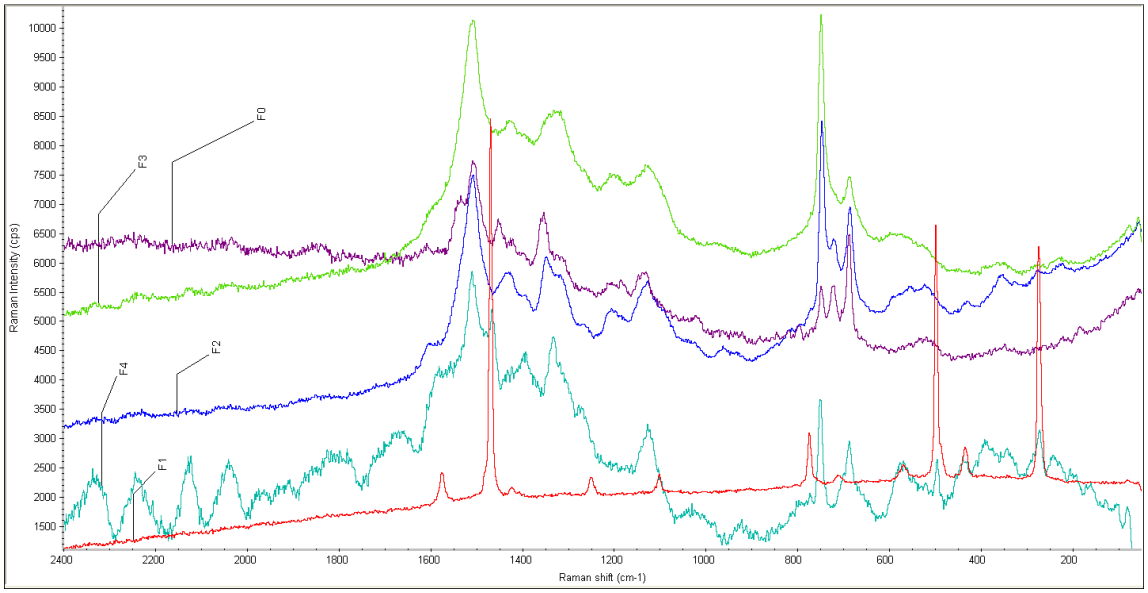

Figure II-37: RAMAN spectra for F0, F1, F2, F3, F4

In the case of UV-VIS spectroscopy (Figure II-38), characteristic for **F0** is the absorption at 717 nm corresponding to the Q band, compared to the fullerene which has characteristic high absorbance in the UV range at 295 nm and 334 nm and only a very weak response at 407 nm and in the visible range 430-650 nm. By comparing the absorption of the **F2**, **F3** and **F4** a different degree of modification with fullerene can be noticed, resulting from the modification of the absorption intensity of each moiety. Considering that the intensity is directly proportional with the concentration of the excited components, the ratio between the intensity of the peaks corresponding to the absorption of the fullerene moiety and the Q band intensity decreases in the order **F4**>**F2**>**F3**. There was also a small bathochromic shift in the Q band absorption value compared with the **F0**, which is due to the loss of symmetry of the phthalocyanine moiety.

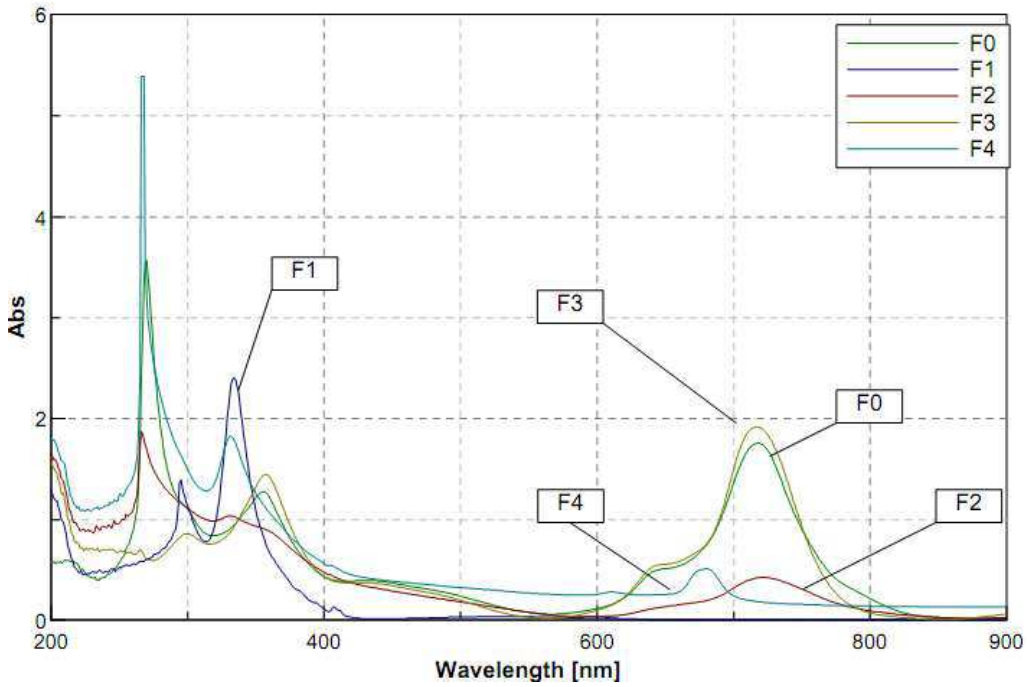

Figure II-38: UV-VIS spectra for F0, F1, F2, F3 and F4

To further study the optical properties of the compounds the next step for their characterization was fluorescence spectroscopy. Using this technique, the wavelength of the emitted light on the irradiation of a sample with a monochromatic light is recorded (emission spectra). The 3D spectra are obtained by recording all the emission spectra for an interval of excitation wavelengths. In the present case, the fluorescence modification gives an insight into the interactions between the phthalocyanine and fullerene moieties since a donor-acceptor interaction is usually coupled with a fluorescence quenching.

In the fluorescence spectra recorded for the compound **F0**, the most important signal is in the emission range of 730-770 nm for an excitation wavelength of 700-750 nm. For **F3** the same characteristics are present, with a quenching of the fluorescence. In contrast, for **F2** and **F4**, new signals are observed. In the case of **F2** for an excitation wavelength of 280-440 nm, the compound emits in the range of 500-570 nm and 800-880 nm. For **F4** the conservation of the emission at 800-880 nm was noticed.

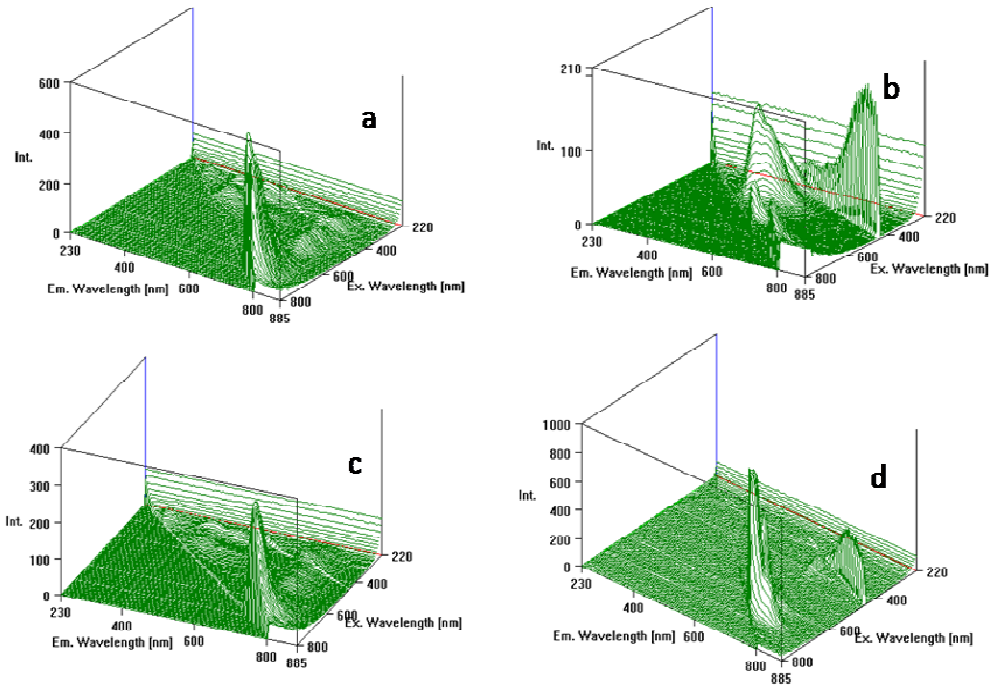

Figure II-39: Fluorescence 3D spectra for a) F0, b) F2, c) F3 and d) F4

Both the UV-VIS and the fluorescence spectroscopy prove the influence of the linkage of the C_{60} on spectroscopic properties of the compounds revealing changes both in absorption and fluorescence properties.

TGA analysis has been used to study the thermal stability of the materials (Figure II-40). High temperature stability has been obtained, which is a characteristic of phthalocyanines[187], and the thermal resistance was directly proportional to the quantity of fullerene attached (noticed when comparing **F2** to **F4**). The high stability of **F0** may be due to its symmetry and the electron donor effect of the amino group, both elements that are disrupted in the case of **F2**. Although the addition of the C_{60} should have as a result an increasing of the thermal stability of the molecule, the symmetry and the electron-donor properties of the substituting groups on the phthalocyanine have a more important role in the overall stability of the adduct.

[187] T. M. M. Kumar and B. N. Achar, *Journal of Organometallic Chemistry,* **2006,** *691*, 331-336.

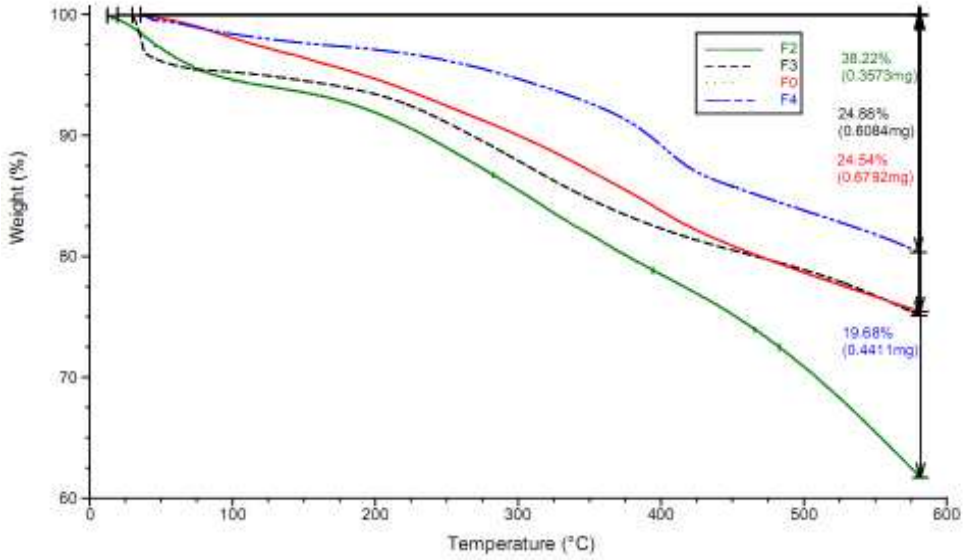

Figure II-40: TGA analysis F0, F2, F3 and F4

Further analyses including cyclic voltammetry or MALDI-TOF have not been possible due to the low solubility of the materials, this characteristic supporting a high mass adduct possibility.

In conclusion phthalocyanine-fullerene adducts have been obtained. The fluorescence quenching observed for the obtained compounds suggests a donor-acceptor interaction between phthalocyanine and fullerene. The linking possibility and reaction types, between the two components, have been chosen in order to obtain polymer-like structures. Differences in the fluorescence properties of compounds involving direct linking and the ones with a short spacer have been observed. RAMAN spectroscopy has also been used for the characterization of adducts.

The thermal stability of the compounds has also been studied using thermogravimetric analysis. The presence of the fullerene does not induce a higher thermal stability due to the characteristics and symmetry of starting phthalocyanine which are only disrupted by the presence of fullerene. These types of materials could present interesting applications in photovoltaics as semiconducting materials.

3. Perylene-3,4:9,10–bis(dicarboximide) (PDI) – fullerene C60 light-harvesting dyads state of the art

Although, less investigated, fullerene-C_{60} has been covalently attached to electron acceptor systems.[188] Recently, a new approach toward the synthesis of fullerene derivatives with C_{60} covalently linked to electron accepting perylenediimide (PDI) dyes has emerged as a results of research into energy transfer processes from PDI to C_{60} allowing the developing of antenna effect concept[189] (Figure II-41). This concept could find applications in the development of photovoltaic solar cells by blending the appropriate semiconducting polymer with the functionalized C_{60} derivatives. Also, due to the possible triplet state of the dye molecules, possible applications in photodynamic therapy can also be envisaged.

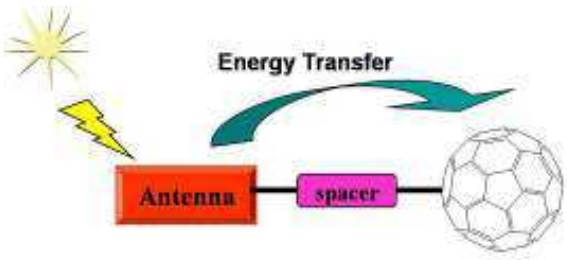

Figure II-41 the concept of the PDI antenna effect

Perylene -3,4:9,10-bis(dicarboximide) (PDI) are chromophores used as dyes and pigments[190] in a wide variety of application thanks to their outstanding chemical, thermal and photochemical stability[191].

Recently, many new electro- and photoactive C_{60}-based systems associating PDI acceptor unit have been reported. A brief description of these results will be presented in the following paragraphs.

Some of the first examples of dyads and triads involving C_{60} and PDI are presented in Figure II-42. The dyad **1** has been obtained by Li et al. [192]. Significant interaction between PDI singlet state and fullerene was evidenced through significant quenching of the fluorescence of dyad **1.** PDI singlet state energy level is higher than that of C_{60}, thus energy transfer is possible. A fast and highly efficient photoinduced energy transfer process was demonstrated on this system by Fu et al. [193], this confirms that PDI functions as light-

[188] B. M. Illescas and N. Martín, *Comptes Rendus Chimie, 9*, 1038-1050.
[189] D'Souza, F.; Kadish, K. M., *Fundamentals and Applications of Carbon Nano Materials*. World Scientific Pub Co Inc: 2010.
[190] Smith, H. M. D., *High performance pigments*. Wiley-VCH: 2002.
[191] Y. Nagao, *Prog. Org. Coat., 31*, 43-49.
[192] Y. Li, N. Wang, X. He, S. Wang, H. Liu, Y. Li, X. Li, J. Zhuang and D. Zhu, *Tetrahedron,* **2005,** *61*, 1563-1569.
[193] F. Li-Min and et al., *Chinese Physics Letters,* **2004,** *21*, 2525.

harvesting antenna and improves the photosensitization efficiency of fullerene-C_{60} in the visible spectral domain.

In the case of the triad **2** (Figure II-42), the fluorescence properties of PDI were found to be strongly influenced by the presence of the ferrocene (Fc) substituent. This behavior can be explained by intramolecular interaction in the triad, a photoinduced intramolecular electron transfer being proven as thermodynamically feasible. First, there is no spectral overlap between the absorption spectrum of Fc and the emission spectrum of PDI, the singlet excited state of Fc (2.46 eV) is higher than PDI (2.29 eV), thus a quenching by energy transfer from PDI to Fc by Förster mechanism is not possible. Thus, a cascade electron transfer mechanism is proposed for triad **2**. This has been demonstrated by Wu et al. using femtosecond time-resolved absorption spectroscopy in solution[194], showing the formation of a charge separated state $Fc^{+\cdot}$-PDI-$C_{60}^{-\cdot}$ as result of the cascade electron transfer.

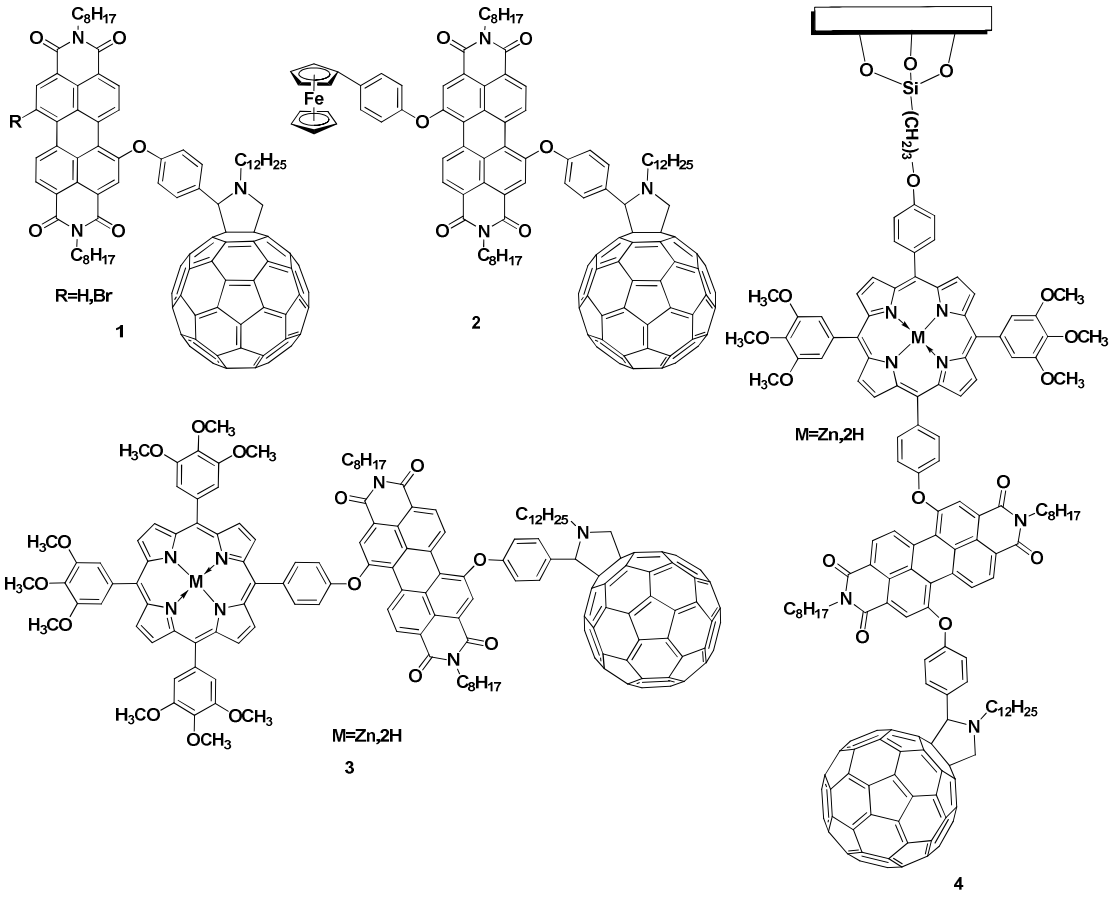

Figure II-42 Dyads and triads PDI-C_{60}

[194] Y. Wu, Y. Li, H. Li, Q. Shi, H. Fu and J. Yao, *Chemical Communications,* **2009**, 6955-6957.

Another interesting triad obtained by the same Beijing group has been triad **3**[195] (Figure II-42). Photoinduced electron-transfer processes within the triad were confirmed through preliminary fluorescence and steady-state photolysis. The fabrication of photovoltaic devices using the dyad afforded moderately efficient devices. An extension of this work was the obtaining of self-assembled monolayers (SAMs) using triad **4**[196]. The PDI association to porphyrins and C_{60} was considered in order to increase the absorption spectrum due to the fact that the chromophores have complementary absorption spectrum. Photoelectrochemical measurement of the SAMs indicated prompt, steady and reproducible photocurrent generation for irradiation with light. The results clearly demonstrate that this system exhibits wide absorption spectra (400–650 nm) in the visible light region and that this system is highly promising in light-energy conversion applications.

The dyad, PDI-C_{60}, **5**[197] and triad, C_{60}-PDI-C_{60}, **6**[198] have been obtained as thermally-stable and highly soluble systems (Figure II-43). The photophysical characterization proved the existence of efficient photoinduced energy transfer from the PDI to the C_{60} moiety. A photovoltaic device utilizing **5** allowed the demonstration of photoinduced electron transfer which however is negligible compared to the energy transfer process.

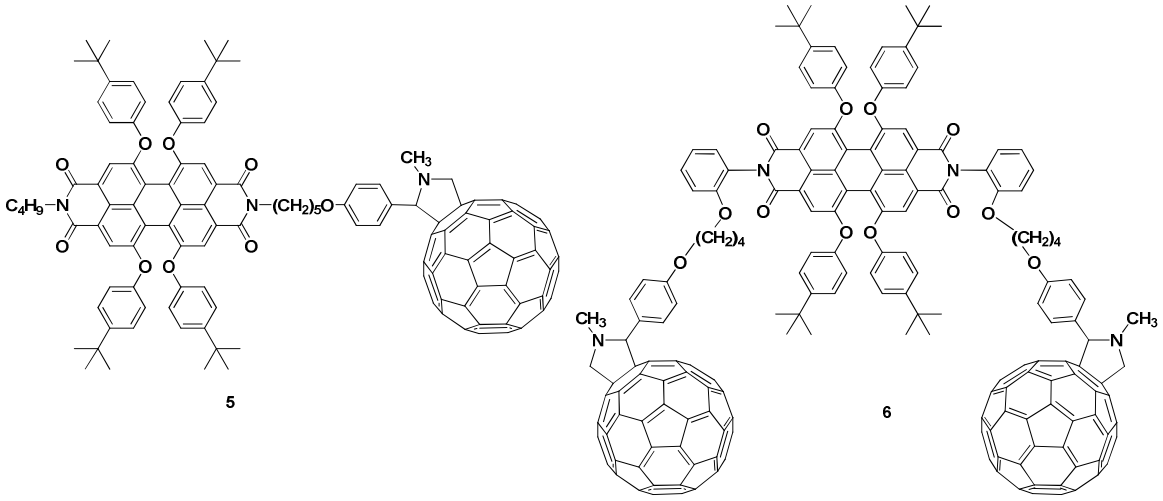

Figure II-43 highly soluble PDI-C_{60} systems

Diphenylmethanofullene-perylenediimide dyad 7 and triad 8 have been also obtained[199], representing highly efficient light-harvesting organofullerenes (Figure II-44). The

[195] S. Xiao, Y. Li, Y. Li, J. Zhuang, N. Wang, H. Liu, B. Ning, Y. Liu, F. Lu, L. Fan, C. Yang, Y. Li and D. Zhu, *The Journal of Physical Chemistry B,* **2004,** *108*, 16677-16685.
[196] Y. Li and et al., *Nanotechnology,* **2005,** *16*, 1899.
[197] J. Hua, F. Meng, F. Ding, F. Li and H. Tian, *Journal of Materials Chemistry,* **2004,** *14*, 1849-1853.
[198] J. Hua, F. Meng, F. Ding and H. Tian, *Chem. Lett.,* **2004,** *33*, 432-433.
[199] R. Gómez, J. L. Segura and N. Martín, *Organic Letters,* **2005,** *7*, 717-720.

aliphatic tail chains allow better solubility of the compounds. In the case of dyad 7 a quenching above 99% was observed which corresponds to almost quantitative energy transfer between the PDI moiety and C60. It should be noted that in the case of the triad 8 the quenching is a little lower (95%), this means a less efficient energy transfer compared to 7. In contrast, surprisingly, for the triad 9 there was no clear evidence for the existence of singlet-singlet energy transfer from PDI to C60. It was suggested that the strong quenching of the PDI fluorescence is due to intramolecular charge-transfer within triad 10200. Another important characteristic of this triad is the tendency to form aggregates due to π-π stacking which is common for perylene molecules. This tendency was evidenced through SEM analysis which shows the uniform formation nanofibers with a diameter of 50 nm (Figure II-44).

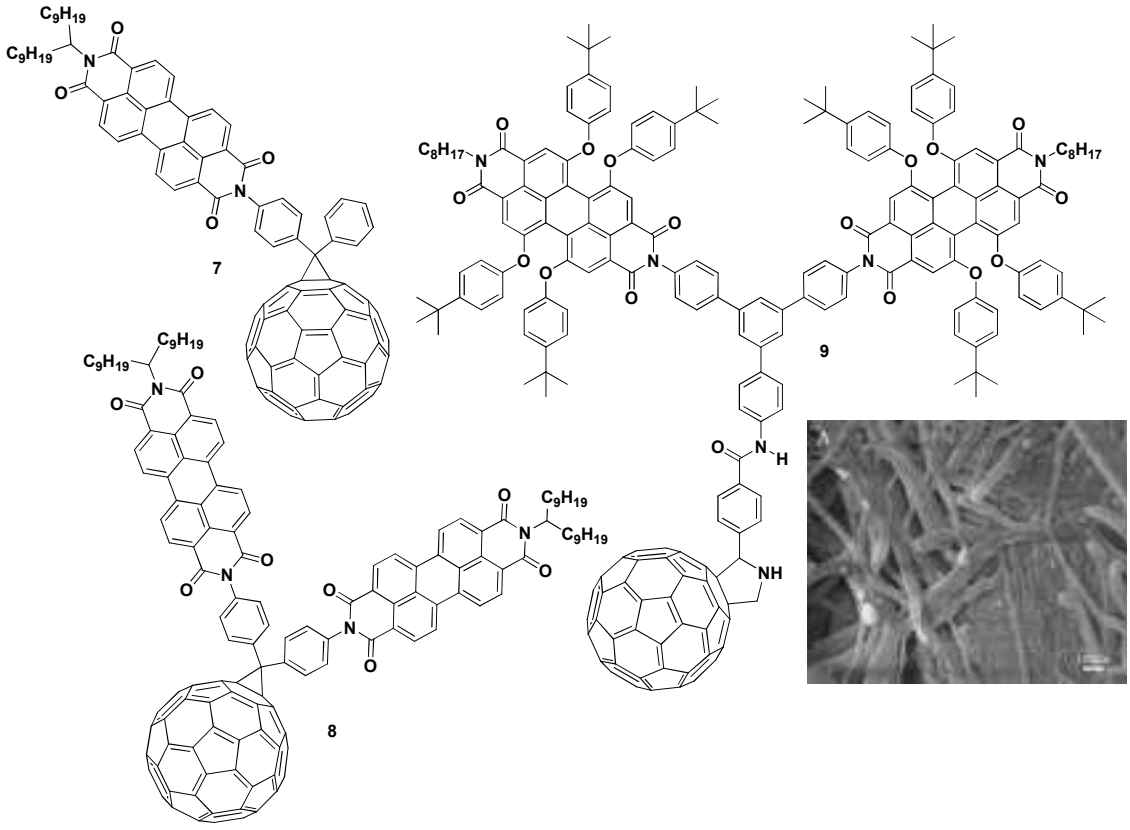

Figure II-44 dyad and triads PDI-C_{60} and SEM analysis of triad 9

[200] N. Wang, Y. Li, X. He, H. Gan, Y. Li, C. Huang, X. Xu, J. Xiao, S. Wang, H. Liu and D. Zhu, *Tetrahedron,* **2006,** *62*, 1216-1222.

Recently, Chamberlain et al presented the synthesis and characterization of dyad **10** and triad **11**, Figure II-45[201]**.** Triad **11** is a mixture of 1, 6 and 1, 7 isomers, with 1, 7 isomers as the major component (90%). The cyclic voltammetry analysis of the compounds revealed the possibility to reversibly inject up to four electrons into the dyad **10** and up to six into the triad **11.**

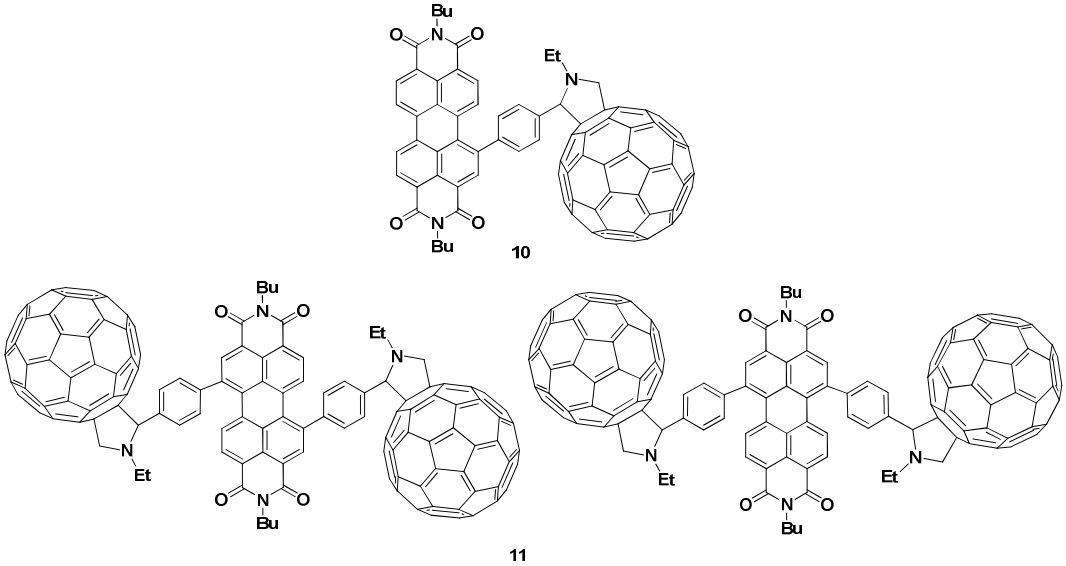

Figure II-45 Dyad and triad systems

Compared to **8**, **12**[202, 203] is a flexible PDI-C_{60}-PDI triad, the two PDI antennas being covalently attached to the C_{60} by flexible spacers. It has been found that the π-π stacking of the antenna subunits is significant and that in steady state only 40% of the triads reside in a non-stacked conformation. As a consequence of the stacking, the effective light-harvesting ability per molecule is reduced with respect to a dyad consisting of a single PDI covalently linked to C_{60}. Moreover, experimental evidence for the population of an antenna-associated triplet-state with lifetime of 10^{-7} s was found. Thus, in order to maximize the light-harvesting efficiency, π-π stacking of antennas should be avoided, for example by using long, nonflexible spacers between the antenna and fullerene units. This would have as a side effect the reduction of triplet-triplet energy transfer between fullerene and the antennas due to the fact that this process is governed by short-range exchange interaction (Dexter mechanism).

[201] T. W. Chamberlain, E. S. Davies, A. N. Khlobystov and N. R. Champness, *Chemistry – A European Journal,* **2011,** *17*, 3759-3767.
[202] C. C. Hofmann, S. M. Lindner, M. Ruppert, A. Hirsch, S. A. Haque, M. Thelakkat and J. Kohler, *PCCP,* **2010,** *12*, 14485-14491.
[203] C. C. Hofmann, S. M. Lindner, M. Ruppert, A. Hirsch, S. A. Haque, M. Thelakkat and J. r. Köhler, *The Journal of Physical Chemistry B,* **2010,** *114*, 9148-9156.

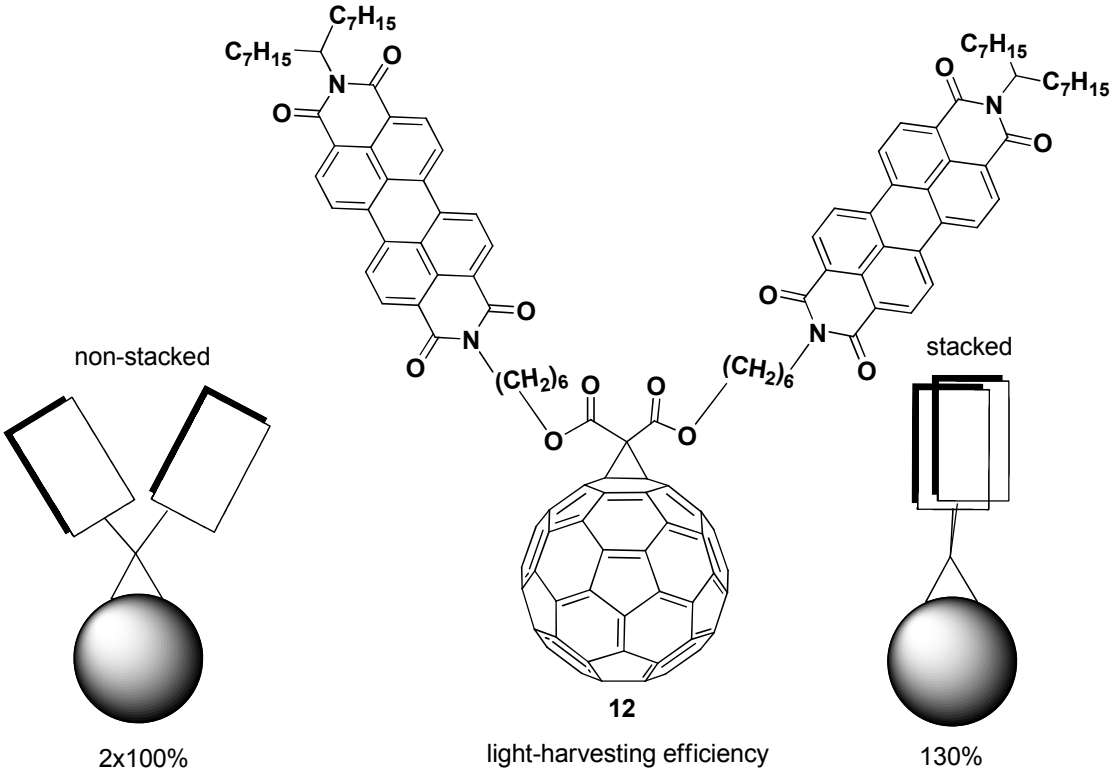

Figure II-46 π-π stacking effect in a flexible PDI-C_{60} dyad

PDI and C_{60} have been also covalently linked through the use of polymers, the examples are presented in Figure II-47, **13**[204], **14**[205], **15**[206].

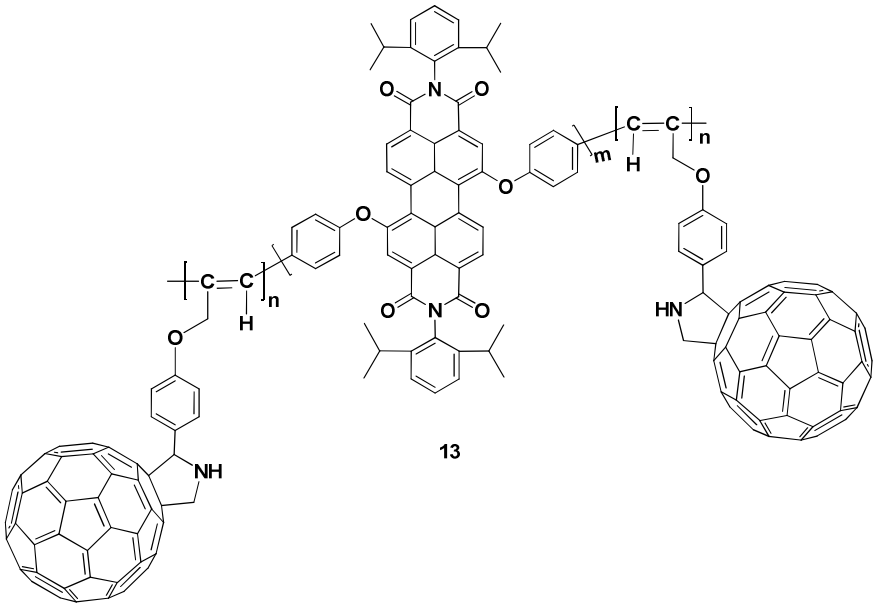

[204] Y. Liu, N. Wang, Y. Li, H. Liu, Y. Li, J. Xiao, X. Xu, C. Huang, S. Cui and D. Zhu, *Macromolecules,* **2005,** *38*, 4880-4887.
[205] C. Huang, F. Lu, Y. Li, H. Gan, T. Jiu, J. Xiao, X. Xu, S. Cui, H. Liu and D. Zhu, *Journal of Nanoscience and Nanotechnology,* **2007,** *7*, 1472-1478.
[206] N. Wang, F. Lu, C. Huang, Y. Li, M. Yuan, X. Liu, H. Liu, L. Gan, L. Jiang and D. Zhu, *Journal of Polymer Science Part A: Polymer Chemistry,* **2006,** *44*, 5863-5874.

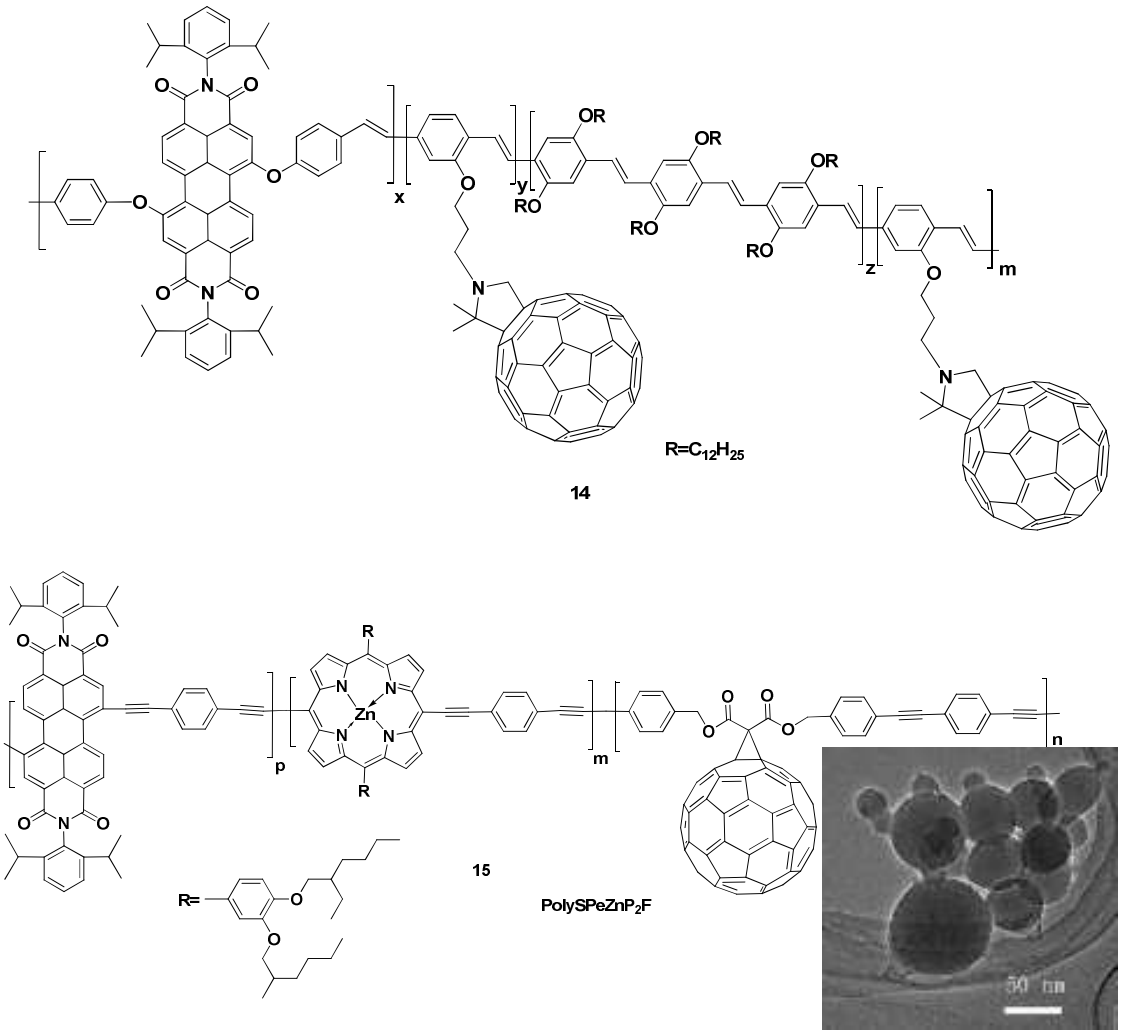

Figure II-47 Polymers incorporating PDI and C_{60} moieties; SEM images for aggregates of 13 formed in toluene

In all these examples the PDI and C_{60} moieties are separated by polymeric spacers. The photocurrent measurements showed that the films of these conjugated polymers could produce steady and rapid cathodic photocurrent responses, indicating that efficient charge transfer takes place in these polymers. These results indicate that fullerene units are able to increase charge separation efficiency[207]. Thus, in the case of **14** the photocurrent increased with the content of fullerene in the polymers. Another interesting characteristic of this type of materials is the tendency to form aggregates. An example is shown for **15**, which form both in $CHCl_3$ and toluene spherical nanoparticles.

Only recently it was shown that an efficient photoinduced electron transfer occurs in the C_{60}-PDI dyad **16**[208] which contains electro-donating pyrrolidino groups introduced as

[207] C. Li and Y. Li, *Macromol. Chem. Phys.,* **2008,** *209*, 1541-1552.
[208] Y. Shibano, T. Umeyama, Y. Matano, N. V. Tkachenko, H. Lemmetyinen and H. Imahori, *Organic Letters,* **2006,** *8*, 4425-4428.

substituent of PDI bay region. The presence of the substituent determines a low oxidation potential of the PDI moiety, thus allowing the electron transfer from the PDI to C_{60}. For **16** fast charge separation was observed (~$4x10^9$ s^{-1}) in polar solvents followed by a faster charge recombination. In nonpolar solvents, such as toluene, relatively slow energy transfer was observed form the singlet PDI unit to the singlet C_{60} ($2.3x10^8$ s^{-1}) followed by triplet-triplet energy transfer from C_{60} to the PDI moiety ($2.3x10^6$ s^{-1}).

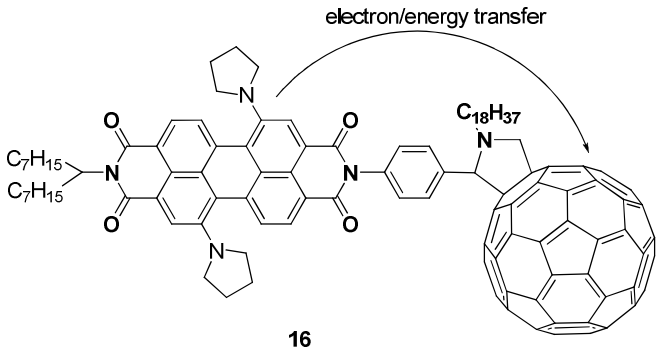

Figure II-48 Electron enriched bay substituted PDI-C_{60} dyads

The Angers group, in which I had the opportunity to work, has previously been interested in the investigation of the antenna effect in molecules consisting of dye molecules covalently linked to fullerene-C_{60}. The objective is to consider that the dye molecule could act as an antenna by absorption of sunlight inducing an intramolecular energy transfer towards the fullerene. Solar cells utilizing this concept should be designed taking into account that inside the photoactive layer a combination of the following processes occurs: self-assembly into an interpenetrating nanoscopic network; an energy transfer from PDI towards fullerene-C_{60} with the dye acting as light-harvesting antenna; a selective electron transfer between p-type polymer (donor polymer) such as poly 3-hexylthiophene (P3HT) to the C_{60} (Figure II-49).

The dyads **17 (A, B, C, D)**[209] had as objectives to study the effect that PDI bay region substituents nature has on the electronic properties of these dyads for applications in solar cell design and also the importance of the distance between the PDI and C_{60} moieties on energy transfer efficiency and kinetics.

[209] J. Baffreau, S. Leroy-Lhez, N. Vân Anh, R. M. Williams and P. Hudhomme, *Chemistry – A European Journal,* **2008,** *14*, 4974-4992.

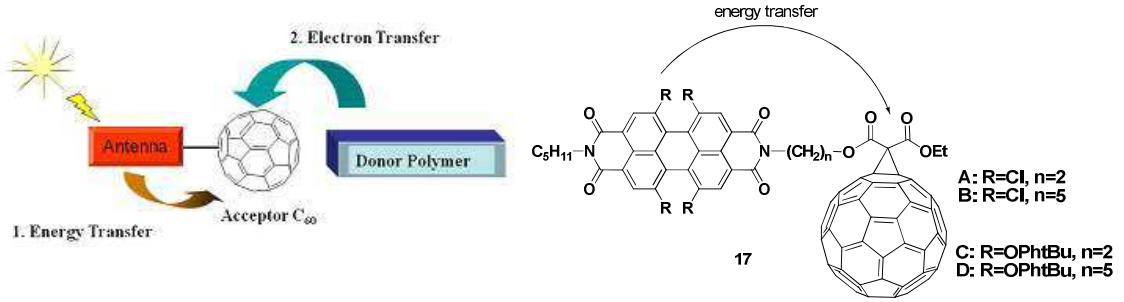

Figure II-49 Concept of antenna effect in bulk-heterojunction solar cells and dyads developed by the Angers group

The synthesis strategy included as first step the preparation of unsymmetrical PDI derivatives. This was followed by the transformation of the alcohol derivatives into malonate functional groups. Using the malonate functionality the covalent linking to the fullerene derivative was realized by Bingel cyclopropanation reaction. The bay area substituents have been chlorine and tert-butylphenoxy obtained by nucleophilic substitution of the chlorine atoms.[210]

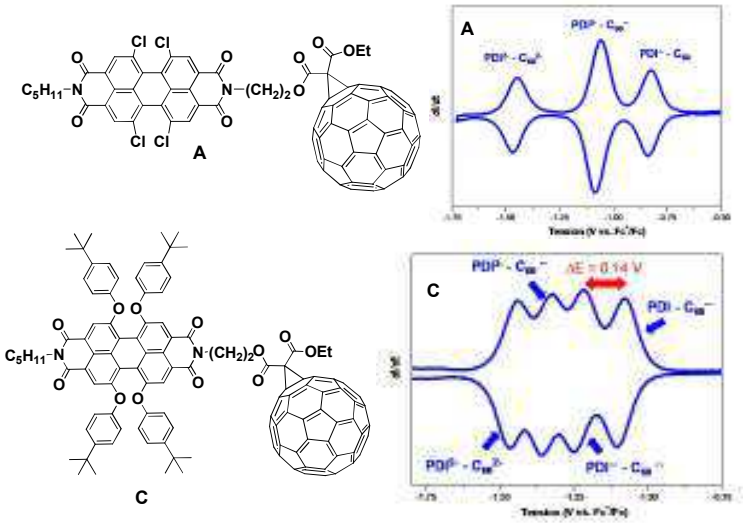

Figure II-50 Deconvoluted cyclic voltammograms of C_{60}-PDI recorded in CH_2Cl_2 solution using Bu_4NPF_6 0.1 M as electrolyte, Ag wire as the reference, platinum wires as counter and working electrodes, adapted from *Fundamentals and Applications of Carbon Nano Materials*. World Scientific Pub Co Inc: 2010

Electrochemical properties revealed that the first reduction clearly occurs on the PDI moiety in the case of **17A** and **17B** dyads. Moreover, the reduction potentials of the PDI are shifted to more negative values when chlorine atoms were substituted by tert-butylphenoxy groups. Consequently, the C_{60} moiety appears to be the favored electron acceptor inside dyad **17C** and **17D,** thus demonstrating that electronic properties can be tuned by an appropriate substitution of the PDI bay region (Figure II-50). These differences between the dyads can be

[210] J. Baffreau, L. Perrin, S. Leroy-Lhez and P. Hudhomme, *Tetrahedron Letters,* **2005,** *46*, 4599-4603.

explained by the electronic effects of substituents and their influence on the PDI core electron density. The enhancement of the electron affinity for the PDI was explained by the electron-withdrawing inductive effect of the chlorine atoms stabilizing the anion radical $PDI^{-\cdot}$, this minimizing their possible electron-donating mesomeric effect. On the contrary, the electron-donating mesomeric effect of phenoxy groups appeared predominant with less consideration for their possible electron-withdrawing inductive effect.

This electrochemical behavior and considering that this phenomenon observed in solution occurs in the same manner in solid state, we can imagine that the electron transfer from the donor polymer will take place principally onto the PDI unit for dyads **A** and **B** (containing the chlorine substituents) and onto the C_{60} unit in dyads **C** and **D** (containing tertbutylphenoxy group). For the second case, the difference of 0.14 V between the first reduction potential of C_{60} and that of PDI should favor the electron transfer from the p-type polymer donor to the n-type C_{60} acceptor in the corresponding bulk-heterojunction.[211]

[211] J. Baffreau, S. Leroy-Lhez, H. Derbal, A. R. Inigo, J.-M. Nunzi, M. M. Groeneveld, R. M. Williams and P. Hudhomme, *Eur. Phys. J. Appl. Phys.,* **2006,** *36*, 301-305.

4. Versatile light-harvesting dyad PDI-fullerene C_{60} building block (Original contribution)

4.1. Introduction

The objective of the research has been the construction of a platform allowing the attachment of light-harvesting dyads PDI-C_{60} including a free functional group for further applied developments. In order to achieve this objective, the strategy adopted was to utilize a building block unit that could act as anchoring unit for the antenna and the fullerene. The building block also has to present a free functional group, thus a total of three functional groups are required. Another important characteristic of the building block is its mobility or rigidity. Due to more accessible synthesis a rigid benzene ring was the logical choice. In order to reduce the steric hindrance of the bulky substituents (C_{60} and PDI), a 1, 3, 5 tri-substituted benzene template was chosen. For the fullerene attachment two alternatives were considered: a Bingel cyclopropanation reaction and a Prato cycloaddition reaction. (Figure II-51). For the PDI attachment an esterification reaction was considered. To play the role of the desired free group, the hydroxy (phenolic) was chosen due to its stability, protection possibilities and reactivity. By using this reasoning two building-blocks were chosen for synthesis (building block A and building block B Figure II-51).

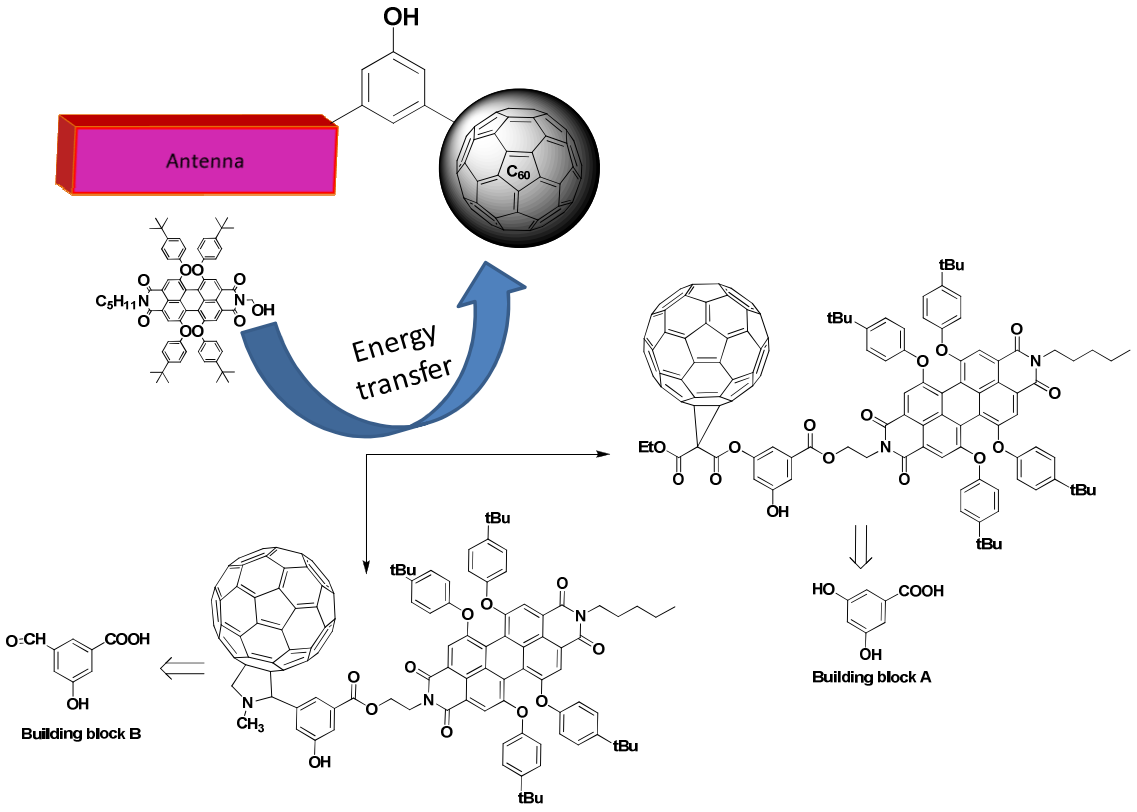

Figure II-51 Objective and target molecules

The reactive group on the dyad has been employed for the grafting onto a polymer chain (Figure II-52). This approach should increase the processability of the dyad allowing easier access to films and possibly better interpenetration and self-assembly properties in the interpenetrating layer of the bulk-heterojunction solar cells.

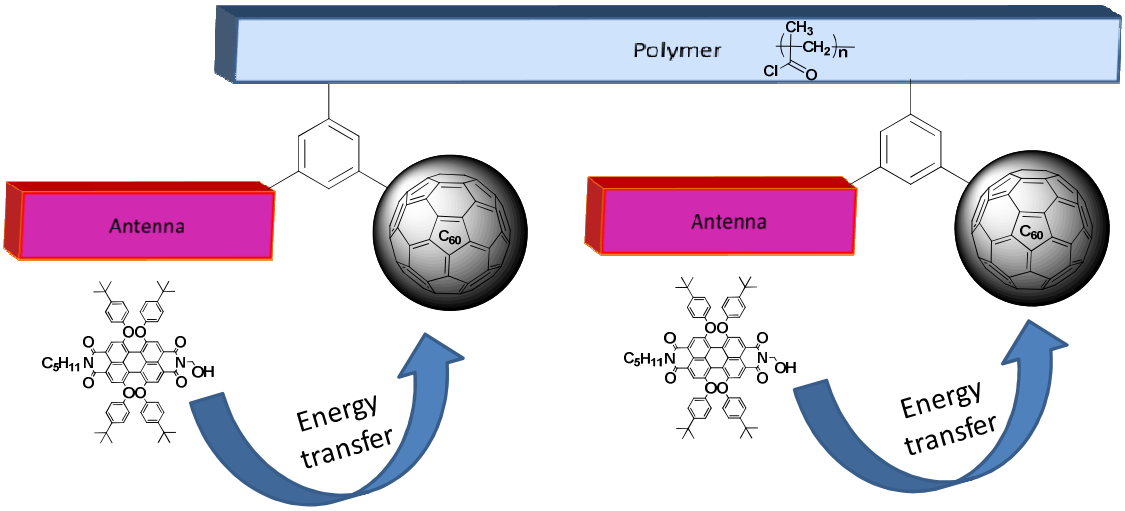

Figure II-52 Utilization of the reactive group for attachment onto a polymer chain

4.2.Synthesis

The first step of the synthesis consists in the access to the unsymmetrical derivative of PDI precursor. This was realized by direct condensation of 1,6,7,10-tetrachloroperylenedianhydride with amylamine (n-pentylamine) and ethanolamine in 1:1 ratio (Scheme II-2). After separation by chromatography on silica gel, dissymmetrical PDI **3** was isolated in nearly 30% yield.

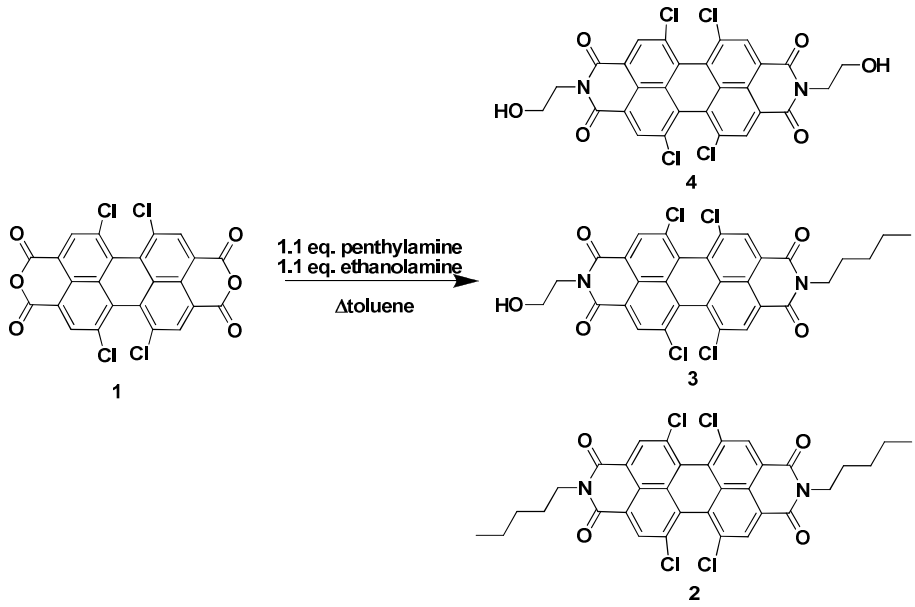

Scheme II-2 Obtaining of the unsymmetrical PDI derivative

The next step was the substitution of the chlorine with *p*-tert-butylphenol in the presence of potassium carbonate in NMP as solvent (Scheme II-3). The choice for using p-tert-butylphenol substituted PDI was motivated by the increase the solubility this groups provide and due to previously presented studies in which the dyad containing p-tBu-phenoxy substituted PDI presented the first reduction potential on C_{60} (Figure II-50 comparison between dyad **15 A** and **15 C**).

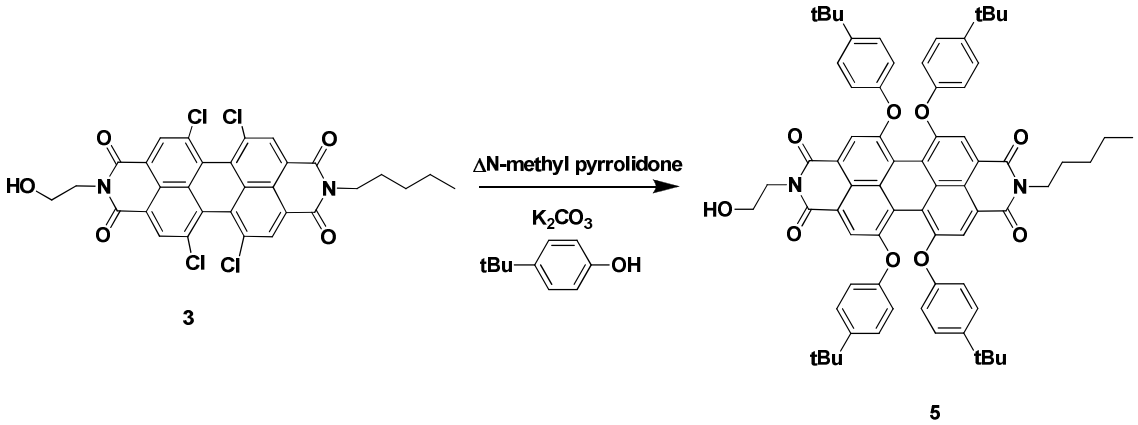

Scheme II-3 Chlorine substitution, obtaining the PDI precursor

Building block A

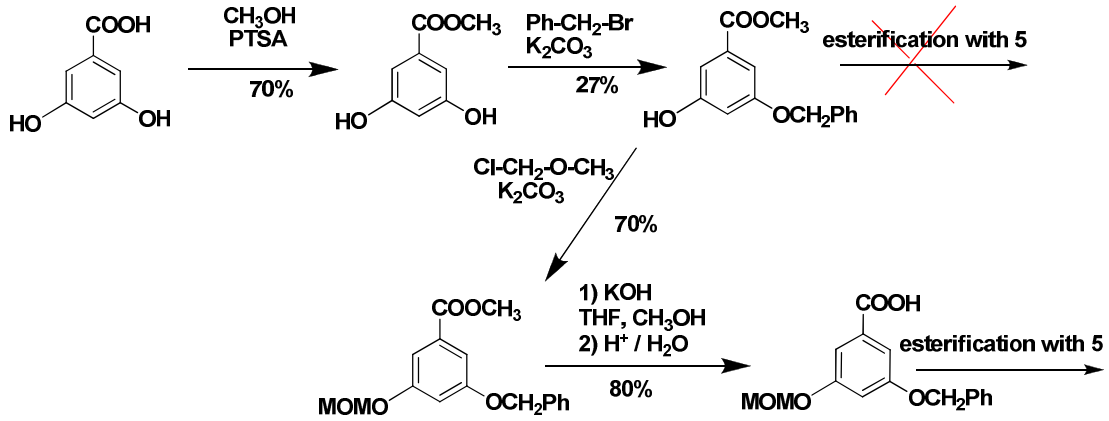

Scheme II-4 Building block A synthesis

The first building block investigated for obtaining of these dyads was 3,5-dihydroxybenzoic acid. Due to the presence of two OH groups with identical reactivity it was necessary to selectively protect one of them. First, the acid group had to be transformed into the corresponding methyl ester. As protection method that allows the reaction of only one of the phenolic groups, benzyl protection proved to be an efficient choice.[212] Other methods utilized have been tried with the use of silane protection methods which proved either

[212] P. Sörme, P. Arnoux, B. Kahl-Knutsson, H. Leffler, J. M. Rini and U. J. Nilsson, *Journal of the American Chemical Society,* **2005,** *127*, 1737-1743.

selectivity for obtaining the disubstituted phenols ($tBuPh_2SiCl$) or weak stability ($tBuMe_2SiCl$) (personal not presented results).

A different protection group for the second phenolic group (MOM-methoxymethyl) was necessary due to the fact that the esterification of methyl 3-(benzyloxy)-5-hydroxybenzoate with **5** (using Steglich esterification – carbodiimide initiation Figure II-53**)** failed, one explanation for this being the acidic properties of the free phenolic group.

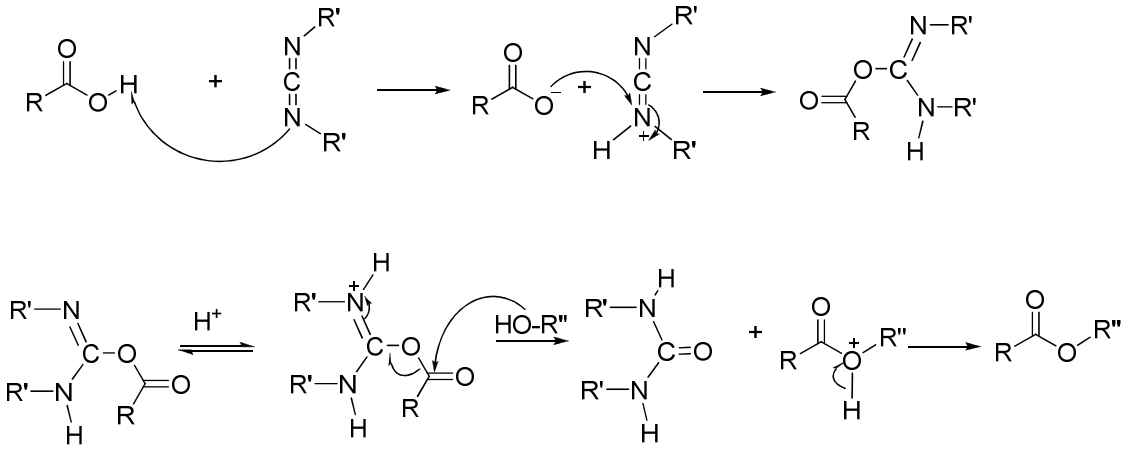

Figure II-53 Steglich esterification mechanism

The ^{1}H and ^{13}C-NMR spectra for 3-(benzyloxy)-5-(methoxymethoxy) benzoic acid (building block A) are presented in Figure II-54, confirming the obtaining of these compounds.

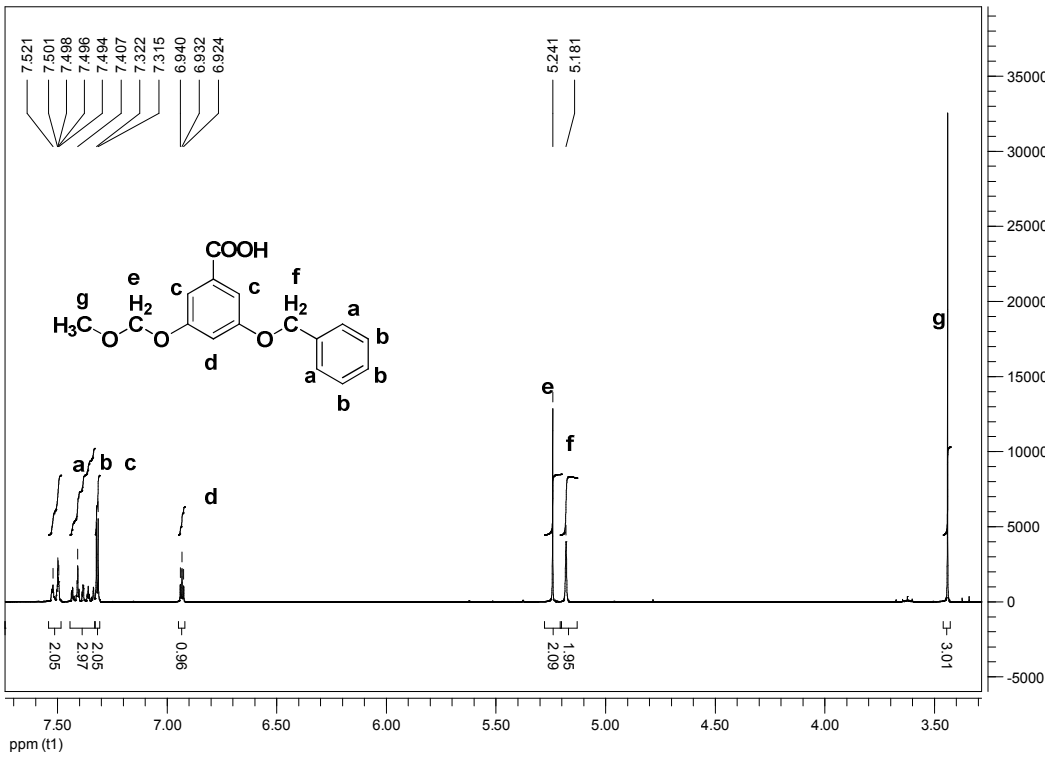

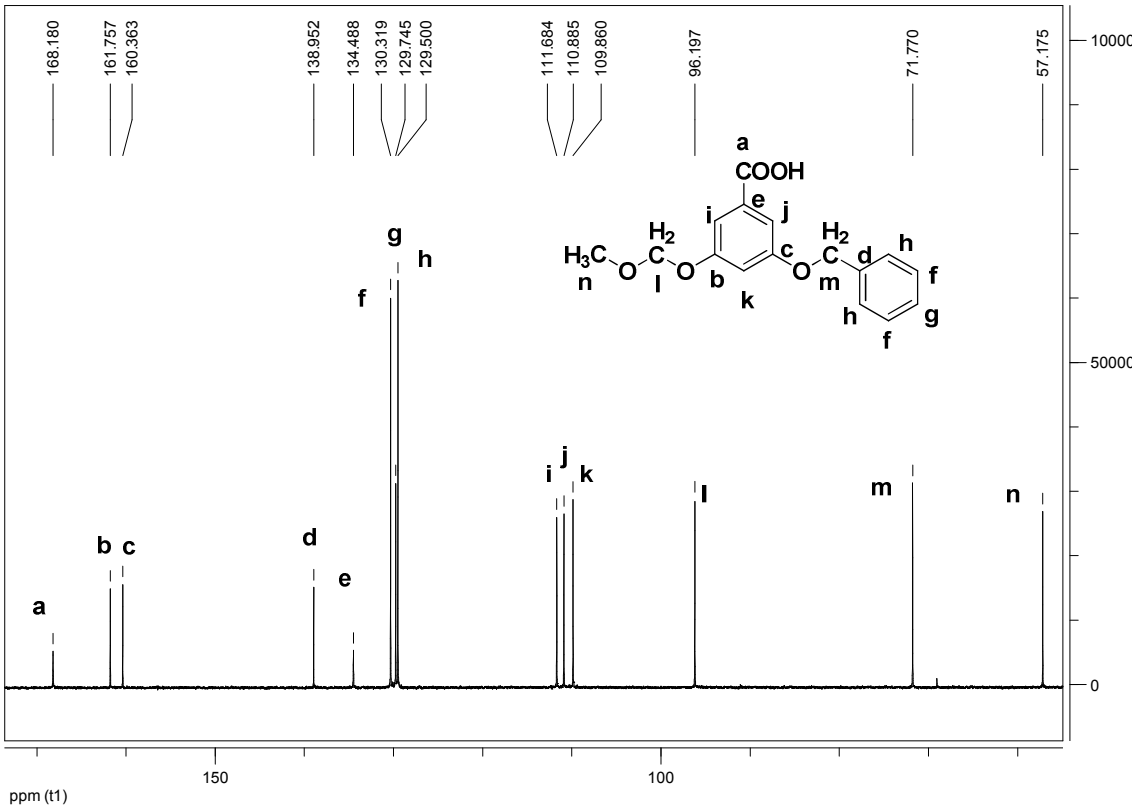

Figure II-54 ^{1}H and ^{13}C-NMR spectra for 3-(benzyloxy)-5-(methoxymethoxy) benzoic acid (acetone-d_6, 300 MHz)

Building block B

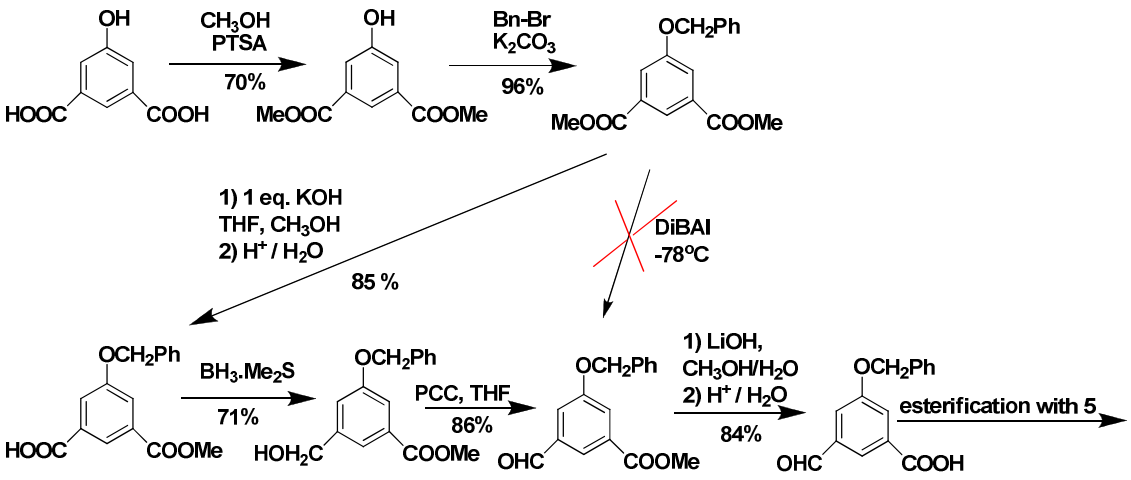

Scheme II-5 Building block B synthesis

The second building block is represented by the 3-formyl-5-hydroxybenzoic acid compound. The synthesis steps are presented in Scheme II-5. A search of the literature revealed a variant for obtaining of 3-formyl-5-methoxymethylbenzoate starting from

dimethyl-3-methoxyisophthalate[213] using diisobutylaluminium hydride (DiBAl), for our benzyl protected derivative this proved to be troublesome. The second alternative found in the literature[214], also for the methyl protected phenol group, was used as support to design our route, with modifications.

The benzyl protective group was chosen in order to protect the phenol group and to allow a more facile removal, so the esterification with the PDI precursor **5** was realized in presence of the protected phenolic group.

The key step of the synthesis route for the building block B is the mono deprotection/hydrolysis of the diester (dimethyl 5-(benzyloxy)isophthalate). This is followed by the reduction of the carboxy group using borane dimethyl sulfide complex to the corresponding alcohol which was then oxidized using pyridinum chlorochromate to obtain the methyl 3-(benzyloxy)-5-formylbenzoate. The following hydrolysis was realized with LiOH in a methanol/water mixture.

The ^{1}H and ^{13}C-NMR spectra for 3-(benzyloxy)-5-formylbenzoic acid (building block B) are presented in Figure II-55, confirming the structure of the compound.

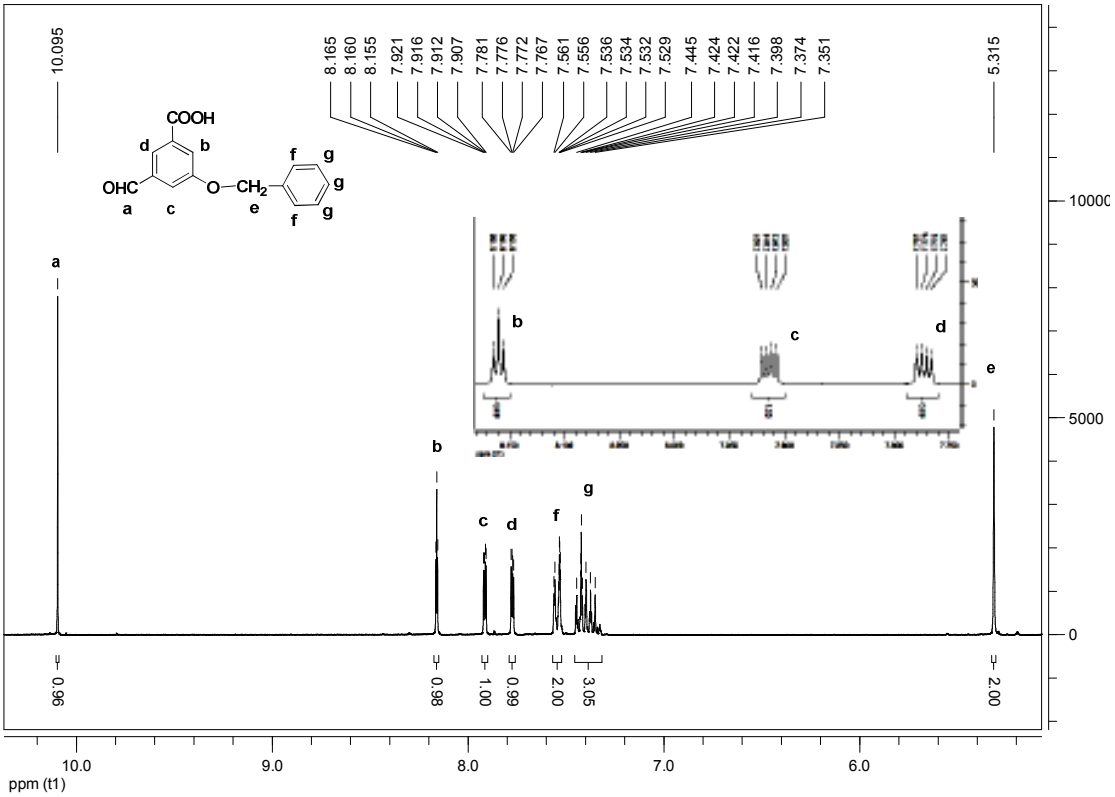

[213] M. R. Johnson and L. S. Melvin, *U.S Patent Office,* **1978,** *4,118,559*.

[214] H. Zhao and A. Thurkauf, *Synthetic Communications: An International Journal for Rapid Communication of Synthetic Organic Chemistry,* **2001,** *31*, 1921 - 1926.

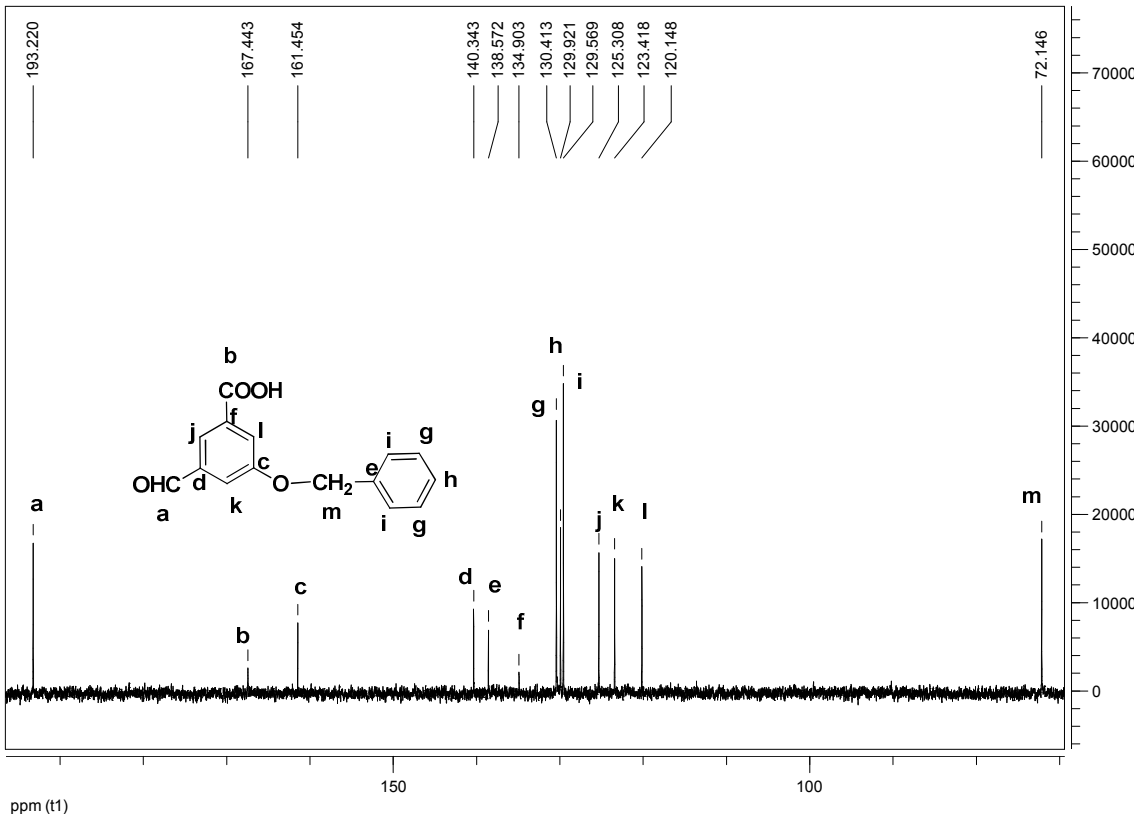

Figure II-55 ^{1}H, ^{13}C-NMR spectra for 3-(benzyloxy)-5-formylbenzoic acid (acetone-D_6, 300 MHz)

The attachment of the PDI derivative **5** to the trisubtituted benzene moieties was realized through a Steglich esterification reaction, as mentioned above Figure II-53, using N-(3-dimethylaminopropyl) N'-carbodiimide (EDC) as initiator.

In the case of **building block A**, the esterification was followed by the removal of the MOM protecting group which allowed the reaction with ethyl malonyl chloride. Three methods have been utilized for the removal of MOM, the highest yield (70%) being obtained using NaI and HCl (catalytic amounts)[215] in acetone as solvent (Scheme II-6). The obtained product **7** was then reacted with ethyl malonyl chloride in dry CH_2Cl_2 and pyridine, resulting **8.** The benzyl protecting group present in **8** was then removed by catalytic hydrogenation, resulting in the formation of **9.** Bingel cyclopropanation reaction was attempted on compound **9,** using DBU and iodide, but despite many efforts to modify experimental conditions we could not isolate the expected dyad. One explanation for the failure of the reaction could be the acidic characteristic of the OH which blocks the proton extraction from the malonyl

[215] D. R. Williams, B. A. Barner, K. Nishitani and J. G. Phillips, *Journal of the American Chemical Society,* **1982,** *104*, 4708-4710.

component. A solution for this could be utilization of **8** for the Bingel reaction with fullerene. Initial attempts have been made, but for the moment the dyad has not been isolated.

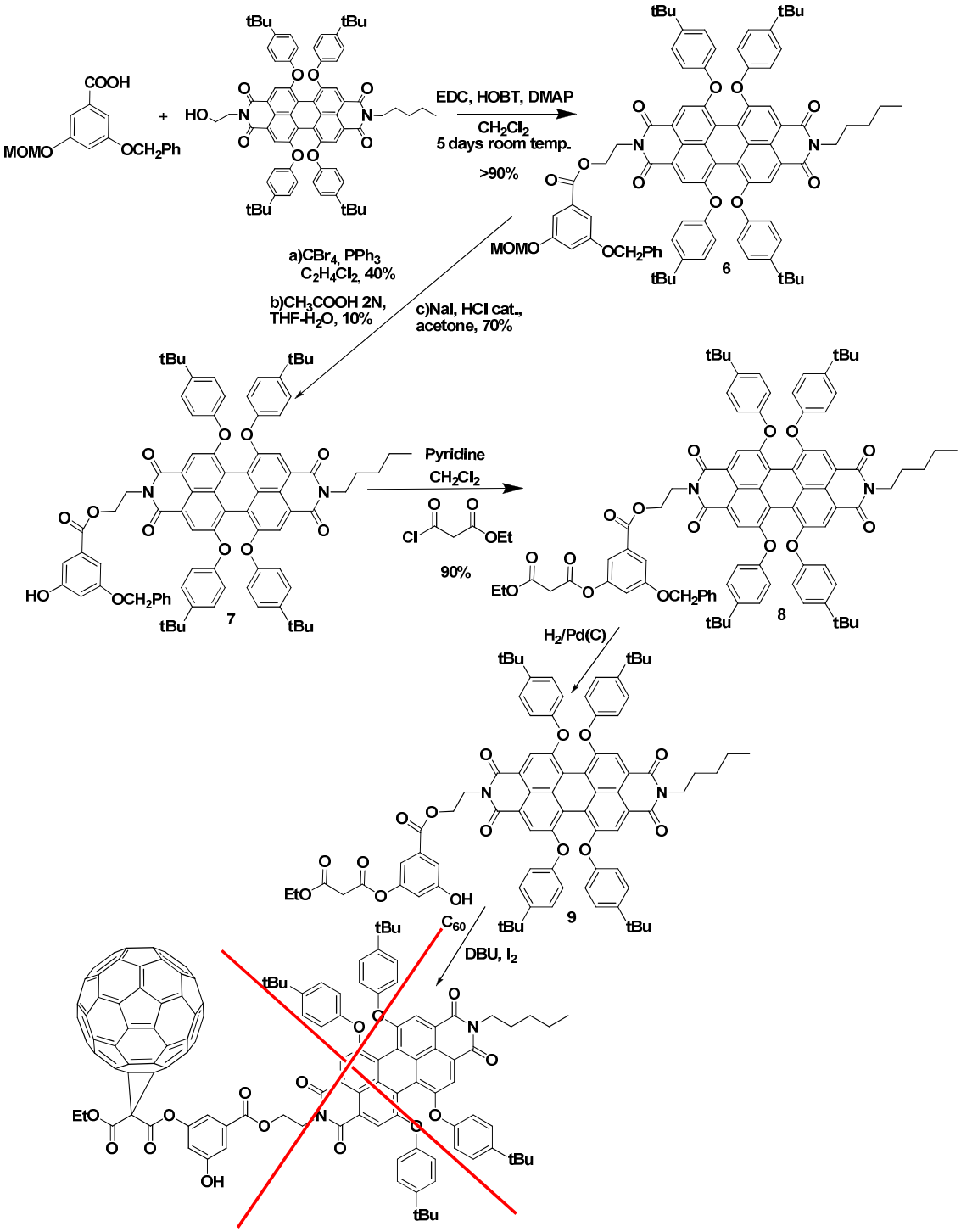

Scheme II-6 Building block A PDI-C_{60} dyad synthesis route

The ^{1}H-NMR spectra for **9** is presented in Figure II-56, coupled with the MALDI-TOF analysis demonstrate the obtaining of the proposed structure.

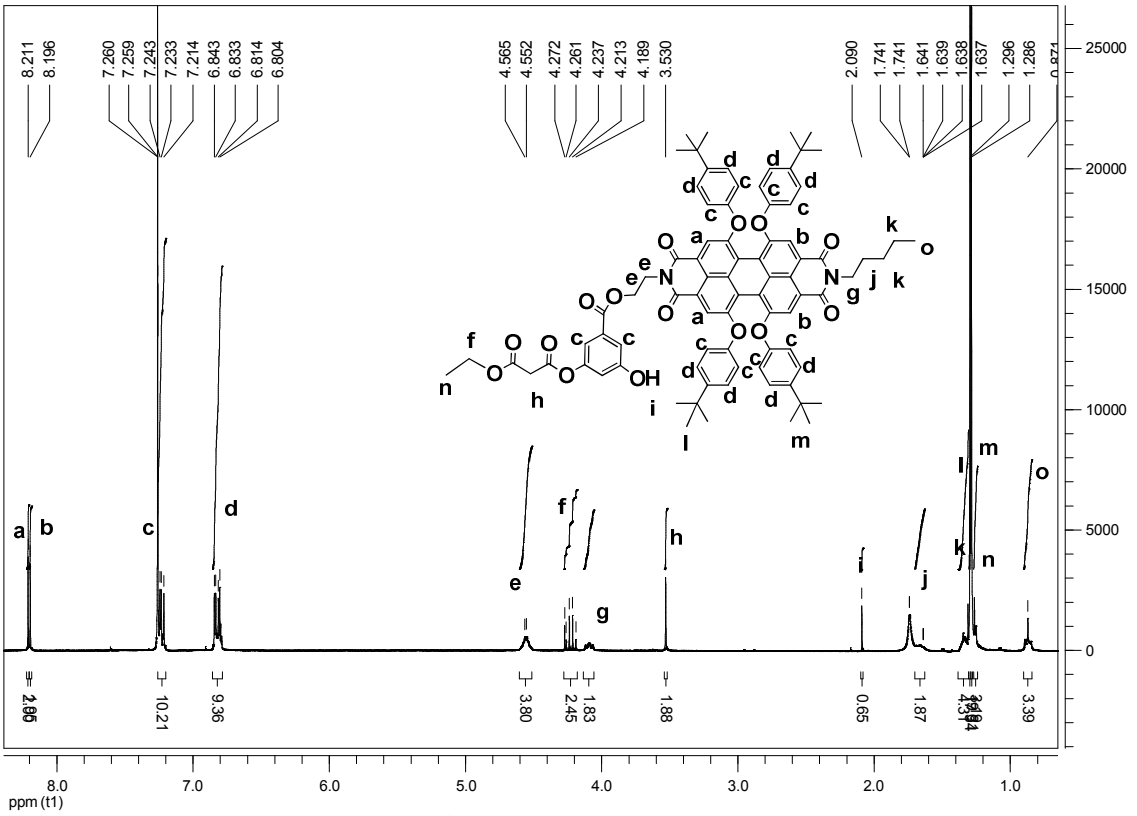

Figure II-56 ^{1}H-NMR spectrum for compound 9

In the case of **building block B**, the esterification with the PDI precursor **5** is realized also by using a carbodiimide initiator resulting in the obtaining of **10**. The linking in of the fullerene in this case involved the use of Prato cycloaddition reaction which was realized using sarcosine. The obtained **Dyad 1** presented a benzyl protecting group on the phenolic group. For the deprotection of the OH several alternatives (H_2, Pd/C, BCl_3/-78°C, HBr and imidazolium salt[216]) have been tested in order to obtain a reasonable yield. Thus, BCl_3 was found to be the best suited method for the deprotection of the benzyl in the case of **Dyad 1**.

For a complete characterization of the dyads ^{1}H, ^{13}C, DEPT, COSY, HMQC, HMBC and MALDI-TOF analysis have been employed. Also, the electrochemical properties have been investigated using cyclic voltammetry and the optical characteristics using UV-Vis and fluorescence spectroscopy.

The obtained Dyad 2 has been grafted onto a polymer chain using poly(methacryloyl chloride).

[216] S. K. Boovanahalli, D. W. Kim and D. Y. Chi, *The Journal of Organic Chemistry,* **2004,** *69*, 3340-3344.

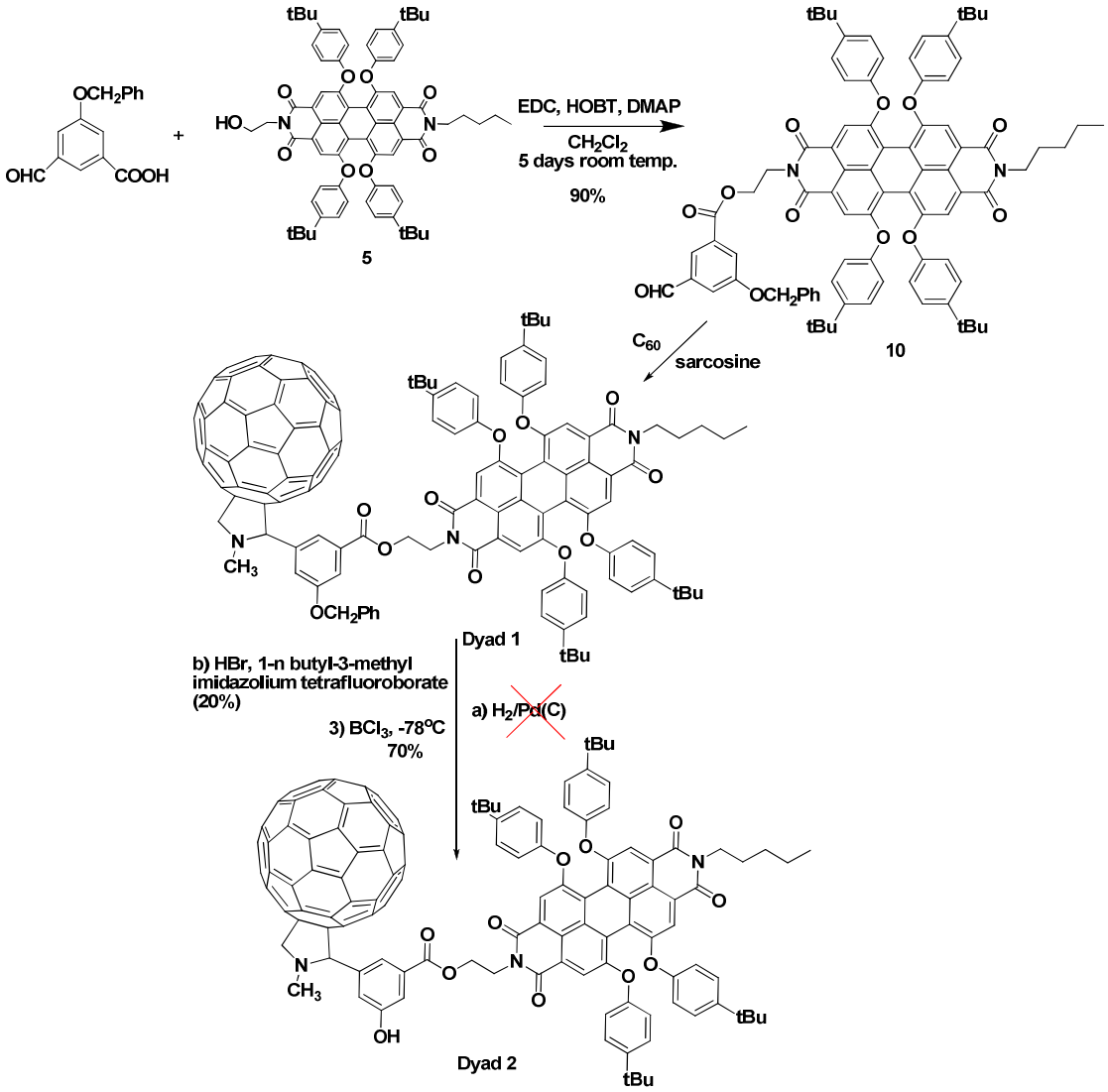

Scheme II-7 Building block B PDI-C_{60} dyad synthesis route

4.3. Dyad structure determination

The ^{1}H-NMR spectra for the Dyad 1 and Dyad 2 at room temperature exhibit coalescence effect for the signals belonging to the protons on the perylene macrocycle. Variable temperature NMR spectra recorded in $CDCl_3$ show modification of the shape of one of the two characteristic singlet signals when temperature is increased to 55°C (Figure II-57). Hua et al.[197] and Eckert et al.[169] observed similar behavior for other fulleropyrrolidine derivatives, but in their cases, the protons affected by the broadening of the signals were the ones corresponding to the phenyl group substituted on the pyrrolidines ring. This behavior indicates a restricted rotation of the phenyl substitute on the pyrrolidine ring. The relaxation of the molecule increases with temperature, the signal that undergoes the shape modification being attributed to the two protons closest to the fullerene moiety. Thus, at lower temperature

the molecule adopts a packed configuration while the increase of temperature allows a relaxed configuration. Also, the energy transfer process decreases with the increase of temperature.

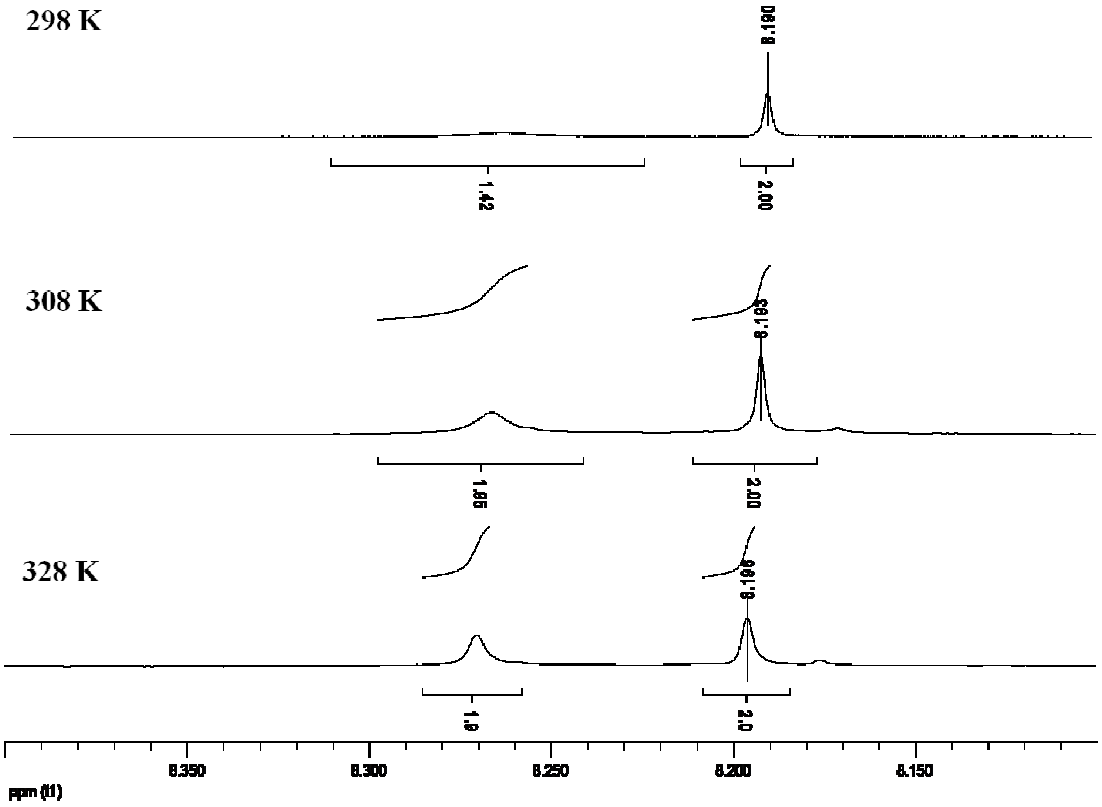

Figure II-57 Variable temperature ^{1}H-NMR spectra of Dyad 1 ($CDCl_3$, 300 MHz)

Dyad 2:

In order to determine the structure of the dyad 2, ^{1}H-NMR at 300 MHz and 500 MHz coupled with temperature dependent experiments have been carried out. Also, for correct assignment of the signals 2D-NMR analyses consisting in COSY (proton-proton coupling), HMQC (direct C-H coupling) and HMBC (C-H coupling over long distance) have been employed. The steps followed for structure determination will be outlined in the following paragraphs.

I: ^{1}H NMR analysis

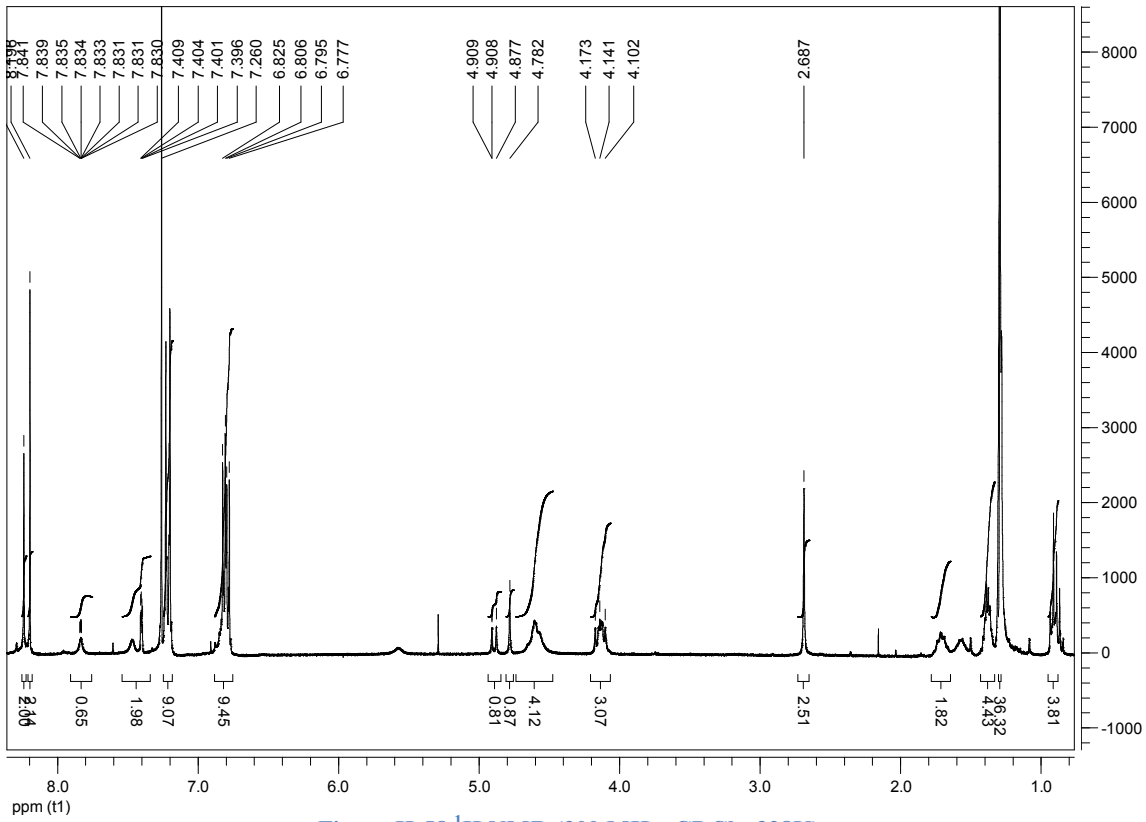

Figure II-58 ^{1}H NMR (300 MHz, $CDCl_3$, 328K)

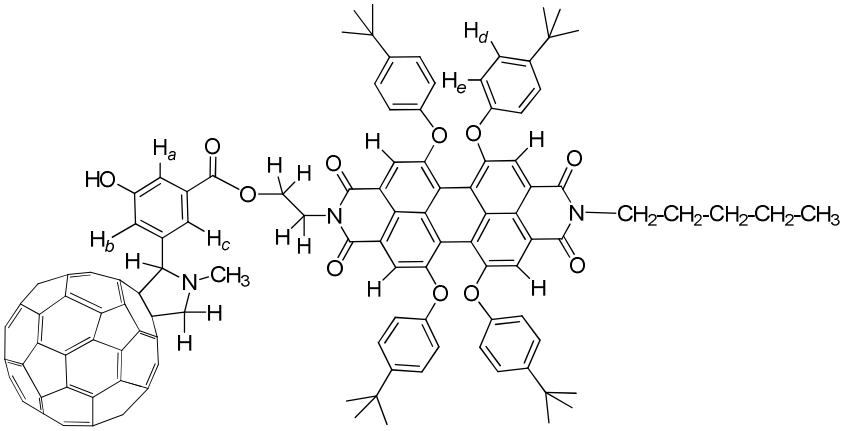

δ =
- 8.24 (s, 2H, H perylene)
- 8.20 (s, 2H, H perylene)
- 7.83 (br s, 1H, Ha or Hb or Hc)
- 7.47 (br s, 1H, Ha or Hb or Hc)
- 7.40 (dd, ^{3}J= 1,5 and 2,4 Hz, Ha or Hb or Hc)
- 7.21 (d, ^{3}J = 9Hz, 8H, H_D or H_E)
- 6.78 et 6,81 (2d, ^{3}J = 9Hz, 8H, H_D or H_E)
- 5.57 (br s, 1H, OH)

- 4.89 (d, J = 9.3 Hz, 1H)
- 4.78 (s, 1H, CH pyrrolidine)
- 4.60 (m, 4H)
- 4.14 (m, 3H)
- 2.68 (s, 3H, N-CH_3)
- 1.71 (m, 2H, -CH_2-)
- 1.39 (m, 4H, -CH_2CH_2-)
- 1.29 and 1,30 (2s, 36H, tBu)
- 0.91 (t, J = 7 Hz , 3H, CH_3)

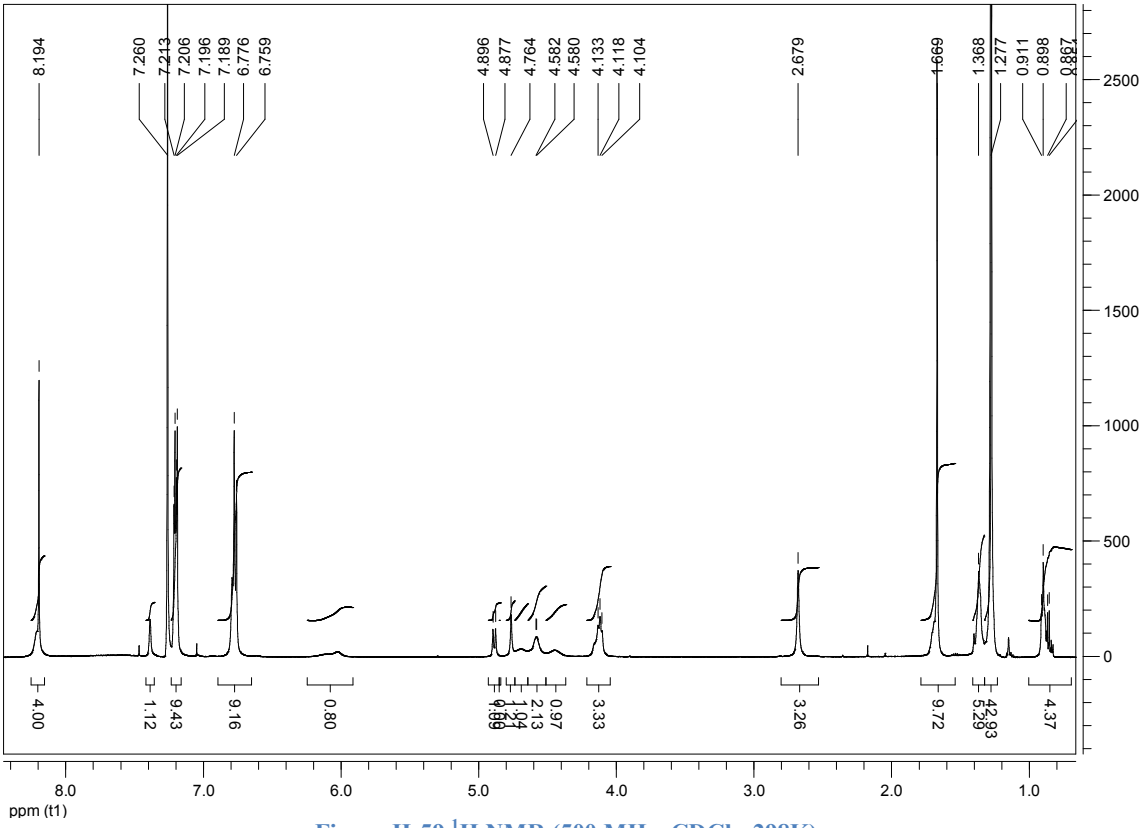

Figure II-59 ^{1}H NMR (500 MHz, $CDCl_3$, 298K)

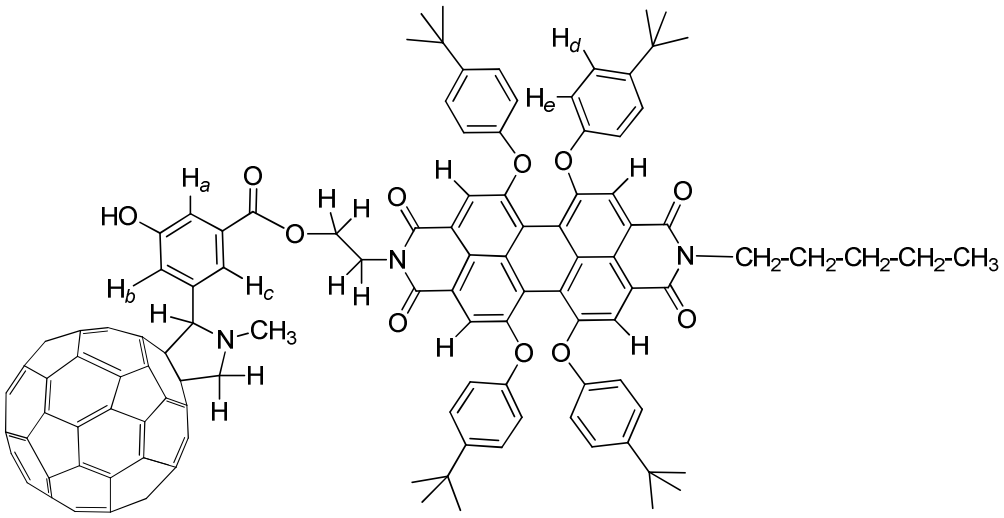

δ =
- 8.21 (br s, 2H, H perylene)
- 8.19 (s, 2H, H perylene)
- Two protons of the aromatic platform are missing due to problems of relaxation
- 7,39 (br s, 1H, Ha or Hb or Hc)
- 7,20 and 7.19 (2d, ^3J = 8.5 Hz, 8H, H_D or H_E)
- 6.78 and 6.76 (2d, ^3J = 8.5 Hz, 8H, H_D or H_E)
- 6.03 (br s, 1H, OH)
- 4.88 (d, J = 9.5 Hz, 1H, -NCH_2CH_2O- group)
- 4.76 (s, 1H, CH pyrrolidine)
- 4.69 (br s, 1H, -NCH_2CH_2O- group)
- 4.58 (br s, 2H, CH_2 pyrrolidine)
- 4.45 (br s, 1H, -NCH_2CH_2O- group)
- 4.16 (br s, 1H, -NCH_2CH_2O- group)
- 4.10 (t, J = 7.5 Hz, 2H, N$\underline{CH_2}(CH_2)_3CH_3$)
- 2,68 (s, 3H, N-CH_3)
- 1,67 (m, 2H, -CH_2-)
- 1,37 (m, 4H, -CH_2CH_2-)
- 1,28 (s, 36H, tBu)
- 0,90 (t, J = 7 Hz, 3H, CH_3)

II : Protons of the perylene core and of the aromatic platform

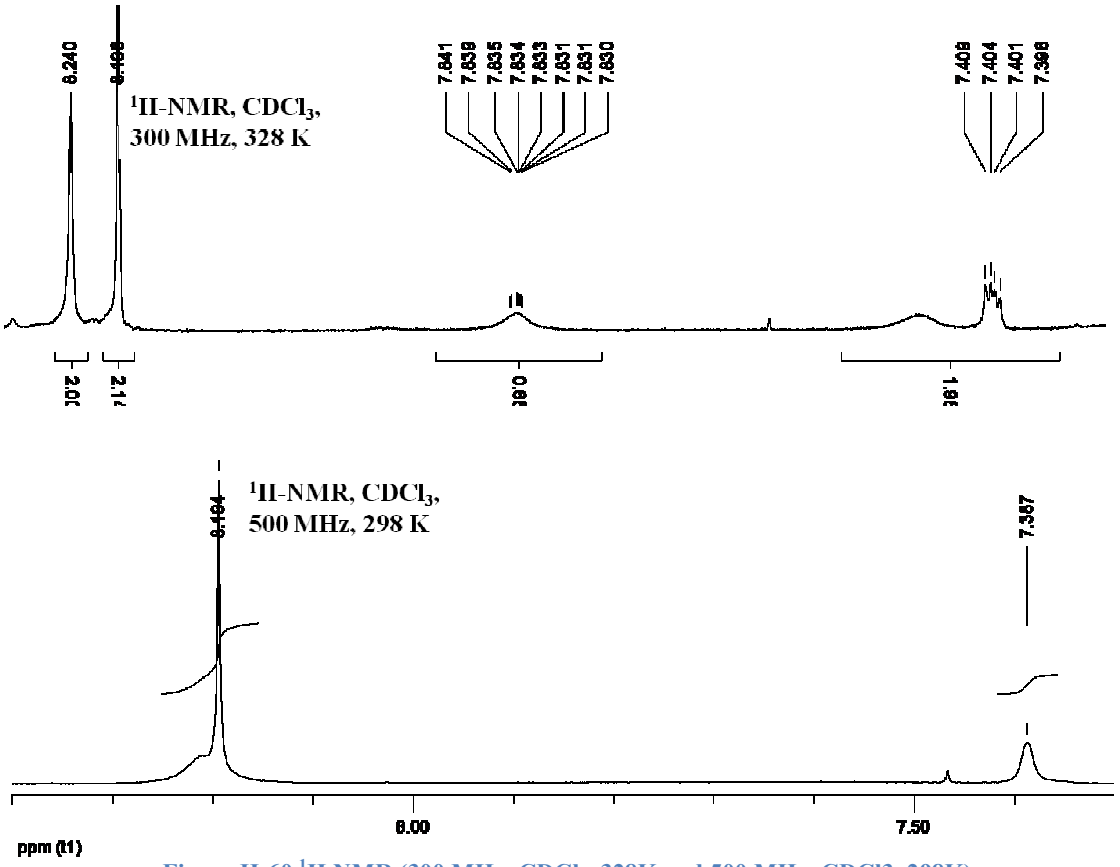

Figure II-60 ^{1}H NMR (300 MHz, $CDCl_3$, 328K and 500 MHz, CDCl3, 298K)

The ^{1}H NMR spectrum at 298 K showed for protons of the perylene core a well defined singlet for two protons and a broad singlet for the two others. This suggested a problem of relaxation which was demonstrated by the obtention in the spectrum recorded at 328 K of the two expected singlets at 8.20 and 8.24 ppm.

Concerning the three protons of the aromatic platform, noted H_A, H_B and Hc, only one of these protons at 7.38 ppm is observed in the spectrum at 298 K. This problem of relaxation due to the presence of both fullerene and PDI substituents around this aromatic platform is partially solved at 328 K. In the latter case, a well defined doublet of doublet at 7.40 ppm (^{3}J = 1,5 and 2,4 Hz) is observed accompanied with two broad singlets at 7.47 and 7.83 ppm. For the attribution of these Ha, Hb and Hc protons of the aromatic platform, it should be reasonable to consider that both protons exhibiting higher problems of relaxation correspond to H_B and H_C protons which are closer to bulky C_{60} fullerene. Consequently, H_A could be attributed to the proton at 7.40 ppm. The other possibility considers the table of increments for aromatic protons, following the formula:

$$\delta = 7.27 + \text{ortho} + \text{meta} + \text{para}$$

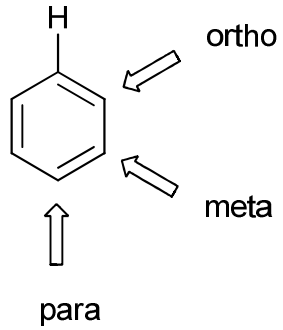

Table 4.6. $S(\delta)$ values for substituted benzenes (after Jackman and Sternhell[8])

Substituent	$S(\delta)$ (ppm) Ortho	Meta	Para
NO_2	0.95	0.17	0.33
CHO	0.58	0.21	0.27
COCl	0.83	0.16	0.3
COOH	0.8	0.14	0.2
$COOCH_3$	0.74	0.07	0.20
$COCH_3$	0.64	0.09	0.3
CN	0.27	0.11	0.3
C_6H_5	0.18	0.00	0.08
CCl_3	0.8	0.2	0.2
$CHCl_2$	0.1	0.06	0.1
CH_2Cl	−0.0	0.01	−0.0
CH_3	−0.17	−0.09	−0.18
CH_2CH_3	−0.15	−0.06	−0.18
$CH(CH_3)_2$	−0.14	−0.09	−0.18
$C(CH_3)_3$	0.01	−0.10	−0.24
CH_2OH	−0.1	−0.1	−0.1
CH_2NH_2	−0.0	−0.0	−0.0
F	−0.30	−0.02	−0.22
Cl	0.02	−0.06	−0.04
Br	0.22	−0.13	−0.03
I	0.40	−0.26	−0.03
OCH_3	−0.43	−0.09	−0.37
$OCOCH_3$	−0.21	−0.02	—
OH	−0.50	−0.14	−0.4
$p\text{-}CH_3C_6H_4SO_3$	−0.26	−0.05	—
NH_2	−0.75	−0.24	−0.63
SCH_3	−0.03	−0.0	—
$N(CH_3)_2$	−0.60	−0.10	−0.62

Figure II-61 δ values for substituted benzenes[217]

	OH	CO_2CH_3	CH_2NH_2
Ortho	**- 0,50**	**+ 0,74**	**+ 0**
Meta	**- 0,14**	**+ 0,07**	**+ 0**
Para	**- 0,40**	**+ 0,20**	**+ 0**

Consequently:

$\delta H_A = 7.27 - 0.50 + 0.74 + 0 = 7.51$

$\delta H_B = 7.27 - 0.50 + 0.07 + 0 = 6.84$

$\delta H_C = 7.27 + 0.74 - 0.40 + 0 = 7.61$

Nevertheless, this technique suffers from the lack of information in the table of increments about the influence of the pyrrolidine ring on the chemical shift. Using this table, the proton H_B should be the more shielded and the proton H_C the more deshielded.

This increment table could be used for attribution of H_D and H_E protons:

	C(CH3)3	OCH3
Ortho	**+ 0.01**	**0.10**
Meta	**- 0,43**	**- 0,09**

Consequently: $\delta H_D = 7.27 + 0.01 - 0.09 = 7.19$

$\delta H_E = 7.27 - 0.43 - 0.10 = 6.74$

[217] Günther, H., *NMR spectroscopy: an introduction*. Wiley: 1980.

These calculated chemical shifts are in good agreement with those observed on the ^1H NMR spectrum. Consequently, protons H_D can be attributed to the two doublets at 7.20 ppm and protons H_E to the two doublets at 6.78 ppm.

III : Protons of the linkers $-OCH_2CH_2N-$ and pyrrolidine ring

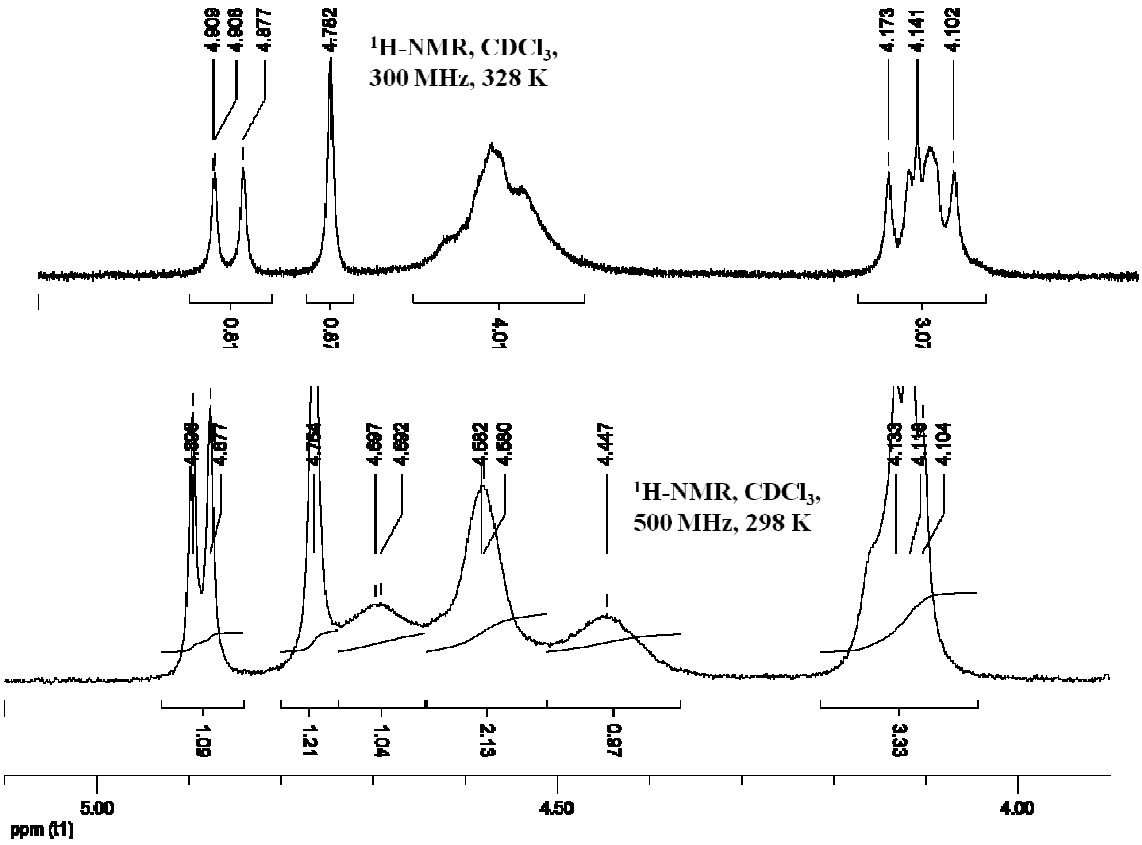

Figure II-62 ^1H NMR (300 MHz, $CDCl_3$, 328K and 500 MHz, $CDCl_3$, 298K)

The ^1H NMR spectrum at 298 K presents signals in the range 4 – 5 ppm for which the better resolution allows an easier attribution :

- 4.88 (d, J = 9.5 Hz, 1H, $-NCH_2CH_2O-$ group)
- 4.76 (s, 1H, CH pyrrolidine)
- 4.69 (br s, 1H, $-NCH_2CH_2O-$ group)
- 4.58 (br s, 2H, CH_2 pyrrolidine)
- 4.45 (br s, 1H, $-NCH_2CH_2O-$ group)
- 4.16 (br s, 1H, $-NCH_2CH_2O-$ group)
- 4.10 (t, J = 7.5 Hz, 2H, $N\underline{CH_2}(CH_2)_3CH_3$)

This attribution is conforted thanks to the COSY spectrum :

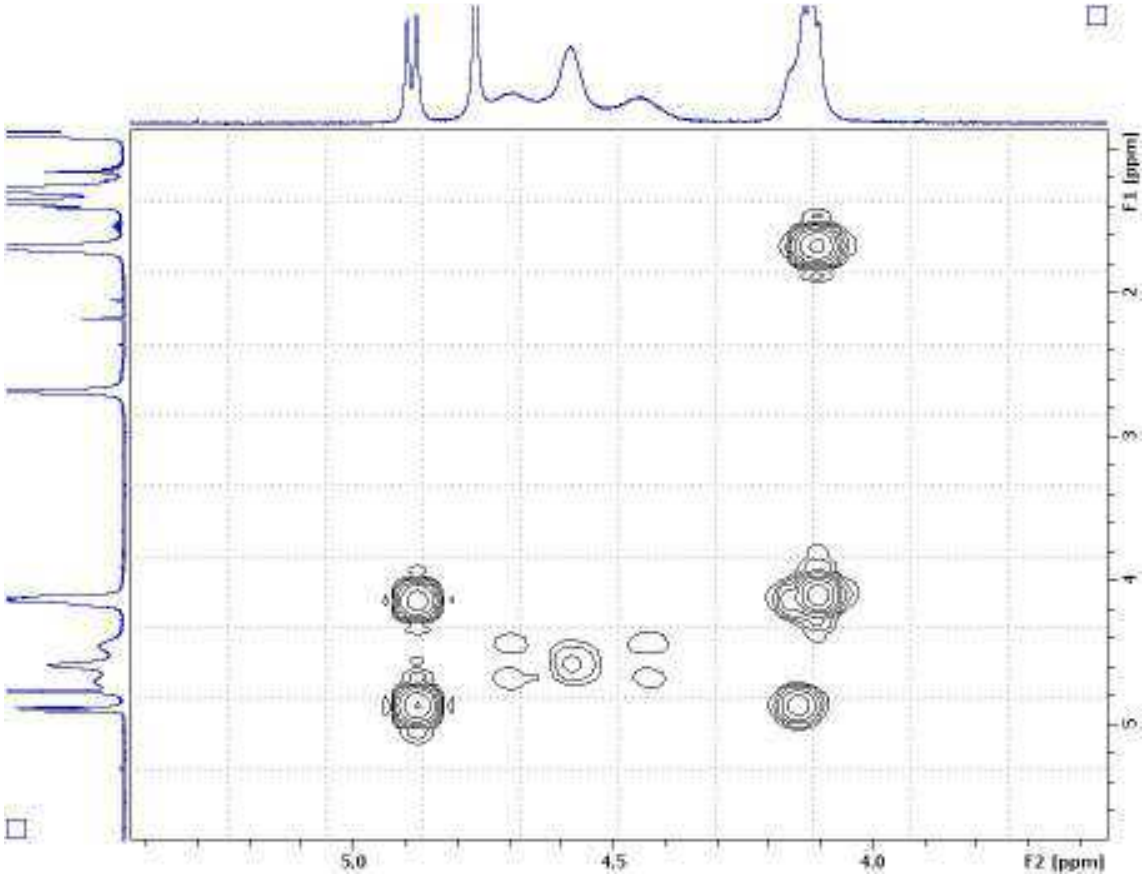

Figure II-63 COSY spectrum

Protons at 4.10 ppm (t, J = 7.5 Hz, 2H) are correlated with the CH_2 groups at 1.7 ppm and can be attributed to the $–NCH_2-$ group of the pentyl chain.

Protons at 4.58 ppm (br s, 2H) present no correlation and can be attributed to the CH_2 group of the pyrrolidine ring.

Consequently, the doublet at 4.88 ppm and three broad singlets at 4.69, 4.45 and 4.16 ppm correspond to the $-NCH_2-CH_2O-$ group. Proton at 4.16 ppm (br s, 1H) is correlated with the proton appearing at 4.88 ppm (d, J = 9.5 Hz, 1H) whereas proton at 4.45 ppm (br s) is correlated to the proton at 4.69 ppm (br s). The coupling constant (J = 9.5 Hz) is in agreement with a ^2J coupling of a methylene group.

IV : DEPT ^{13}C spectrum (125 MHz)

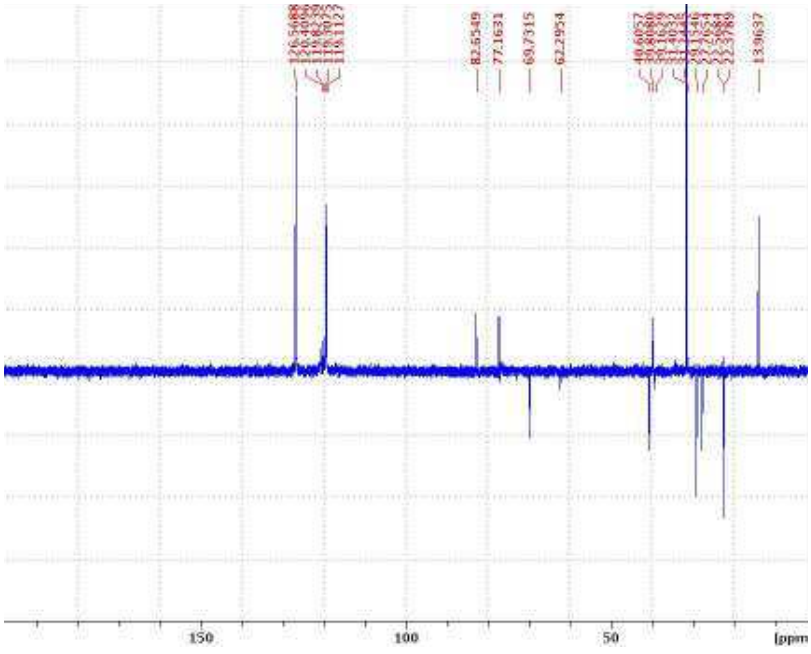

Figure II-64 DEPT spectrum

In the range 0 – 100 ppm:

- 7 groups CH_2 are observed : 22.4, 27.8, 29.1, 39.2, 40.6, 62.3, 69.7 ppm
- 13.9, 31.2, 39.8, 82.6 (the peak at 77.2 ppm corresponds to $CDCl_3$)

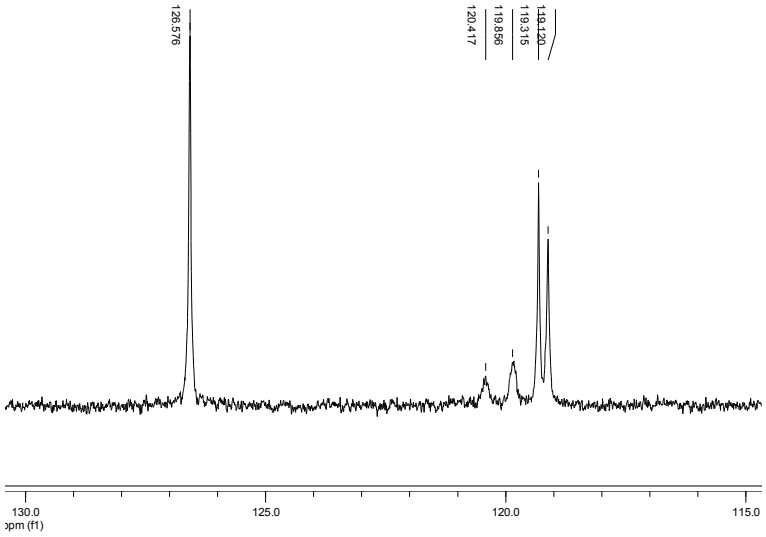

Figure II-65 ^{13}C-NMR 500MHz, $CDCl_3$, 298K

In the range from 115 to 130 ppm, five signals corresponding to the CH group of the aromatic platform and the perylenediimide core are observed at 126.6, 120.4, 119.8, 119.3 and 119.1 ppm.

V : HMQC spectrum

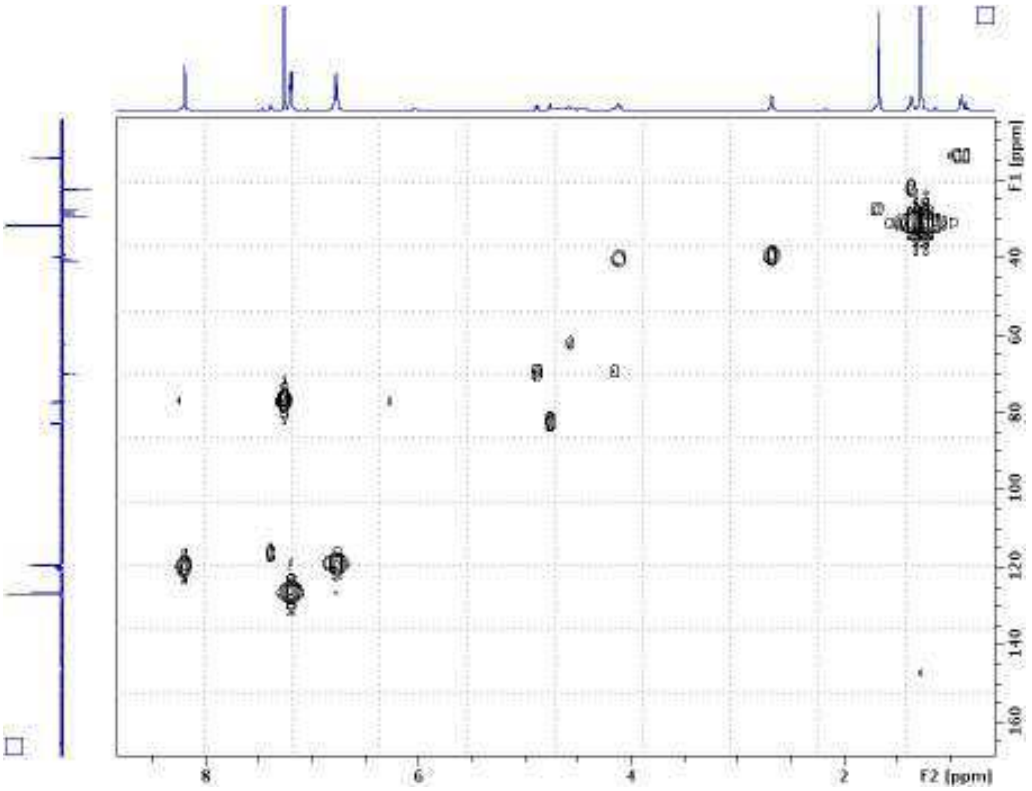

The proton signal at 2,68 ppm attributed to the N-CH_3 group of the pyrrolidine ring is correlated with the carbon at 39.8 ppm

The broad singlet at 4.58 ppm attributed to the CH_2 group of the pyrrolidine ring is correlated with the carbon at 40.6 ppm.

4.4. Electrochemical characterization

The electrochemical properties of the **Dyad 1** have been analyzed by cyclic voltammetry in dicholoromethane (or a mixture with CS_2 in the case of compound **FP**), in the presence of 0.10 M tetrabutylammonium hexafluorophosphate as supporting electrolyte and the results are presented in Figure II-66 and Table II-1. Compounds **5**, **10** and **FP** were used as model derivatives allowing the determination of the reduced species. The voltammograms have been deconvoluted in order to obtain the number of electrons involved in the processes.

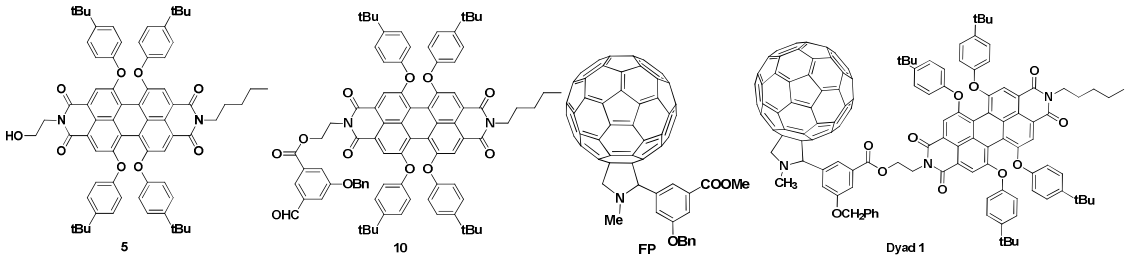

Compound 5

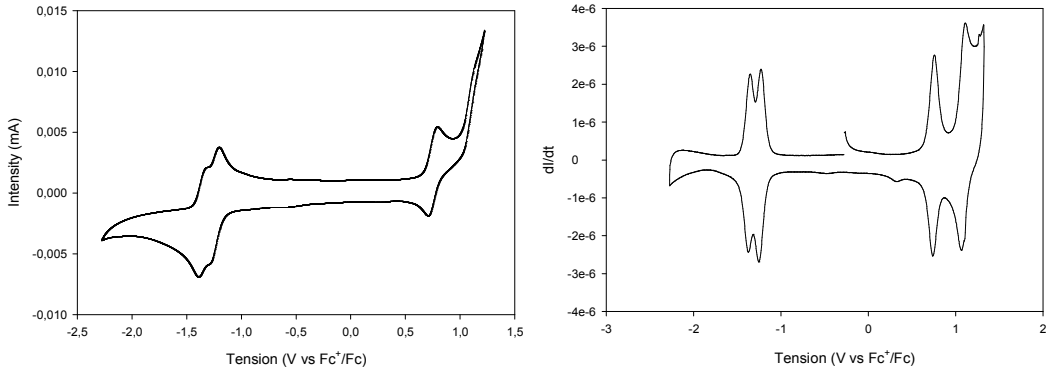

Compound 10

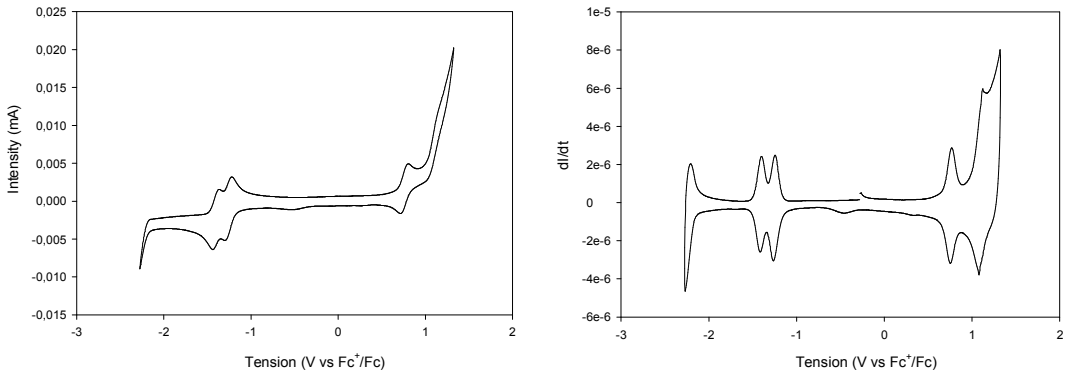

Compound FP

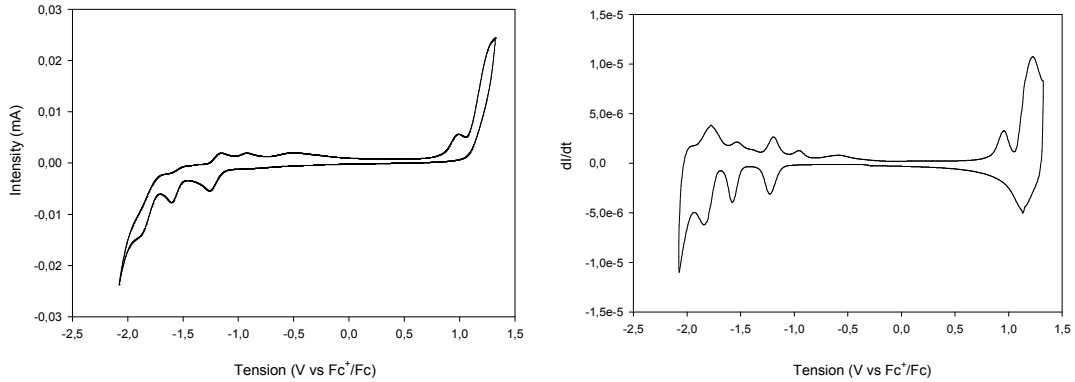

Compound Dyad 1

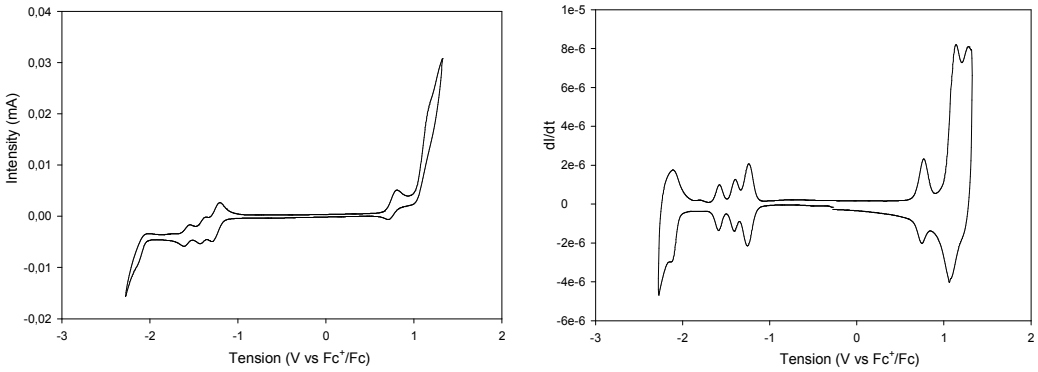

Figure II-66 Cyclic voltammograms and deconvoluted cyclic voltammograms (c=5x10^{-4}M, Pt electrodes, CH_2Cl_2 (20%CS_2 for FP)/n-Bu_4NPF_6 (0.1M)

Table II-1 Oxidation and reduction potentials for 5, 10, FP, and Dyad 1 (*vs.* Fc^+/Fc)

Compound	E^0_{red3} (V)	E^0_{red2} (V)	E^0_{red1} (V)	E^0_{ox1} (V)	E^0_{ox2} (V)	E^0_{ox3} (V)
5	-	-1.34	-1.22	+0.72	+1.11	-
10	-	-1.4	-1.24	+0.77	+1.12	-
FP	-1.78	-1.55	-1.18	+0.98 [(b)]	-	-
Dyad 1	-1.55	-1.38	-1.22[(a)]	+0.81[(a)]	+1.18[(a)]	+1.29[(b)]

[(a)] 2 electrons process; [(b)] irreversible process

Dyad 1 showed three reversible reduction waves. The first two-electron process at E^o_{red1}= -1.22 V (vs Fc^+/Fc) was assigned to the formation of the $C_{60}^{-\cdot}$-PDI $^{-\cdot}$ species. This process suggests that the first reduction wave of fullerene and the first reduction wave of the PDI are overlapping. The second one electron reduction process corresponding to the formation of the moiety $C_{60}^{-\cdot}$-PDI^{2-} was at E^o_{red2}= -1.38 V. The third one electron reduction wave appearing at E^o_{red3}= -1.55 V resulted from the formation of C_{60}^{2-}-PDI^{2-}. A first reversible two electron oxidation process arises at E^o_{ox1}=0.81 V.

Considering the cyclic voltammetry of **Dyad 1**, it could present excellent light-harvesting capabilities due to the formation of the $C_{60}^{-\cdot}$-PDI $^{-\cdot}$ that allows the energy transfer between the PDI moiety and C_{60}. The energy level of the dyad is a combination between the energy values of the dye and the fullerene. Also, this characteristic could allow rapid transfer between the PDI and C_{60}.

4.5. Photophysical characterization

UV-Vis and fluorescence spectroscopy have been employed in order to study the optical properties and to prove the transfer processes between the two moieties of **Dyad 1**.

The solvent influence on the absorption properties has been studied by using toluene and dichloromethane.

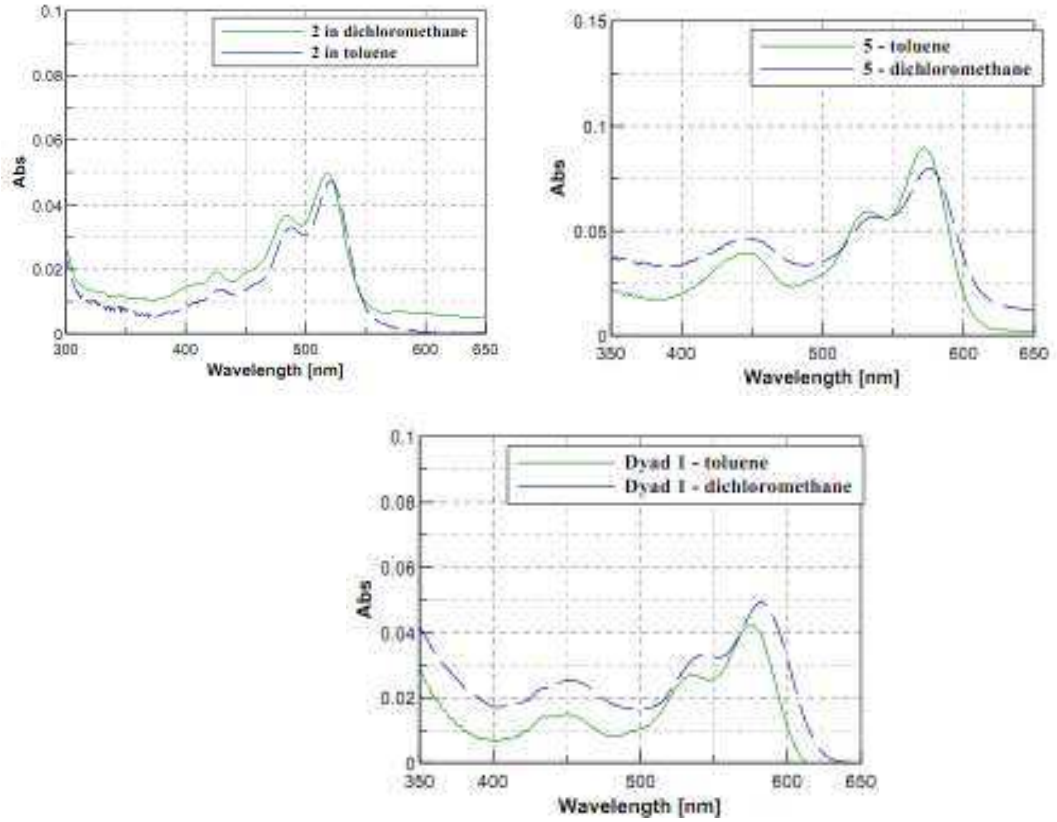

Figure II-67 Absorption spectra in toluene and dichloromethane

Table II-2 UV-Vis characteristics in CH_2Cl_2 and toluene

Compound	Maximum (nm)	
	CH_2Cl_2	Toluene
2	426, 484, 518	431, 488, 522
5	452, 540, 580	448, 535, 575
Dyad 1	229, 452, 543, 579	283, 451, 535, 573

For the PDI derivative **5** and dyad 1 it is noticed an inverse solvatochromic shift is noticed in toluene probably due to the particularly interaction between this solvent and the substituting groups of PDI (tBuPhO-).

Electronic absorption spectra of **3, 5, 10** and **Dyad 1** have been recorded in dichloromethane at room temperature.

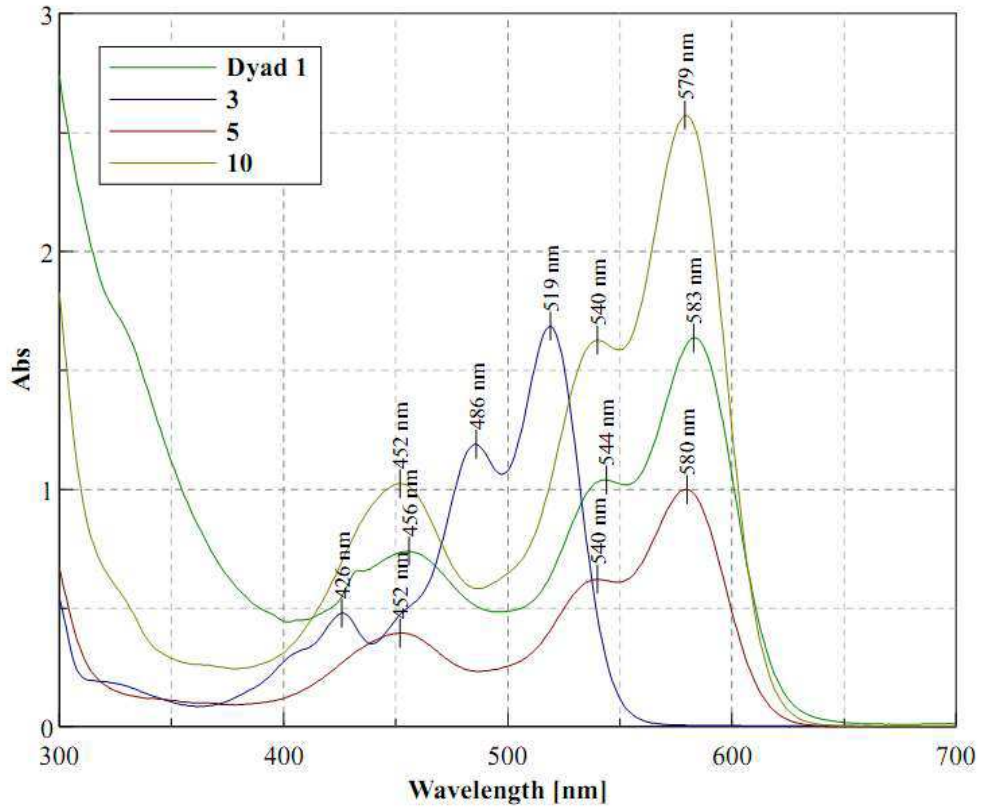

Figure II-68 UV-Vis absorption spectra for 3, 5, 10 and Dyad 1 in CH_2Cl_2

All compounds analyzed exhibit the three typical absorption peaks characteristic for PDI derivatives, at approximately 430, 485 and 520 nm for **3** or 450, 540 and 580 nm for **5**, **10** and **Dyad 1**.

Fluorescence properties

Fluorescence emission spectra of **3**, **5** and **Dyad 1** were recorded in dichloromethane and toluene.

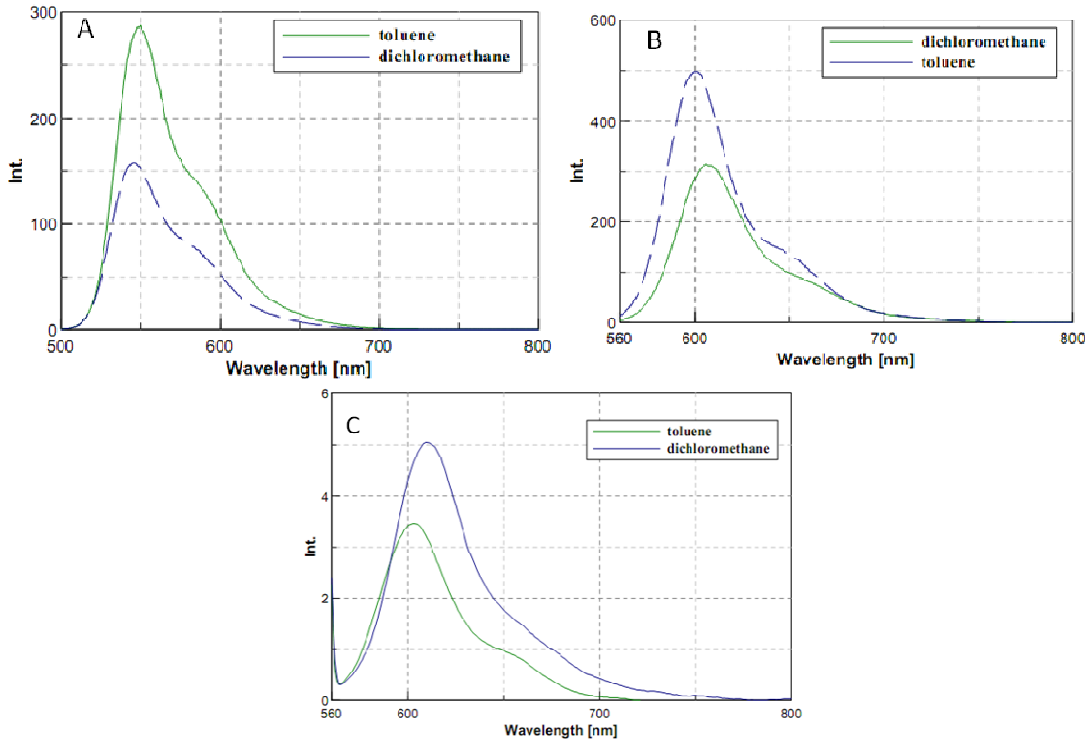

Figure II-69 Emission of: A) 2 for λ_{ex} 485 nm; B) 5 for λ_{ex} of 520 nm C) Dyad 1 for λ_{ex} of 550 nm

As expected **3**, **5** and **10** are also strongly emissive in the visible range with high fluorescence quantum yields at room temperature.

A strong quenching was observed in the case of **Dyad 1**, this is due to the strong interaction between the PDI and C_{60} in the excited state. The quantum yields were calculated using cresyl violet perchlorate as reference (ϕ_F=0.54 in ethanol)[218] and the following equation:

$$\Phi_F = \Phi_{ref} \times \frac{I}{I_{ref}} \times \frac{OD_{ref}}{OD} x \frac{n^2}{n_{ref}{}^2}, \text{ where}$$

Φ_{ref} – quantum yield of the reference;

I - the integrated intensity of fluorescence spectra for the studied compound;

I_{ref} - the integrated intensity of fluorescence spectra for the reference compound;

OD – optical density of the studied compound at $\lambda_{excitation}$;

OD_{ref} – optical density of the reference compound at $\lambda_{excitation}$;

n – refractive index of solvent for the studied compound;

n_{ref} – refractive index of solvent for the reference compound.

[218] H. Du, R.-C. A. Fuh, J. Li, L. A. Corkan and J. S. Lindsey, *Photochemistry and Photobiology,* **1998,** *68*, 141-142.

Table II-3 emission characteristics in CH_2Cl_2 and toluene

Compound	Maximum (nm)		ϕ_F	
	CH_2Cl_2	Toluene	CH_2Cl_2	Toluene
3	546	549	~ 1	~ 1
5	607	601	~ 1	~ 1
Dyad 1	610, 710	603	$2.8x10^{-3}$	$1,1x10^{-2}$

For the **Dyad 1** a fluorescence emission (in CH_2Cl_2) at 710 nm characteristic for fullerene C_{60} can be observed in the normalized spectrum Figure II-70, b, this can be interpreted as a proof of the energy transfer that takes place between the two moieties.

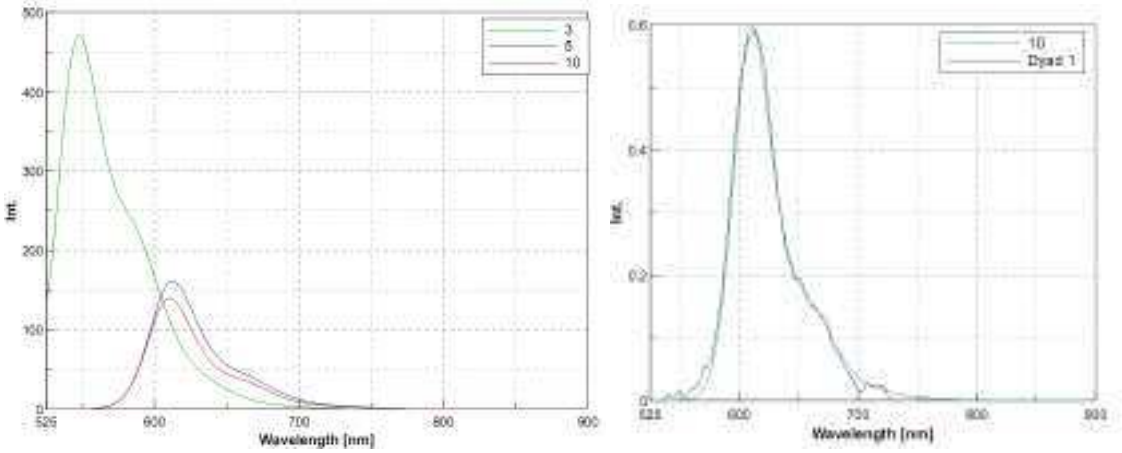

Figure II-70 a) Fluorescence at room temperature in CH_2Cl_2, b) normalized fluorescence intensity (ex. 520 nm) c=$5x10^{-6}$ M.

The obtained quantum yield for **Dyad 1** presents a strong quenching, around 99.7%. The high quenching is present both in dichloromethane and toluene; although a lower value of around 99% was obtained for toluene.

4.6. Preparation of polymer derivatives

The next objective was to obtain a polymeric structure containing grafted units of Dyad 2. The approach adopted was the utilization of a polymer containing reactive groups (poly(metacryloyl chloride)) that can be attached to the free phenolic group of Dyad 2. Other possibilities, for example the attachment of a monomer unit onto the dyad followed by subsequent polymerization can also be considered. In choosing the use of an approach it is important to take into consideration the steric hindrance and radical scavenger properties of fullerene-C_{60}. Thus, the use of poly(metacryloyl chloride) can serve as a model to investigate bulky substituent influence.

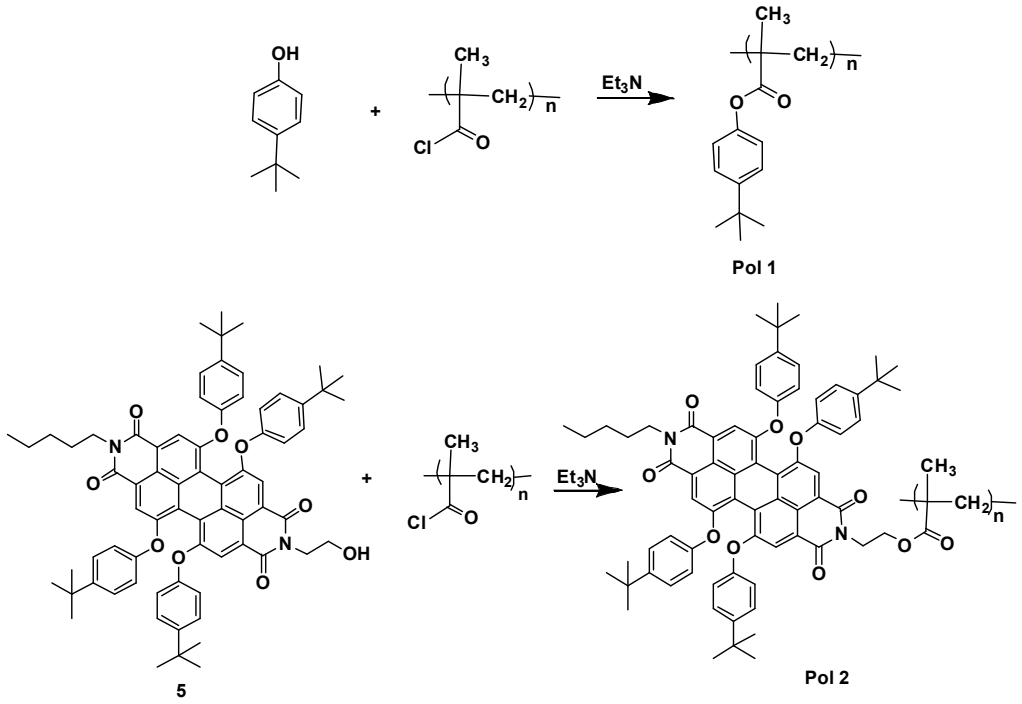

Scheme II-8 Polymer derivatives synthesis

The substitution of the poly(methacryloyl chloride) was realized in dry dioxane in the presence of triethylamine . The synthesis of the polymer derivatives is presented in Scheme II-8. Three derivatives where obtained: **Pol 1** using *p*-tert-butylphenol, **Pol 2** using **5** PDI precursors, **Pol 3** using **Dyad 2**.

IR characterization

A first characterization of the obtained polymers consisted in **IR spectroscopy**, using ATR Bruker equipment. In the case of **Pol 1** a comparison with tBuPhOH was made. The disappearing of the signal characteristic for the vibration of the OH υ_{OH}=3220 cm^{-1} was observed in the polymer. The characteristic signals for $(CH_3)_2C$- $\nu_{CH_3 as}$=2962 cm^{-1} and for ester vibration $\upsilon_{C=O}$=1748 cm^{-1} υ_{C-O}= 1204-1014 cm^{-1} are presented in the **Pol 1** spectra.

IR analysis was also performed on PDI derivative **5** and **Pol 2**. The signal for υ_{OH}=3470 cm^{-1} disappeared in **Pol 2.** The signal for $\upsilon_{C=O}$=1759 cm^{-1} (ester) appeared in **Pol 2** and also presented for C=O can be observed the signal at 1654 cm^{-1} (C=O imidic) and for C-O (1340-1100 cm^{-1}). The signal for $(CH_3)_2C$- vibration $\nu_{CH_3 as}$=2957 cm^{-1} was also observed. For the **Pol 3** the IR spectra is similar to **Pol 2**.

DSC and TGA analysis

An important characteristic of polymeric materials is the glass transition temperature, T_g. This is the temperature at which the chain segments become mobile. The glass transition is a second order transition separating the glassy state from the high elastic state of the amorphous polymers.

The most important factors influencing the glass transition temperature are:

- chemical nature of the polymer - T_g depends on the torsion potential and will be influenced by the chemical structure of the depending units-volume and polarity of substituents
- cross-linking density - due to even low degree of cross-linking, the reciprocal movement of the chain are prevented resulting in a higher T_g
- molecular weight – at glass transition temperature it is the chain segments that become mobile, not the molecule; thus, T_g is practically independent of the molecular weight
- Copolymerization – the glass transition temperature for random or alternate copolymers can be computed as an average between the characteristic transition temperatures of the two corresponding copolymers weighted by the mass fraction of each type of unit in the copolymer: $\frac{1}{T_g} = \frac{w_1}{T_{g1}} + \frac{w_2}{T_{g2}}$.

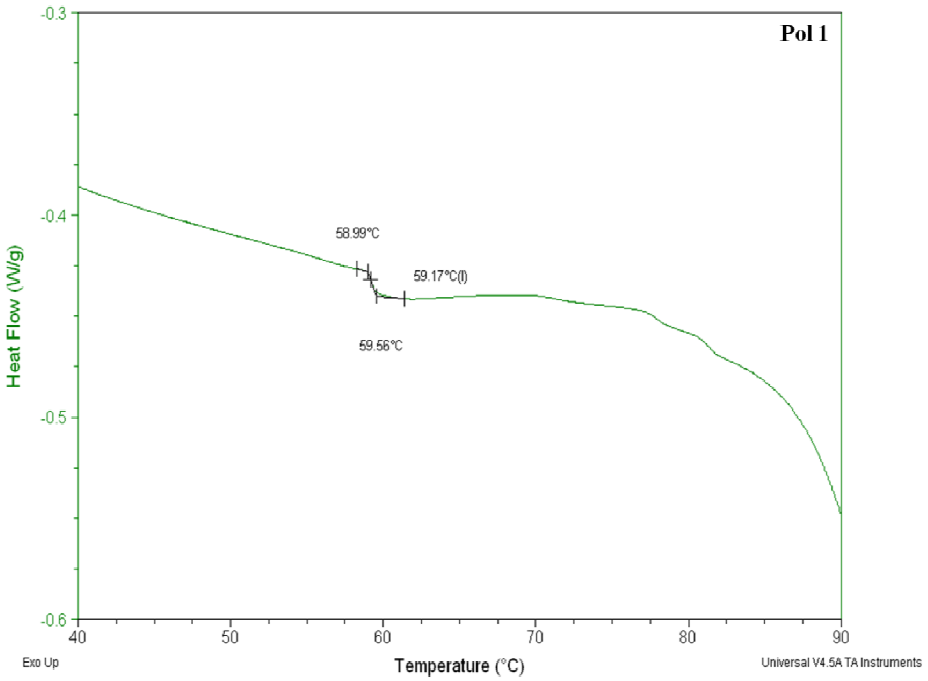

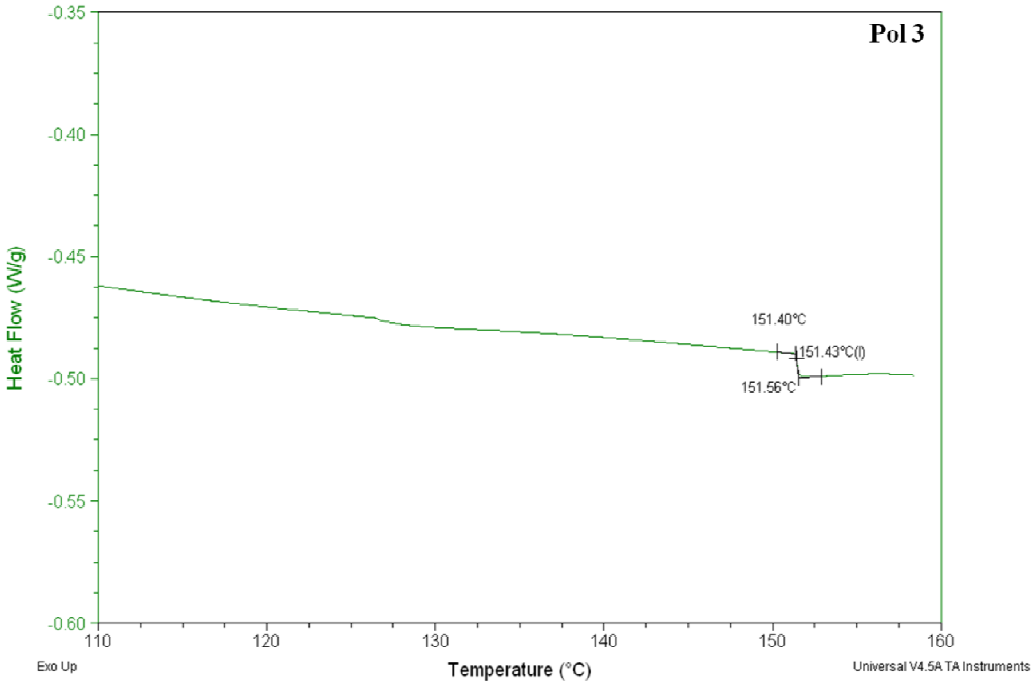

Figure II-71 DSC analysis, determination of the T_g for Pol 1 and Pol 3

Utilizing the DSC (differential scanning calorimetry) analysis the T_g (Figure II-71) values have been obtained for **Pol 1** (59°C) and **Pol 3** (151°C). A good reference for these values can be considered the polymethylmethacrylate (PMMA) that has a T_g value of 105°C. In the case of **Pol 1** the substitution of COCl with p-tert-butylphenol leads to chain segments having bulkier pending groups tBuPhO- compared to MeO- in PMMA. This leads to an increase mobility of the chain segments, thus a lower T_g value.

The value of the T_g for **Pol 3** which is higher than PMMA can be explained by several interconnected factors:

- due to the steric hindrance, the degree of substitution on the polymeric chain is reduced. The unreacted –COCl groups also undergo a hydrolysis to COOH groups which lead to an increase in the T_g as result of hydrogen bond interaction that reduces the mobility. As reference the polymetacrylic acid has a glass transition temperature of 228°C.
- although the substituent represented by the **Dyad 2** represents a bulky group, it can also form aggregates due to π-π stacking interactions limiting the mobility of segment chain.

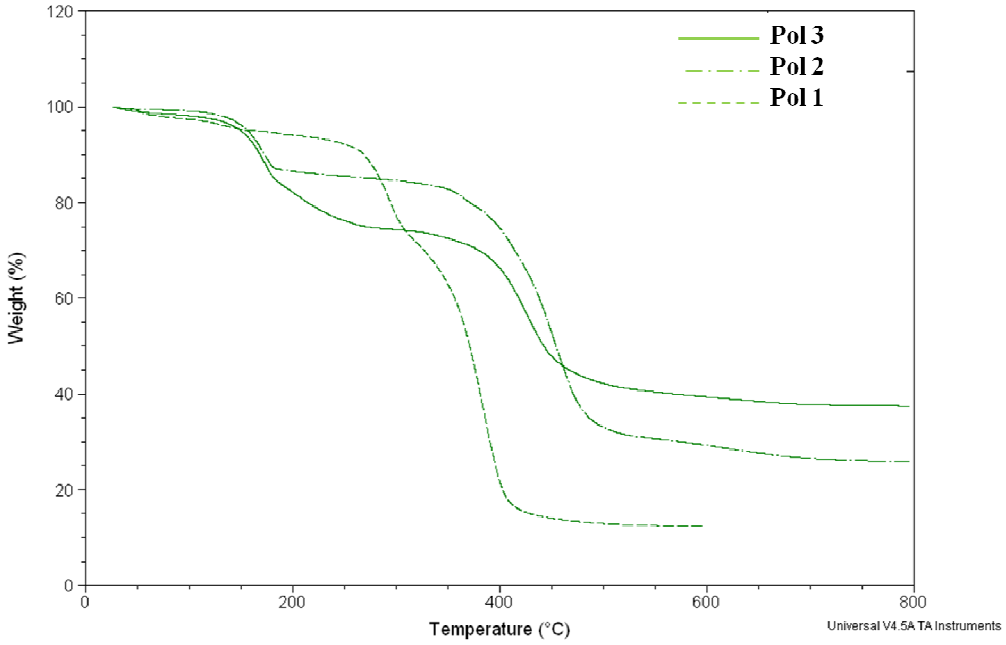

Figure II-72 TGA analysis for Pol 1, Pol 2 and Pol 3

TGA (thermogravimetric analysis) has also been conducted on the three polymeric derivatives at a heating rate of 10°C min^{-1} under nitrogen atmosphere. The data presented in Figure II-72 shows the highest thermal stability in the case of **Pol 3.** This is explained by the presence of PDI and fullerene units. For **Pol 2** is observed also an increased thermal stability compared to **Pol 1**, but lower than **Pol 3**.

The TGA analysis and DTA analysis for **Pol 3** are presented in more detail in Figure II-73.

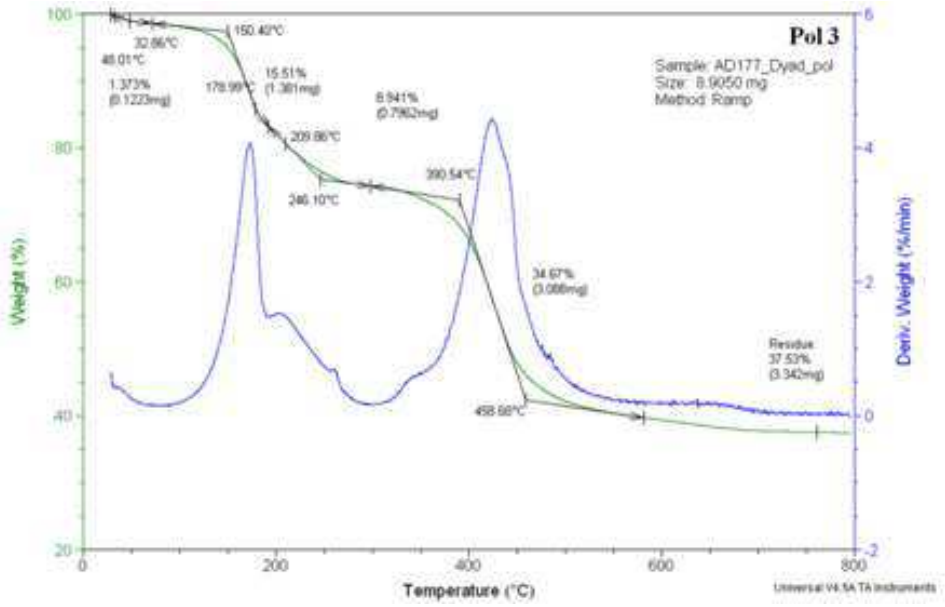

Figure II-73 TGA and DTA analysis for Pol 3

The concentration of dye/dyad in the polymer samples was determined using a colorimetric technique employing Lambert Beers' law ($A = \varepsilon \cdot c \cdot l$). A calibration curve was obtained by plotting the absorbance against concentration of dye solutions of known concentrations.

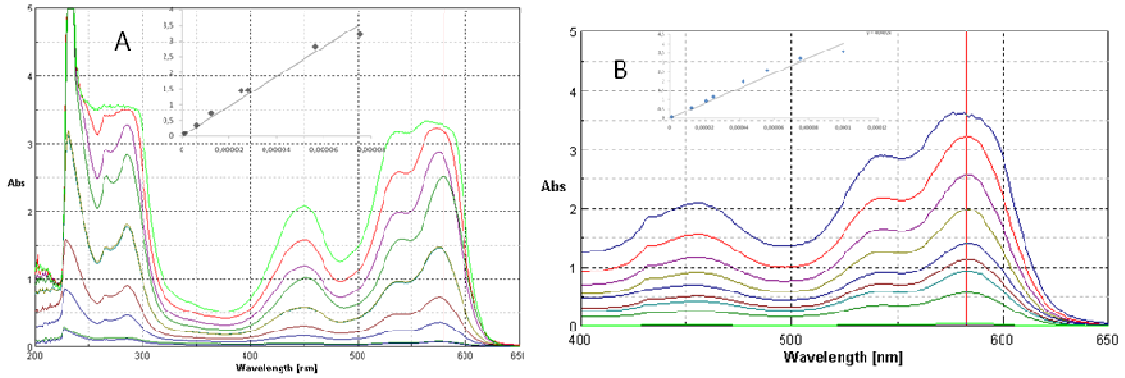

Figure II-74 UV-VIS spectra and calibration curve for (A) POL 2 and (B) POL 3

The technique permitted the determination of a 73% (weight ration, 18% molar ration) content of perylene dye in the polymer sample POL 2.

The same approach was used for POL 3 resulting in the determination of a 62% (weight ratio, 6.5% molar ration) dyad content.

The molar ratios were calculated considering the acyl chloride units hydrolyzed to acidic functions.

4.7. Conclusions

Novel light-harvesting dyads incorporating PDI and C_{60} that allow subsequent modification have been synthesized. The dyad was grafted onto a polymer chain by using its free phenol group. The dyad and the compounds used as references (5, 10, FP) have been characterized by MALDI-TOF, NMR, cyclic voltammetry, UV-Vis and fluorescence spectroscopy.

The strong quenching of the fluorescence in the case of Dyad 1 is a proof of an efficient energy transfer between the PDI and fullerene moieties. The first reduction potential of the dyad presents a two electron transfer which corresponds to the formation of $C_{60}^{\cdot-}$-$PDI^{\cdot-}$ radical species. The following process involves further reduction of C_{60}. This behavior we consider to be beneficial for obtaining bulk-heterojunction solar cells using the antenna effect.

Polymeric derivatives using the fullerene pyrrolidine PDI dyad have been obtained and characterized by DSC, TGA and IR. The high thermal stability and easy processability

makes these derivatives suitable for application bulk heterojunction solar cell manufacture. Also, the polymer chain on which the dyad is grafted presents the advantage of influencing the morphology of the heterojunction by modifying the diffusion and the self-assembly of the components. This polymer can act as a matrix for the dyad conferring the bulk-heterojunction layer an increased lifetime.

Outlook

Future investigation is needed in order to obtain the dyad using the Bingel reaction, in order to obtain another system with the only modification being the attachment of the fullerene moiety.

Comparative testing of the **dyad 1** and **Pol 3** can be performed in the obtaining of bulk heterojunction solar cells. These tests can give on insight on the influence that the polymer chain can have on the self-assembly of the component inside the heterojunction. We estimate that the polymer can have a beneficial role by modifying the morphology of the layer.

Another aspect that can be studied due to the phenolic reactive group is the self-assembly properties of the dyad in different solvents. This approach would serve for obtaining complex systems, aggregates resulted from π-π interaction and hydrophilic/hydrophobic interaction due to other substituents covalently linked to the dyad. (Scheme II-9)

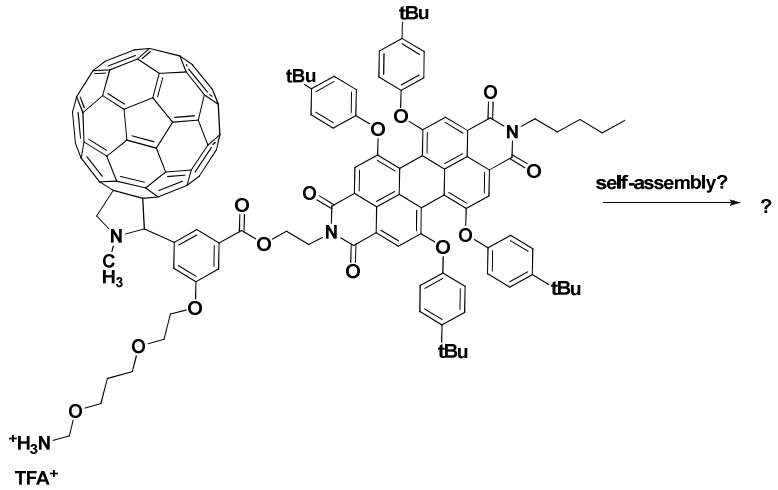

Scheme II-9 Structure envisaged in order to study the self-assembly properties in different solvents

Other important future projects involve the utilization of Dyad 2 in order to obtain novel structures like a PDI-C_{60}-TTF triad. This would represent the first triad PDI-C_{60}-TTF. An important characteristic of this triad would be the intramolecular transfer processes that are possible (energy transfer PDI-C_{60}, electron transfer TTF-C_{60}, electron transfer TTF-PDI) (Scheme II-1010).

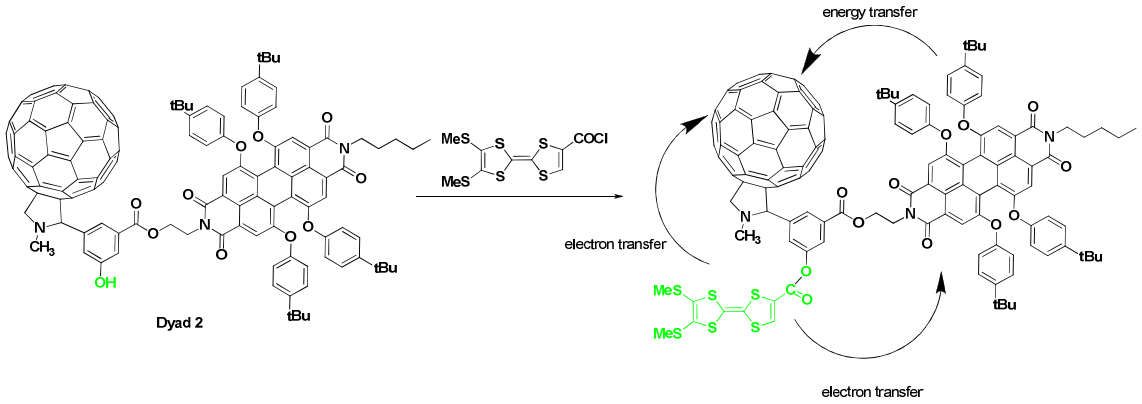

Scheme II-10 Synthesis of the first triad PDI-C_{60}-TTF

Further studies are needed in order to characterize the singlet and triplet energy-transfer in the dyads. The triplet state coupled with the transfer properties of the dyad may allow the utilization in photodynamic therapy. The Dyad 2 posses the advantage of permitting further functionalization allowing the construction of a targeting or delivery system covalently linked. Such systems can be envisaged by using a sugar (delivery system) or a peptide (targeting system).

VI. *EXPERIMENTAL*

1. New phthalocyanine-fullerene derivatives (Original Contribution)

a) Tetranitrophthalocyanine zinc (II) synthesis (Figure II-33)**:** In a three-neck round bottom flask, equipped with a mechanical stirrer, thermometer and reflux condenser, 17.3 g (0.1 mol) 4-nitro phthalodinitrile, 5 g (0.025 mol) $Zn(CH_3COO)_2$, 15 mL formamide (0.1 moli) and 40 mL N- methylpyrrolidone have been added, together with a small amount of DBU, playing the role of catalyst. The reaction mixture has been heated under stirring at 50°C. After the beginning of the reaction the temperature was increased at 125°C, then at 150°C for 1h; after another 30 minutes at 170°C, the mixture was cooled at 50°C and 50 mL of methanol were added under continuous stirring for 30 minutes. The hot mixture was filtered and was washed with methanol. The precipitate was added to 100 mL of HCl 5%, heated for 30 minutes, filtered and washed with water. A blue-violet powder was obtained (9.9 g, 50% yield).

b) Tetraaminophthalocyanine zinc (II) (F0) synthesis: (Figure II-33) In a three-neck round bottom flask, equipped with a mechanical stirrer, thermometer and reflux condenser, 9.9 g tetranitrophthalocyanine zinc (II) and 55 mL N, N-dimethylformamide (DMF) were added and the mixture was stirred at 40°C for 30 minutes to allow the dissolution of the dye. Then, a solution of $Na_2S{\cdot}9H_2O$ in 26 mL of water was added. The mixture was heated under stirring at 50-55°C for 6 h. The reaction mixture was cooled, diluted with 50 mL H_2O, filtered and washed with water. The precipitate was dissolved in 400 mL of HCl 2N and heated for 3 h at reflux, filtered to remove impurities and cooled at room temperature. The solution was neutralized with aqueous NaOH solution, filtered, washed with water and dried. A green powder was obtained (5.8 g, 70% yield).

c) Fused fullerene/phthalocyanine dyads

Synthesis of F2 (Figure II-34): 0.05 g tetraaminophthalocyanine zinc (II), 0.025 g fullerene C_{60} (F1) and 15 mL of dichlorobenzene were introduced in a round bottom flask. The mixture was stirred at 80°C, under nitrogen, for 48 h. After being cooled at room temperature, the reaction mixture was precipitated in acetone, filtered, washed with CS_2 to remove the excess fullerene and dried. A dark blue powder was obtained (0.07 g)

Synthesis of compound F4 (Figure II-34): 0.03 g monoamino phthalocyanine zinc (II), 0.03 g fullerene C_{60} (F1) and 15 mL of dichlorobenzene were introduced in a round bottom flask. The mixture was stirred at 80°C, under nitrogen, for 48 h. After being cooled at room temperature, the reaction mixture was precipitated in acetone, filtered, washed with CS_2 to remove the excess fullerene and dried. A dark blue powder was obtained (0.06 g)

d) Short spacer fullerene/phthalocyanine dyads

Synthesis of compound F3 (Figure II-35): To a solution of 0.5 g zinc tetraamino phthalocyanine in 50 mL DMF, 4 mL epichlorohydrin were added. The mixture has been stirred at 80°C for 24 h. The product was precipitated in acetone and washed with diethyl ether. A blue powder has been obtained.

To a solution of 0.4 g epichlorohydrin derivative in 50 mL DMF, 0.2 g of NaN_3 was added. The mixture was stirred at 80°C for 24h. The product was precipitated in water and separated by centrifugation, then washed with acetone and diethyl ether. A blue powder was obtained.

To a solution of 0.030 g fullerene C_{60} in 15 mL DCB, 0.045 g azide derivative was added. The mixture was stirred, under nitrogen, at 80°C for 24h. The product was precipitated in diethyl ether, filtered, washed with CS_2 to remove the excess fullerene and dried. A dark blue powder has been obtained.

2. Versatile light-harvesting dyad PDI-fullerene C_{60} building-block (Original contribution)

Synthesis of the perylene dye

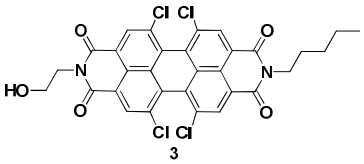

3

Exact Mass: 640,01
Molecular Weight: 642,31

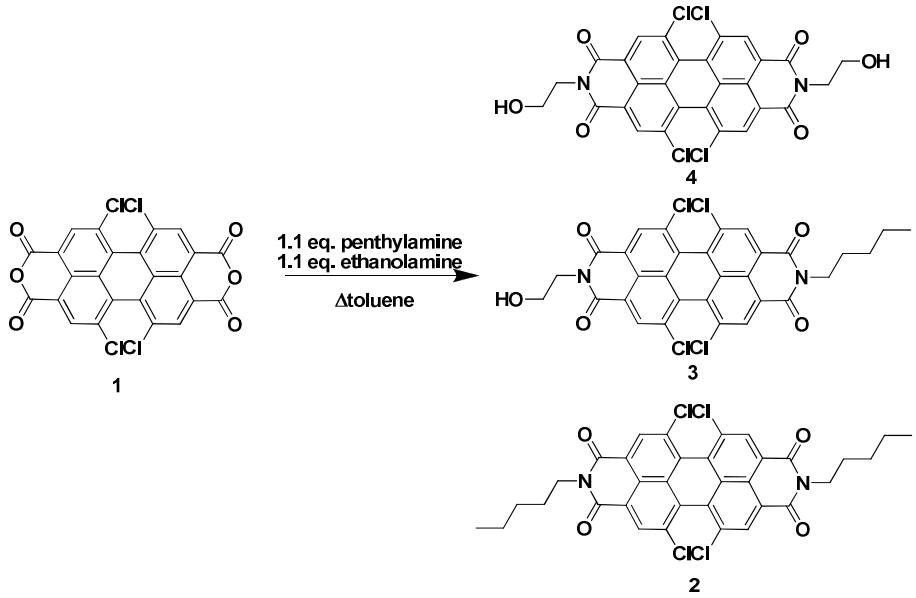

Experimental

N-2'-Hydroxyethyl-N'-pentyl-1,6,7,12-tetrachloroperylene-3,4:9,10-bis(dicarboximide) (3): To a solution of 1,6,7,12-tetrachloroperylene-3,4:9,10-tetracarboxylic dianhydride **1** (10 g; 18.9 mmol) in toluene (110 mL) was added a mixture of n-pentylamine (2.2 mL, 18.9 mmol) and ethanolamine (1.2 mL, 18.9 mmol). The reaction mixture was heated at reflux for 24 h and after cooling the solvent was concentrated under reduced pressure. The products were separated by column chromatography on silica gel. The symmetrical derivative **2** was first isolated by using CH_2Cl_2, and then the unsymmetrical compound **3** was obtained as a red powder using CH_2Cl_2/EtOAc 4:1. (2.4 g)

^{1}H NMR ($CDCl_3$ -500 MHz): δ=8.62 (s, 2H), 8.60 (s, 2H), 4.50 (t, ^3J=7.5 Hz, 2H), 4.30-4.10 (brs, 1H), 4.20 (t, ^3J=7.5 Hz, 2H), 4.00 (t, ^3J=7 Hz, 2H), 1.80 (m, 2H), 1.50 (m, 4H), 0.95 ppm (t, ^3J=7.5 Hz, 3H).

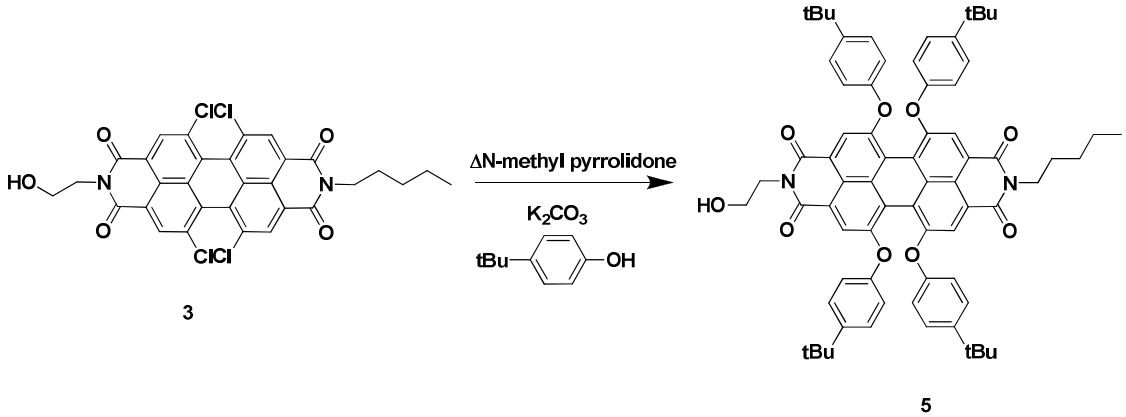

Experimental

N-2'-Hydroxyethyl-N'-pentyl-1,6,7,12-tetra(*p*-tertiobutyl)phenoxyperylene-3,4:9,10-bis(dicarboximide) (5): A mixture of perylenediimide **3** (860 mg, 1.4 mmol), *p*-tertiobutylphenol (2.1 g, 14 mmol), and K_2CO_3 (2 g, 14.5 mmol) in *N*-methylpyrrolidone (NMP) (50 mL) was stirred at 130°C under nitrogen for 14 h. After being cooled to room temperature, the reaction mixture was neutralized with HCl 1N. The precipitate was filtrated, washed thoroughly with water until neutrality, dried under vacuum at 100°C and then purified by column chromatography on silica gel using successively CH_2Cl_2 then CH_2Cl_2/acetone 30:1. Recrystallization from CH_2Cl_2/petroleum ether afforded compound **5** as a purple powder (920 mg, 60%).

^{1}H NMR ^{1}H NMR($CDCl_3$, 500 MHz): d=8.24 (s, 2 H), 8.22 (s, 2 H), 7.25 (d, ^3J=9 Hz, 8 H), 6.80 (d, ^3J =9 Hz, 8 H), 4.40 (t, ^3J =7 Hz, 2H,), 4.40–4.20 (br s, 1 H), 4.10(t, ^3J=7 Hz, 2 H), 3.93 (t, ^3J =7 Hz, 2 H), 1.70 (br t, 2 H), 1.40–1.35 (m, 4H), 1.30 (s, 36 H), 0.95 ppm (t, ^3J =7 Hz, 3H).

The synthesis of the building blocks

Building block A

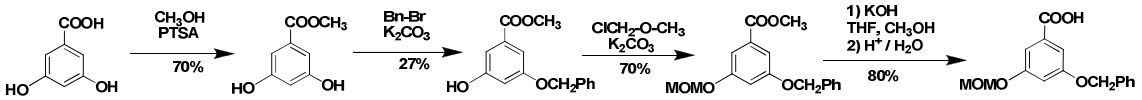

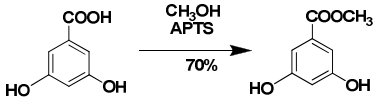

Experimental[219]

Methyl 3,5-dihydroxybenzoate: 3,5-Dihydroxybenzoic acid (15 g, 0.1 mol), p-toluenesulfonic acid (3 g, 0.016 mol), and methanol (100 mL) were heated at reflux under N_2 for 24 h before methanol was removed in vacuum. The product was dissolved in ether, then washed with water and saturated $NaHCO_3$ solution. The organic layer was dried over $MgSO_4$, filtered, and concentrated in vacuum. Recrystallization from a mixture of CH_2Cl_2 and methanol and gave a white powder in 80% yield.

^{1}H NMR (Acetone-d_6, 300 MHz): δ=8.57 (s, 2H; OH), δ=7.08 (d, *J*=2.4 Hz, 2H; PhH), δ=6.58 (t, *J*= 2.4 Hz, 1H; PhH), δ=3.82 ppm (s, 3H; OCH_3).

[219] D. Xie, M. Jiang, G. Zhang and D. Chen, *Chemistry - A European Journal,* **2007,** *13*, 3346-3353.

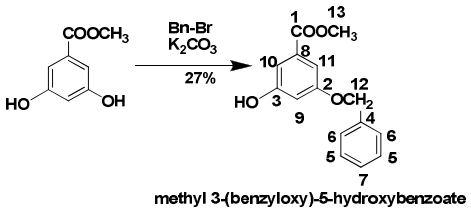

Experimental

Methyl 3-(benzyloxy)-5-hydroxybenzoate: Methyl 3,5-dihydroxybenzoate (5 g, 0.03 mol), K_2CO_3 (8.21 g, 0.06 mol) were added in 60 mL dry acetone and were degassed with N_2 before the addition of benzyl bromide (3.53 mL, 0.03 mol). The mixture was heated at reflux under N_2 for 24 h. The acetone was removed in vacuum; the remaining solid was taken with ethyl acetate and then washed with water. The aqueous layer was extracted with ethyl acetate, and the combined organic products were washed with brine, dried over $MgSO_4$, filtered, and concentrated in vacuum. The product was separated using column chromatography on silica gel petroleum ether/ethyl acetate 4:1 (2.07g, 27%).

^{1}H NMR (Acetone-d_6, 300 MHz): δ=8.7 (s, 1H; OH), δ=7.5-7.33 (m, 5H; OPhH), δ=7.15 (dd, *J*= 1.2 Hz, *J*= 2.4 Hz, 1H; PhH), δ=7.11 (dd, *J*= 1.2 Hz, *J*= 2.4 Hz, 1H; PhH), δ=6.73 (t, *J*= 2.4 Hz, 1H; PhH), δ=5.14 ppm (s, 2H; OCH_2), δ=3.84 ppm (s, 3H; OCH_3).

^{13}C NMR (Acetone-d_6, 300 MHz): δ=166.98; 160.98; 159.45; 138.05; 133.12; 129.31; 128.70; 128.42; 109.92; 107.74; 107.72; 70.64; 52.36 ppm.

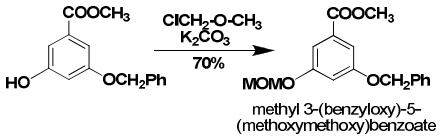

Experimental

Methyl 3-(benzyloxy)-5-(methoxymethoxy) benzoate: Methyl 3-(benzyloxy)–5-hydroxybenzoate (1.5 g, 0.006 mol), K_2CO_3 (0.82 g, 0.006 mol) were added in 60 mL dry acetone and were degassed with N_2 before the addition of chloro(methoxy)methane (0.88 mL, 0.012 mol). The mixture was stirred at room temperature for 24h. The acetone was removed in vacuum, HCl 1N was added and the solution was extracted with ethyl acetate. The organic layer was washed with brine and dried over $MgSO_4$, filtered, and concentrated in vacuum. The product was separated using column chromatography on silica gel petroleum ether/ethyl acetate 4:1. (1.75 g, 70%). ^{1}H NMR (Acetone-d_6, 300 MHz): δ=7.52-7.31 (m, 5H; OPhH), δ=7.28 (m, 2H; PhH), δ=6.93 (t, *J*= 2.4 Hz, 1H; PhH), δ=5.24 ppm (s, 2H; OCH_2), δ=5.17 (s, 2H; OCH_2), δ=3.86 (s, 3H; OCH_3), δ=3.43 ppm (s, 3H; OCH_3).

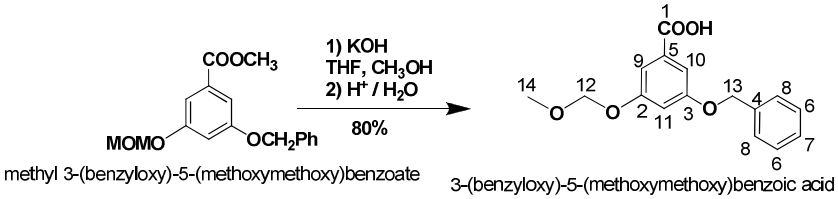

Experimental

3-(benzyloxy)-5-(methoxymethoxy) benzoic acid: To a solution of methyl 3-(benzyloxy)-5-(methoxymethoxy) benzoate (0.7 g, 0.002 mol) in 15 mL THF were added a solution of KOH (0.224 g, 0.004 mol) in 5 mL H_2O and CH_3OH (10 mL) and the mixture was heated at reflux for 24h. Dichloromethane was added and HCl 1N was used to bring the pH to 3. The organic layer was washed with brine, dried over $MgSO_4$, filtered and concentrated under vacuum. A white precipitate was obtained (0.53 g, 80%).

^{1}H NMR (Acetone-d_6, 300 MHz): δ=11.3 (brs, 1H), δ=7.52 -7.33 (m, 5H; OPhH), δ=7.32 (d, *J*= 2.1 Hz, 2H; PhH); OPhH), δ=6.93 (t, *J*= 2.4 Hz, 1H; PhH), δ=5.24 (s, 2H; OCH_2), δ=5.18 (s, 2H; OCH_2), δ=3.44 ppm (s, 3H; OCH_3).

^{13}C NMR (Acetone-d_6, 300 MHz): δ=168.18; 161.75; 160.36; 138.95; 134.48; 130.32; 129.74; 129.50; 111.68; 110.88; 109.85; 96.19; 71.76; 57.17 ppm.

Building block B

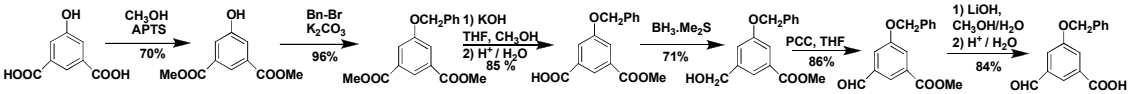

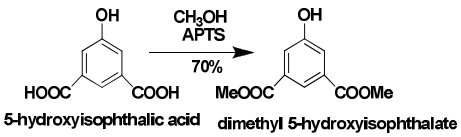

Experimental

Dimethyl 5-hydroxyisophthalate: 5-hydroxyisophthalic acid (6.34 g, 0.035 mol), p-toluenesulfonic acid (1.21 g, 0.007 mol), and methanol (120 mL) were heated at reflux under N_2 for 24 h before 2/3 of the methanol was removed in vacuum. The product was dissolved in ether, and NaOH was used to neutralize the solution, the organic layer was washed with water, dried over $MgSO_4$, filtered, and concentrated in vacuum. The product was obtained as a white powder with a 80% yield.

^{1}H NMR (Acetone-d_6, 300 MHz): δ=9.2 (s, 1H; OH), δ=8.1 (t, *J*= 1.5 Hz, 1H; PhH), δ=7.68 (d, *J*= 1.5 Hz, 2H; PhH), δ=3.9 ppm (s, 6H; OCH_3).

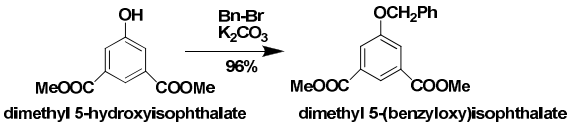

dimethyl 5-hydroxyisophthalate — dimethyl 5-(benzyloxy)isophthalate

Experimental

Dimethyl 5-(benzyloxy)isophthalate: Dimethyl 5-hydroxyisophthalate (5.8 g, 0.027 mol), K_2CO_3 (5.7 g, 0.041 mol) were added in 120 mL dry acetone and were degassed with N_2 before the addition of benzyl bromide (3.4 mL, 0.027 mol). The mixture was heated at reflux under N_2 for 24 h. The acetone was removed in vacuum; the remaining solid was taken with ethyl acetate and then washed with water. The aqueous layer was extracted with ethyl acetate, and the combined organic products were washed with brine, dried over $MgSO_4$, filtered, and concentrated in vacuum (8 g, 96.6%).

^{1}H NMR (Acetone-d_6, 300 MHz): δ=8.2 (t, *J*= 1.5 Hz, 1H; PhH), δ=7.83 (d, *J*= 1.5 Hz, 2H; PhH), δ=7.55-7.35 (m, 5H; OPhH), δ=5.28 (s, 2H; OCH_2), δ=3.92 ppm (s, 6H; OCH_3).

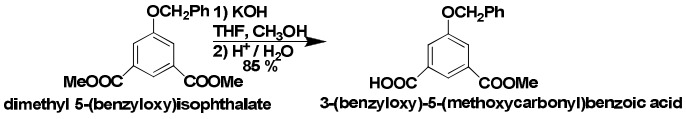

dimethyl 5-(benzyloxy)isophthalate — 3-(benzyloxy)-5-(methoxycarbonyl)benzoic acid

Experimental[214]

3-(benzyloxy)-5-(methoxycarbonyl) benzoic acid: Potassium hydroxide (85%, 0.84 g, 0.013 mol) was added to a solution of dimethyl 5-(benzyloxy)isophthalate (4 g, 0.013 mol) in methanol (60 mL) and THF (30 mL). The mixture was stirred at room reflux under N_2 overnight. The solvent was removed under vacuum, the remaining slurry was dissolved in water and washed with CH_2Cl_2. Concentrated HCl was added to the aqueous layer to pH=3. The resulting white precipitate was collected by vacuum filtration and dried in vacuum to give 3-(benzyloxy)-5-(methoxycarbonyl) benzoic acid (3.2 g, 85%).

^{1}H NMR (Acetone-d_6, 300 MHz): δ=8.24 (m, 1H; PhH), δ=7.86 (m, 1H; PhH), δ=7.86 (m, 1H; PhH), δ=7.83 (m, 1H; PhH), δ=7.55-7.34 (m, 5H; OPhH), δ=5.28 (s, 2H; OCH_2), δ=3.92 ppm (s, 3H; OCH_3).

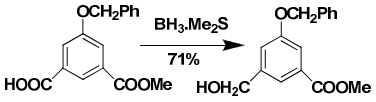

methyl 3-(benzyloxy)-5-(hydroxymethyl)benzoate

Experimental

Methyl 3-(benzyloxy)-5-(hydroxymethyl)benzoate: $BH_3(CH_3)_2S$ complex (2.0 M in THF, 4.2 mL, 8 mmol) was added dropwise to a solution of 3-(benzyloxy)-5-(methoxycarbonyl) benzoic acid (2 g, 7 mmol) in dry THF (25 mL) at 0°C. The mixture was then heated at reflux overnight. The reaction was quenched and neutralized by the addition of 1:2 H_2O/CH_3COOH (6 mL). The solvents were removed under vacuum and the slurry was dissolved in ethyl acetate, washed with 30% $K_2CO_3$1N HCl, saturated $NaHCO_3$, brine, and dried over anhydrous Na_2SO_4. The solution was then filtered concentrated. The product was purified using column chromatography on silica gel petroleum ether/ethyl acetate 4:1.The product was obtained as colorless oil (1.36 g, 70%).

^{1}H NMR (Acetone-d_6, 300 MHz): δ=7.62 (m, 1H; PhH), δ=7.52-7.28 (m, 7H; PhH), δ=5.18 (s, 2H; OCH_2), δ=4.68 (d, *J*= 5.7 Hz, 2H; OCH_2), δ=4.4 (t, *J*= 5.7 Hz, 1H; OH), δ=3.86 ppm (s, 3H; OCH_3).

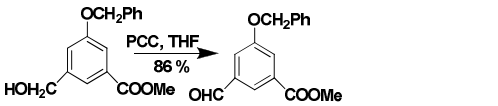

methyl 3-(benzyloxy)-5-formylbenzoate

Experimental

Methyl 3-(benzyloxy)-5-formylbenzoate: A solution of pyridinum chlorochromate in THF (PCC, 2.77 g, 0.013 mol in 25 mL) was added to a solution of methyl 3-(benzyloxy)-5-(hydroxymethyl)benzoate in THF (2.8 g, 0.011 mol, 25 mL). The mixture was heated at reflux for 24 h, diluted with CH_2Cl_2 (30 mL), filtered through Hyflo, washed with NH_4Cl and water, dried on $MgSO_4$ and concentrated under vacuum. The product was purified using column chromatography on silica gel petroleum ether/ethyl acetate 4:1, resulting as a white precipitate (2.41 g, 86%).

^{1}H NMR (Acetone-d_6, 300 MHz): δ=10.09 (s, 1H; -CHO), δ=8.12 (t, , *J*= 1.5 Hz 1H; PhH), δ=7.88 (dd, , *J*= 1.2 Hz, *J*= 1.5 Hz 1H; PhH), δ=7.77 (dd, *J*= 1.2 Hz , *J*= 1.5 Hz, 1H; PhH), δ=7.55-7.35 (m, 5H; PhH), δ=5.31 (s, 2H; OCH_2), δ=3.93 ppm (s, 3H; OCH_3).

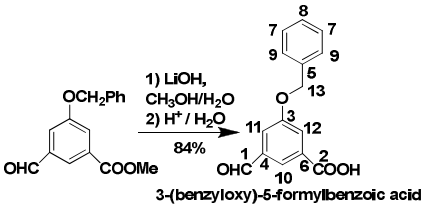

Experimental

3-(benzyloxy)-5-formylbenzoic acid: To a solution of 3-(benzyloxy)-5-formylbenzoate (0.6g, 2.2 mmol) in methanol and water (48 mL, 3:1) was added lithium hydroxide (0.1 g, 4.4 mmol). The mixture was stirred at room temperature overnight and most of the methanol was removed under vacuum. The aqueous solution was diluted with water and washed with CH_2Cl_2. Concentrated HCl was added to neutralize the solution to pH=3. The product was collected by filtration and dried under vacuum to give the 3-(benzyloxy)-5-formylbenzoic acid as a white solid (0.48 g, 84%).

^{1}H NMR (Acetone-d_6, 300 MHz): δ=10.09 (s, 1H; -CHO), δ=8.15 (t, *J*= 1.5 Hz, 1H; PhH), δ=7.91 (dd, *J*= 1.5 Hz, *J*= 2.7 Hz, 1H; PhH), δ=7.77 (dd, *J*= 1.5 Hz, *J*= 2.7 Hz, 1H; PhH), δ=7.56-7.35 (m, 5H; PhH), δ=5.31 ppm (s, 2H; OCH_2).

^{13}C NMR (Acetone-d_6, 300 MHz): δ=193.22; 167.44; 161.45; 140.34; 138.57; 134.90; 130.41; 129.92; 129.57; 125.30; 123.41; 120.14; 72.14 ppm.

<u>Attachment of the perylene dye to the building blocks and dyads synthesis building block A</u>

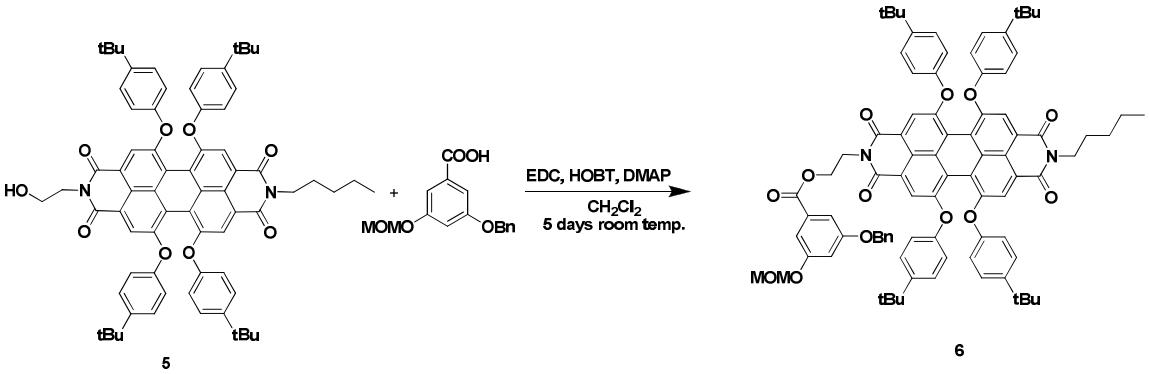

Experimental

To a degassed solution of 3-(benzyloxy)-5-(methoxymethoxy) benzoic acid (0.15 g, 0.5 mmol) in dry CH_2Cl_2 (35 mL) was added hydroxybenzotriazole (HOBt) (0.07 g, 0.5 mmol), N-(3-dimethylaminopropyl) N'-carbodiimide (EDC) (0.1 mL, 0.55 mmol), 4-dimethylaminopyridine (0.063 g, 0.5 mol) and N-2'-Hydroxyethyl-N'-pentyl-1,6,7,12-tetra(*p*-

tertiobutyl)phenoxyperylene-3,4:9,10-bis(dicarboximide) **(5)** (0.57 g, 0.5 mmol). The mixture was stirred at room temperature under argon for 5 days. The solvent was removed under reduced pressure and the residue was purified by column chromatography on silica gel using CH_2Cl_2/Acetone 30:1, resulting in a purple powder (0.62 g, 90%).)

^{1}H NMR ($CDCl_3$, 300 MHz): δ=8.24 (s, 2H), δ=8.20 (s, 2H), δ=7.36-7.27 (m, 5H), δ=7.24-7.19 (m, 10H), δ= 6.81-7.78 (m, 9H), δ= 5.05 (s, 2H), δ= 4.97 (s, 2H), δ= 4.57 (s, 4H,OCH_2CH_2N), δ= 4.10 (br t, 2H, NCH_2), δ= 3.34 (s, 3H, OCH_3), δ= 1.66 (br t, 2H), δ= 1.35 (m, 4H), δ=1.34 (s, 18H), δ=1.31 (s, 18H), δ=0.87 ppm (t, *J*=7.2 Hz, 3H).

MS (MALDI-TOF, pos. mode, dithranol): m/z: calcd for: 1366.61; found: 1366.6 $[M]^+$

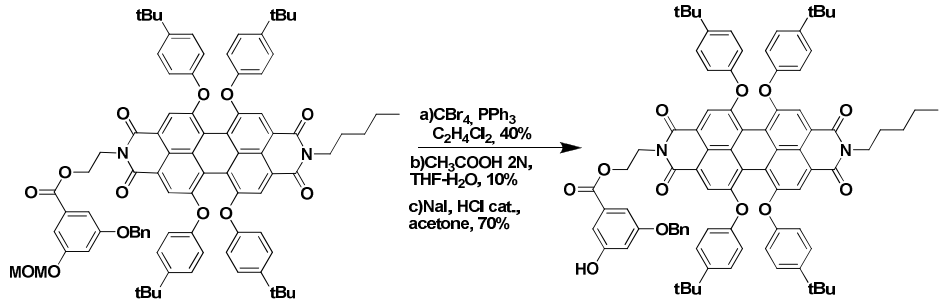

6 7

Experimental (method c)

To a solution of **6** (0.15 g, 0.11 mmol) in acetone (30 mL) was added NaI (0.025g, 0.16 mmol) and a catalytic quantity of concentrated HCl. The mixture was heated at reflux overnight. The solvent was removed under reduced pressure and the residue was dissolved in CH_2Cl_2 and washed with $NaHCO_3$, then it was dried on $MgSO_4$, filtered and concentrated under reduced pressure. The product **(7)** was purified by column chromatography on silica gel using CH_2Cl_2/Acetone 30:1, resulting in a purple powder (0.1 g, 70%).)

^{1}H NMR ($CDCl_3$, 300 MHz): δ=8.21 (s, 2H), δ=8.20 (s, 2H), δ=7.36-7.27 (m, 5H), δ=7.24 (d, *J*=8.5 Hz, 8H), δ= 7.14 (dd, *J*=1.2 Hz, *J*=2.4 Hz, 1H), 6.99 (dd, *J*=1.2 Hz, *J*=2.4Hz, 1H), δ= 6.82 and δ= 6.81 (2d, *J*=8.5 Hz, 8H), δ=6.62 (t, *J*=2.4 Hz, 1H), δ= 4.97 (s, 2H), δ= 4.56 (s, 4H, OCH_2CH_2N), δ= 4.10 (br t, 2H, NCH_2), δ= 1.66 (t br, 1H), δ= 1.35 (m, 4H), δ=1.35 (s, 18H), δ=1.28 (s, 18H), δ=0.87 ppm (t, *J*=7.2 Hz, 3H).

MS (MALDI-TOF, pos. mode, dithranol): m/z: calcd for: 1322.59; found: 1322.6 $[M]^+$

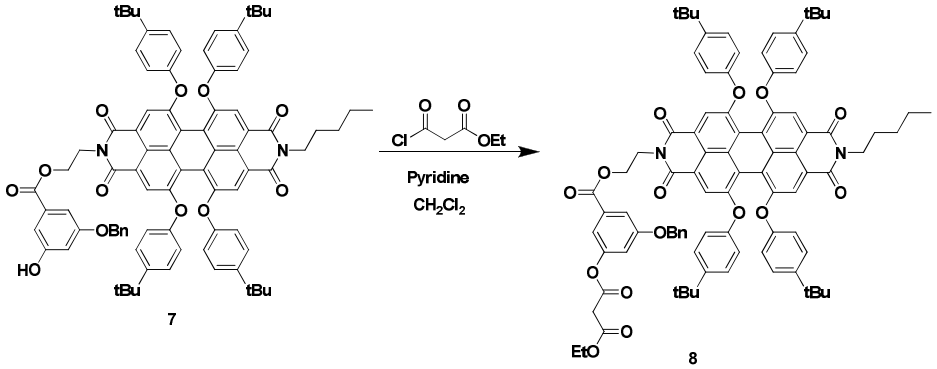

Experimental

To a solution of **(7)** (0.15 g, 0.11 mmol) in dry CH_2Cl_2 (50 mL) were added under argon at 0°C pyridine (30 µL, 0.33 mmol) and ethyl malonyl chloride 90% (50 µL, 0.33 mmol). The mixture was heated at reflux for 24 h. After cooling at room temperature, the solvent was removed under reduced pressure. The residue was purified by column chromatography on silica gel using CH_2Cl_2/acetone 30:1, resulting in a purple powder **(8)** (0.155g, 95%).

^{1}H NMR ($CDCl_3$, 300 MHz): δ=8.24 (s, 2H), δ=8.20 (s, 2H), δ=7.47 (dd, *J*=1.2 Hz, *J*=2.4 Hz 5H), δ=7.33-7.28 (m, 6H), δ= 7.24-7.18 (m, 8H), 6.99 (t, *J*=2.4 Hz, 1H), δ= 6.82 and δ= 6.81 (2d, *J*=8.5 Hz, 8H), δ= 4.98 (s, 2H), δ= 4.58 (s, 4H, OCH_2CH_2N), δ= 4.2 (q, *J*=7.2 Hz, 2H), δ= 4.1 (br t, 2H), δ= 3.5 (s, 2H), δ= 1.67 (te, 2H), δ= 1.35 (m, 4H), δ=1.29 (s, 18H), δ=1.27 (s, 18H), δ=0.87 ppm (t, *J*=7.2 Hz, 3H).

MS (MALDI-TOF, pos. mode, dithranol): m/z: calcd for: 1436.62; found: 1436.6 $[M]^+$

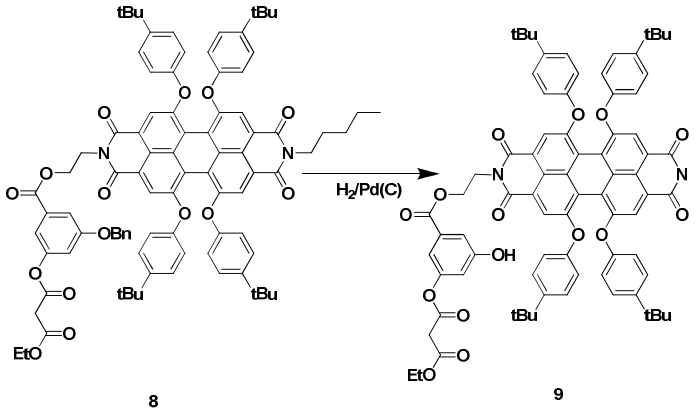

Experimental

Compound **8 (**0.245 g, 0.17 mmol) was dissolved in a mixture of CH_2Cl_2/EtOAc 3:2 (50 mL) under stirring in a three neck round-bottom flask. 10% Pd/C (30 mg) was added to the solution. A latex balloon was fitted to the flask and after degassing with nitrogen, it was filled with H_2. After stirring at room temperature for 4 days the mixture was filtered on Hyflo, the

solvent was removed under reduced pressure. The product **(9)** was purified by column chromatography on silica gel using CH_2Cl_2/acetone 30:1, resulting in a purple powder. (0.16 g, 70%).
^{1}H NMR ($CDCl_3$, 300 MHz): δ=8.21 (s, 2H), δ=8.19 (s, 2H), δ=7.25-7.21 (m, 10H), δ= 7.6.84-6.80 (m, 9H), δ= 4.58 (s, 4H, OCH_2CH_2N), δ= 4.2 (q, *J*=7.2 Hz, 2H), δ= 4.1 (br t, 2H), δ= 3.5 (s, 2H), δ= 1.68 (br t, 2H), δ= 1.35 (m, 4H), δ=1.29 (s, 18H), δ=1.27 (s, 18H), δ=0.87 ppm (t, *J*=7.2 Hz, 3H).
MS (MALDI-TOF, pos. mode, dithranol): m/z: calcd for: 1346.57; found: 1346.5 $[M]^+$

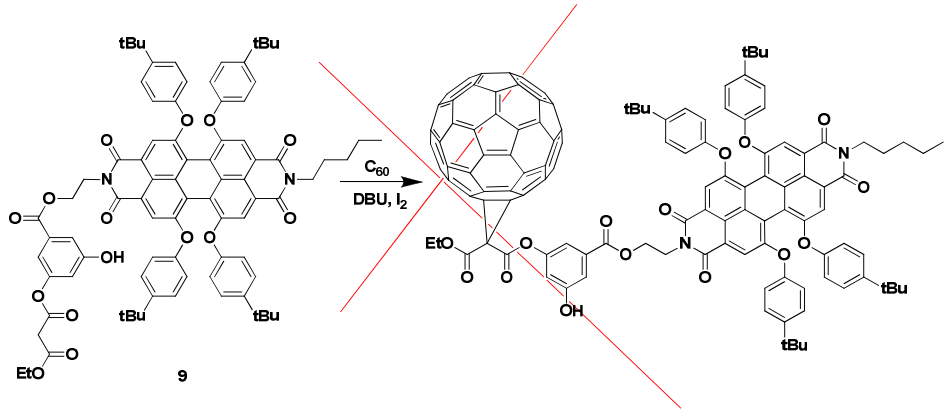

Experimental

To a solution of **9** (120 mg, 0.088 mmol) in anhydrous toluene (40 mL) were added successively fullerene C_{60} (100 mg, 0.13 mmol), iodine (34 mg, 0.34 mmol), and DBU (56 µL, 0.35 mmol). The reaction mixure was stirred at room temperature under nitrogen for 2 days. After addition of water (50 mL), the resulting emulsion was extracted with CH_2Cl_2 (3x30 mL). The combined organic phases were washed with 1N HCl (50 mL), water (2x50 mL), dried over $MgSO_4$ and concentrated under reduced pressure. The residue was purified by column chromatography on silica gel by using CS_2 to remove the excess C_{60}, then CH_2Cl_2.

<u>Attachment of the perylene dye to the building blocks and dyads synthesis building block B</u>

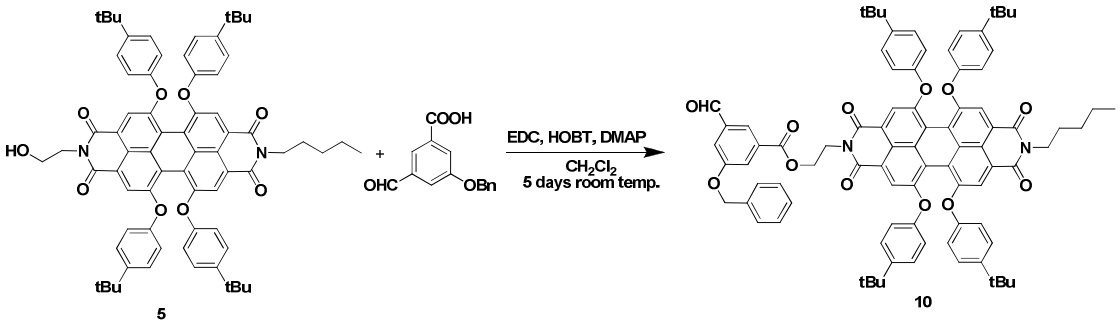

Experimental

To a degassed solution of 3-(benzyloxy)-5-formylbenzoic acid (100 mg, 0.390 mmol) in dry CH_2Cl_2 (30 mL) was added hydroxybenzotriazole (HOBt) (53 mg, 0.390 mmol), N-(3-dimethylaminopropyl) N'-carbodiimide (EDC) (82 µL, 0.429 mmol), 4-dimethylaminopyridine (48 mg, 0.39 mmol) and N-2'-Hydroxyethyl-N'-pentyl-1,6,7,12-tetra(*p*-tertiobutyl)phenoxyperylene-3,4:9,10-bis(dicarboximide) **(5)** (428 mg, 0.39 mmol). The mixture was stirred at room temperature under argon for 5 days. The solvent was removed under reduced pressure and the residue was purified by column chromatography on silica gel using CH_2Cl_2/Acetone 30:1, resulting in a purple powder (0.47 g, 90%).

^{1}H NMR ($CDCl_3$, 300 MHz): δ=9.89 (s, 1H), δ=8.23 (s, 2H), δ=8.20 (s, 2H), δ=7.99 (t, *J*=1.5 Hz,1H), δ=7.83 (dd, *J*= 1.5 Hz, *J*= 2.7Hz, 1H; PhH), δ=7.61 (dd, *J*= 1.5 Hz, *J*= 2.7Hz, 1H; PhH), δ=7.38-7.28 (m, 5H), δ= 7.24 and 7.23 (2d, *J*=9 Hz, 8H), δ= 6.82 and 6.81 (2d, *J*=8.7 Hz, 8H), δ= 5.07 (s, 2H), δ= 4.66-4.55 (br t, 4H), 4.12-4.07 (te, 2H), δ= 1.66 (br t, 2H), δ= 1.35 (m, 4H), δ=1.29 (s, 18H), δ=1.28 (s, 18H), δ=0.87 ppm (t, *J*=7.2 Hz, 3H).

^{13}C NMR ($CDCl_3$, 300 MHz) δ=191.18; 165.23; 163.68; 163.55; 159.37; 156.30; 155.95; 153.02; 152.87; 147.50; 147.47; 137.92; 135.94; 132.39; 128.79; 128.39; 127.68; 126.83; 122.76; 122.13; 121.15; 120.32; 119.53; 119.30; 77.36; 70.57; 34.52; 34.51; 31.60; 31.58; 29.34; 22.51; 14.11 ppm

MS (MALDI-TOF, pos. mode, dithranol): m/z: calcd for: 1334.59; found: 1334.6 $[M]^+$

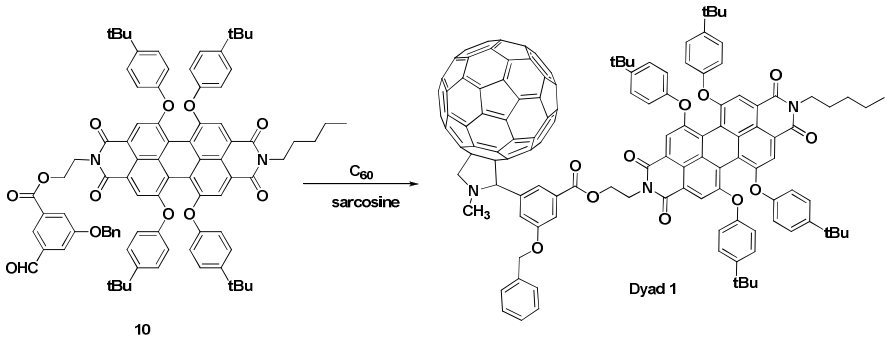

Experimental

To a solution of **(10)** (250 mg, 0.18 mmol) in anhydrous toluene (70 mL) were added fullerene-C_{60} (200 mg, 0.27 mmol) and N-methylglycine (sarcosine) (60 mg, 0.67 mmol). The reaction mixture was refluxed under nitrogen for 24 h. After the solution was cooled to room temperature, the solvent was removed under reduced pressure and the residue was purified by column chromatography on silica gel. A first column was used to remove the excess C_{60} with

CS_2, followed by a second one using toluene: ethyl acetate 100:1. The dyad was isolated as a red powder (225 mg, 60%).

Temperature dependent NMR – no very well resolved. The effect of the temperature on the two signals corresponding to the protons on the perylene bay area was studied.

^{1}H NMR ($CDCl_3$, 300 MHz 25°C): δ=8.26 (br s, 2H), δ=8.19 (s, 2H), δ=7.58 (m,1H), δ=7.38-7.28 (m, 4H), δ= 7.21-7.17 (m,10H), δ= 6.77 (m, 9H), δ= 5.06 (s, 2H), δ= 4.66-4.55 (br t, 2H), 4.12-4.07 (br t, 2H), δ= 2.7 (s, 2H),δ= 1.70 (br t, 2H), δ= 1.35 (m, 4H), δ=1.27 (s, 18H), δ=1.26 (s, 18H), δ=0.89 ppm (t, 3H).

^{1}H NMR ($CDCl_3$, 300 MHz 55°C): δ=8.26 (s, 2H), δ=8.19 (s, 2H) further discussion in the text.

MS (MALDI-TOF, pos. mode, dithranol): m/z: calcd for: 2081.53; found: 2082.5 $[M]^+$

Synthesis of model compound FP

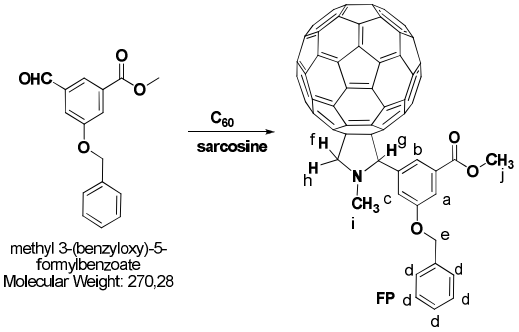

To a solution of **methyl 3-(benzyloxy)-5-formylbenzoate** (50 mg, 0.185 mmol) in anhydrous toluene (30 mL) were added fullerene-C_{60} (220 mg, 0.3 mmol) and N-methylglycine (sarcosine) (60 mg, 0.67 mmol). The reaction mixture was refluxed under nitrogen for 24 h. After the solution was cooled to room temperature, the solvent was removed under reduced pressure and the residue was purified by column chromatography on silica gel. A first column was used to remove the excess C_{60} with CS_2, followed by a second one using CH_2Cl_2. The dyad was isolated as a brown powder (30 mg, 60%).

^{1}H NMR ($CDCl_3/CS_2$, 300 MHz 25°C): 8.00 (br m, 1H), 7.66 (br m, 1H), 7.59 (m, 1H), 7.34 (m, 5H), 5.11 (s, 2H), 5.01 (d, J=9.3, 1H), 4.95 (s, 1H), 4.30 (d, J=9.4, 1H), 3.90 (s, 3H), 2.80 (s, 3H).

MS (MALDI-TOF, pos. mode, dithranol): m/z: calcd for: 1017.14; found: 1017.2 $[M]^+$

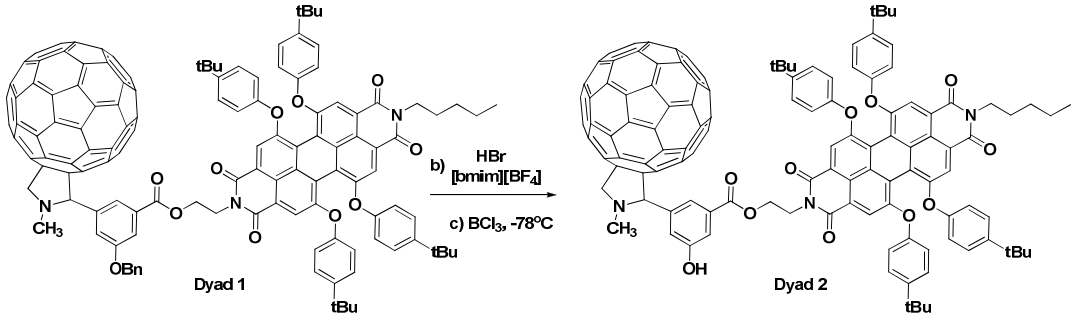

Experimental (b)

Dyad 1 (100 mg, 0.048 mmol) and concentrated hydrobromic acid (47%, 0.96 mmol) in 1-n-butyl-3-methylimidazolium tetrafluoroborate (1.5 ml) were stirred at 115°C for 36 h. The reaction mixture was extracted with CH_2Cl_2, washed with water, dried on $MgSO_4$, filtered and concentrated under vacuum. The product was purified by column chromatography on silica gel using CH_2Cl_2/acetone 30:1 to furnish a red powder (20 mg, 21%).

Experimental (c)

To a solution of Dyad 1 (372 mg) in 40 ml dry CH_2Cl_2, cooled to -78°C under argon, were added 3.5 ml BCl_3 1M in CH_2Cl_2. The reaction mixture was stirred at -78°C for 2 h after which 1 ml CH_3OH was slowly added and the temperature was left to increase to room temperature. The solvent was removed under reduced pressure and the cycle of methanol addition was repeated 3 times. The mixture was then neutralized with NH_3 solution. After extraction with CH_2Cl_2 and concentration under reduce pressure, the mixture was purified by column chromatography on silica gel using CH_2Cl_2/acetone 30:1 and reprecipitated using CH_2Cl_2/Petroleum ether resulting 250 mg red powder(70%).

MS (MALDI-TOF, pos. mode, dithranol): m/z: calcd for: 1991.59; found: 1992.3 $[M]^+$

^{13}C NMR ($CDCl_3$, 300 MHz) δ=165.94, 165.94, 163.53, 163.53, 163.36, 163.36, 156.14, 156.14, 155.72, 155.65, 155.65, 153.05, 153.05, 152.76, 152.76, 147.20, 147.20, 147.12, 147.12, 146.23, 146.18, 146.18, 146.01, 145.90, 145.90, 145.85, 145.75, 145.75, 145.68, 145.68, 145.58, 145.58, 145.28, 145.28, 145.19, 145.19, 145.12, 145.12, 144.90, 144.90, 144.37, 144.37, 144.27, 144.17, 144.17, 143.93, 142.71, 142.48, 142.48, 142.37, 142.37, 142.17, 142.10, 142.00, 141.96, 141.96, 141.86, 141.86, 141.76, 141.70, 141.70, 141.65, 141.59, 141.46, 141.46, 141.24, 139.96, 139.96, 139.54, 139.54, 139.25, 139.25, 139.15, 139.15, 136.56, 136.56, 136.10, 135.59, 135.59, 132.95, 132.95, 132.86, 132.86, 126.60, 126.60, 122.51, 122.51, 121.82, 121.82, 121.31, 121.31, 120.48, 120.34, 120.34, 119.87, 119.87, 119.60, 119.60, 119.34, 119.34, 119.12, 119.12, 82.69, 69.77, 68.83, 40.65, 39.85, 39.19, 34.34, 31.45, 29.20, 27.81, 22.61, 22.42, 14.01 ppm.

Analysis including ^{1}H-NMR, ^{13}C, DEPT, COSY, HMBC and HMQC presented in the text.

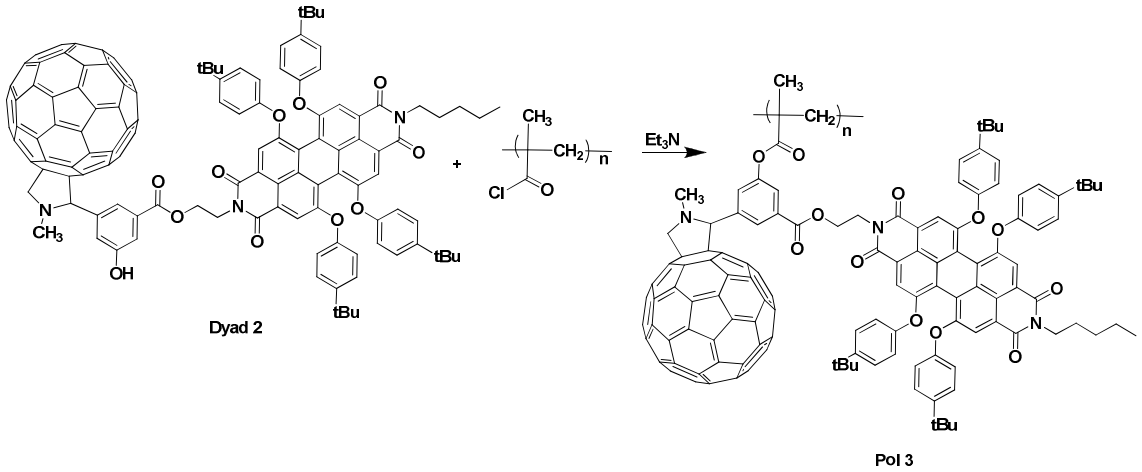

Experimental

To a solution of Dyad 2 (100 mg) in distilled dioxane (3.5 mL) under argon, were added Et_3N (10 µl) Et_3N and poly(methacryloyl chloride) 25% solution in dioxane (Polyscience) (40 µl). The reaction was stirred at room temperature for 24h before being refluxed for 2h. The mixture was concentrated under reduced pressure. The product was purified by successive precipitation using $CHCl_3$/CH_3OH and $CHCl_3$/hexane.

The characterization through IR, DSC and TGA for all polymer derivatives is presented in the discussion part.

CHAPTER III: Photonic crystals and dye interaction

I. *Introduction*

Photonic crystals, as the name suggests, are materials that present an interaction with light (photons) and have an ordered structure (a crystal is a periodic arrangement of atoms/ions or molecules).

The pattern with which the atoms/ions or molecules are repeated in space is the crystal lattice. The crystal presents a periodic potential to an electron propagating through it, and both the constituents of the crystal and the geometry of the lattice dictate the conduction properties of the crystal. Similarly, in the photonic crystal, the arrangement of particles with differing refractive index controls how photons are able to move through the crystal. Thus, photonic crystals are periodic dielectric nanostructures that affect the propagation of electromagnetic waves. The lattice structure can prevent the propagation in certain directions of specific wavelengths range, this domain representing the photonic crystal band-gap or stop-band. The arrangement of the dielectric materials can take place over one, two or all three dimensions; a simple representation of these cases is presented in Figure III-1. In a one-dimensional photonic crystal, layers of different dielectric constant may be deposited or adhered together to form a band gap in a single direction; a Bragg grating is an example of this type of photonic crystal. In two dimensions, holes may be drilled in a substrate transparent to the wavelength of radiation that the band-gap is designed to block. A three dimensional photonic crystal can be obtained using colloidal-particles by their assembly.

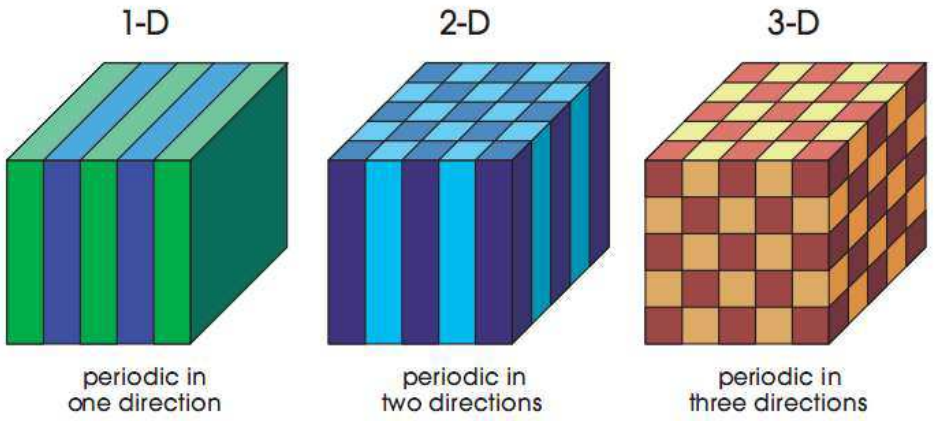

Figure III-1 Simple representation of one, two and three-dimensional arrangement, the different colors representing materials with different dielectric constants[220]

Although photonic crystals have been studied since 1887, one of the pioneers being lord Rayleigh, the term has been introduced only in 1987 after the papers of two physicist

[220] Joannopoulos, J. D., *Photonic crystals: molding the flow of light*. Princeton University Press: 2008.

working independently: Eli Yablonovitch[221] and Sajeev John[222]. Both papers dealt with high dimensional periodic optical structures – photonic crystals. Yablonovitch's objective was to engineer the photonic density of states, to control spontaneous emission of materials embedded within the photonic crystal whereas John's main motivation was to use photonic crystals to affect the localization and control of light. The first successful 3D photonic crystal that demonstrated the band-gap in the microwave region was formed by drilling three intersecting arrays of holes into a block of ceramic material. Each array is angled 35 degrees from vertical, producing a structure called yablonovite[223]. The pattern of six-millimeter-diameter holes blocks radio waves from 13 to 16 gigahertz.

The first 2D photonic crystal at optical wavelengths (in the range 800-900 nm) demonstration was made by Krauss et al.[224]. This led to the development of photonic crystals fabricated in semiconductor materials using specific techniques from this domain.

The study of three-dimensional photonic crystals has proceeded more slowly than their two-dimensional counterparts. This is because of the increased difficulty in fabrication; there was no inheritance of readily applicable techniques from the semiconductor industry for fabricators of three-dimensional photonic crystals to draw on.

Polymer chemistry permits the obtaining of monodisperse particles of a lower density compared to inorganic materials. Thus, one of the new strategies in the field of photonic crystals is to use the advantage of polymer chemistry and polymer colloids. Monodisperse particles are not sufficient for the obtaining of photonic crystals they also need to be coupled with the formation of assemblies: the crystal lattice formation. In cases where interparticle forces are sufficiently balanced (a balance being needed between attraction and repulsion forces) in a colloidal system, self-assembly can occur.

The investigation of colloidal (not only polymer colloids) self-assembly as technique of nanostructure fabrication holds technological implication. The structures obtained through this method may find applications in: photonic/plasmonic devices, nanoscale electronics, high efficiency energy-conversion/energy-storage, diagnostic systems, drug delivery and obtaining structured catalysts.[225]

[221] E. Yablonovitch, *Physical Review Letters,* **1987,** *58*, 2059.
[222] S. John, ibid., 2486.
[223] E. Yablonovitch, T. J. Gmitter and K. M. Leung, ibid. **1991,** *67*, 2295.
[224] T. F. Krauss, R. M. D. L. Rue and S. Brand, *Nature,* **1996,** *383*, 699-702.
[225] G. A. Ozin, K. Hou, B. V. Lotsch, L. Cademartiri, D. P. Puzzo, F. Scotognella, A. Ghadimi and J. Thomson, *Mater. Today,* **2009,** *12*, 12-23.

1. Polymeric nanoparticles preparation

Polymer nanoparticles can be conveniently prepared either from preformed polymers or by polymerization of the monomers using different techniques. From the preformed polymers methods like solvent evaporation, salting-out, dialysis and supercritical fluid technology involving the rapid expansion of a supercritical solution into liquid solvent, can be utilized for the preparation of polymer nanoparticles. On the other hand, polymer nanoparticles can be directly synthesized by the polymerization of monomers using various polymerization techniques such as micro-emulsion, mini-emulsion, surfactant-free (soap-free) emulsion and interfacial polymerization (Figure III-1). The choice of preparation is made on the basis of a number of factors like: area of application, polymer system, size requirement etc.

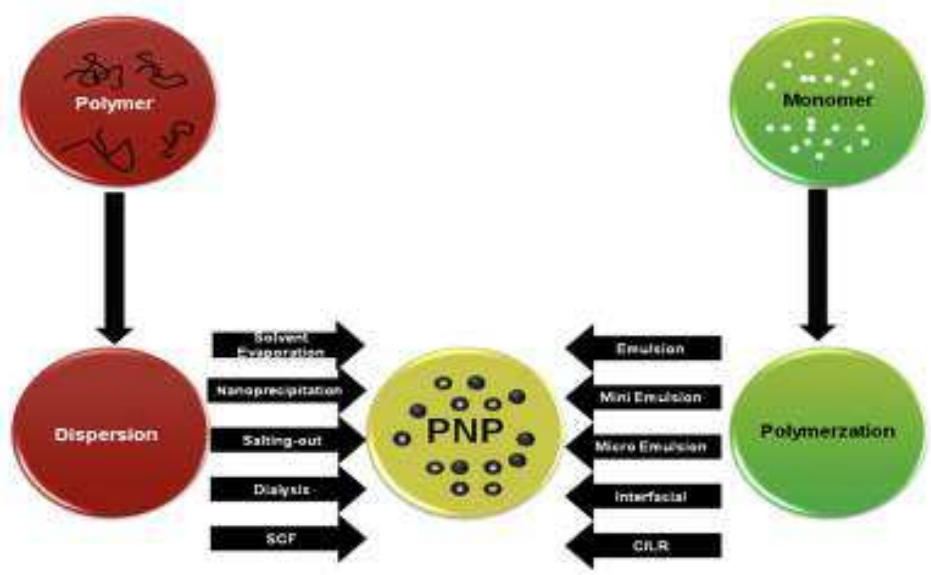

Figure III-2 Schematic representation of various techniques for the preparation of polymer nanoparticles; SCF-supercritical fluid technology; C/LR: controlled/living radical[226]

2. Emulsion polymerization

Emulsion polymerization process was first commercialized in the early 1930s for the production of synthetic rubber latexes as an alternative to the use of natural rubber latexes in tyre manufacture. During the World Word II, as natural rubber resources were limited the process was more developed and implemented. This polymerization represents one of the most widely used polymer synthesis methods for producing waterborne resins with various colloidal and physicochemical properties. This heterogeneous free radical process involves emulsification of the relatively hydrophobic monomer in water by an oil-in-water emulsifier,

[226] J. P. Rao and K. E. Geckeler, *Progress in Polymer Science,* **2011,** *36*, 887-913.

followed by the initiation reaction with usually a water soluble initiator (sodium persulfate).[227] Typical monomers used in emulsion polymerization are: syterene, acrylonitrile, methacrylate and acrylate esters etc. As the particle nuclei form and grow in size the progress of polymerization an extremely large surface area organic phase – water phase is formed. Thus, an effective stabilizer such as non-ionic and ionic surfactants is required to prevent latex particles coagulation. The amphiphilic nature of surfactant molecules causes them to partition between the water and monomer/polymer (organic phase) by adsorbing at the droplet/particle interface. Thus, satisfactory colloidal stability can be achieved via the electrostatic stabilization mechanism and/or the steric stabilization mechanism[228].

In the electrostatic stabilization mechanism, surfactant molecules provide an ionic charge when they are adsorbed at the droplet surface. The surface-charged particles repel one another electrostatically. In the steric stabilization mechanism, the surfactant molecules are water-soluble, polymeric chains that have some conformational mobility. When two particles covered with non-ionic surfactant approach one another, the adsorbed layer is compressed, thus limiting the mobility of the stabilizer chains. There is an associated, thermodynamically-undesirable increase in the free energy that causes the particles to be repelled from one another.

Surfactants lower the surface tension between the water and the monomer (organic phase). This allows smaller droplets to be formed in the water phase. In addition, the thermodynamic driving force for coalescence is lowered as a consequence of decreasing in the interfacial tension. This reasons and emulsion stabilization mechanisms make the emulsion prepared with surfactants more colloidally stable[229]. Besides coalescence, diffusional degradation is another mechanism by which emulsion can degrade into fewer, larger droplets. Monomer from smaller diffuses to larger ones as the result of the process to interfacial free energy minimization. This phenomenon is called Ostwald ripening. Most monomers have slight solubility in water so they can be transported through the water phase from the monomer droplets to the sites of polymerization (the polymer particles), the monomer concentration will overcome Ostwald ripening forces, and diffusion of monomer from large droplets to smaller monomer-swollen particles will occur. The extent of monomer diffusion can be reduced by the incorporation of a costabilizer. The extremely hydrophobic costabilizer molecules in the small monomer droplet are incapable of being dissolved in water, diffusing

[227] C. S. Chern, ibid. **2006,** *31*, 443-486.
[228] Goodwin, J. W., *Colloids and interfaces with surfactants and polymers: an introduction*. J. Wiley: 2004.
[229] Anderson, C. D.; Daniels, E. S., *Emulsion Polymerisation and Latex Applications*. Rapra Technology: 2003.

across the water phase and then entering the large droplet. Thus, monomer molecules in the large droplet are forced to migrate back to the small droplet in order to reduce the concentration gradient for costabilizer (the osmotic pressure effect) resulting in a relatively stable mini-emulsion product (Figure III-3). In addition to the conventional long-chain alkanes (hexadecane) and alcohols (cetyl alcohol), the hydrophobic species that have been evaluated as costabilizer in preparation of mini-emulsions include polymer, oil-soluble initiator (lauryl peroxide), chain transfer agent (n-dodecyl mercaptan), dye[230] and reactive costabilizers (lauryl methacrylate).

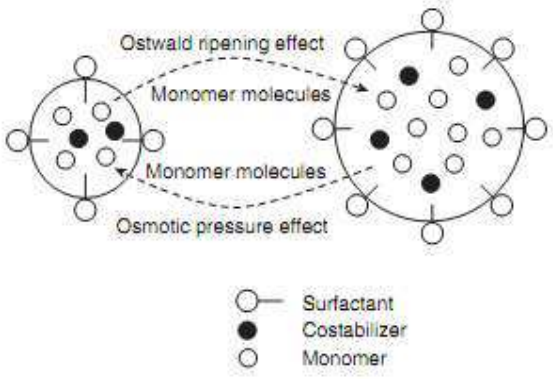

Figure III-3 Ostwald ripening effect and costabilizer effect[231]

Most emulsion polymerizations are free radical processes, but other types of polymerizations (RAFT-reversible addition-fragmentation transfer[232], ATRP- atom transfer radical polymerization[233]) have also been carried out in emulsion polymerization. There are several steps in the free radical polymerization mechanism: initiation, propagation and termination. The initiator thermal decomposition generates the free radicals which initiate the polymerization by reaction with neighboring monomer molecule. This event is the start of a new polymer chain. Because initiator molecules constantly decompose to form radicals, new polymer chains are also constantly formed. During propagation, the initiated monomeric molecules, containing an active free radical end group, come into contact with uninitiated monomer molecules and react to form dimers containing active end groups. The dimers react with monomer to become oligomers which then by propagation continue to develop in molecular weight.

$$I \xrightarrow{k_d} 2R\cdot$$

[230] C. S. Chern, T. J. Chen and Y. C. Liou, *Polymer,* **1998,** *39*, 3767-3777.
[231] Chern, C. S., *Principles and applications of emulsion polymerization*. Wiley: 2008.
[232] H. de Brouwer, J. G. Tsavalas and F. J. Schork, *Macromolecules,* **2000,** *33*, 9239-9246.
[233] J. Qiu, S. G. Gaynor and K. Matyjaszewski, ibid. **1999,** *32*, 2872-2875.

- initiation with $R_{iw} = \frac{d[R\cdot]_w}{dt} = 2k_{dw}[I]_w$ rate of initiation (the initiator being usually soluble in water, w-subscript was added for processes taking place in the water phase);

$$R_w \cdot + M_w \xrightarrow{k_{iw}} M_w \cdot$$

- initiator reaction with monomer molecules with $R_{iw} = \frac{d[M\cdot]_w}{dt} = 2k_{iw}[R\cdot]_w[M]_w$;

$$M_{jw} \cdot + M_w \xrightarrow{k_{pw}} M_{(j+1)w} \cdot$$

When the free radical end group on the growing polymer chain is deactivated, the chain stops growing, thus termination step taking place. This is realized either by combination, in which two active radical end groups meet, or by disproportionation, in which the active radical is lost from the growing polymer chain by abstraction of hydrogen from another growing chain. Chain growth may also be terminated by chain transfer to another species (monomeric or polymeric), as result branching and crosslinking (gel formation) may result. At higher conversions of monomer to polymer, the internal viscosity of the latex particles is substantial. The rate of termination drops under these conditions and the rate of polymerization accelerates. This autoaccelaration phenomenon is known as the Tromsdorff gel effect.

The surfactant keeps the emulsion droplets and latex particles colloidally stable against coalescence/aggregation. It also plays an important role in the nucleation mechanism (how the particles are formed) of the polymer latex. The amount of surfactant is critical in controlling the latex particle size distribution. As the free surfactant concentration in the water phase increases it reaches a point at which no additional surfactant is soluble – the critical micelle concentration (CMC). Any surfactant added after CMC will form aggregates called micelles. The core of the micelles is hydrophobic and attracts monomer from the stabilized droplets, thereby swelling the micelles. Radicals generated by the initiator react with the monomer dissolved in the water phase to form oligoradicals. Once the radicals reach a critical chain length, they can either aggregate to form primary particles by micellar nucleation, or enter monomer droplets directly to cause nucleation. An illustration of the various possible nucleation mechanisms is presented in Figure III-4. There are other nucleation mechanisms theories in emulsion polymerization, such as coagulative nucleation, that expand on these fundamental principles.

Fitch and Tsai proposed the homogeneous nucleation mechanism for the formation of particle nuclei in the continuous aqueous phase. First, waterborne initiator radicals are generated by the thermal decomposition of initiator and they can grow in size via the

propagation reaction with those monomer molecules dissolved in the aqueous phase. The oligomeric radicals then become water-insoluble when a critical chain length is reached. The hydrophobic oligomeric radical may thus coil up and form a particle nucleus in the aqueous phase. This is followed by formation of stable primary particles via the limited flocculation of the relatively unstable particle nuclei and adsorption of surfactant molecules on their particle surfaces. The surfactant species required to stabilize these primary particles come from those dissolved in the aqueous phase and those adsorbed on the monomer droplet surfaces.

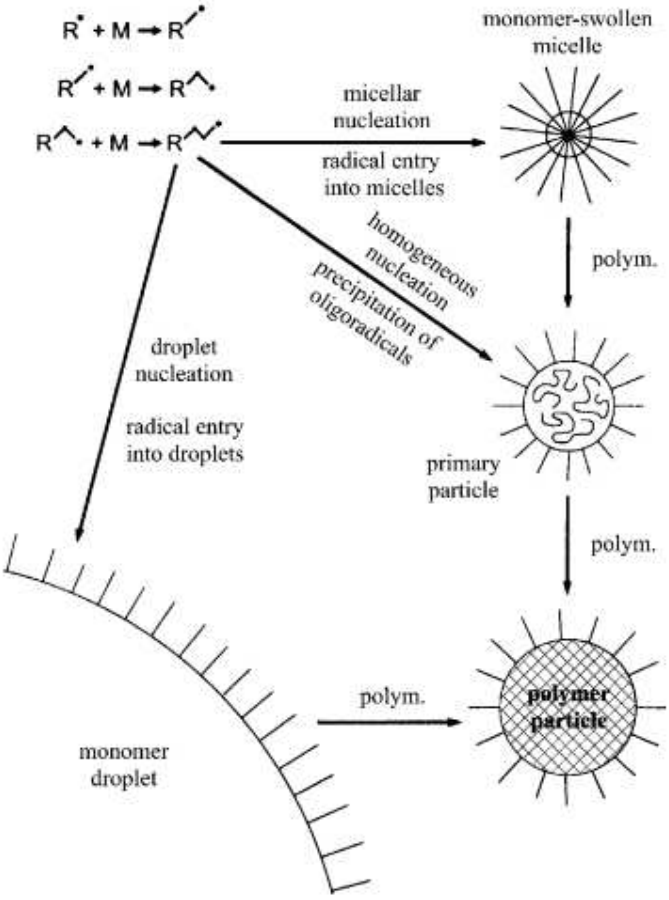

Figure III-4 Nucleation possible mechanisms: homogenous, micellar and droplet nucleation[229]

Having in mind this brief description of emulsion polymerization two characteristics important for the obtaining of photonic crystals must be repeated: the possibility to control the size of the polymer particles and to obtain monodisperse systems. The key element governing the obtaining photonic crystals structures using polymer nanoparticles is the possibility to obtain periodic assemblies. The colloidal assembly is strongly dependent on the surface characteristics of the nanoparticles and on the interactions between each particle.

As result of emulsion polymerization surfactant molecules may remain adsorbed on the surface of the polymer particles. This represents an inherent draw-back for classical

emulsion polymerization. The solution is represented by soap-free polymerization which is capable of providing the monodispersity and particle dimension control coupled with the high purity of the obtained latexes. A short presentation of the method will be made in the following paragraphs.

3. Soap-free emulsion polymerization

Soap-free or surfactant-free emulsion polymerization is an important industrial process for the manufacture of polymeric materials with excellent water resistance and adhesion properties. One of the main advantages of this technique is the fact that it leads to high purity monodisperse submicronic particles in macroscopic amounts. In the absence of surfactant, limited flocculation of latex particles greatly reduces the number of particles per unit volume of water (or increases the particle size) with progress of the polymerization. This makes the particle nucleation and growth mechanisms more complicated. Also, intensive coagulation of the particles resulting in deposits adhering to the reactor wall or agitator could become a serious problem in plant production. Thus, the colloidal stability must be addressed from the theoretical and practical view. Micellar nucleation is general ruled out for the polymerization in the absence of monomer-swollen micelles.

As early as 1965[234], monodisperse latexes of polystyrene, polymethylmethacrylate and polyvinyl acetate with particle dimension raging from 97 to 1370 nm have been obtained by soap-free polymerization using potassium persulfate as initiator.

The stabilization of the radical propagating oligomers and finally of the latexes containing particles can be achieved by different paths:

- the utilization of higher concentrations of initiator which have as results higher concentration of ions. Thus, in the case of persulfate initiator more sulfate groups will be present at the polymer particles surface Figure III-5.
- the copolymerization of hydrophobic monomers with small quantities of water-soluble monomers. Using this approach the hydrophilic functional groups remain at the surface of the polymer particles providing stabilization of the final polymer particles.
- the addition of the polyethylene containing macromonomers which induce a stabilization by a steric mechanism.

[234] A. R. Goodall, M. C. Wilkinson and J. Hearn, *Journal of Polymer Science: Polymer Chemistry Edition,* **1977,** *15*, 2193-2218.

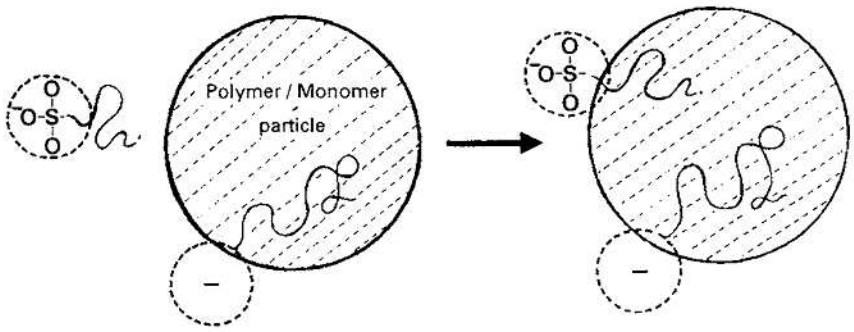

Figure III-5 Capture of surface active oligoradical to introduce functional end group at the polymer/water interface[235]

The mechanisms regarding the formation, growth and stabilization of nuclei particles are not fully understood yet in the case of surfactant-free emulsion homopolymerization, and even less in case of surfactant-free emulsion copolymerization[236]. Kinetically, the concentrations of the monomers in aqueous phase are very important for both homopolymerization and copolymerization. In the case of monomers characterized by a high solubility in water, at the reaction temperature, the homogeneous mechanism is considered as the dominant nucleation mechanism.[234] The evolution in time of the system may involve the automicellization of the oligomers radicals exceeding their solubility limit (critical chain length), as well as aggregation phenomena.[237]

Tauer et al.[238] studied the surfactant-free emulsion polymerization of styrene initiated by potassium persulfate. At the moment of particle nucleation, the number of particle nuclei per unit volume of water increased rapidly to $2 \cdot 10^{16}$ dm^{-3} and more than one polymer chain per particle was obtained. It was the aggregation nucleation (or homogeneous nucleation accompanied with limited flocculation) mechanism that controlled the particle size and particle size distribution of latex products.

Yamamoto et al.[239] used atomic force microscopy in order to clarify the growth mechanism of polystyrene particles in soap-free polymerization using a cationic initiator. They presented a schematic representation of the possible processes of the growth of polystyrene particles in the soap-free polymerization (Figure III-6). Their conclusions were: (1) As far as the initiators and monomers remain in the bulk solution, the polymeric materials (oligomers, embryo, nucleus and solidified nucleus) are born in the bulk continuously,

[235] Fitch, R. M. L., *Polymer colloids: a comprehensive introduction*. Academic Press: 1997.
[236] H.-S. Chang and S.-A. Chen, *Journal of Polymer Science Part A: Polymer Chemistry,* **1988,** *26*, 1207-1229.
[237] S. C. Thickett and R. G. Gilbert, *Polymer,* **2007,** *48*, 6965-6991.
[238] K. Tauer, R. Deckwer, I. Kühn and C. Schellenberg, *Colloid & Polymer Science,* **1999,** *277*, 607-626.
[239] T. Yamamoto, M. Nakayama, Y. Kanda and K. Higashitani, *Journal of Colloid and Interface Science,* **2006,** *297*, 112-121.

because of the slow decomposition rate of initiators. In the present case, the polymeric materials remain in the bulk even after the polymerization is terminated. (2) The growth of particles at the early stage of $t_r \geq 0.75$ h is considered to be attributable mainly to the particle swelling by absorbing monomers from the bulk. The rapid growth at the intermediate stage is due to the deposition of polymeric materials in the bulk on the particle surface and their simultaneous swelling by monomers in the bulk. Hence the particles are composed of the core solidified by polymerization and the soft shell of deposited polymeric materials. (3) The reason why the particle size increases with increasing concentration of initiator is that the growth process is controlled by the deposition rate of polymeric materials in the bulk whose amount increases with the initiator concentration. (4) The particle size and the smoothness of particle surface depend on the relative concentration of initiators and monomers remained. If the initiator concentration is relatively small, small particles with smooth surface will be formed. On the other hand, if the initiator concentration is relatively large, large particles with rough surfaces will be formed.

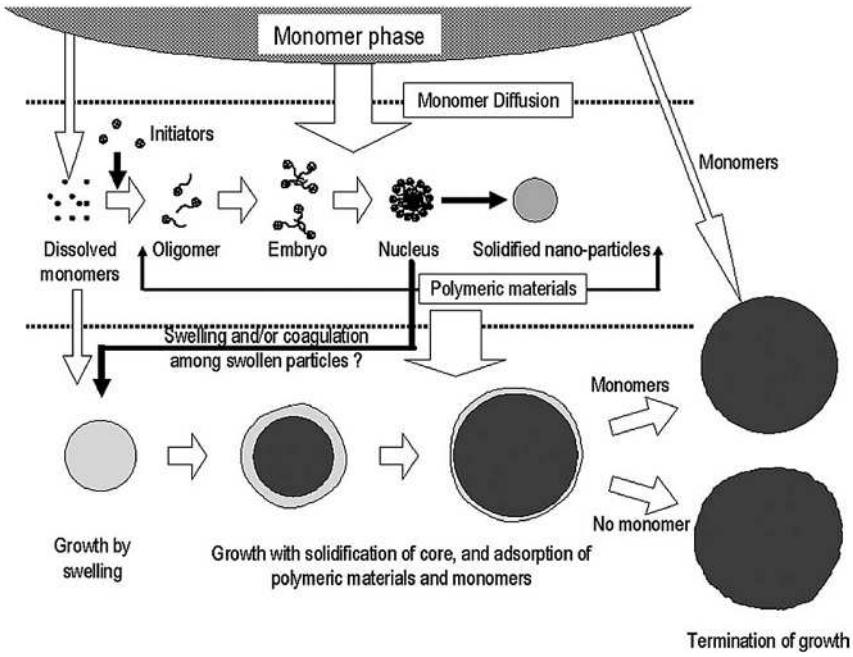

Figure III-6 Possible mechanisms for polymer particles formation in soap-free polymerization

The surfactant-free emulsion copolymerization of styrene, methyl methacrylate and acrylic acid initiated by ammonium persulfate was investigated by Yan et al.[240] As expected, both the rates of particle nucleation and polymerization increased with increasing the concentration of acrylic acid or initiator. The persulfate initiator and temperature were the

[240] C. e. Yan, S. Cheng and L. Feng, *Journal of Polymer Science Part A: Polymer Chemistry,* **1999,** *37*, 2649-2656.

predominant parameters that governed the particle nucleation process (homogeneous nucleation accompanied with limited flocculation). A shell growth mechanism was proposed to describe the particle growth stage (Figure III-7)

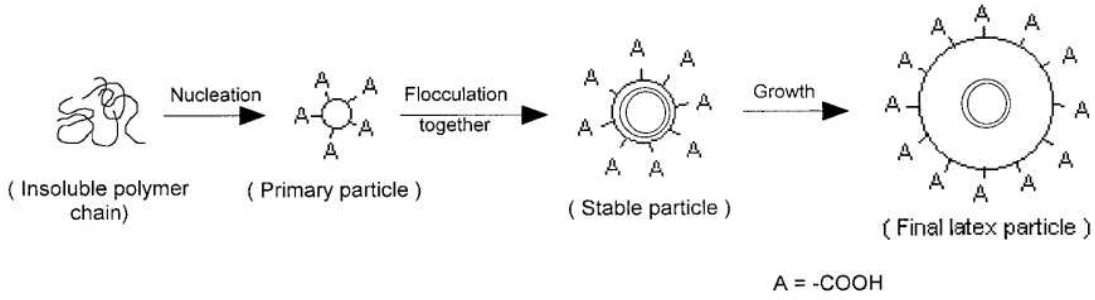

Figure III-7 Soap-free polymerization shell growth mechanism of styrene, methyl methacrylate and acrylic acid proposed by Yan et al.

Preda et al.[241] studied the effect of aqueous comonomer solubility on the emulsion copolymerization of methyl methacrylate. They evidenced both the influence of MMA saturation concentration and the solubility in aqueous phase of the comonomer (hydroxyethylacrylate or hydroxypropylacrylate) on the soap-free emulsion copolymerization. The initiator concentration influence on the particle size has been studied the selected copolymer systems. Control over particle size in soap-free polymerization was also obtained by seeded polymerization using fullerene-C_{60}. Rusen et al[242] showed that presence of fullerene is responsible for a significant decrease of the particle size as well as for the dimensional monodispersity of the obtained systems.

4. Polymer nanoparticles assemblies

The useful properties of the particle assemblies such as high surface-to-volume ration, periodicity at mesoscale, large packing density, and long-range ordering, can be utilized in optical, electronic and biosensing devices.

Self-assembly is a spontaneous process, guided by information content intrinsic to the assembling units, in which multiple levels of structural organization are built into a product[243]. The ease of spontaneous organization and the complexity of the resulting structures have made self-assembly a highly studied subject. It is akin to crystallization except

[241] N. Preda, E. Matei, M. Enculescu, E. Rusen, A. Mocanu, B. Marculescu and I. Enculescu, *Journal of Polymer Research,* **2011,** *18*, 25-30.
[242] E. Rusen, A. Mocanu, C. Corobea and B. Marculescu, *Colloids and Surfaces A: Physicochemical and Engineering Aspects,* **2010,** *355*, 23-28.
[243] Ulman, A., *Organic thin films and surfaces: directions for the nineties*. Academic Press: 1995.

that the complexity of the structural elements involved is greater in self-assembly and length-scales beyond a single lattice constant emerge in the product.

Table III-1 Processes Incorporating Self-Assembly[244]

Processes Incorporating Self-Assembly
• Adsorption of multicomponent polymers
• Cooperative supramolecular self-assembly of surfactant-inorganic mesostructures
• Grafting of polymers on interfaces
• Langmuir-Blodgett deposition
• Layer-by-layer deposition or sequential adsorption
• Micellar control of reactions
• Microcontact printing
• Organization of colloids into arrays and crystals
• Self-assembly of monolayers
• Spin and dip coating of supramolecular solutions and dispersions
• Surface directed ordering of molecules at interfaces (liquid crystals)
• Surface modification by monolayer or multilayer deposition
• Templating
• Vesicle fusion

Various methods for obtaining films of colloidal particles, such as gravitational sedimentation[245], centrifugation, vertical deposition[246], physical confinement, interfacial[247] or electric field induced self-assembly[248], spin-coating[249] have been described in the literature.

A graphical representation of the methods for 3D crystallization is presented in Figure III-8

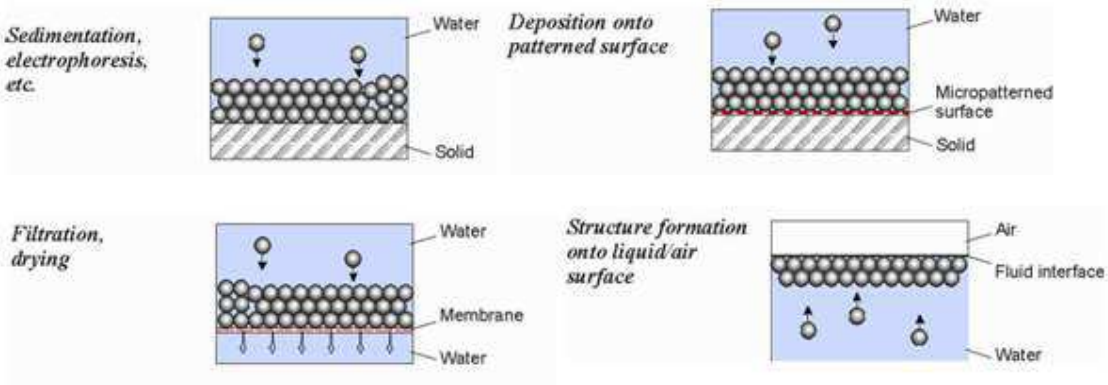

Figure III-8 Schematic representation of various methods for obtaining nanoparticles assemblies (adapted from O. D. Velev lecture available online http://crystal.che.ncsu.edu/colloidal/4_1_3D_all.html)

[244] J. Texter and M. Tirrell, *AlChE J.,* **2001,** *47*, 1706-1710.
[245] G. I. N. Waterhouse and M. R. Waterland, *Polyhedron,* **2007,** *26*, 356-368.
[246] H. Ge, Y. Song, L. Jiang and D. Zhu, *Thin Solid Films,* **2006,** *515*, 1539-1543.
[247] L. Zhang and Y. Xiong, *Journal of Colloid and Interface Science,* **2007,** *306*, 428-432.
[248] J. Zhang, Z. Sun and B. Yang, *Current Opinion in Colloid & Interface Science,* **2009,** *14*, 103-114.
[249] A. Chiappini, C. Armellini, A. Chiasera, M. Ferrari, L. Fortes, M. Clara Gonçalves, R. Guider, Y. Jestin, R. Retoux, G. Nunzi Conti, S. Pelli, R. M. Almeida and G. C. Righini, *Journal of Non-Crystalline Solids,* **2009,** *355*, 1167-1170.

Although many alternative methods for obtaining colloidal crystals by deposing spherical, monodisperse particles, on plane surface have been reported, the assembly process always involves three distinctive stages[250]:

- a concentration of the colloidal particles on the substrate surface, phenomenon based on the reciprocal adherence;
- a compact disposition of the particles in a planar 2D network due to the lateral inter-particles attractions;
- an increase of the thickness of the layer by successive deposition of new crystalline planes on the initial planar area, thus leading to a 3D – spatial network, with a compact hexagonal (hcp) or centered cubic (ccp) geometry.

None of the above stages was proven as dominant for the entire process, thus it is reasonable to consider that the relative importance of the stages is the same as their chronological order. One of the major problems is to define the driving forces nature of the assembly process. An exhaustive and pertinent analysis of the complex physical interaction phenomena involved during concentration of the disperse particles revealed the fact that the capillary forces play a decisive role, both due to their intensity and their interaction radius.

The ordering starts when the thickness of the water layer containing particles becomes approximately equal to the particle diameter. Denkov et al[251] proved that neither the electrostatic repulsion nor the van der Waals attraction between the particles is responsible for the formation of two-dimensional crystals (Figure III-9). The direct observations revealed the main factors governing the ordering – the convective transport of particles toward the ordered region due to water evaporation and only at the nucleus formation stages the attractive capillary forces.

[250] Laine, V. E., *Photonic Crystals: Fabrication, Band Structure and Applications*. Nova Science Pub Inc: 2010.
[251] N. Denkov, O. Velev, P. Kralchevski, I. Ivanov, H. Yoshimura and K. Nagayama, *Langmuir,* **1992,** *8*, 3183-3190.

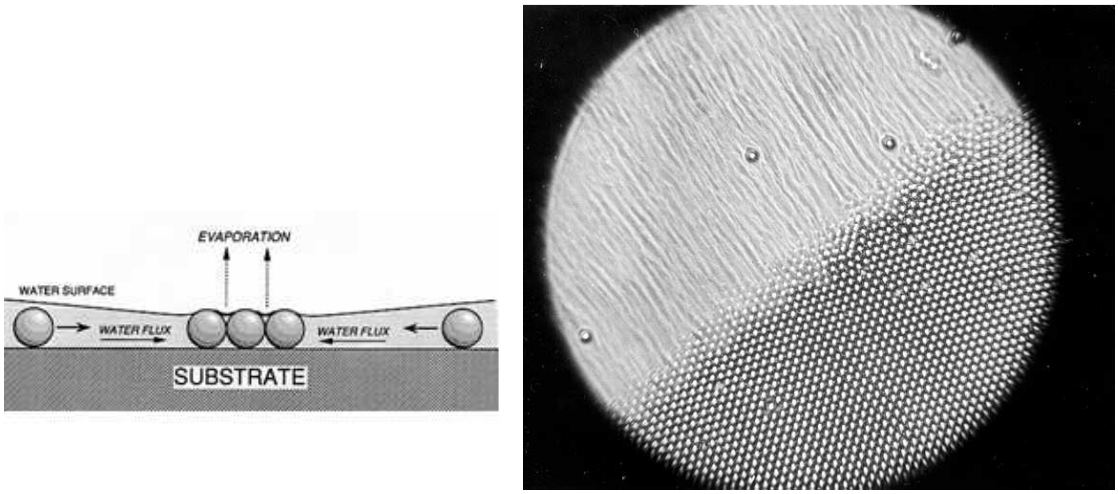

Figure III-9 First stage in 2D crystal formation and microphotograph of the "live" process of 2D array formation. The "worm-like" traces on the top left side of the photograph are the actual trajectories of the particles moving during the exposure period. Particle diameter is 1.7 µm

However, the capillary force does not represent a sufficient explanation. Cardoso et al.[252] have explained the importance of a hydrophilic comonomer, leading both to a decrease in the water evaporation rate and to a slower decrease of the interstitial zones, thus excluding the problems related to the mass transfer and facilitating attaining an equilibrium state of the ordered particles.

[252] A. Herzog Cardoso, C. A. P. Leite, M. E. D. Zaniquelli and F. Galembeck, *Colloids and Surfaces A: Physicochemical and Engineering Aspects,* **1998,** *144*, 207-217.

II. *Photophysical properties of dye doped photonic crystals (Original Contribution)*

As presented in the previous paragraphs, photonic crystals (PC) are generally characterized by artificial structures with a periodic dielectric arrangement which does not allow propagation of light in all directions (3D arrangements) for a given frequency range.

The aim of this research was to study the influence of photonic crystals on emmision properties of fluorescent dyes. The presentation of the results will be devided into the two topics studied.

First the use of a highly perrylene diimide derivative (PDI) during soap free emulsion polymerization of resulted in the obtaining of monodisperse core-shell particles which allowed the fabrication of PC films. The properties of the hybrid material were studied in comparison with hybrid materials obtained by impregnation of films with chromophores solutions. In both cases an increase of the fluorescence response was observed and also a blue shift for the PDI core particles proving the incorporation of the dye inside the copolymer particles. [253]

The second topic involved the obtaining photonic crystal heterostructures using monodisperse polymer particles dispersion and a colloidal gold solution. The obtained structures served as platform for the self-assembly of aliphatic chains containing hydroxy-thiol groups (HO-R-SH). The hydroxyl group allowed the attachment of Rhodamine B dye. The fluorescence properties of the obtained structure have been compared to a Rhodamine B film deposited on a simple glass surface. Also, by modifying Rhodamine B with TETA (triethylentetraamine) the chemosensor properties of the obtained materials have been investigated.[254]

1. Photonic crystals doped with fluorescent dyes

Organic dyes are commonly used due to their high fluorescence quantum yields for investigating stimulated emissions from photonic structures with stop bands such as synthetic opals[255, 256]. From a general point of view the localization of light emitters in PCs-based architectures allows the investigation of the stop-band influence on the photoluminescence

[253] A. Diacon, E. Rusen, A. Mocanu, P. Hudhomme and C. Cincu, *Langmuir,* **2011,** *27*, 7464-7470.
[254] E. Rusen, A. Mocanu, A. Diacon and B. Marculescu, *The Journal of Physical Chemistry C,* **2011,** *115*, 14947-14953.
[255] Z. Yang, J. Zhou, X. Huang, G. Yang, Q. Xie, L. Sun, B. Li and L. Li, *Chemical Physics Letters,* **2008,** *455*, 55-58.
[256] R. Withnall and et al., *Journal of Optics A: Pure and Applied Optics,* **2003,** *5*, S81.

properties[257, 258]. Near the stop-band of PCs, light propagates at reduced group velocities owing to resonant Bragg scattering, which can enhance luminescence owing to stimulated emission and amplify the absorption of incident light. Hybrid materials have been fabricated by incorporation of dye molecules into PCs through an emulsion polymerization process in case of water soluble chromophores[259]. Another strategy consists in incorporating dyes by a swelling and deswelling process of the already synthesized colloids[260].

Perylenediimide (PDI) dyes represent a well-recognized class of functional chromophores and fluorophores[261] which have been extensively used as organic n-type semiconducting materials for a wide range of applications including organic field effect transistors[262], organic light-emitting diodes[263] and organic solar cells[264]. These building-blocks have also been incorporated in architectures to obtain artificial photosynthetic systems[265], logic gates[266], molecular optical switches[267], sensors[268] and photosensitizers[269].

In this study, hybrid materials comprised of PDI and PCs have been obtained by two different methods:

- soap free emulsion polymerization of styrene (ST) and acrylic acid (AA) in the presence of PDI, despite poor solubility of the dye in water. The substitution on the bay area and the imide functionalization[261, 270] of PDI enhances the solubility in organic solvents, such as styrene, thus making possible the polymerization process. Consequently, we have chosen a dissymmetrical PDI derivative for which the substitution at the bay region allows the solubility in organic solvent and the presence of the alcohol functionality increases the hydrophilic character.

[257] M. Muller, R. Zentel, T. Maka, S. G. Romanov and C. M. Sotomayor Torres, *Chemistry of Materials,* **2000,** *12*, 2508-2512.
[258] F. Fleischhaker and R. Zentel, ibid. **2005,** *17*, 1346-1351.
[259] S. G. Romanov, T. Maka, C. M. S. Torres, M. Muller and R. Zentel, *Applied Physics Letters,* **1999,** *75*, 1057-1059.
[260] B. Lange, R. Zentel, C. Ober and S. Marder, *Chemistry of Materials,* **2004,** *16*, 5286-5292.
[261] F. Wurthner, *Chemical Communications,* **2004**, 1564-1579.
[262] B. A. Jones, M. J. Ahrens, M.-H. Yoon, A. Facchetti, T. J. Marks and M. R. Wasielewski, *Angewandte Chemie International Edition,* **2004,** *43*, 6363-6366.
[263] M. A. Angadi, D. Gosztola and M. R. Wasielewski, *Materials Science and Engineering B,* **1999,** *63*, 191-194.
[264] L. Schmidt-Mende, A. Fechtenkötter, K. Müllen, E. Moons, R. H. Friend and J. D. MacKenzie, *Science,* **2001,** *293*, 1119-1122.
[265] M. R. Wasielewski, *Accounts of Chemical Research,* **2009,** *42*, 1910-1921.
[266] X. Guo, D. Zhang and D. Zhu, *Advanced Materials,* **2004,** *16*, 125-130.
[267] S. Leroy-Lhez, J. Baffreau, L. Perrin, E. Levillain, M. Allain, M.-J. Blesa and P. Hudhomme, *The Journal of Organic Chemistry,* **2005,** *70*, 6313-6320.
[268] X. He, H. Liu, Y. Li, S. Wang, N. Wang, J. Xiao, X. Xu and D. Zhu, *Advanced Materials,* **2005,** *17*, 2811-2815.
[269] J. Baffreau, S. Leroy-Lhez, P. Hudhomme, M. M. Groeneveld, I. H. M. van Stokkum and R. M. Williams, *The Journal of Physical Chemistry A,* **2006,** *110*, 13123-13125.
[270] F. Wurthner, *Pure Appl. Chem.,* **2006,** *78*, 2341-2349.

- impregnation of PCs with a PDI solution. The characteristics of solubility of this PDI derivative appeared particularly adapted, making possible the impregnation method without disturbing the crystal arrangement of PCs.

The characterization of the obtained materials started with the analysis of the latexes and the containing particles using DLS and SEM techniques.

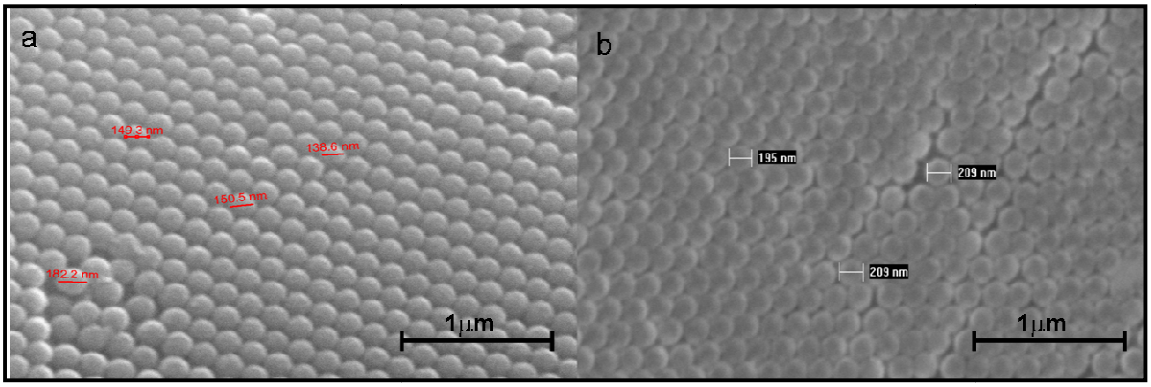

Figure III-10 SEM images for particles from ST-AA-PDI (a) and ST-AA (b) latexes

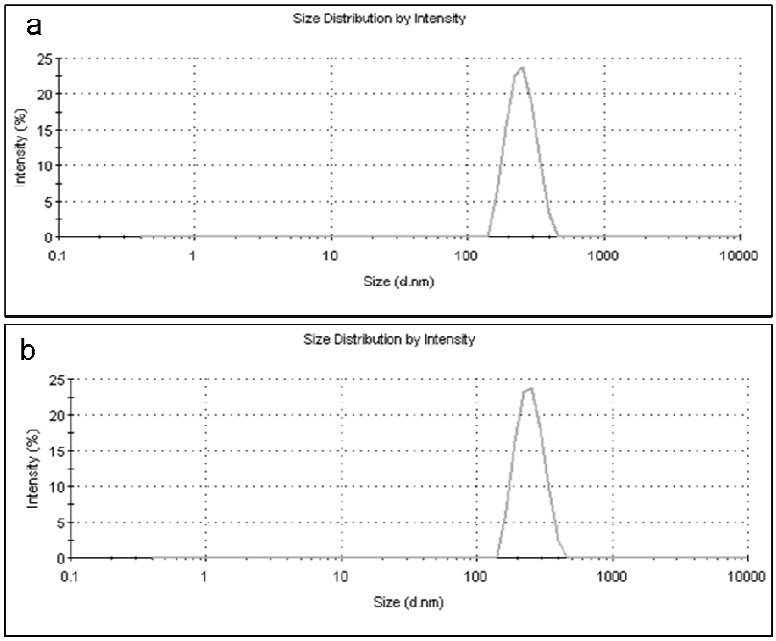

Figure III-11 DLS analysis for latexes: ST-AA (a) and ST-AA-PDI (b)

The SEM analysis confirms the presence of ordered structures, in both cases, having a cubic close packing structure (ccp) presenting photonic crystal characteristics. The major difference concerns the particle, namely a decrease in particle size from 210 nm (ST-AA) to 150 nm (ST-AA-PDI). DLS technique was employed to sustain the dimensional uniformity of obtained particles. The particle size variation may be due to the scavenger capability of PDI during the soap free polymerization process. In previous studies, this effect was observed

during the polymerization reaction in the presence of fullerene C_{60}[271]. Thus, by homogeneous nucleation, a higher number of particles with smaller dimensions are formed, due to the inhibition in the water phase of the propagating radicals by the PDI molecules transported by the ST from the organic phase. In agreement with previous investigations proving that the majority of hydrophilic groups from the monomer are arranged by homogeneous nucleation at the surface[240, 241], the PDI moieties should be reasonably arranged inside the copolymer particles.

In order to study the presence of dye and the optical properties of modified PCs we have employed UV-VIS and fluorescence spectroscopy. For the UV-VIS characterization a reflection integration sphere was used, due to the PCs properties.

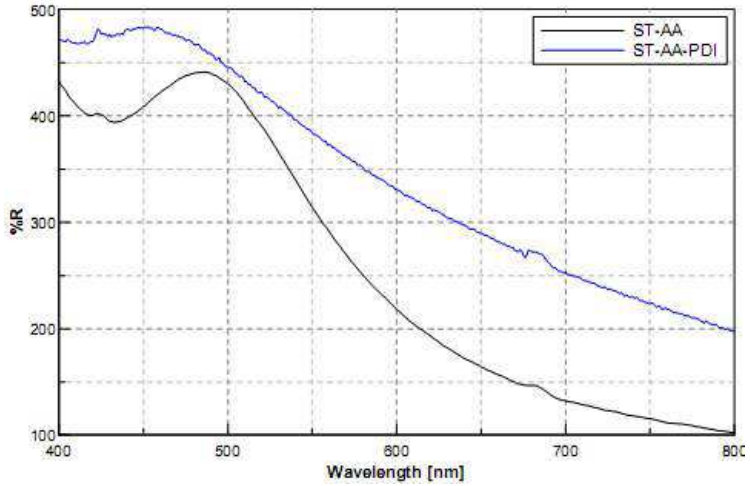

Figure III-12 UV-VIS spectra for the obtained films: (ST-AA) and (ST-AA-PDI)

The analysis of the spectra in Figure III-12 shows a hypsochromic shift of the signal in the case of the PDI containing film from 475 to 450 nm, which is consistent with the decrease in particle size[245, 246, 272, 273]. For the ST-AA-PDI film (Figure III-12) a decrease in the reflection response in the absorption domain of PDI is not observed. This can be explained by the incorporation of PDI (scavenger) in the particles and the overlay of the absorption domain and the stop-band of the PC. Consequently, the influence of absorption band corresponding to free dye is not observed, due to the core-shell structure of the hybrid material obtained. All the dye molecules have been incorporated in the polymer particles. In the Scheme III-1 are presented comparatively, the structure of the hybrid material (a) obtained by us, the material obtained by classical impregnation method (b) and the structure of the PDI (*N*-2'-

[271] E. Rusen, A. Mocanu and B. Marculescu, *Colloid & Polymer Science,* **2010,** *288*, 769-776.
[272] X. Wang, S. M. Husson, X. Qian and S. R. Wickramasinghe, *Materials Letters,* **2009,** *63*, 1981-1983.
[273] X. He, Y. Thomann, R. J. Leyrer and J. Rieger, *Polymer Bulletin,* **2006,** *57*, 785-796.

hydroxyethyl -*N'*-pentyl- 1,6,7,12- tetra (*p*-tertiobutyl) phenoxyperylene - 3,4:9,10 bis(dicarboximide) – see **Chapter II**- for the synthesis).

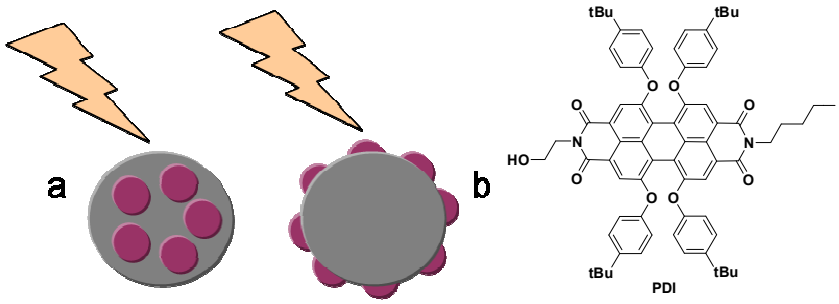

Scheme III-1 a) our case with the dye molecules incorporated in polymer particles; b) dye molecules on the surface of polymer particles and the used PDI dye structure

In order to study the influence of the dye on the optical properties of the PCs relatively to its insolubility in water, studies have been carried out for comparison with the dye ZnPc (tetracarboxy zinc phthalocyanine), as its potassium salt. We have confirmed the PC characteristics for the ST-AA-ZnPc film with the conservation of the particles size and the lack of aggregation.

For more information, the ST-AA-PDI films have been further characterized by fluorescence spectroscopy. In Figure III-13 are presented the 3D fluorescence spectra which consist of emission intensity versus emission wavelength and excitation wavelength.

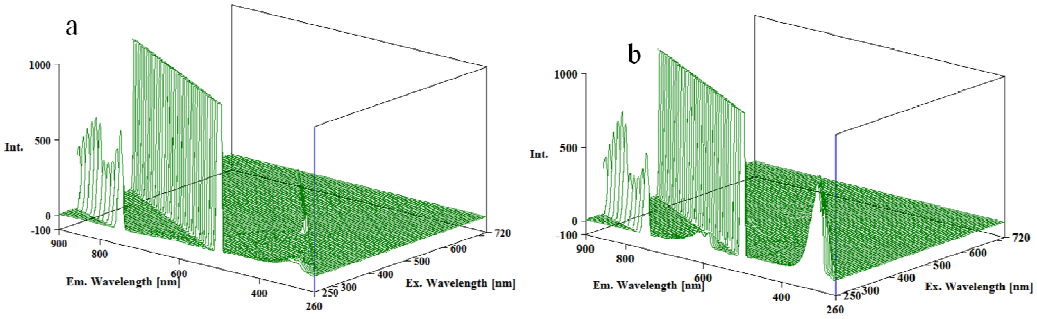

Figure III-13 3D fluorescence spectra (emission intensity versus emission wavelength and excitation wavelength) for: (a) ST-AA; (b) ST-AA-PDI

It was previously reported that the PCs may act as a Bragg mirror and can effectively increase fluorescence intensity of organic dyes because they enhance excitation and/or emission light[274]. A condition for fluorescence enhancement is that the excitation wavelength should be in the stop-band of the PCs. The excitation light reflected by a Bragg mirror can

[274] Y.-Q. Zhang, J.-X. Wang, Z.-Y. Ji, W.-P. Hu, L. Jiang, Y.-L. Song and D.-B. Zhu, *Journal of Materials Chemistry,* **2007,** *17*, 90-94.

stimulate more dye molecules, which is also in favor of fluorescence enhancement. In our case, the excitation wavelength is higher than the maximum reflection value of the stop-band. However, in Figure III-13, the response of the ST-AA-PDI shows new signals that require a more detailed analysis.

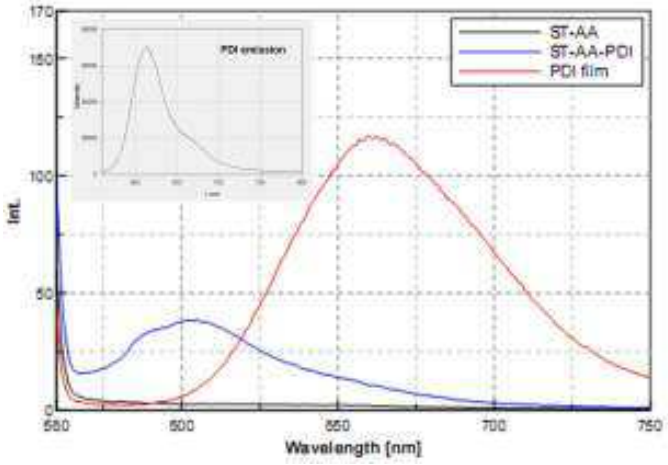

Figure III-14 Fluorescence spectra at an excitation wavelength of 550 nm of the films: ST-AA; ST-AA-PDI and PDI; in caption fluorescence emission of PDI solution (10^{-6}M in CH_2Cl_2)

Figure III-14 presents the response of the films at an excitation wavelength of 550 nm, in the stop-band of the photonic crystal. The emission spectrum of the PDI film is characterized by a large band centered at around 660 nm. By comparison with the emission spectra of the ST-AA and ST-AA-PDI, a new but less intense band centered at around 600 nm is observed for PC containing dye. The blue shift of emission maximum can be explained by light confinement in defects of the PC lattice and by the optical path up to the PDI core particle[275, 276]. The lack of fluorescence enhancement for the ST-AA-PDI system may be due to weak interaction between the excitation wavelength of PDI and the stop-band of the colloidal crystal (weak reflection of the excitation wavelength). But, the decrease in the intensity compared to the PDI film is explained by the incorporation of the dye inside the polymer particles which could lead to a weaker excitation of the molecules.

Because of the substitution on the bay area which induces a twist of the molecule[270], the formation of excimers appears not favorable for the PDI derivative used in this study. However, in the solid film the excimer like emission is present.

The emission spectrum of PDI in solution (10^{-6}M (CH_2Cl_2), λ_{ex}=550 nm) is inserted in Figure III-14. The emission takes place at 614 nm for monomeric species[209]. For the film ST-AA-PDI (the dye inside the polymer particles) the emission is situated to the same band (614

[275] X. Juan, D. Hong, X. Zi-qiang, L. Yan and H. Jun, *Materials Science in Semiconductor Processing,* **2006,** *9*, 136-140.
[276] J. Liu and et al., *Journal of Optics A: Pure and Applied Optics,* **2007,** *9*, 325.

nm). That behavior could be explained by the low concentration of PDI in the polymerization systems, which induce a small amount of PDI in the polymer particle, respectively a weak interaction between the PDI molecules, inside the polymer particles. The behavior of PDI inside of polymer particle is same like in solution (monomeric species).

As a result of geometric relaxation in the excited state, the emission takes place from an excimer like species, *i.e.*, an electronic intermediate, at 660 nm strongly red-shifted band emission (Figure III-14) for PDI film[277]. The fluorescent nature of PDI in the solid state (film) may be related to its crystal structure[278].

The analysis of the 3D fluorescence spectra shows a high intensity emission of the ST-AA-PDI for an excitation wavelength of 250 nm (Figure III-15).

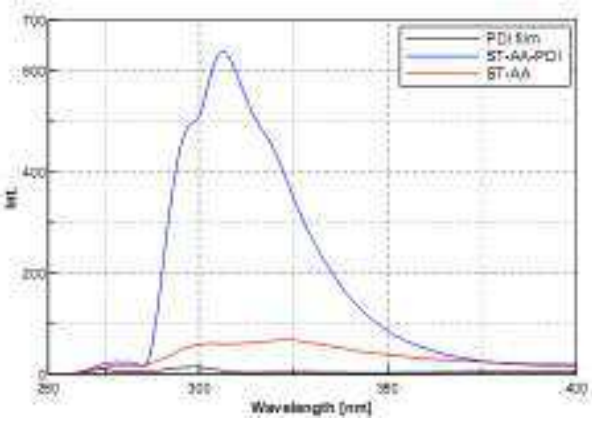

Figure III-15 Fluorescence spectra at an excitation wavelength of 250 nm of the films:

ST-AA-PDI system presents a high increase of fluorescence at 280-360 nm, which is not characteristic to PDI. In order to find an explanation for this behavior, the next step was the impregnation of a ST-AA film with a PDI solution in carbon tetrachloride (10^{-3} mol.L^{-1}).

Figure III-16 a) and b) illustrate the results related to Figure III-15 explaining the increase of the fluorescence noticed in the case of ST-AA-PDI system at an excitation wavelength of 250 nm. There are only small modifications (signal overlapping for the signals at 300-325 nm), for the surface adsorbed PDI film, compared to the ST-AA film. Thus, an explanation for the increase of fluorescence for a 250 nm excitation wavelength in the case of ST-AA-PDI film could be the result of the difference in diameter and a better compactness of the particles. The emission around 300 nm (Figure III-16 a) is present in the case of ST-AA and PDI film. In the case of ST-AA film the signal is due to the polystyrene structure, up-converted emission is believed to result from the second singlet excited state through

[277] C. Hippius, I. H. M. van Stokkum, E. Zangrando, R. M. Williams, M. Wykes, D. Beljonne and F. Würthner, *The Journal of Physical Chemistry C,* **2008,** *112*, 14626-14638.
[278] W. E. Ford and P. V. Kamat, *The Journal of Physical Chemistry,* **1987,** *91*, 6373-6380.

multiphoton process[279]. Many perylene derivatives have been demonstrated to aggregate in solid films where head-to-tail interaction and face-to-face packing occurs[270]. The peak at 300 nm could be due to the Bragg diffraction of dye molecules aggregates. Moreover, this behaviour could be assigned to the resonance effect between the incident electromagnetic radiation and the electron's polarization, which leads to the coupling of electrons in PDI films to the oscillating electric field.

A fluorescence enhancement in the case of the PDI impregnated PC is noticed (Figure III-16 c), although the excitation wavelength of 550 nm is not in the maximum reflection domain of the PC stop-band.

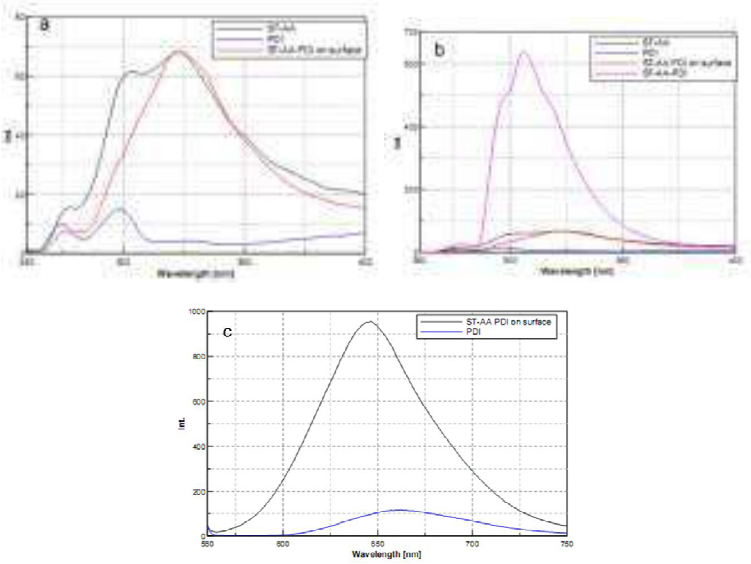

Figure III-16 Fluorescence spectra at an excitation wavelength of 550 nm of the films: a) ST-AA; ST-AA PDI on surface and PDI; b) ST-AA; ST-AA PDI on surface, PDI and ST-AA-PDI; c) fluorescence spectra at an excitation wavelength of 250 nm of the films ST-AA PDI on surface and PDI

To obtain a fluorescence enhancement for the ST-AA-PDI system, the maximum reflection value of the stop-band should be around 550 nm, which would be characteristic to colloidal particles with an increased diameter, according to formula (1)[257]:

$$\lambda_{(111)} = n_{eff} \times 1.632 \times d \qquad (1)$$

where the effective refractive index is given by $n_{eff} = f\, n_{ST\text{-}AA} + (1\text{-}f)\, n_{air}$, the refractive index of ST-AA, can be estimated as the refractive index of polyST, is given by $n_{PST}=1.55$, $n_{air}=1$, and the filling factor for ideal face-centered cubic packing is $f=0.74$. According to the formula (1) the ideal diameter should be 240 nm, which will represent the topic of the future work.

[279] K. Dou, Z. Xu, X. J. Wang, Y. Chen and T. Collins, *Journal of Luminescence,* **2003,** *102-103*, 476-480.

In general, taking into account the excitation and/or the emission wavelength of the dye, respectively the composition and the size of the polymer particles which allows the control of the stop band domain of the PC, fluorescence enhancement can be achieved.

The comparative macroscopic characterization of the films (ST-AA, ST-AA-PDI, ST-AA PDI on surface) was studied. These were obtained by deposition on glass plates having an area of 4 cm^2 and the volume of the used latexes of 0.3 mL. This characterization has been performed in order to gain information on the quality of the obtained systems. In Figure III-17 are presented images using optic microscopy at different magnifications.

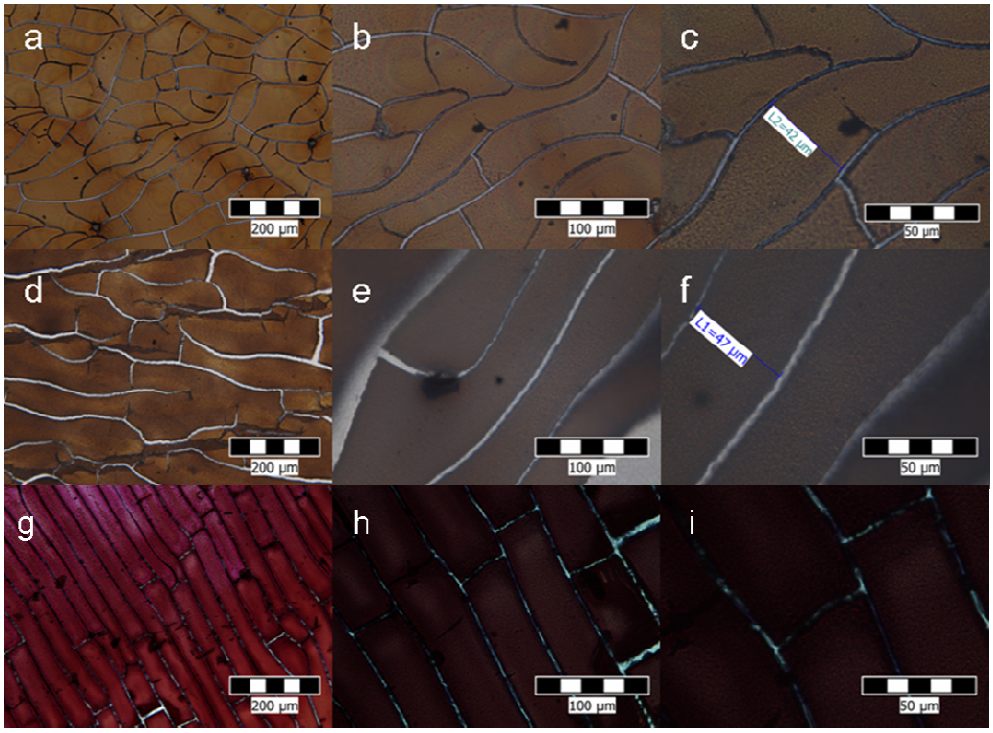

Figure III-17 Optical microscopy images: latex ST-AA (a, b, c); latex ST-AA-PDI (d, e, f) and latex ST-AA PDI on surface (g, h, i)

The analysis of images in Figure III-17 shows a better quality of the film in the case of ST-AA-PDI. The improvement is explained by the lower density of cracks, and the higher distance between them sustaining a higher continuity of the film.

In order to study the influence of the dye on the optical properties of the PCs, an alternative method consisted in the physical immobilization of the dye on polymer particles surface and the analysis of the obtained film. Due to the insolubility in water and the absorption properties of the PDI, a new dye has been used ZnPc (tetracarboxy zinc phthalocyanine), as potassium salt. Thus, the ST-AA latex (5 mL) has been mixed with the aqueous solution of ZnPc ($2 \cdot 10^{-3}$mol/L) and then the film has been obtained (ST-AA-ZnPc),

by deposition on a glass surface. By comparing the behavior of ST-AA and ST-AA-ZnPc (Figure III-18 a) we have noticed the same signals centered at around 500 nm, which confirm the conservation of the particles size, the lack of aggregation and the conservation of PC characteristics. The influence of the surface adsorbed dye is put into evidence by a decrease of the reflection around 700 nm (Figure III-18 a), which corresponds to the absorption band of the ZnPc material. In Figure III-18 b) are presented the absorption spectra of PDI and ZnPc. For the ST-AA-PDI film a decrease in the reflection response in the absorption domain of PDI is not observed, which can be explained by the incorporation of PDI (scavenger) in the particles and the overlay of the absorption domain and the stop-band of the PC.

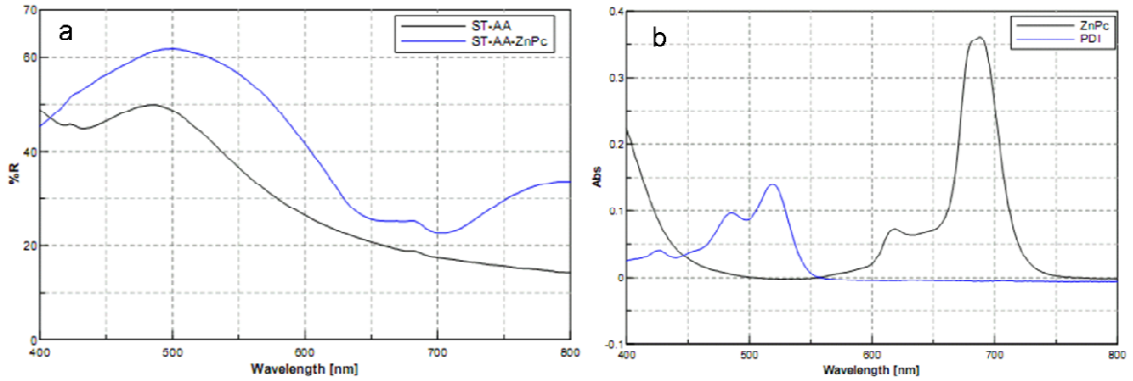

Figure III-18 UV-VIS spectra for: a) the obtained films ST-AA, ST-AA-ZnPc and b) solutions of ZnPc, PDI

Both the UV-VIS analysis and the optical microscopy (Figure III-19) prove that the adsorption of the ZnPc on the surface of the polymer particles has not hindered the self-assembly properties of the latexes.

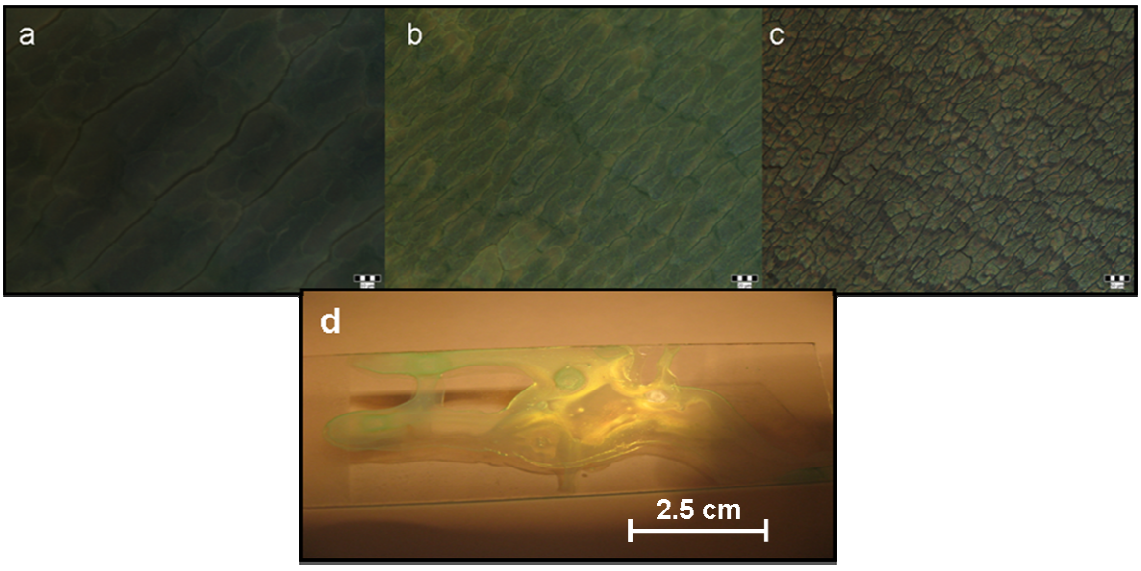

Figure III-19 Optical microscopy images at different magnifications (a) 20x; (b) 50x; (c) 100x si (d) photo image for the ST-AA-ZnPc

In conclusion photonic crystals modified with fluorescent chromophores have been obtained, by employing: soap free emulsion polymerization in the presence of PDI, physical mixture of an aqueous solution of the potassium salt of ZnPc with ST-AA latex and the impregnation of the ST-AA film with a PDI solution. This study demonstrated that PDI influence on the soap free polymerization of ST-AA led to a decrease in particle size by its scavenger effect. The PCs have been characterized by UV-Vis and fluorescence spectroscopies and the shift in the emission response observed in the case of the ST-AA-PDI system can be explained by light confinement in defects of the PC lattice and by the optical path up to the PDI core particle. The lack of fluorescence enhancement for the ST-AA-PDI system may be due to weak interaction between the excitation wavelength of PDI and the stop-band of the colloidal crystal corresponding to a weak reflection of the excitation wavelength. It was also demonstrated that the decrease in the intensity compared to the PDI film was resulting from the incorporation of the dye in the polymer particles which led to a weaker excitation of the molecules. Moreover, the impregnation of the PC with PDI resulted to a fluorescence enhancement, although the excitation wavelength of 550 nm is not in the maximum reflection domain of the PC stop-band.

2. Photonic crystals heterostructures

Introducing defects into photonic crystals in a controlled manner has attracted great interest. One of the possibilities to introduce defects consists in the photonic crystal heterostructures, combining two or more photonic crystals composed of particles of different sizes[280, 281, 282]. Thus, photonic crystals heterostructures can exhibit a broader band gaps[283, 284], which may offer functionality for engineered photonic behavior. Therefore, it is very important to improve the quality of photonic crystal heterostructures and to reduce the space of the interface. One of the possibilities to decrease the space occupied by air could consist in the surface modification, for a type of particles which form photonic crystal heterostructures. In addition, self-assembled monolayers (SAM) are a versatile tool for the modification of surfaces allowing for the creation of well ordered molecular assemblies. These SAM on the surface of gold offer an attractive means for building chemical functionality onto a surface with the eventual goal of defining and controlling interfacial activity. The possible arrangement of photonic crystal heterostructures consisted by two type of particles, polymeric and gold nanoparticles with SAM on the surface presented in Scheme III-2.

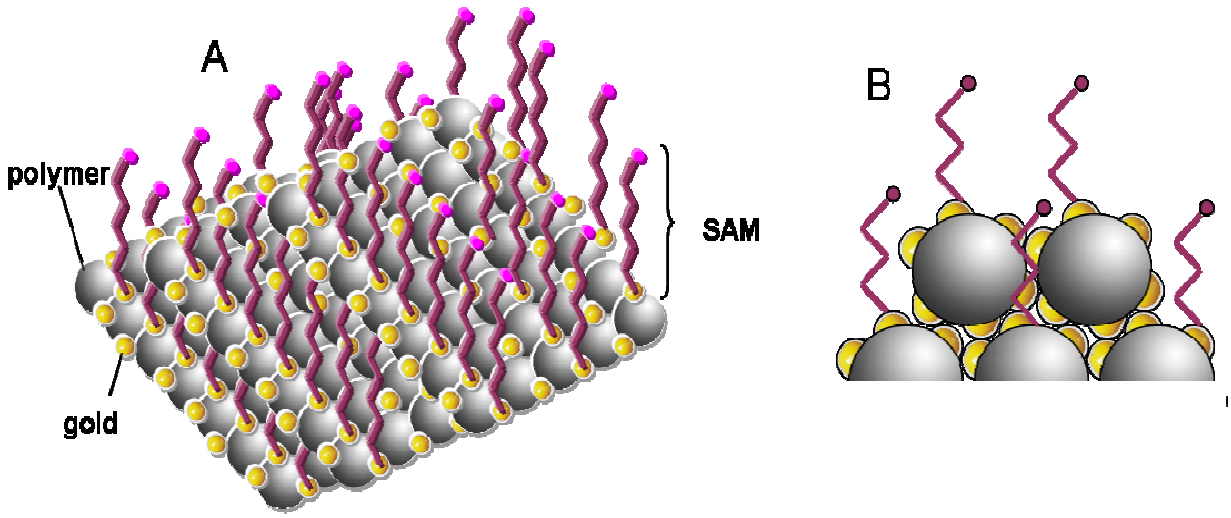

Scheme III-2 The possible arrangement of photonic crystal heterostructures modified with SAM: A) view from above; B) view from cross section

[280] P. Jiang, G. N. Ostojic, R. Narat, D. M. Mittleman and V. L. Colvin, *Advanced Materials,* **2001,** *13*, 389-393.
[281] M. Egen, R. Voss, B. Griesebock, R. Zentel, S. Romanov and C. S. Torres, *Chemistry of Materials,* **2003,** *15*, 3786-3792.
[282] H.-L. Li and F. Marlow, ibid. **2005,** *17*, 3809-3811.
[283] R. Rengarajan, P. Jiang, D. C. Larrabee, V. L. Colvin and D. M. Mittleman, *Physical Review B,* **2001,** *64*, 205103.
[284] G. Q. Liu, H. H. Hu, Y. B. Liao, Z. S. Wang, Y. Chen and Z. M. Liu, *Optik - International Journal for Light and Electron Optics,* **2011,** *122*, 9-13.

In order to improve the optical properties of photonic crystal heterostructures, SAM was functionalized with a dye. Thus, Rhodamine B is an important laser dye with excellent photophysical properties, such as long wavelength absorption and emission, high fluorescence quantum yield, large extinction coefficient and high stability against light[285, 286]. There are various methods to fabricate organic dyes thin films, but each method has some disadvantages. The photonic crystal heterostructures could be considerate as a physical support for Rhodamine film.

Due to the increasing interest of optical properties of photonic crystal heterostructures, the current investigation first attempt has been to prepare high quality fluorescent film. The film has been obtained by covalent attachment of Rhodamine B to the SAM, contained in the photonic crystal heterostructures.

Rhodamine B derivatives have recently gained much interest in obtaining fluorescent chemosensors since the dye framework offers selectivity based on its particular structural property[287, 288, 289, 290]. Due to the roughness of the surface, (presented in Scheme III-2) Rhodamine B has been adsorbed on the surface in a certain amount. The unreacted carboxylic group of adsorbed Rhodamine B makes possible the reaction with substances containing multifunctional amine groups. Thus, the presence of heavy metal ions induce ring opening of the spirolactam, gives rise to strong fluorescence emission and a strong pink color. The aim of this study consisted in obtaining a high fluorescent chemosensor film.

The first stage in this study consisted in preliminary characterization of the ST-HEMA film using optical microscope. The distance between the defaults (resulted from the water evaporation) was around 200 μm, an evidence of the good quality of the final opal film (Figure III-20).

[285] M. Obata, M. Morita, K. Nakase, K. Mitsuo, K. Asai, S. Hirohara and S. Yano, *Journal of Polymer Science Part A: Polymer Chemistry,* **2007,** *45*, 2876-2885.
[286] I. Zareba-Grodz, R. Pazik, K. Hermanowicz, W. Strek and K. Maruszewski, *Journal of Luminescence,* **2006,** *119-120*, 148-152.
[287] Y. Xiang, Z. Li, X. Chen and A. Tong, *Talanta,* **2008,** *74*, 1148-1153.
[288] S. Bae and J. Tae, *Tetrahedron Letters,* **2007,** *48*, 5389-5392.
[289] X. Zhang, Y. Shiraishi and T. Hirai, ibid., 5455-5459.
[290] X.-F. Yang, X.-Q. Guo and H. Li, *Talanta,* **2003,** *61*, 439-445.

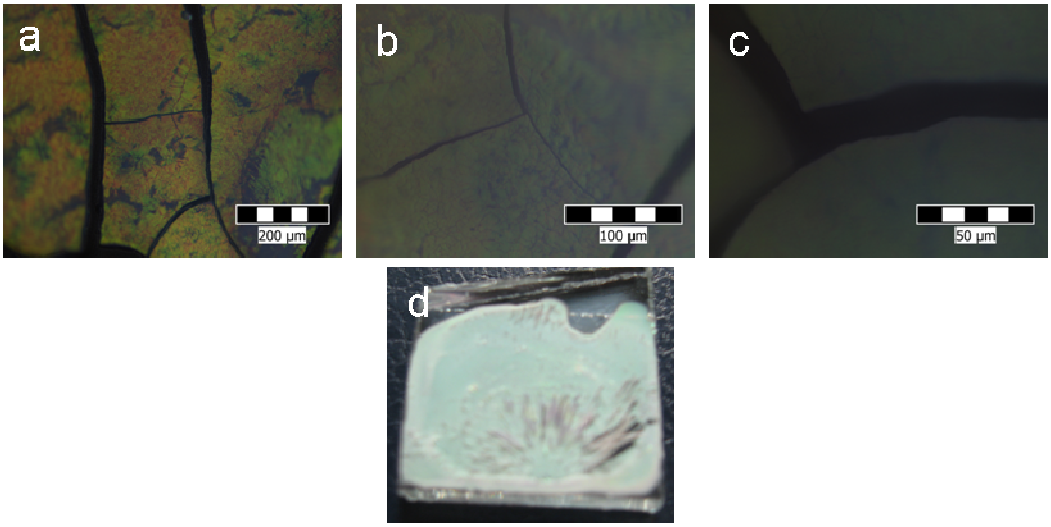

Figure III-20 Optical microscope image at various magnifications: a) 20X; b) 50X; c) 100X; d) photo image

In order to obtain more information about the ST-HEMA film, respectively the particles size, SEM analysis was performed. The SEM images Figure III-21 a) show a regular lattice structure, characteristic for photonic crystals, with particles size of 200 nm, also confirmed by AFM (Figure III-21 b). FFT data (insertion in Figure III-21 b) shows that particles arrange in a compact hexagonal lattice (hcp).

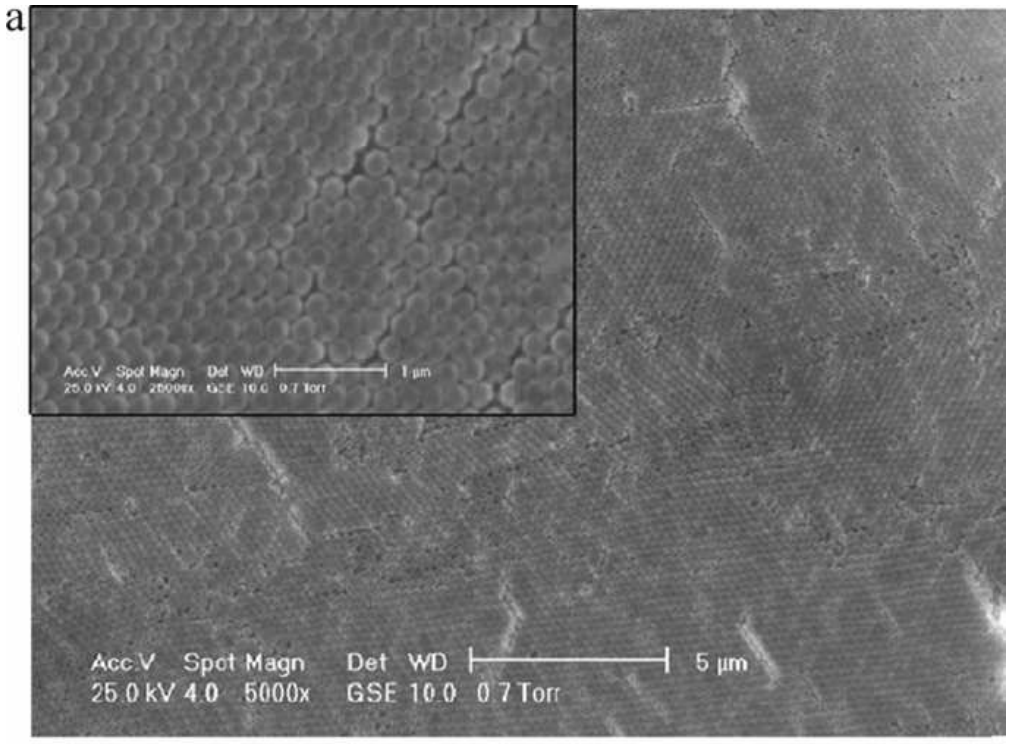

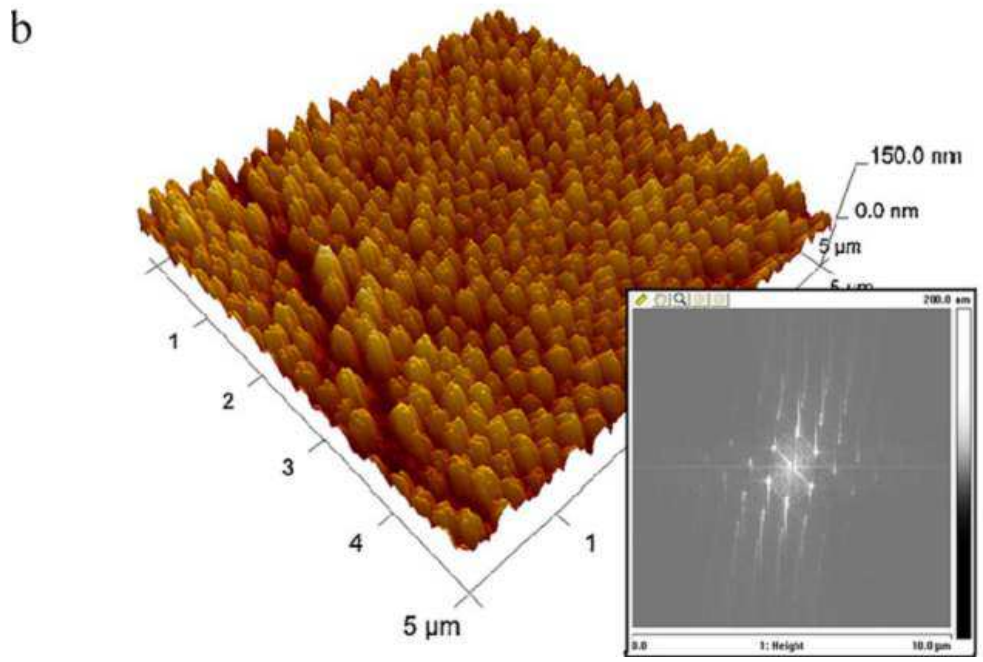

Figure III-21 SEM image of the film obtained from the ST-HEMA dispersion (a) and the AFM results for the same system (b). Insertion gives the FFT data

Photonic crystals possess photonic band gaps: ranges of frequency in which light cannot propagate through the structure. The enhancement of the intensity and the far stronger interaction of the conned light with any kind of material make photonic crystals ideal candidates for optical sensing devices. To put in evidence the band gap in our case, the UV-VIS spectra has been recorded. The characteristic band gap is not well defined (Figure III-22), due to the compact structure (fractions occupied by spheres and air for a hcp lattice is 74%, respectively 26%)[245, 291].

[291] T.-S. Deng, J.-Y. Zhang, K.-T. Zhu, Q.-F. Zhang and J.-L. Wu, *Colloids and Surfaces A: Physicochemical and Engineering Aspects,* **2010,** *356*, 104-111.

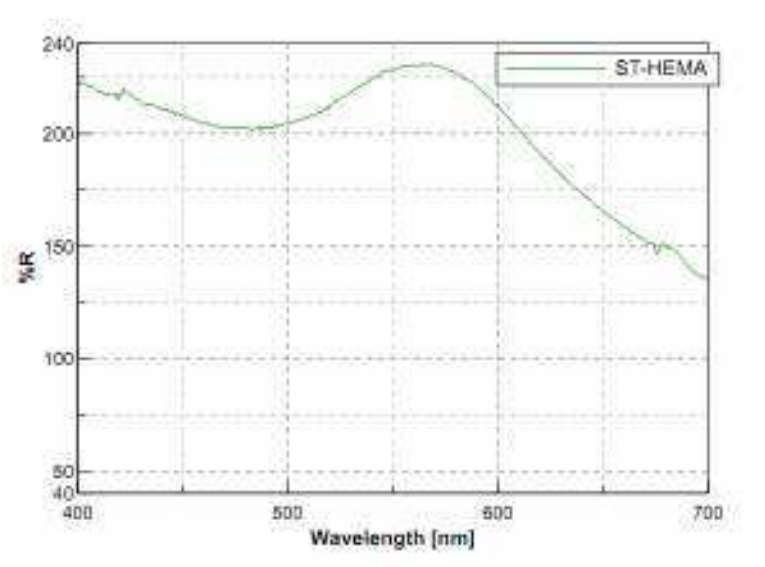

Figure III-22 UV-VIS spectrum for ST-HEMA film

Photonic crystal heterostructures can exhibit a broader band gap by manipulating the sphere sizes of the two constitutional components, which may offer functionality for engineered photonic behavior. Taking into account this reasoning, the ST-HEMA colloidal dispersion has been mixed with Au colloidal solution (1:5 volume ratio). The size of Au particles and the stability of colloidal mixture have been investigated by TEM and DLS.

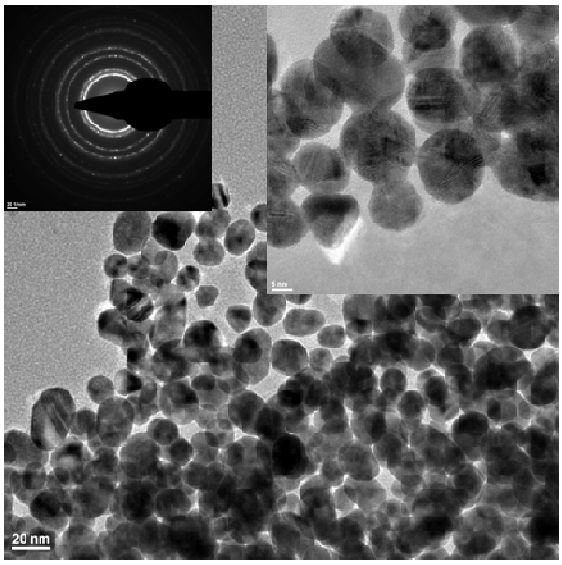

Figure III-23 TEM image of Au nanoparticles

The diameter of metallic particles was 10 nm (Figure III-23) and the Zeta Potential of the mixture was -39 mV. This value indicated the colloidal stability of the mixture and the size of the hybrid particles becomes 260 nm (Figure III-24). The monodispersity of the hybrid particles has been observed in the same figure. The size of the aggregates corresponds to a

cluster of seven particles (six Au particles around the one ST-HEMA particle). The possible structure is inserted in Figure III-24.

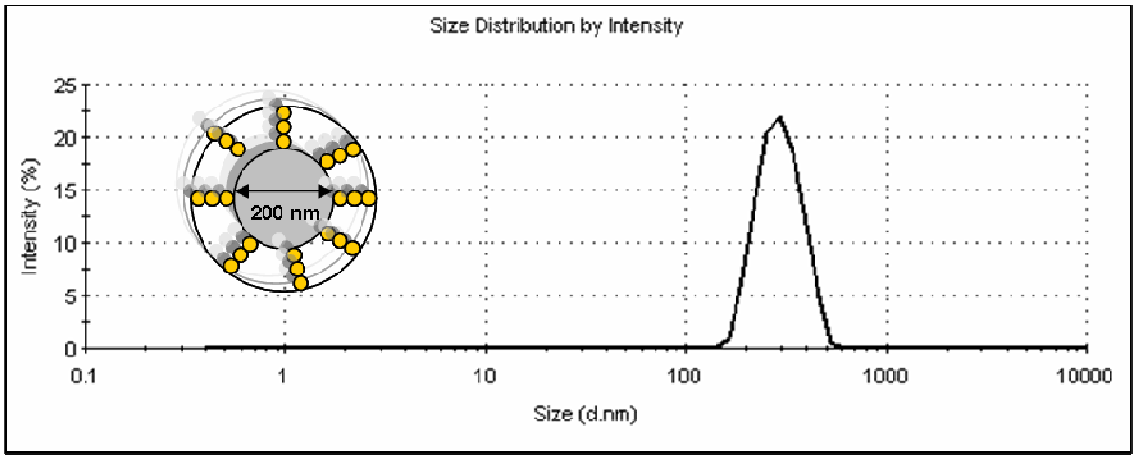

Figure III-24 The DLS analysis of the colloidal mixture

The film obtained by mixing the two colloidal dispersions has been primary/initially investigated using optical microscope (Figure III-25). The distance between the defaults (resulted from the water evaporation) was around 100 µm, a proof of the good quality of the final opal film.

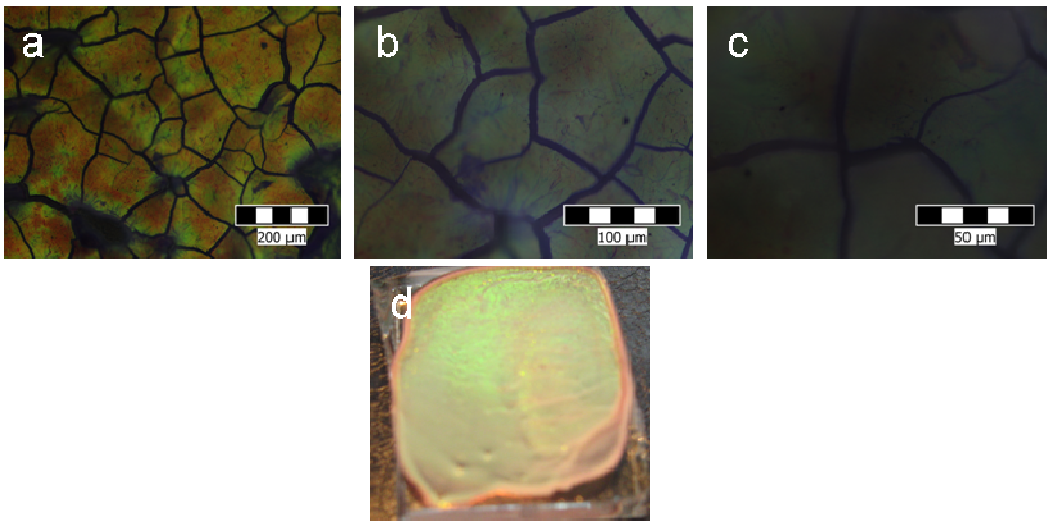

Figure III-25 Optical microscope image at various magnifications: a) 20X; b) 50X; c) 100X; d) photo image

The next step consisted in the UV-VIS characterization of the heterostructures photonic crystal. In Figure III-26 broader and shifted band gap has been noticed for the

system ST-HEMA-Au, due to the increase of the particles size and due to the volume occupied by the air (insertion in the Figure III-26 of the arrangement of the particle).

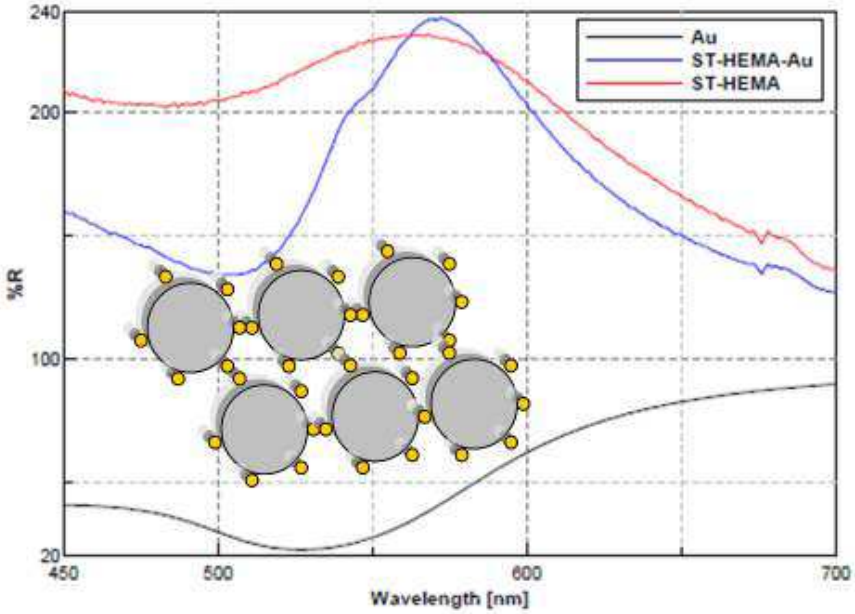

Figure III-26 UV-VIS spectra of the photonic crystals heterostructures

In order to modify the photonic crystal heterostructures with Rh, the first step has been the chemical attachment of HO-R-SH to the surface of Au particles. The FT-IR analysis of the obtained structure shows the characteristic peak of the hydroxyl group 3300 cm^{-1}. The next reaction was the esterification of hydroxyl modified photonic crystal with Rh. In FT-IR spectrum appear new peaks specific to rhodamine B appear: aromatic C=C 1593–1595 cm^{-1}, C=O ester band at 1705cm^{-1}, the 3100 cm^{-1} absorption band assigned to C–H aromatic. In addition, the 1709.9 cm^{-1} absorption band is assigned to C = N stretching vibration and the 2963 cm^{-1} absorption can be assigned to C–H asymmetric stretching. The aromatic skeletal C–C stretch and C–O–C stretch were observed at 1339 and 1220 cm^{-1}, respectively. The aromatic C–H in plane bending was observed at 1115.5 cm^{-1}. The C–H out of plane bending was observed at 824 cm^{-1} and the band at 680 cm^{-1} can be assigned to the aromatic C–H vibrations[292]. The values found for the ester band are in agreement with several Rh ester bands at 1707–1728 cm^{-1}.

[292] Z. S. Guan, Y. Zhang, Q. Zhang and D. X. Li, *Journal of Colloid and Interface Science,* **2006,** *302*, 113-122.

As shown in Figure III-27, the hybrid material modified with Rh has not maintained the good quality of the opal film.

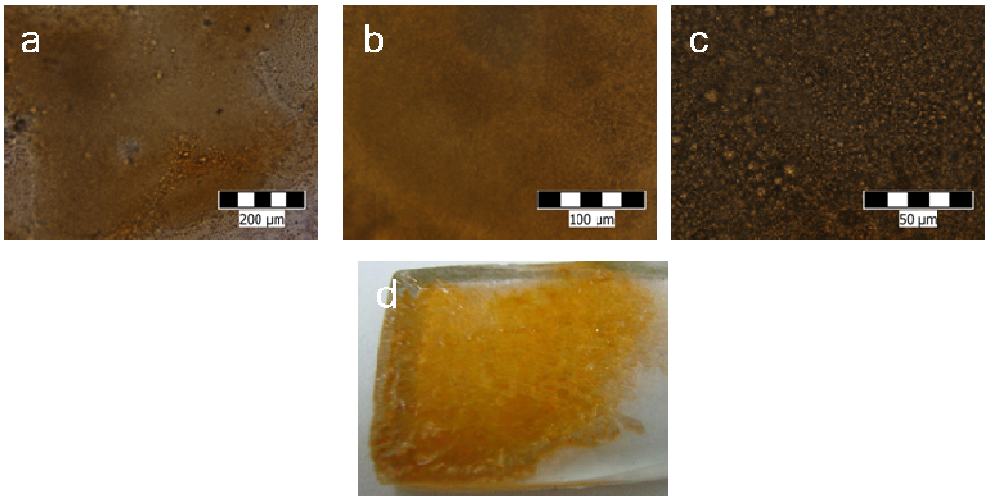

Figure III-27 Optical microscope image at various magnifications: a) 20X; b) 50X; c) 100X; d) photo image for hybrid material modified with Rh

In order to obtain more information about the optical properties of hybrid material modified with Rh, it has been compared with Rh film deposited on a glass surface.

In the UV-VIS spectra showed in Figure III-28, for Rh film the reflexion response has been noticed at 600 nm. According to recent studies[293], the refractive index n of Rh thin film shows anomalous dispersion in the spectral range 400-900 nm. This anomalous behavior is due to the resonance effect between the incident electromagnetic radiation and the electron's polarization, which leads to the coupling of electrons in Rh films to the oscillating electric field. Moreover, the peak in the refractive index corresponds to the fundamental energy gap of Rh film. The peak at 600 nm is possible due to the Bragg diffraction of dye molecules aggregates (insertion of Rh optical image). In the case of ST-HEMA-Au-SH-Rh, the same signal has been shifted to 625 nm, induced by the existence of preformed particles.

A decrease in the reflection response of Rh is noticed to 500 nm that correspond to the absorption domain of dye, namely Q-band, assigned to the first π–π* transition[294]. The large decrease area for particles ST-HEMA-Au-SH-Rh could be attributed to the overlapping of Rh reflection band to photonic crystal stop band.

[293] A. A. M. Farag and I. S. Yahia, *Optics Communications,* **2010,** *283*, 4310-4317.
[294] I. Moreno-Villoslada, M. Jofré, V. Miranda, P. Chandía, R. González, S. Hess, B. L. Rivas, C. Elvira, J. San Román, T. Shibue and H. Nishide, *Polymer,* **2006,** *47*, 6496-6500.

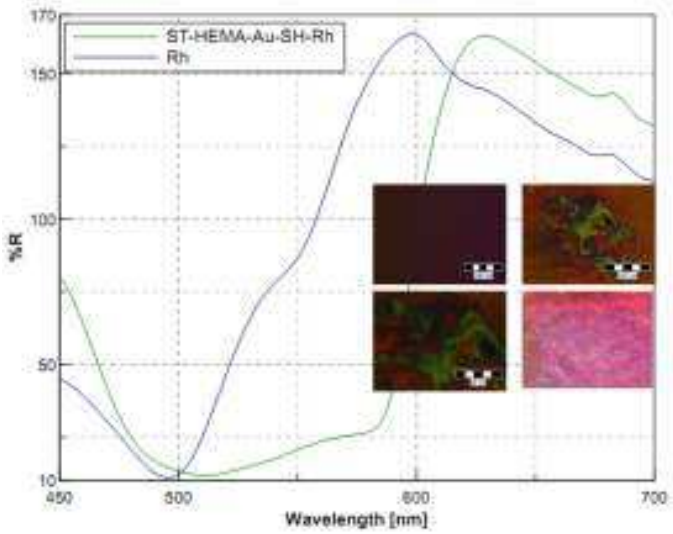

Figure III-28 UV-VIS spectra (insertion Rh optical image)

The films have been further characterized by fluorescence spectroscopy. In Figure III-29 are presented the 3D fluorescence spectra which consist of emission intensity versus emission wavelength and excitation wavelength.

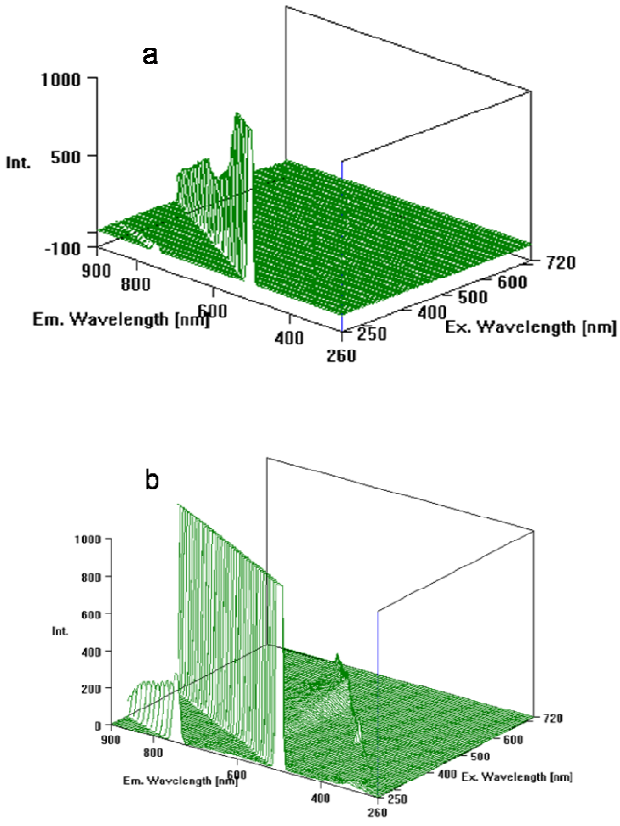

Figure III-29 3D fluorescence spectra: (a) Rh film; (b) ST-HEMA-Au-SH-Rh film

According to previous articles[295, 248] the photonic crystal may act as a Bragg mirror and can effectively increase fluorescence intensity of organic dyes because they enhance excitation and/or emission light. A condition for fluorescence enhancement is that the excitation wavelength to be in the stop-band of the photonic crystal. The excitation light reflected by a Bragg mirror can stimulate more dye molecules, which is also in favor of fluorescence enhancement. In our case, the emission response for Rh film is observed at 500 and 750 nm for a 250 nm excitation wavelength (Figure III-29 a). To the same excitation wavelength, in the case of ST-HEMA-Au-SH-Rh film, the emissions have been amplified (Figure III-29 b). Although, the excitation wavelength is not in the stop-band region of the photonic crystal, a fluorescent enhancement was noticed.

In order to put into evidence the chemosensor properties of photonic crystal heterostructures, the free amine groups provided from TETA has been reacted with Rh adsorbed on the surface. These are potentially available to interact with specific metal ions[296, 297, 298]. Preliminary test has been performed putting in contact an aqueous solution (20%) of $Pb(CH_3COO)_2$ with the ST-HEMA-Au-SH-Rh film. The reactions are presented in Scheme III-3.

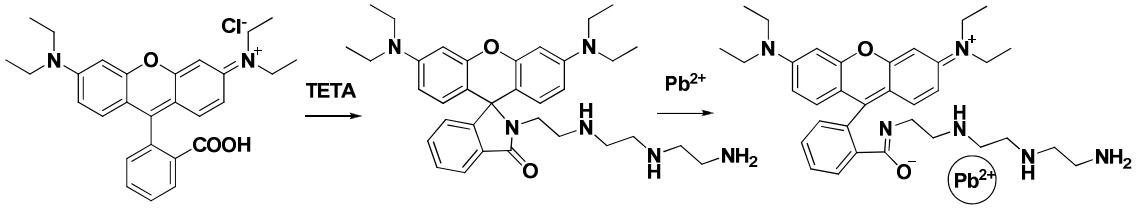

Scheme III-3 Modification reaction of Rh

The surface exposed to Pb^{+2} showed fluorescence, indicating a Pb^{+2} induced ring opening of the spirolactam. Comparing the fluorescent emission of ST-HEMA-Au-SH-Rh (580 nm Rh emission) film with the ST-HEMA-Au-SH-Rh-TETA exposed to Pb^{+2} one could notice the appearance of a new band situated to 520 nm[299, 300, 301].This peak has been attributed to ring opening of the spirolactam (Figure III-30).

[295] H. Li, J. Wang, F. Liu, Y. Song and R. Wang, *Journal of Colloid and Interface Science,* **2011,** *356*, 63-68.
[296] M. Zhao, X.-F. Yang, S. He and L. Wang, *Sensors and Actuators B: Chemical,* **2009,** *135*, 625-631.
[297] L. Dong, ChongWu, X. Zeng, L. Mu, S.-F. Xue, Z. Tao and J.-X. Zhang, ibid. **2010,** *145*, 433-437.
[298] F.-J. Huo, J. Su, Y.-Q. Sun, C.-X. Yin, H.-B. Tong and Z.-X. Nie, *Dyes and Pigments,* **2010,** *86*, 50-55.
[299] H. Sasaki, K. Hanaoka, Y. Urano, T. Terai and T. Nagano, *Biorg. Med. Chem.,* **2011,** *19*, 1072-1078.
[300] H. Liu, P. Yu, D. Du, C. He, B. Qiu, X. Chen and G. Chen, *Talanta,* **2010,** *81*, 433-437.
[301] H. Ju, M. H. Lee, J. Kim, J. S. Kim and J. Kim, ibid. **2011,** *83*, 1359-1363.

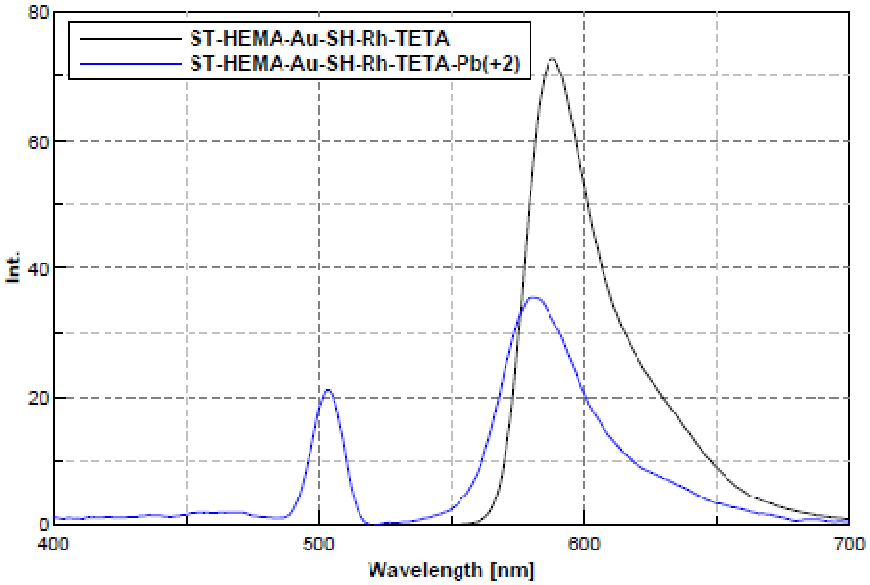

Figure III-30 Fluorescence spectra at 250 nm excitation wavelength

The film obtained after the contact with Pb^{+2} has been analyzed to the optical microscope (Figure III-31). It has been noticed a strong pink color, specific to identification reaction.

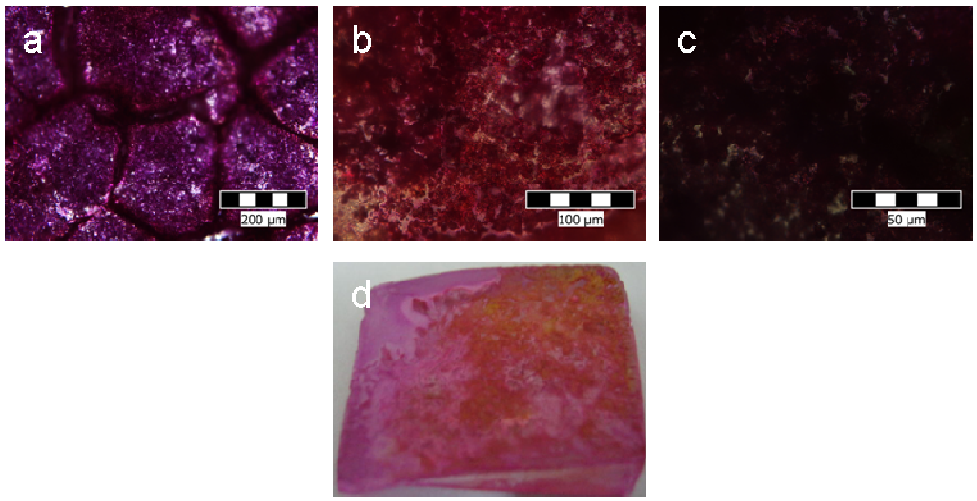

Figure III-31 Optical microscope image at various magnifications: a) 20X; b) 50X; c) 100X; d) photo image of film after the contact with Pb^{2+}

In conclusion, photonic crystal heterostructures has been obtained by mixing a ST-HEMA colloidal dispersion with Au solution (1:5 volume ratio). The size of the aggregates corresponds to a cluster of seven particles (six Au particles around the one ST-HEMA particle). In UV-VIS analysis a broader and shifted band gap has been noticed for the system ST-HEMA-Au, due to the increase of the particles size and due to the volume occupied by the

air. In order to modify the heterogeneous photonic crystal with Rh, the first step has been the chemical attachment of HO-R-SH to the surface of Au particles. The next reaction was the esterification of hydroxyl modified photonic crystal with Rh.

In UV-VIS spectra the peak at 600 nm is possible due to the Bragg diffraction of dye molecules aggregates. In the case of ST-HEMA-Au-SH-Rh, the same signal has been shifted to 625 nm, induced by the existence of preformed particles. A decrease in the reflection response of Rh is noticed that correspond to the absorption domain of dye, namely Q-band. The large decrease area for particles ST-HEMA-Au-SH-Rh could be attributed to the overlapping of Rh reflection band to photonic crystal stop band. In the case of fluorescence, to the same excitation wavelength, for the ST-HEMA-Au-SH-Rh film, the emissions have been amplified compared with the signal of Rh film. Preliminary test has been performed for putting into evidence the chemosensor properties of ST-HEMA-Au-SH-Rh film modified with TETA.

III. *EXPERIMENTAL*

1. Photonic crystals doped with fluorescent dyes

1) Preparation of the ST-AA colloidal dispersion

6.5 mL ST and 2mL AA were added in 100 mL distilled water together with 62.5 mg KPS. The reaction mixture was nitrogen purged and then maintained for 8h at 75 °C under continuous stirring. The final dispersion was dialyzed in distilled water for 7 days, using cellulose dialysis membranes (molecular weight cut-off: 12,000–14,000), in order to remove the unreacted monomers and initiator.

2) Preparation of the ST-AA-PDI colloidal dispersion

A mixture of 6.5 mL ST and 25 mg PDI were added in 100 mL distilled water together with 62.5 mg KPS and 2mL AA. The reaction mixture was nitrogen purged and then maintained for 8h at 75°C under continuous stirring. The final dispersion was dialyzed in distilled water for 7 days, using cellulose dialysis membranes (molecular weight cut-off: 12,000–14,000), in order to remove the unreacted monomers and initiator.

3) Preparation of the PDI film

A 10^{-2} mol.L^{-1} solution of PDI in carbon tetrachloride was prepared and the PDI was deposited on glass substrate by dip-coating method.

4) Preparation of ST-AA PDI on surface film

ST-AA film with synthetic opal properties was obtained by gravitational sedimentation on glass substrate and dried at 70^0C for 1h. A PDI solution in carbon tetrachloride (10^{-3} mol.L^{-1}) was deposited on ST-AA surface by dip-coating method.

2. Photonic crystals heterostructures

1). Soap-free emulsion polymerization[302]

6.5 ml ST and 2ml HEMA have been added in 100 ml distilled water together with 0.0625 g KPS. The reaction mixture has been nitrogen purged and then maintained for 8h at 75^0 C under continuous stirring. The final dispersion has been dialyzed in distilled water for 7

[302] E. Rusen, A. Mocanu, B. Marculescu, R. Somoghi, L. Butac, F. Miculescu, C. Cotrut, I. Antoniac and C. Cincu, *Colloids and Surfaces A: Physicochemical and Engineering Aspects,* **2011,** *375*, 35-41.

days, using cellulose dialysis membranes (molecular weight cut-off: 12,000–14,000), in order to remove the unreacted monomer and initiator.

2). Preparation of gold (Au) nanoparticles

Au colloids were prepared by Na3C6O7·2H2O reduction of HAuCl4. 90 ml of 3×10-4 M aqueous solution of HAuCl4 was allowed to boil, at which point 3.6 ml of 6.8×10-2 M Na3C6O7·2H2O was added dropwise with stirring. Following the addition of Na3C6O7·2H2O, the solution began to darken and turn bluish-gray or purple. After approximately 10 min, the reaction was completed and the final color of solution was a deep wine red. The solution was cooled to room temperature with continued stirring.

3). Chemical attachment of HO-R-SH to Au particles/ SAM preparation

The ST-HEMA colloidal dispersion has been mixed with Au colloidal solution (1:5 volume ratio) and has been deposed on glass substrate (drying at 60^0C in an air current). The obtained film has been immersed in 20 ml of an aqueous HO-R-SH solution (1%). The reaction has been kept 24 h at room temperature. The modified film has been washed with distillate water and dried to vacuum.

4). Esterifcation with Rh (ST-HEMA-Au-SH-Rh)

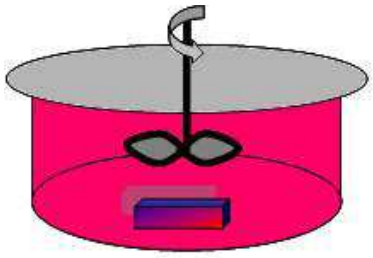

The thiol modified film/SAM has been immersed in a dichloromethane solution. The 20 ml solution of dichloromethane contained 0.02 g Rh, 0.03 g DCC and 0.008g DMAP. The reaction has been kept 24 h at room temperature with stirring. The modified film has been washed with dichloromethane and dried to vacuum.

5). Reaction of ST-HEMA-Au-SH-Rh with TETA

The ST-HEMA-Au-SH-Rh film has been immersed in a 20% aqueous solution of TETA. The reaction has been kept for 5h at 70^0C with stirring. The modified film has been washed with water and dried to vacuum.

Bibliography

[1]. M. R. Peres, *Focal encyclopedia of photography: digital imaging, theory and applications, history, and science*. Elsevier/Focal Press: 2007.

[2]. S. Namba; Y. Hishiki, *The Journal of Physical Chemistry,* **1965,** *69*, 774-779.

[3]. H. Tributsch; H. Gerischer, *Berichte der Bunsengesellschaft für physikalische Chemie,* **1969,** *73*, 251-260.

[4]. H. Tsubomura; M. Matsumura; Y. Nomura; T. Amamiya, *Nature,* **1976,** *261*, 402-403.

[5]. J. Desilvestro; M. Graetzel; L. Kavan; J. Moser; J. Augustynski, *Journal of the American Chemical Society,* **1985,** *107*, 2988-2990.

[6]. B. O'Regan; M. Gratzel, *Nature,* **1991,** *353*, 737-740.

[7]. M. A. Green; K. Emery; Y. Hishikawa; W. Warta, *Progress in Photovoltaics: Research and Applications,* **2011,** *19*, 84-92.

[8]. M. Grätzel, *Inorganic Chemistry,* **2005,** *44*, 6841-6851.

[9]. M. Grätzel, *Journal of Photochemistry and Photobiology C: Photochemistry Reviews,* **2003,** *4*, 145-153.

[10]. A. Hagfeldt; M. Graetzel, *Chemical Reviews,* **1995,** *95*, 49-68.

[11]. A. Hagfeldt; G. Boschloo; L. Sun; L. Kloo; H. Pettersson, *Chemical Reviews,* **2010,** *110*, 6595-6663.

[12]. K. Tennakone; et al., *Semiconductor Science and Technology,* **1995,** *10*, 1689.

[13]. B. O'Regan; D. T. Schwartz, *Journal of Applied Physics,* **1996,** *80*, 4749-4754.

[14]. M. Grätzel, *Journal of Photochemistry and Photobiology A: Chemistry,* **2004,** *164*, 3-14.

[15]. J. Halme; P. Vahermaa; K. Miettunen; P. Lund, *Advanced Materials,* **2010,** *22*, E210-E234.

[16]. M. K. Nazeeruddin; A. Kay; I. Rodicio; R. Humphry-Baker; E. Mueller; P. Liska; N. Vlachopoulos; M. Graetzel, *Journal of the American Chemical Society,* **1993,** *115*, 6382-6390.

[17]. H. Mao; H. Deng; H. Li; Y. Shen; Z. Lu; H. Xu, *Journal of Photochemistry and Photobiology A: Chemistry,* **1998,** *114*, 209-212.

[18]. M. K. Nazeeruddin; R. Humphry-Baker; M. Gratzel; B. A. Murrer, *Chemical Communications,* **1998**, 719-720.

[19]. J. M. Rehm; G. L. McLendon; Y. Nagasawa; K. Yoshihara; J. Moser; M. Gratzel, *The Journal of Physical Chemistry,* **1996,** *100*, 9577-9578.

[20]. A. S. Polo; M. K. Itokazu; N. Y. Murakami Iha, *Coordination Chemistry Reviews,* **2004,** *248*, 1343-1361.

[21]. S. Ferrere; A. Zaban; B. A. Gregg, *The Journal of Physical Chemistry B,* **1997,** *101*, 4490-4493.

[22]. B. C. O'Regan; I. López-Duarte; M. V. Martínez-Díaz; A. Forneli; J. Albero; A. Morandeira; E. Palomares; T. Torres; J. R. Durrant, *Journal of the American Chemical Society,* **2008,** *130*, 2906-2907.

[23]. R. K. Lammi; R. W. Wagner; A. Ambroise; J. R. Diers; D. F. Bocian; D. Holten; J. S. Lindsey, *The Journal of Physical Chemistry B,* **2001,** *105*, 5341-5352.

[24]. F. Odobel; E. Blart; M. Lagree; M. Villieras; H. Boujtita; N. El Murr; S. Caramori; C. Alberto Bignozzi, *Journal of Materials Chemistry,* **2003,** *13*, 502-510.

[25]. M. K. Nazeeruddin; R. Humphry-Baker; D. L. Officer; W. M. Campbell; A. K. Burrell; M. Grätzel, *Langmuir,* **2004,** *20*, 6514-6517.

[26]. Y. Liu; N. Xiang; X. Feng; P. Shen; W. Zhou; C. Weng; B. Zhao; S. Tan, *Chemical Communications,* **2009**, 2499-2501.

[27]. M. K. Nazeeruddin; R. Humphry-Baker; M. Gratzel; D. Wohrle; G. Schnurpfeil; G. Schneider; A. Hirth; N. Trombach, *J. Porphyrins Phthalocyanines,* **1999,** *3*, 230-237.

[28]. J. He; A. Hagfeldt; S.-E. Lindquist; H. Grennberg; F. Korodi; L. Sun; B. Åkermark, *Langmuir,* **2001,** *17*, 2743-2747.
[29]. J. He; G. Benkö; F. Korodi; T. Polívka; R. Lomoth; B. Åkermark; L. Sun; A. Hagfeldt; V. Sundström, *Journal of the American Chemical Society,* **2002,** *124*, 4922-4932.
[30]. K. Kalyanasundaram; M. Grätzel, *Coordination Chemistry Reviews,* **1998,** *177*, 347-414.
[31]. P. Pechy; F. P. Rotzinger; M. K. Nazeeruddin; O. Kohle; S. M. Zakeeruddin; R. Humphry-Baker; M. Gratzel, *J. Chem. Soc., Chem. Commun.,* **1995**, 65-66.
[32]. A. Ehret; L. Stuhl; M. T. Spitler, *The Journal of Physical Chemistry B,* **2001,** *105*, 9960-9965.
[33]. H. Choi; S. Kim; S. O. Kang; J. Ko; M.-S. Kang; J. N. Clifford; A. Forneli; E. Palomares; M. K. Nazeeruddin; M. Grätzel, *Angewandte Chemie International Edition,* **2008,** *47*, 8259-8263.
[34]. B. E. Hardin; E. T. Hoke; P. B. Armstrong; J.-H. Yum; P. Comte; T. Torres; J. M. J. Frechet; M. K. Nazeeruddin; M. Gratzel; M. D. McGehee, *Nat Photon,* **2009,** *3*, 406-411.
[35]. J.-H. Yum; B. E. Hardin; S.-J. Moon; E. Baranoff; F. Nüesch; M. D. McGehee; M. Grätzel; M. K. Nazeeruddin, *Angewandte Chemie International Edition,* **2009,** *48*, 9277-9280.
[36]. K. Hara; T. Horiguchi; T. Kinoshita; K. Sayama; H. Arakawa, *Solar Energy Materials and Solar Cells,* **2001,** *70*, 151-161.
[37]. J. Wu; Z. Lan; J. Lin; M. Huang; P. Li, *J. Power Sources,* **2007,** *173*, 585-591.
[38]. B. O'Regan; D. T. Schwartz, *Chemistry of Materials,* **1995,** *7*, 1349-1354.
[39]. N. Papageorgiou; Y. Athanassov; M. Armand; P. Bonhote; H. Pettersson; A. Azam; M. Gratzel, *J. Electrochem. Soc.,* **1996,** *143*, 3099-3108.
[40]. S. Cukierman, *Biochimica et Biophysica Acta (BBA) - Bioenergetics,* **2006,** *1757*, 876-885.
[41]. M. Gorlov; L. Kloo, *Dalton Transactions,* **2008**, 2655-2666.
[42]. D. Kuang; S. Uchida; R. Humphry-Baker; S. M. Zakeeruddin; M. Grätzel, *Angew. Chem.,* **2008,** *120*, 1949-1953.
[43]. Y. Bai; Y. Cao; J. Zhang; M. Wang; R. Li; P. Wang; S. M. Zakeeruddin; M. Gratzel, *Nat Mater,* **2008,** *7*, 626-630.
[44]. W. Kubo; K. Murakoshi; T. Kitamura; Y. Wada; K. Hanabusa; H. Shirai; S. Yanagida, *Chem. Lett.,* **1998,** *27*, 1241-1242.
[45]. W. Kubo; K. Murakoshi; T. Kitamura; S. Yoshida; M. Haruki; K. Hanabusa; H. Shirai; Y. Wada; S. Yanagida, *The Journal of Physical Chemistry B,* **2001,** *105*, 12809-12815.
[46]. F. Call; N. A. Stolwijk, *The Journal of Physical Chemistry Letters,* **2010,** *1*, 2088-2093.
[47]. Z. Lan; J. Wu; J. Lin; M. Huang; S. Yin; T. Sato, *Electrochim. Acta,* **2007,** *52*, 6673-6678.
[48]. M.-S. Kang; K.-S. Ahn; J.-W. Lee, *J. Power Sources,* **2008,** *180*, 896-901.
[49]. A. F. Nogueira; J. R. Durrant; M. A. De Paoli, *Advanced Materials,* **2001,** *13*, 826-830.
[50]. J. Wu; S. Hao; Z. Lan; J. Lin; M. Huang; Y. Huang; P. Li; S. Yin; T. Sato, *Journal of the American Chemical Society,* **2008,** *130*, 11568-11569.
[51]. P. Wang; Q. Dai; S. M. Zakeeruddin; M. Forsyth; D. R. MacFarlane; M. Grätzel, *Journal of the American Chemical Society,* **2004,** *126*, 13590-13591.

[52]. S. Murai; S. Mikoshiba; H. Sumino; S. Hayase, *Journal of Photochemistry and Photobiology A: Chemistry,* **2002,** *148*, 33-39.
[53]. B. Li; L. Wang; B. Kang; P. Wang; Y. Qiu, *Solar Energy Materials and Solar Cells,* **2006,** *90*, 549-573.
[54]. J. Nemoto; M. Sakata; T. Hoshi; H. Ueno; M. Kaneko, *J. Electroanal. Chem.,* **2007,** *599*, 23-30.
[55]. J. Kang; W. Li; X. Wang; Y. Lin; X. Xiao; S. Fang, *Electrochim. Acta,* **2003,** *48*, 2487-2491.
[56]. J. Kang; W. Li; X. Wang; Y. Lin; X. Li; X. Xiao; S. Fang, *J. Appl. Electrochem.,* **2004,** *34*, 301-304.
[57]. M. Toivola; F. Ahlskog; P. Lund, *Solar Energy Materials and Solar Cells,* **2006,** *90*, 2881-2893.
[58]. Z.-S. Wang; K. Sayama; H. Sugihara, *The Journal of Physical Chemistry B,* **2005,** *109*, 22449-22455.
[59]. H. Nusbaumer; J.-E. Moser; S. M. Zakeeruddin; M. K. Nazeeruddin; M. Grätzel, *The Journal of Physical Chemistry B,* **2001,** *105*, 10461-10464.
[60]. J. G. Rowley; B. H. Farnum; S. Ardo; G. J. Meyer, *The Journal of Physical Chemistry Letters,* **2010,** *1*, 3132-3140.
[61]. G. Redmond; D. Fitzmaurice, *The Journal of Physical Chemistry,* **1993,** *97*, 1426-1430.
[62]. Y. Liu; A. Hagfeldt; X.-R. Xiao; S.-E. Lindquist, *Solar Energy Materials and Solar Cells,* **1998,** *55*, 267-281.
[63]. H. Wang; J. Bell; J. Desilvestro; M. Bertoz; G. Evans, *The Journal of Physical Chemistry C,* **2007,** *111*, 15125-15131.
[64]. S. Pelet; J.-E. Moser; M. Grätzel, *The Journal of Physical Chemistry B,* **2000,** *104*, 1791-1795.
[65]. S. Nakade; S. Kambe; T. Kitamura; Y. Wada; S. Yanagida, *The Journal of Physical Chemistry B,* **2001,** *105*, 9150-9152.
[66]. G. P. Smestad; S. Spiekermann; J. Kowalik; C. D. Grant; A. M. Schwartzberg; J. Zhang; L. M. Tolbert; E. Moons, *Solar Energy Materials and Solar Cells,* **2003,** *76*, 85-105.
[67]. K. Tennakone; et al., *Journal of Physics D: Applied Physics,* **1999,** *32*, 374.
[68]. G. R. A. Kumara; S. Kaneko; M. Okuya; K. Tennakone, *Langmuir,* **2002,** *18*, 10493-10495.
[69]. V. P. S. Perera; K. Tennakone, *Solar Energy Materials and Solar Cells,* **2003,** *79*, 249-255.
[70]. J. Bandara; H. Weerasinghe, *Solar Energy Materials and Solar Cells,* **2005,** *85*, 385-390.
[71]. C. K. Chiang; C. R. Fincher; Y. W. Park; A. J. Heeger; H. Shirakawa; E. J. Louis; S. C. Gau; A. G. MacDiarmid, *Physical Review Letters,* **1977,** *39*, 1098.
[72]. H. Shirakawa; E. J. Louis; A. G. MacDiarmid; C. K. Chiang; A. J. Heeger, *J. Chem. Soc., Chem. Commun.,* **1977**, 578-580.
[73]. S. Stafström; J. L. Brédas; A. J. Epstein; H. S. Woo; D. B. Tanner; W. S. Huang; A. G. MacDiarmid, *Physical Review Letters,* **1987,** *59*, 1464.
[74]. Y. Cao; P. Smith; A. J. Heeger, *Synthetic Metals,* **1992,** *48*, 91-97.
[75]. K. Murakoshi; R. Kogure; Y. Wada; S. Yanagida, *Chem. Lett.,* **1997,** *26*, 471-472.
[76]. D. Gebeyehu; C. J. Brabec; N. S. Sariciftci; D. Vangeneugden; R. Kiebooms; D. Vanderzande; F. Kienberger; H. Schindler, *Synthetic Metals,* **2001,** *125*, 279-287.
[77]. C. D. Grant; A. M. Schwartzberg; G. P. Smestad; J. Kowalik; L. M. Tolbert; J. Z. Zhang, *J. Electroanal. Chem.,* **2002,** *522*, 40-48.

[78]. S. A. Haque; T. Park; C. Xu; S. Koops; N. Schulte; R. J. Potter; A. B. Holmes; J. R. Durrant, *Advanced Functional Materials,* **2004,** *14*, 435-440.
[79]. R. Zhu; C.-Y. Jiang; B. Liu; S. Ramakrishna, *Advanced Materials,* **2009,** *21*, 994-1000.
[80]. R. Senadeera; N. Fukuri; Y. Saito; T. Kitamura; Y. Wada; S. Yanagida, *Chemical Communications,* **2005**, 2259-2261.
[81]. J. Xia; N. Masaki; M. Lira-Cantu; Y. Kim; K. Jiang; S. Yanagida, *Journal of the American Chemical Society,* **2008,** *130*, 1258-1263.
[82]. X. Liu; W. Zhang; S. Uchida; L. Cai; B. Liu; S. Ramakrishna, *Advanced Materials,* **2010,** *22*, E150-E155.
[83]. J. K. Koh; J. Kim; B. Kim; J. H. Kim; E. Kim, *Advanced Materials,* **2011,** *23*, 1641-1646.
[84]. J.-K. Lee; W.-S. Kim; H.-J. Lee; W. S. Shin; S.-H. Jin; W.-K. Lee; M.-R. Kim, *Polym. Adv. Technol.,* **2006,** *17*, 709-714.
[85]. N. Ikeda; K. Teshima; T. Miyasaka, *Chemical Communications,* **2006**, 1733-1735.
[86]. C.-P. Lee; P.-Y. Chen; R. Vittal; K.-C. Ho, *Journal of Materials Chemistry,* **2010,** *20*, 2356-2361.
[87]. U. Bach; D. Lupo; P. Comte; J. E. Moser; F. Weissortel; J. Salbeck; H. Spreitzer; M. Gratzel, *Nature,* **1998,** *395*, 583-585.
[88]. H. J. Snaith; A. J. Moule; C. Klein; K. Meerholz; R. H. Friend; M. Grätzel, *Nano Letters,* **2007,** *7*, 3372-3376.
[89]. G. Schlichthörl; S. Y. Huang; J. Sprague; A. J. Frank, *The Journal of Physical Chemistry B,* **1997,** *101*, 8141-8155.
[90]. C. J. Barbé; F. Arendse; P. Comte; M. Jirousek; F. Lenzmann; V. Shklover; M. Grätzel, *Journal of the American Ceramic Society,* **1997,** *80*, 3157-3171.
[91]. C. C. Leznoff; A. B. P. Lever, *Phthalocyanines: properties and applications*. VCH: 1996.
[92]. G. Schneider; D. Wohrle; W. Spiller; J. Stark; G. Schulz-Ekloff, *Photochemistry and Photobiology,* **1994,** *60*, 333-342.
[93]. C. Boscornea; L. Hinescu; C. Moldovan; S. Tomas; A. Diacon, *Proceedings of the 16th Romanian International Conference on Chemistry and Chemical Engineering RICCCE XVI 9-12 September 2009,* **2009**, S. VI.2-S.VI.11.
[94]. A. Diacon; E. Rusen; C. Boscornea; C. Zaharia; C. Cincu, *Journal of Optoelectronics and Advanced Materials,* **2010,** *12*, 199-204.
[95]. R. D. McCullough, *Advanced Materials,* **1998,** *10*, 93-116.
[96]. V. M. Niemi; P. Knuuttila; J. E. Österholm; J. Korvola, *Polymer,* **1992,** *33*, 1559-1562.
[97]. M. R. Andersson; D. Selse; M. Berggren; H. Jaervinen; T. Hjertberg; O. Inganaes; O. Wennerstroem; J. E. Oesterholm, *Macromolecules,* **1994,** *27*, 6503-6506.
[98]. T. Olinga; B. François, *Synthetic Metals,* **1995,** *69*, 297-298.
[99]. G. Barbarella; M. Zambianchi; R. Di Toro; M. Colonna; D. Iarossi; F. Goldoni; A. Bongini, *The Journal of Organic Chemistry,* **1996,** *61*, 8285-8292.
[100]. D. Yang; P. N. Adams; L. Brown; B. R. Mattes, *Synthetic Metals,* **2006,** *156*, 1225-1235.
[101]. S. W. Ng; K. G. Neoh; J. T. Sampanthar; E. T. Kang; K. L. Tan, *The Journal of Physical Chemistry B,* **2001,** *105*, 5618-5625.
[102]. V. P. Parkhutik; E. Matveeva, *The Journal of Physical Chemistry B,* **1998,** *102*, 1549-1555.
[103]. R. J. Ellingson; M. C. Beard; J. C. Johnson; P. Yu; O. I. Micic; A. J. Nozik; A. Shabaev; A. L. Efros, *Nano Letters,* **2005,** *5*, 865-871.

[104]. R. P. Raffaelle; S. L. Castro; A. F. Hepp; S. G. Bailey, *Progress in Photovoltaics: Research and Applications,* **2002,** *10*, 433-439.
[105]. A. Diacon; L. Fara; C. Cincu; M. R. Mitroi; C. Zaharia; E. Rusen; C. Boscornea; C. Rosu; D. Comaneci, *Optical Materials,* **2010,** *32*, 1583-1586.
[106]. J. I. Langford; A. J. C. Wilson, *J. Appl. Crystallogr.,* **1978,** *11*, 102-113.
[107]. A. Diacon; E. Rusen; B. Mărculescu; C. Andronescu; C. Cotruţ; C. Zaharia; A. Mocanu; C. Cincu, *International Journal of Polymer Analysis and Characterization,* **2011,** *16*, 1 - 8.
[108]. G. McDermott; S. M. Prince; A. A. Freer; A. M. Hawthornthwaite-Lawless; M. Z. Papiz; R. J. Cogdell; N. W. Isaacs, *Nature,* **1995,** *374*, 517-521.
[109]. H. Zuber, *Trends Biochem. Sci,* **1986,** *11*, 414-419.
[110]. H. van Amerongen; R. van Grondelle, *The Journal of Physical Chemistry B,* **2000,** *105*, 604-617.
[111]. G. S. Beddard; G. Porter, *Nature,* **1976,** *260*, 366-367.
[112]. Z. Liu; H. Yan; K. Wang; T. Kuang; J. Zhang; L. Gui; X. An; W. Chang, *Nature,* **2004,** *428*, 287-292.
[113]. C. I. Brändén; J. Tooze, *Introduction to protein structure*. Garland Pub.: 1999.
[114]. M. N. Paddon-Row, *Electron and Energy Transfer*. Wiley-VCH Verlag GmbH & Co. KGaA: 2005; p 267-291.
[115]. T. Forster, *Discussions of the Faraday Society,* **1959,** *27*, 7-17.
[116]. D. L. Dexter, *The Journal of Chemical Physics,* **1953,** *21*, 836-850.
[117]. H. Imahori; K. Hagiwara; T. Akiyama; M. Aoki; S. Taniguchi; T. Okada; M. Shirakawa; Y. Sakata, *Chemical Physics Letters,* **1996,** *263*, 545-550.
[118]. M. R. Wasielewski, *Chemical Reviews,* **1992,** *92*, 435-461.
[119]. D. M. Guldi, *Chemical Society Reviews,* **2002,** *31*, 22-36.
[120]. E. Osawa, *Kagaku,* **1970,** *25*, 854-863.
[121]. Z. Yoshida; E. Osawa, *Hokozokusei (Aromaticity),* **1971**, 174.
[122]. W. Kratschmer; L. D. Lamb; K. Fostiropoulos; D. R. Huffman, *Nature,* **1990,** *347*, 354-358.
[123]. S. Iijima, *Nature,* **1991,** *354*, 56-58.
[124]. H. Ajie; M. M. Alvarez; S. J. Anz; R. D. Beck; F. Diederich; K. Fostiropoulos; D. R. Huffman; W. Kraetschmer; Y. Rubin; et al., *The Journal of Physical Chemistry,* **1990,** *94*, 8630-8633.
[125]. Q. Xie; E. Perez-Cordero; L. Echegoyen, *Journal of the American Chemical Society,* **1992,** *114*, 3978-3980.
[126]. K. M. Kadish; R. S. Ruoff, *Fullerenes: chemistry, physics, and technology*. Wiley-Interscience: 2000.
[127]. Q. Xie; F. Arias; L. Echegoyen, *Journal of the American Chemical Society,* **1993,** *115*, 9818-9819.
[128]. J. Catalán; J. L. Saiz; J. L. Laynez; N. Jagerovic; J. Elguero, *Angewandte Chemie International Edition in English,* **1995,** *34*, 105-107.
[129]. S. Leach; M. Vervloet; A. Desprès; E. Bréheret; J. P. Hare; T. John Dennis; H. W. Kroto; R. Taylor; D. R. M. Walton, *Chem. Phys.,* **1992,** *160*, 451-466.
[130]. R. Taylor; D. R. M. Walton, *Nature,* **1993,** *363*, 685-693.
[131]. A. Hirsch, *The chemistry of the fullerenes*. G. Thieme Verlag: 1994.
[132]. A. Skiebe; A. Hirsch; H. Klos; B. Gotschy, *Chemical Physics Letters,* **1994,** *220*, 138-140.
[133]. A. Hirsch, *J. Phys. Chem. Solids,* **1997,** *58*, 1729-1740.
[134]. M. A. Yurovskaya; I. V. Trushkov, *Russ. Chem. Bull.,* **2002,** *51*, 367-443.

[135]. A. Vasella; P. Uhlmann; C. A. A. Waldraff; F. Diederich; C. Thilgen, *Angewandte Chemie International Edition in English,* **1992,** *31*, 1388-1390.
[136]. M. Prato; T. Suzuki; H. Foroudian; Q. Li; K. Khemani; F. Wudl; J. Leonetti; R. D. Little; T. White, *Journal of the American Chemical Society,* **1993,** *115*, 1594-1595.
[137]. M. Prato; M. Maggini; G. Scorrano; V. Lucchini, *The Journal of Organic Chemistry,* **1993,** *58*, 3613-3615.
[138]. M. Maggini; G. Scorrano; M. Prato, *Journal of the American Chemical Society,* **1993,** *115*, 9798-9799.
[139]. M. Cases; M. Duran; J. Mestres; N. Martín; M. Solà, *The Journal of Organic Chemistry,* **2000,** *66*, 433-442.
[140]. C. Bingel, *Chemische Berichte,* **1993,** *126*, 1957-1959.
[141]. J.-F. Nierengarten; V. Gramlich; F. Cardullo; F. Diederich, *Angewandte Chemie International Edition in English,* **1996,** *35*, 2101-2103.
[142]. X. Camps; A. Hirsch, *J. Chem. Soc., Perkin Trans. 1,* **1997**, 1595-1596.
[143]. A. Bagno; S. Claeson; M. Maggini; M. L. Martini; M. Prato; G. Scorrano, *Chemistry – A European Journal,* **2002,** *8*, 1015-1023.
[144]. C. G. Claessens; U. Hahn; T. Torres, *The Chemical Record,* **2008,** *8*, 75-97.
[145]. P. A. Liddell; J. P. Sumida; A. N. Macpherson; L. Noss; G. R. Seely; K. N. Clark; A. L. Moore; T. A. Moore; D. Gust, *Photochemistry and Photobiology,* **1994,** *60*, 537-541.
[146]. H. Imahori; Y. Sakata, *Advanced Materials,* **1997,** *9*, 537-546.
[147]. R. M. Williams; J. M. Zwier; J. W. Verhoeven, *Journal of the American Chemical Society,* **1995,** *117*, 4093-4099.
[148]. R. M. Williams; M. Koeberg; J. M. Lawson; Y.-Z. An; Y. Rubin; M. N. Paddon-Row; J. W. Verhoeven, *The Journal of Organic Chemistry,* **1996,** *61*, 5055-5062.
[149]. J. M. Lawson; A. M. Oliver; D. F. Rothenfluh; Y.-Z. An; G. A. Ellis; M. G. Ranasinghe; S. I. Khan; A. G. Franz; P. S. Ganapathi; M. J. Shephard; M. N. Paddon-Row; Y. Rubin, *The Journal of Organic Chemistry,* **1996,** *61*, 5032-5054.
[150]. K. G. Thomas; V. Biju; D. M. Guldi; P. V. Kamat; M. V. George, *The Journal of Physical Chemistry A,* **1999,** *103*, 10755-10763.
[151]. K. G. Thomas; V. Biju; D. M. Guldi; P. V. Kamat; M. V. George, *The Journal of Physical Chemistry B,* **1999,** *103*, 8864-8869.
[152]. D. M. Guldi; M. Maggini; G. Scorrano; M. Prato, *Journal of the American Chemical Society,* **1997,** *119*, 974-980.
[153]. M. Even; B. Heinrich; D. Guillon; D. M. Guldi; M. Prato; R. Deschenaux, *Chemistry – A European Journal,* **2001,** *7*, 2595-2604.
[154]. T. Nakamura; H. Kanato; Y. Araki; O. Ito; K. Takimiya; T. Otsubo; Y. Aso, *The Journal of Physical Chemistry A,* **2006,** *110*, 3471-3479.
[155]. M. Maggini; A. Dono; G. Scorrano; M. Prato, *J. Chem. Soc., Chem. Commun.,* **1995**, 845-846.
[156]. J. A. Schlueter; J. M. Seaman; S. Taha; H. Cohen; K. R. Lykke; H. H. Wang; J. M. Williams, *J. Chem. Soc., Chem. Commun.,* **1993**, 972-974.
[157]. H. Imahori; S. Cardoso; D. Tatman; S. Lin; L. Noss; G. R. Seely; L. Sereno; J. C. d. Silber; T. A. Moore; A. L. Moore; D. Gust, *Photochemistry and Photobiology,* **1995,** *62*, 1009-1014.
[158]. T. Otsubo; Y. Aso; K. Takimiya, *Journal of Materials Chemistry,* **2002,** *12*, 2565-2575.
[159]. B. Jousselme; P. Blanchard; E. Levillain; R. de Bettignies; J. Roncali, *Macromolecules,* **2003,** *36*, 3020-3025.
[160]. T. Gu; J.-F. Nierengarten, *Tetrahedron Letters,* **2001,** *42*, 3175-3178.

[161]. N. Martín; L. Sánchez; B. Illescas; S. González; M. Angeles Herranz; D. M. Guldi, *Carbon,* **2000,** *38*, 1577-1585.
[162]. M. Bendikov; F. Wudl; D. F. Perepichka, *Chemical Reviews,* **2004,** *104*, 4891-4946.
[163]. D. Kreher; S.-G. Liu; M. Cariou; P. Hudhomme; A. Gorgues; M. Mas; J. Veciana; C. Rovira, *Tetrahedron Letters,* **2001,** *42*, 3447-3450.
[164]. S.-G. Liu; D. Kreher; P. Hudhomme; E. Levillain; M. Cariou; J. Delaunay; A. Gorgues; J. Vidal-Gancedo; J. Veciana; C. Rovira, *Tetrahedron Letters,* **2001,** *42*, 3717-3720.
[165]. N. Martin; L. Sanchez; D. M. Guldi, *Chemical Communications,* **2000**, 113-114.
[166]. L. Sánchez; I. Pérez; N. Martín; D. M. Guldi, *Chemistry – A European Journal,* **2003,** *9*, 2457-2468.
[167]. N. Martín; L. Sánchez; M. a. Á. Herranz; B. Illescas; D. M. Guldi, *Accounts of Chemical Research,* **2007,** *40*, 1015-1024.
[168]. J.-F. Nierengarten; J.-F. Eckert; J.-F. Nicoud; L. Ouali; V. Krasnikov; G. Hadziioannou, *Chemical Communications,* **1999**, 617-618.
[169]. J.-F. Eckert; J.-F. Nicoud; J.-F. Nierengarten; S.-G. Liu; L. Echegoyen; F. Barigelletti; N. Armaroli; L. Ouali; V. Krasnikov; G. Hadziioannou, *Journal of the American Chemical Society,* **2000,** *122*, 7467-7479.
[170]. M. Maggini; G. Possamai; E. Menna; G. Scorrano; N. Camaioni; G. Ridolfi; G. Casalbore-Miceli; L. Franco; M. Ruzzi; C. Corvaja, *Chemical Communications,* **2002**, 2028-2029.
[171]. C. M. Atienza; G. Fernandez; L. Sanchez; N. Martin; I. S. Dantas; M. M. Wienk; R. A. J. Janssen; G. M. A. Rahman; D. M. Guldi, *Chemical Communications,* **2006**, 514-516.
[172]. P. Vivo; M. Ojala; V. Chukharev; A. Efimov; H. Lemmetyinen, *Journal of Photochemistry and Photobiology A: Chemistry,* **2009,** *203*, 125-130.
[173]. T. G. Linssen; K. Durr; M. Hanack; A. Hirsch, *J. Chem. Soc., Chem. Commun.,* **1995**, 103-104.
[174]. D. M. Guldi; A. Gouloumis; P. Vazquez; T. Torres, *Chemical Communications,* **2002**, 2056-2057.
[175]. D. M. Guldi; I. Zilbermann; A. Gouloumis; P. Vázquez; T. Torres, *The Journal of Physical Chemistry B,* **2004,** *108*, 18485-18494.
[176]. A. Gouloumis; A. de la Escosura; P. Vázquez; T. Torres; A. Kahnt; D. M. Guldi; H. Neugebauer; C. Winder; M. Drees; N. S. Sariciftci, *Organic Letters,* **2006,** *8*, 5187-5190.
[177]. M. Quintiliani; A. Kahnt; T. Wölfle; W. Hieringer; P. Vázquez; A. Görling; D. M. Guldi; T. Torres, *Chemistry – A European Journal,* **2008,** *14*, 3765-3775.
[178]. T. J. Marks, *Angewandte Chemie International Edition in English,* **1990,** *29*, 857-879.
[179]. D. M. Guldi; A. Gouloumis; P. Vázquez; T. Torres; V. Georgakilas; M. Prato, *Journal of the American Chemical Society,* **2005,** *127*, 5811-5813.
[180]. G. Bottari; D. Olea; C. Gómez-Navarro; F. Zamora; J. Gómez-Herrero; T. Torres, *Angewandte Chemie International Edition,* **2008,** *47*, 2026-2031.
[181]. B. Ballesteros; G. de la Torre; T. Torres; G. L. Hug; G. M. A. Rahman; D. M. Guldi, *Tetrahedron,* **2006,** *62*, 2097-2101.
[182]. Y. Chen; M. E. Ei-Khouly; M. Sasaki; Y. Araki; O. Ito, *Organic Letters,* **2005,** *7*, 1613-1616.
[183]. M. S. Rodríguez-Morgade; M. E. Plonska-Brzezinska; A. J. Athans; E. Carbonell; G. de Miguel; D. M. Guldi; L. Echegoyen; T. s. Torres, *Journal of the American Chemical Society,* **2009,** *131*, 10484-10496.

[184]. F.-D. Cong; B. Ning; X.-G. Du; C.-Y. Ma; H.-F. Yu; B. Chen, *Dyes and Pigments,* **2005,** *66*, 149-154.
[185]. R. Aroca; C. Jennings; G. J. Kovac; R. O. Loutfy; P. S. Vincett, *The Journal of Physical Chemistry,* **1985,** *89*, 4051-4054.
[186]. M. Diem; P. L. Polavarapu; M. Oboodi; L. A. Nafie, *Journal of the American Chemical Society,* **1982,** *104*, 3329-3336.
[187]. T. M. M. Kumar; B. N. Achar, *Journal of Organometallic Chemistry,* **2006,** *691*, 331-336.
[188]. B. M. Illescas; N. Martín, *Comptes Rendus Chimie, 9*, 1038-1050.
[189]. F. D'Souza; K. M. Kadish, *Fundamentals and Applications of Carbon Nano Materials*. World Scientific Pub Co Inc: 2010.
[190]. H. M. D. Smith, *High performance pigments*. Wiley-VCH: 2002.
[191]. Y. Nagao, *Prog. Org. Coat., 31*, 43-49.
[192]. Y. Li; N. Wang; X. He; S. Wang; H. Liu; Y. Li; X. Li; J. Zhuang; D. Zhu, *Tetrahedron,* **2005,** *61*, 1563-1569.
[193]. F. Li-Min; et al., *Chinese Physics Letters,* **2004,** *21*, 2525.
[194]. Y. Wu; Y. Li; H. Li; Q. Shi; H. Fu; J. Yao, *Chemical Communications,* **2009**, 6955-6957.
[195]. S. Xiao; Y. Li; Y. Li; J. Zhuang; N. Wang; H. Liu; B. Ning; Y. Liu; F. Lu; L. Fan; C. Yang; Y. Li; D. Zhu, *The Journal of Physical Chemistry B,* **2004,** *108*, 16677-16685.
[196]. Y. Li; et al., *Nanotechnology,* **2005,** *16*, 1899.
[197]. J. Hua; F. Meng; F. Ding; F. Li; H. Tian, *Journal of Materials Chemistry,* **2004,** *14*, 1849-1853.
[198]. J. Hua; F. Meng; F. Ding; H. Tian, *Chem. Lett.,* **2004,** *33*, 432-433.
[199]. R. Gómez; J. L. Segura; N. Martín, *Organic Letters,* **2005,** *7*, 717-720.
[200]. N. Wang; Y. Li; X. He; H. Gan; Y. Li; C. Huang; X. Xu; J. Xiao; S. Wang; H. Liu; D. Zhu, *Tetrahedron,* **2006,** *62*, 1216-1222.
[201]. T. W. Chamberlain; E. S. Davies; A. N. Khlobystov; N. R. Champness, *Chemistry – A European Journal,* **2011,** *17*, 3759-3767.
[202]. C. C. Hofmann; S. M. Lindner; M. Ruppert; A. Hirsch; S. A. Haque; M. Thelakkat; J. Kohler, *PCCP,* **2010,** *12*, 14485-14491.
[203]. C. C. Hofmann; S. M. Lindner; M. Ruppert; A. Hirsch; S. A. Haque; M. Thelakkat; J. r. Köhler, *The Journal of Physical Chemistry B,* **2010,** *114*, 9148-9156.
[204]. Y. Liu; N. Wang; Y. Li; H. Liu; Y. Li; J. Xiao; X. Xu; C. Huang; S. Cui; D. Zhu, *Macromolecules,* **2005,** *38*, 4880-4887.
[205]. C. Huang; F. Lu; Y. Li; H. Gan; T. Jiu; J. Xiao; X. Xu; S. Cui; H. Liu; D. Zhu, *Journal of Nanoscience and Nanotechnology,* **2007,** *7*, 1472-1478.
[206]. N. Wang; F. Lu; C. Huang; Y. Li; M. Yuan; X. Liu; H. Liu; L. Gan; L. Jiang; D. Zhu, *Journal of Polymer Science Part A: Polymer Chemistry,* **2006,** *44*, 5863-5874.
[207]. C. Li; Y. Li, *Macromol. Chem. Phys.,* **2008,** *209*, 1541-1552.
[208]. Y. Shibano; T. Umeyama; Y. Matano; N. V. Tkachenko; H. Lemmetyinen; H. Imahori, *Organic Letters,* **2006,** *8*, 4425-4428.
[209]. J. Baffreau; S. Leroy-Lhez; N. Vân Anh; R. M. Williams; P. Hudhomme, *Chemistry – A European Journal,* **2008,** *14*, 4974-4992.
[210]. J. Baffreau; L. Perrin; S. Leroy-Lhez; P. Hudhomme, *Tetrahedron Letters,* **2005,** *46*, 4599-4603.
[211]. J. Baffreau; S. Leroy-Lhez; H. Derbal; A. R. Inigo; J.-M. Nunzi; M. M. Groeneveld; R. M. Williams; P. Hudhomme, *Eur. Phys. J. Appl. Phys.,* **2006,** *36*, 301-305.
[212]. P. Sörme; P. Arnoux; B. Kahl-Knutsson; H. Leffler; J. M. Rini; U. J. Nilsson, *Journal of the American Chemical Society,* **2005,** *127*, 1737-1743.

[213]. M. R. Johnson; L. S. Melvin, *U.S Patent Office,* **1978,** *4,118,559*.
[214]. H. Zhao; A. Thurkauf, *Synthetic Communications: An International Journal for Rapid Communication of Synthetic Organic Chemistry,* **2001,** *31*, 1921 - 1926.
[215]. D. R. Williams; B. A. Barner; K. Nishitani; J. G. Phillips, *Journal of the American Chemical Society,* **1982,** *104*, 4708-4710.
[216]. S. K. Boovanahalli; D. W. Kim; D. Y. Chi, *The Journal of Organic Chemistry,* **2004,** *69*, 3340-3344.
[217]. H. Günther, *NMR spectroscopy: an introduction*. Wiley: 1980.
[218]. H. Du; R.-C. A. Fuh; J. Li; L. A. Corkan; J. S. Lindsey, *Photochemistry and Photobiology,* **1998,** *68*, 141-142.
[219]. D. Xie; M. Jiang; G. Zhang; D. Chen, *Chemistry - A European Journal,* **2007,** *13*, 3346-3353.
[220]. J. D. Joannopoulos, *Photonic crystals: molding the flow of light*. Princeton University Press: 2008.
[221]. E. Yablonovitch, *Physical Review Letters,* **1987,** *58*, 2059.
[222]. S. John, *Physical Review Letters,* **1987,** *58*, 2486.
[223]. E. Yablonovitch; T. J. Gmitter; K. M. Leung, *Physical Review Letters,* **1991,** *67*, 2295.
[224]. T. F. Krauss; R. M. D. L. Rue; S. Brand, *Nature,* **1996,** *383*, 699-702.
[225]. G. A. Ozin; K. Hou; B. V. Lotsch; L. Cademartiri; D. P. Puzzo; F. Scotognella; A. Ghadimi; J. Thomson, *Mater. Today,* **2009,** *12*, 12-23.
[226]. J. P. Rao; K. E. Geckeler, *Progress in Polymer Science,* **2011,** *36*, 887-913.
[227]. C. S. Chern, *Progress in Polymer Science,* **2006,** *31*, 443-486.
[228]. J. W. Goodwin, *Colloids and interfaces with surfactants and polymers: an introduction*. J. Wiley: 2004.
[229]. C. D. Anderson; E. S. Daniels, *Emulsion Polymerisation and Latex Applications*. Rapra Technology: 2003.
[230]. C. S. Chern; T. J. Chen; Y. C. Liou, *Polymer,* **1998,** *39*, 3767-3777.
[231]. C. S. Chern, *Principles and applications of emulsion polymerization*. Wiley: 2008.
[232]. H. de Brouwer; J. G. Tsavalas; F. J. Schork, *Macromolecules,* **2000,** *33*, 9239-9246.
[233]. J. Qiu; S. G. Gaynor; K. Matyjaszewski, *Macromolecules,* **1999,** *32*, 2872-2875.
[234]. A. R. Goodall; M. C. Wilkinson; J. Hearn, *Journal of Polymer Science: Polymer Chemistry Edition,* **1977,** *15*, 2193-2218.
[235]. R. M. L. Fitch, *Polymer colloids: a comprehensive introduction*. Academic Press: 1997.
[236]. H.-S. Chang; S.-A. Chen, *Journal of Polymer Science Part A: Polymer Chemistry,* **1988,** *26*, 1207-1229.
[237]. S. C. Thickett; R. G. Gilbert, *Polymer,* **2007,** *48*, 6965-6991.
[238]. K. Tauer; R. Deckwer; I. Kühn; C. Schellenberg, *Colloid & Polymer Science,* **1999,** *277*, 607-626.
[239]. T. Yamamoto; M. Nakayama; Y. Kanda; K. Higashitani, *Journal of Colloid and Interface Science,* **2006,** *297*, 112-121.
[240]. C. e. Yan; S. Cheng; L. Feng, *Journal of Polymer Science Part A: Polymer Chemistry,* **1999,** *37*, 2649-2656.
[241]. N. Preda; E. Matei; M. Enculescu; E. Rusen; A. Mocanu; B. Marculescu; I. Enculescu, *Journal of Polymer Research,* **2011,** *18*, 25-30.
[242]. E. Rusen; A. Mocanu; C. Corobea; B. Marculescu, *Colloids and Surfaces A: Physicochemical and Engineering Aspects,* **2010,** *355*, 23-28.
[243]. A. Ulman, *Organic thin films and surfaces: directions for the nineties*. Academic Press: 1995.
[244]. J. Texter; M. Tirrell, *AlChE J.,* **2001,** *47*, 1706-1710.

[245]. G. I. N. Waterhouse; M. R. Waterland, *Polyhedron,* **2007,** *26*, 356-368.
[246]. H. Ge; Y. Song; L. Jiang; D. Zhu, *Thin Solid Films,* **2006,** *515*, 1539-1543.
[247]. L. Zhang; Y. Xiong, *Journal of Colloid and Interface Science,* **2007,** *306*, 428-432.
[248]. J. Zhang; Z. Sun; B. Yang, *Current Opinion in Colloid & Interface Science,* **2009,** *14*, 103-114.
[249]. A. Chiappini; C. Armellini; A. Chiasera; M. Ferrari; L. Fortes; M. Clara Gonçalves; R. Guider; Y. Jestin; R. Retoux; G. Nunzi Conti; S. Pelli; R. M. Almeida; G. C. Righini, *Journal of Non-Crystalline Solids,* **2009,** *355*, 1167-1170.
[250]. V. E. Laine, *Photonic Crystals: Fabrication, Band Structure and Applications*. Nova Science Pub Inc: 2010.
[251]. N. Denkov; O. Velev; P. Kralchevski; I. Ivanov; H. Yoshimura; K. Nagayama, *Langmuir,* **1992,** *8*, 3183-3190.
[252]. A. Herzog Cardoso; C. A. P. Leite; M. E. D. Zaniquelli; F. Galembeck, *Colloids and Surfaces A: Physicochemical and Engineering Aspects,* **1998,** *144*, 207-217.
[253]. A. Diacon; E. Rusen; A. Mocanu; P. Hudhomme; C. Cincu, *Langmuir,* **2011,** *27*, 7464-7470.
[254]. E. Rusen; A. Mocanu; A. Diacon; B. Marculescu, *The Journal of Physical Chemistry C,* **2011,** *115*, 14947-14953.
[255]. Z. Yang; J. Zhou; X. Huang; G. Yang; Q. Xie; L. Sun; B. Li; L. Li, *Chemical Physics Letters,* **2008,** *455*, 55-58.
[256]. R. Withnall; et al., *Journal of Optics A: Pure and Applied Optics,* **2003,** *5*, S81.
[257]. M. Muller; R. Zentel; T. Maka; S. G. Romanov; C. M. Sotomayor Torres, *Chemistry of Materials,* **2000,** *12*, 2508-2512.
[258]. F. Fleischhaker; R. Zentel, *Chemistry of Materials,* **2005,** *17*, 1346-1351.
[259]. S. G. Romanov; T. Maka; C. M. S. Torres; M. Muller; R. Zentel, *Applied Physics Letters,* **1999,** *75*, 1057-1059.
[260]. B. Lange; R. Zentel; C. Ober; S. Marder, *Chemistry of Materials,* **2004,** *16*, 5286-5292.
[261]. F. Wurthner, *Chemical Communications,* **2004**, 1564-1579.
[262]. B. A. Jones; M. J. Ahrens; M.-H. Yoon; A. Facchetti; T. J. Marks; M. R. Wasielewski, *Angewandte Chemie International Edition,* **2004,** *43*, 6363-6366.
[263]. M. A. Angadi; D. Gosztola; M. R. Wasielewski, *Materials Science and Engineering B,* **1999,** *63*, 191-194.
[264]. L. Schmidt-Mende; A. Fechtenkötter; K. Müllen; E. Moons; R. H. Friend; J. D. MacKenzie, *Science,* **2001,** *293*, 1119-1122.
[265]. M. R. Wasielewski, *Accounts of Chemical Research,* **2009,** *42*, 1910-1921.
[266]. X. Guo; D. Zhang; D. Zhu, *Advanced Materials,* **2004,** *16*, 125-130.
[267]. S. Leroy-Lhez; J. Baffreau; L. Perrin; E. Levillain; M. Allain; M.-J. Blesa; P. Hudhomme, *The Journal of Organic Chemistry,* **2005,** *70*, 6313-6320.
[268]. X. He; H. Liu; Y. Li; S. Wang; N. Wang; J. Xiao; X. Xu; D. Zhu, *Advanced Materials,* **2005,** *17*, 2811-2815.
[269]. J. Baffreau; S. Leroy-Lhez; P. Hudhomme; M. M. Groeneveld; I. H. M. van Stokkum; R. M. Williams, *The Journal of Physical Chemistry A,* **2006,** *110*, 13123-13125.
[270]. F. Wurthner, *Pure Appl. Chem.,* **2006,** *78*, 2341-2349.
[271]. E. Rusen; A. Mocanu; B. Marculescu, *Colloid & Polymer Science,* **2010,** *288*, 769-776.
[272]. X. Wang; S. M. Husson; X. Qian; S. R. Wickramasinghe, *Materials Letters,* **2009,** *63*, 1981-1983.
[273]. X. He; Y. Thomann; R. J. Leyrer; J. Rieger, *Polymer Bulletin,* **2006,** *57*, 785-796.

[274]. Y.-Q. Zhang; J.-X. Wang; Z.-Y. Ji; W.-P. Hu; L. Jiang; Y.-L. Song; D.-B. Zhu, *Journal of Materials Chemistry,* **2007,** *17*, 90-94.
[275]. X. Juan; D. Hong; X. Zi-qiang; L. Yan; H. Jun, *Materials Science in Semiconductor Processing,* **2006,** *9*, 136-140.
[276]. J. Liu; et al., *Journal of Optics A: Pure and Applied Optics,* **2007,** *9*, 325.
[277]. C. Hippius; I. H. M. van Stokkum; E. Zangrando; R. M. Williams; M. Wykes; D. Beljonne; F. Würthner, *The Journal of Physical Chemistry C,* **2008,** *112*, 14626-14638.
[278]. W. E. Ford; P. V. Kamat, *The Journal of Physical Chemistry,* **1987,** *91*, 6373-6380.
[279]. K. Dou; Z. Xu; X. J. Wang; Y. Chen; T. Collins, *Journal of Luminescence,* **2003,** *102-103*, 476-480.
[280]. P. Jiang; G. N. Ostojic; R. Narat; D. M. Mittleman; V. L. Colvin, *Advanced Materials,* **2001,** *13*, 389-393.
[281]. M. Egen; R. Voss; B. Griesebock; R. Zentel; S. Romanov; C. S. Torres, *Chemistry of Materials,* **2003,** *15*, 3786-3792.
[282]. H.-L. Li; F. Marlow, *Chemistry of Materials,* **2005,** *17*, 3809-3811.
[283]. R. Rengarajan; P. Jiang; D. C. Larrabee; V. L. Colvin; D. M. Mittleman, *Physical Review B,* **2001,** *64*, 205103.
[284]. G. Q. Liu; H. H. Hu; Y. B. Liao; Z. S. Wang; Y. Chen; Z. M. Liu, *Optik - International Journal for Light and Electron Optics,* **2011,** *122*, 9-13.
[285]. M. Obata; M. Morita; K. Nakase; K. Mitsuo; K. Asai; S. Hirohara; S. Yano, *Journal of Polymer Science Part A: Polymer Chemistry,* **2007,** *45*, 2876-2885.
[286]. I. Zareba-Grodz; R. Pazik; K. Hermanowicz; W. Strek; K. Maruszewski, *Journal of Luminescence,* **2006,** *119-120*, 148-152.
[287]. Y. Xiang; Z. Li; X. Chen; A. Tong, *Talanta,* **2008,** *74*, 1148-1153.
[288]. S. Bae; J. Tae, *Tetrahedron Letters,* **2007,** *48*, 5389-5392.
[289]. X. Zhang; Y. Shiraishi; T. Hirai, *Tetrahedron Letters,* **2007,** *48*, 5455-5459.
[290]. X.-F. Yang; X.-Q. Guo; H. Li, *Talanta,* **2003,** *61*, 439-445.
[291]. T.-S. Deng; J.-Y. Zhang; K.-T. Zhu; Q.-F. Zhang; J.-L. Wu, *Colloids and Surfaces A: Physicochemical and Engineering Aspects,* **2010,** *356*, 104-111.
[292]. Z. S. Guan; Y. Zhang; Q. Zhang; D. X. Li, *Journal of Colloid and Interface Science,* **2006,** *302*, 113-122.
[293]. A. A. M. Farag; I. S. Yahia, *Optics Communications,* **2010,** *283*, 4310-4317.
[294]. I. Moreno-Villoslada; M. Jofré; V. Miranda; P. Chandía; R. González; S. Hess; B. L. Rivas; C. Elvira; J. San Román; T. Shibue; H. Nishide, *Polymer,* **2006,** *47*, 6496-6500.
[295]. H. Li; J. Wang; F. Liu; Y. Song; R. Wang, *Journal of Colloid and Interface Science,* **2011,** *356*, 63-68.
[296]. M. Zhao; X.-F. Yang; S. He; L. Wang, *Sensors and Actuators B: Chemical,* **2009,** *135*, 625-631.
[297]. L. Dong; ChongWu; X. Zeng; L. Mu; S.-F. Xue; Z. Tao; J.-X. Zhang, *Sensors and Actuators B: Chemical,* **2010,** *145*, 433-437.
[298]. F.-J. Huo; J. Su; Y.-Q. Sun; C.-X. Yin; H.-B. Tong; Z.-X. Nie, *Dyes and Pigments,* **2010,** *86*, 50-55.
[299]. H. Sasaki; K. Hanaoka; Y. Urano; T. Terai; T. Nagano, *Biorg. Med. Chem.,* **2011,** *19*, 1072-1078.
[300]. H. Liu; P. Yu; D. Du; C. He; B. Qiu; X. Chen; G. Chen, *Talanta,* **2010,** *81*, 433-437.
[301]. H. Ju; M. H. Lee; J. Kim; J. S. Kim; J. Kim, *Talanta,* **2011,** *83*, 1359-1363.
[302]. E. Rusen; A. Mocanu; B. Marculescu; R. Somoghi; L. Butac; F. Miculescu; C. Cotrut; I. Antoniac; C. Cincu, *Colloids and Surfaces A: Physicochemical and Engineering Aspects,* **2011,** *375*, 35-41.

List of publications in non - ISI rated journals:

1. Boscornea, C.; Hinescu, L.; Moldovan, C.; Tomas, S.; **Diacon, A**., New phthalocyanine-type compounds-synthesis, characterization and applications in gas microsensors. *Proceedings of the 16th Romanian International Conference on Chemistry and Chemical Engineering RICCCE XVI 9-12 September 2009* **2009**, S. VI.2-S.VI.11.
2. **Diacon, A**.; Rusen, E.; Boscornea, C.; Pandele, A. M., Cincu, C., New phthalocyanine-fullerene dyads for solar cells, U.P.B. Sci. Bull., Series B, accepted

List of publications in ISI rated journals:

1. **Diacon, A**.; Fara, L.; Cincu, C.; Mitroi, M. R.; Zaharia, C.; Rusen, E.; Boscornea, C.; Rosu, C.; Comaneci, D., New materials for hybrid dye-sensitized solar cells. *Optical Materials* **2010,** *32* (12), 1583-1586.
2. **Diacon, A**.; Rusen, E.; Boscornea, C.; Zaharia, C.; Cincu, C., Hybrid dye sensitized solar cells. *Journal of Optoelectronics and Advanced Materials* **2010,** *12* (2), 199-204
3. **Diacon, A.**; Rusen, E.; Mărculescu, B.; Andronescu, C.; Cotruţ, C.; Zaharia, C.; Mocanu, A.; Cincu, C., Superficial Grafting of Water-Soluble Polymers on Brominated MWCNT by ATRP Technique. *International Journal of Polymer Analysis and Characterization* **2011,** *16* (1), 1 - 8.
4. **Diacon, A.**; Rusen, E.; Mocanu, A.; Hudhomme, P.; Cincu, C., Fluorescence Properties of Photonic Crystals Doped with Perylenediimide. *Langmuir* **2011,** *27* (12), 7464-7470
5. Rusen, E.; Mocanu, A.; **Diacon, A.;** Marculescu, B., Fluorescence Enhancement of Rhodamine B in the Presence of Photonic Crystals Heterostructures. *The Journal of Physical Chemistry C* **2011,** *115* (30), 14947-14953.

Books:

1. Cincu, C.; Iovu, H.; Zaharia, C.; **Diacon, A.**, Biomateriale polimerice şi aplicaţii medicale. Politehnica Press, **2009**, ISBN 978-065-515-068-3

Abstract:

The thesis entitled "Polymers functionalized with chromophores for applications in photovoltaics, photonics and medicine" is structured in three chapters dealing with: a) the obtaining of chromophores and new materials for dye-sensitized solar cells; b) the obtaining of new fullerene-C_{60} derivatives with increased absorption; c) the obtaining of a platform allowing the attachment of light-harvesting dyads PDI-C_{60} including a free functional group for further applied developments of which one consisting in grafting onto a polymeric chain for increased processability; d) the obtaining of polymer photonic crystals and the utilization in dye emission modification and the building of complex heterostructures with chemosensor capabilities.

In the first chapter new materials for hybrid dye-sensitized solar cells are presented with the aim of constructing solid state solar cells using polymers to replace the liquid electrolyte. Furthermore, strategies for improving the cell efficiency by using a dye with better anchoring on the TiO_2 layer capacity, and the use of quantum-dots particles for the increasing of the electron injection rate have been tested.

In the second chapter the obtaining of new fullerene based light-harvesting antennas is presented. Fullerene-phthalocyanine adducts were obtained and electron transfer was proven through fluorescence spectroscopy. A PDI-C_{60} dyad was successfully attached onto a polymeric chain for increasing processability for applications in bulk-heterojunction solar cells.

In the third chapter the optical properties and use as chemosensor of polymer photonic crystals and complex heterostructures modified with fluorescent dyes was investigated.
Key words: solid-state DSSC, fullerene, antenna, photonic crystals, fluorescence

Abstract:

Teza intitulată "Polimeri funcționalizați cu cromofori având utilizări în fotovoltaică, fotonică și medicină" este structurată pe trei capitole ce prezintă: a) obținerea de cromofori și noi materiale pentru celule solare pe bază de coloranți; b) obținerea de noi derivați de fulerenă-C_{60} cu o absorbție ridicată; c) obținerea unei platforme care permite atașarea unei diade colectoare de lumină PDI-C_{60} incorporând și o grupă funcțională liberă ce permite modificări ulterioare, dintre care una constă în grefarea pe un lanț polimeric preformat pentru îmbunătățirea procesabilității; d) obținerea de cristale fotonice polimerice și utilizarea acestora pentru modificarea caracteristicilor de emisie a unui colorant și obținerea de heterostructuri complexe cu caracteristici de chemosenzor.

În primul capitol sunt prezentate noi materiale pentru celule solare pe baza de coloranți utilizate în obținerea de celule în stare solidă utilizând polimeri pentru înlocuirea electrolitului lichid. Au fost testate și strategii pentru îmbunătățirea eficienței celulei prin utilizarea unor coloranți cu o capacitate de ancorare pe stratul de TiO_2 precum și utilizarea de quantum dot-uri pentru creșterea ratei de injectare de electroni.

În al doilea capitol este prezentată obținerea de noi antene colectoare de lumină pe bază de fulerenă-C_{60}. Aducți ftalocianină-fulerenă au fost obținuți și transferul de electroni a fost demonstrat prin spectroscopie de fluorescență. O diadă PDI-C_{60} a fost obținută și atașată pe un lanț polimeric pentru îmbunătățirea procesabilității pentru posibile utilizări în obținerea de celule solare organice.

În al treilea capitol au fost studiate proprietățile optice și utilizarea drept chemosenzori a cristalelor fotonice polimerice și a unor heterostructuri complexe modificate cu cromofori fluorescenți.
Cuvinte cheie: celule solare pe baza de coloranți, fulerenă, antenă, cristale fotonice, fluorescență.

Résumé:

La thèse intitulée ≪ Polymères fonctionnalisés avec des chromophores pour des applications en photovoltaïque, photonique et médecine ≫ est structurée en trois chapitres portant sur: a) l'obtention de chromophores et de nouveaux matériaux pour les cellules solaires à base de colorant; b) l'obtention de dérivés de fullerène C_{60} présentant une absorption élevée; c) l'obtention d'une plateforme permettant la fixation d'une antenne collectrice de lumière PDI-C_{60} intégrant un groupe fonctionnel libre réactif; d) l'obtention des cristaux photoniques polymères et leur utilisation dans la modification des émissions du colorant et la construction d'hétérostructures complexes intégrant ces colorants.

Dans le premier chapitre sont présentés des nouveaux matériaux pour cellules solaires à base de colorant en vue de construire des cellules solaires à l'état solide en utilisant des polymères pour remplacer l'électrolyte liquide. Des stratégies pour améliorer l'efficacité des cellules en utilisant un colorant qui présente une meilleure capacité d'ancrage à la couche de TiO_2, et l'utilisation des quantum dots particules pour l'augmentation du taux d'injection d'électrons ont été testées.

Dans le deuxième chapitre est présentée l'obtention des nouvelles antennes collectrices de lumière à base de fullerène. Des adduits fullerènes phtalocyanine ont été obtenus et le transfert d'électrons a été prouvé par spectroscopie de fluorescence. Une dyade PDI-C_{60} a été attachée avec succès sur une chaîne de polymère pour augmenter la processabilité afin d'envisager des applications dans les cellules solaires organiques.

Dans le troisième chapitre ont été analysées les propriétés optiques des cristaux photoniques et d'hétérostructures complexes modifiées aves des colorants.

Mots clés : cellules solaires état solide, fullerène, antenne, cristaux photonique, fluorescence